Modelling horizontal soil deformations

Validation of the state of the art models with in-situ measurements

Brass, Nigeria

Abcoude, the Netherlands

Master of Science Thesis
C.W.J. te Boekhorst
15 June 2010

Delft University of Technology
Faculty of Civil Engineering and Geosciences
Section of Geo-Engineering

Royal Boskalis Westminster nv
Hydronamic bv

T̃UDelft
Delft University of Technology

Royal Boskalis Westminster nv
International Dredging Contractors

Modelling horizontal soil deformations

Validation of the state of the art models with in-situ measurements

C.W.J. te Boekhorst
Student no. 1404598

T̃U Delft
Delft University of Technology

db Royal Boskalis Westminster nv
International Dredging Contractors

A thesis submitted in partial fulfilment of the requirements for the degree of Master of Science at Delft University of Technology in Civil Engineering and Geosciences, track Geo-Engineering, specialisation Geotechnical Engineering.

Graduation Committee:

Prof. M.A. Hicks, Ph.D.	TU Delft (section Geo-Engineering)
Prof. Drs. Ir. J.K. Vrijling	TU Delft (section Hydraulic Engineering)
Dr. Ir. R.B.J. Brinkgreve	TU Delft (section Geo-Engineering) & Plaxis bv
Ir. F.A.J.M. Mathijssen	TU Delft (section Geo-Engineering) & Hydronamic bv
Ir. C.J. Dykstra	Hydronamic bv

Preface

This thesis is the final product of a research project undertaken to obtain the degree Master of Science at Delft University of Technology. The project started at the end of September 2009 and lasted for approximately 9 months. The realization of this report is the ultimate result of a close collaboration between the engineering department of Boskalis (Hydronamic) and the university. The main objective of this thesis was to gain more insight into the modelling of horizontal soil deformations. To reach this objective the constitutive behaviour of soft soils had to be explored, and numerical implementations had to be analyzed.

Although, this thesis is in principle an individual project. I would not been able to complete this thesis on my own, and therefore I would like to thank all people who supported my research project. First of all I wish to thank my parents. You provided me the opportunity to become a geotechnical engineer. I am grateful to Boskalis and Hydronamic for offering me the possibility to combine my thesis work with commercial work for various projects. I also would like to thank all colleagues for the pleasant working atmosphere, and especially my roommate Arthur Zoon who started about the same time with his graduation project.

Furthermore, I want to thank the members of my graduation committee for their advise and supervision of my research process. A special word of thanks goes to François Mathijssen and Chris Dykstra of Hydronamic, they have invested a lot of time for support and lengthy discussions. Next to the committee members, I also want to thank Minna Karstunen of the University of Strathclyde, she provided the opportunity to investigate the S-Clay1 model and the Anisotropic Creep model in more detail.

Papendrecht, 15 June 2010

Coen te Boekhorst

Summary

Many cities around the world are located in deltaic areas, these areas have a major economic potential due to their strategic location close to seas and waterways. On the other hand, these deltaic regions are generally covered with very compressible soils. When embankments are constructed on such soils large vertical deformations will occur, but also a significant amount of horizontal deformations can be expected at the outer sides of the embankment. These deformations can have an adverse effect on nearby structures, for instance pile foundations, cables and ducts. This research concentrates on the horizontal deformations, which are most prominent at the outer sides of the embankment. A case where horizontal deformations have resulted in damage is reported by Fellenius and Johansson (1972). They presented a case where several piles of a building in Huddinge near Stockholm buckled due to excessive horizontal movements. More recently the HSL railway track near The Hague was damaged due to horizontal soil deformations (Maas and Wuite, 2006). The horizontal deformations slightly deformed the piles under the concrete railway track.

In spite of the several decades of research, geotechnical engineers still have difficulty with predicting the horizontal soil deformations. The currently available design models are not always successful in predicting soil behaviour due to the fact that these models often assume loading situations, effective stress paths and constitutive relations that are not representative for in-situ soil conditions. The traditional models for predicting the horizontal deformations are the analytical models Van IJsseldijk and Loof, which assume undrained linear elastic soil behaviour during loading. De Leeuw (1963) converted these models into normalized tables for terrace and strip loading situations. The normalized tables for both analytical models are included in Appendixes 1 and 2. It is evident that due to these assumptions the analytical models cannot predict horizontal deformations very accurately. In reality, the response of a natural soft soil to an surface loading is highly non-linear. Tavenas and Leroueil (1980) indicated that a fully undrained response during the construction of an embankment is rarely observed; the measured pore pressures are usually much lower. This difference is due to the initially overconsolidated state of soils, during this stage the consolidation coefficients are much higher. It is indicated that the undrained assumption could lead to significant differences even for soft soils with relatively low pre-overburden pressures of about 20 kPa.

For contractors such as Boskalis, the introduction of the Design & Construct contract calls for an update of the standard models for predicting horizontal deformations. The use of the conventional analytical models can be problematic in this type of contract, because very strict deformation requirements can be specified. Therefore, there is an urge for the development of models with an improved reliability. An attractive model that could be used to obtain a quick estimate of the horizontal soil deformations is the empirical model of Bourgens and Mieussens. This model relates the settlements under the centre of an embankment to the horizontal deformations at the toe of an embankment. A substantial benefit of this empirical model is that it implicitly includes complex factors like consolidation and anisotropy. Unfortunately, it is not possible to examine the contributions of each soil aspect individually. In addition, finite element analyses have been performed with Plaxis 2D version 9 for five different constitutive models with varying degree of sophistication. Besides the commercial

available LEPP-MC model, Modified Cam Clay model, and Soft Soil Creep model; the user-defined models S-Clay1 (Wheeler *et al.*, 2003) and the Anisotropic Creep (Leonie *et al.*, 2008) have been investigated. Both user-defined models use a rotational hardening rule to simulate anisotropic behaviour during plastic straining. These models are programmed in the Fortran language, and can be implemented as a dynamic link library in Plaxis. It is noted that most emphasis has been devoted to the simulations with the constitutive formulations in Plaxis, because it enables us to evaluate the contributions of individual soil aspects like consolidation, creep and anisotropy more closely. Apart from the modelling part, basic theories in soil mechanics as the isotache theory and the critical state theory have been related to the phenomenon of horizontal soil deformations.

The predictions obtained with these models are validated with the in-situ measurements of two distinctive case studies. The first case study deals with the construction of a new road embankment near the existing A2 highway in Abcoude. From the borings and CPTs it can be concluded that the subsoil consists of a thick fibrous peat layer and a thin clay layer on top. The other case study is about an embankment construction for a LNG export facility in Brass Nigeria. The subsoil at this location is strongly layered till a depth of at least 100 m below surface level. Such soil profiles are fundamentally different from the soil profiles which are generally observed in the Netherlands. However, the currently available empirical and analytical models are only applicable to a relatively uniform soil profile, which is possibly overlain by a stiff soil layer. This implies that layered soil profiles can only be modelled with Plaxis or another numerical simulation programs. In addition, it is noted that a comparison with the in-situ measurements was not possible a few years after construction, because the inclinometers were in both cases removed shortly after the end of construction. The quality of the long-term predictions is therefore based on the results of the test embankments in Skå Edeby (Neher *et al.*, 1999) and Murro (Koskinen *et al.*, 2002).

In this thesis the horizontal soil deformations are calculated at the crest, the toe and outside the toe of the embankment at various moments in time. The uncertainty in the predictions is evaluated with an extended version of the reliability method of Duncan (2000). The extension embraces the spatial variability of soils and a pragmatic inclusion of the model uncertainty. The model predictions with the mean values and the results of the reliability analyses have led to the following conclusions. It appeared that the predictions with the empirical model of Bourgens and Mieussens are somewhat conservative. Similar findings are reported by Feddema *et al.* (2009) for the embankments in Bricor and the Betuweroute. The quality of the model predictions with the analytical models is usually poor, especially Van IJsseldijk which largely overestimates the magnitude of the in-situ horizontal deformations. It is therefore not advised to apply these models, because the predictions are mostly incorrect. Furthermore, the results of the constitutive models in Plaxis indicate that the best fits and the lowest variation coefficients are generally obtained with the S-Clay1 model. This model is very suitable to simulate the horizontal soil deformations during the construction of the embankment. It performs less well in the long-term, because creep is not included. The Anisotropic Creep model should perform better in the long-term. However, preliminary calculations indicated that this model is not working properly. It is therefore advised to improve the correctness of the constitutive formulation and to increase the stability of numerical algorithms. This will hopefully lead to an Anisotropic Creep model that accurately predicts the horizontal soil deformations during and after construction.

Table of Contents

Notations and Abbreviations

The list of symbols and abbreviations with corresponding unities is not exhaustive, but includes at least the most important symbols used in this report.

Symbol	Description	Unity
a	Direct compression index (Den Haan, 1994)	[-]
a	Destructuration parameter (S-Clay1S model)	[-]
b	Secular compression index (Den Haan, 1994)	[-]
b	Destructuration parameter (S-Clay1S model)	[-]
B	Correction factor for plane strain condition (vertical drainage)	[m]
B	Pore water coefficient (Skempton, 1954)	[-]
c	Coefficient of rate of secular compression (Den Haan, 1994)	[-]
c	Cohesion	[kN/m^2]
c_u	Undrained shear strength	[kN/m^2]
c_v	Vertical consolidation coefficient	[m^2/s]
CR	Compression ratio	[-]
CV	Coefficient of variation	[-]
C_α	Secondary compression ratio	[-]
d_w	Equivalent drain diameter (vertical drainage)	[m]
D	Diameter of the influence zone (vertical drainage)	[m]
e	Void ratio	[-]
e_0	Initial void ratio	[-]
E	Young's modulus	[kN/m^2]
E_{oed}	Tangent stiffness for primary oedometer loading	[kN/m^2]
E_{50}	Secant stiffness in a drained triaxial test	[kN/m^2]
E_{ur}	Unloading / reloading stiffness	[kN/m^2]
f	Yield function	[-]
FS	Factor of safety	[-]
g	Plastic potential function	[-]
h_{max}	Maximum horizontal deformation	[m]
i	Hydraulic gradient	[-]
k_v	Vertical permeability	[m/s]
k_h	Horizontal permeability	[m/s]
K	Earth pressure coefficient	[-]
K_0^{NC}	Normal consolidated value of the earth pressure coefficient	[-]
m	Stress dependency factor	[-]
m_v	Modulus of volume compressibility	[m^2/kN]
M	Slope of the critical state line	[-]
N	Number of independent sample points	[-]
OCR	Vertical overconsolidation ratio	[-]
OCR*	Isotropic overconsolidation ratio	[-]
p'	Mean effective stress invariant (Roscoe $et\ al.$, 1958)	[kN/m^2]
p^{eq}	Isotropic equivalent effective stress	[kN/m^2]

p^{pc}	Isotropic preconsolidation stress	[kN/m²]
p^{ref}	Isotropic reference stress level	[kN/m²]
P	Probability of failure	[%]
POP	Pre-overburden pressure	[kN/m²]
q	Shear stress invariant (Roscoe *et al.*, 1958)	[kN/m²]
RR	Recompression ratio	[-]
s	Mean stress invariant (Lambe, 1967)	[kN/m²]
S_{el}	Elastic settlement	[m]
S_{tot}	Total settlement	[m]
S_t	Soil sensitivity	[-]
t	Shear stress invariant (Lambe, 1967)	[kN/m²]
t_e	Equivalent time	[s]
t_0	Reference time	[s]
T_v	Time factor	[-]
u	Pore pressure	[kN/m²]
Δu	Excess pore pressure	[kN/m²]
x_0	Initial amount of bonding (S-Clay1S model)	[-]
w	Water content	[%]
α	Inclination of the yield surface	[-]
α_0	Initial inclination of the yield surface	[-]
α_p	Primary strain	[-]
α_s	Secondary strain	[-]
β	Reliability index	[-]
β	Rotational hardening parameter (S-Clay1 model)	[-]
γ_b	Bulk volumetric weight	[kN/m³]
γ_{dry}	Dry volumetric weight	[kN/m³]
$\gamma_{in\text{-}situ}$	In-situ volumetric weight	[kN/m³]
γ_{sat}	Saturated volumetric weight	[kN/m³]
γ_{xy}	Shear strain on x-plane in y-direction	[-]
δ	Scale of fluctuation	[m]
ε	Difference between prediction and observation	[m]
ε	Strain	[-]
$\dot{\varepsilon}$	Strain rate	[s⁻¹]
ε_c	Creep strain	[-]
ε^C	Cauchy strain (linear strain)	[-]
ε_d	Direct strain	[-]
ε^e	Elastic strains	[-]
ε^H	Hencky strain (natural strain)	[-]
ε^p	Plastic strains	[-]
ε_P	Volumetric strain	[-]
ε_q	Deviatoric strain	[-]
ε_s	Secular strain	[-]
ε_v	Volumetric strain	[-]
κ	Recompression index	[-]
κ^*	Modified recompression index	[-]
λ	Plastic multiplier	[-]
λ	Compression index	[-]

λ^*	Modified compression index	[-]
μ	Rotational hardening parameter (S-Clay1 model)	[-]
μ	Viscoplastic multiplier (Perzyna, 1963)	[-]
μ^*	Modified creep index	[-]
ν	Specific volume	[-]
ν	Poisson's ratio	[-]
ν_{ur}	Poisson's ratio during unloading / reloading	[-]
ξ	Correlation factor (Tavenas *et al.*, 1979)	[-]
ρ_b	Bulk density	[kN/m^3]
σ'	Effective stress	[kN/m^2]
$\dot{\sigma}'$	Effective stress rate	[kN/m^{2}s]
σ'_{pc}	Effective preconsolidation stress	[kN/m^2]
σ_{point}	Point value of the standard deviation	[m]
σ_{net}	Net value of the standard deviation	[m]
τ_{ref}	Reference intrinsic time	[s]
φ'	Effective friction angle	[°]
φ'_{cv}	Effective friction angle at critical state	[°]
χ	Rotational hardening parameter (S-Clay1 model)	[-]
ψ	Dilatancy angle	[°]
ω	Rotational hardening parameter (AC model)	[-]
ω_d	Rotational hardening parameter (AC model)	[-]
Γ^2	Variance reduction factor	[-]
$\Phi(F)$	Overstress function (Perzyna, 1963)	[-]
AC	Anisotropic creep	[-]
AMSL	Above mean sea level	[m]
CSL	Critical state line	[-]
CRS	Constant rate of strain	[-]
CSS	Current stress surface	[-]
CSSM	Critical state soil mechanics	[-]
EoP	End of primary	[-]
ESP	Effective stress path	[-]
EVP	Elasto-viscoplastic	[-]
FE	Finite element	[-]
HCV	Highest conceivable value	[-]
HD$_{MLV}$	Most likely value of the horizontal deformation	[m]
HD$_{x\%}$	Horizontal deformation that relates to a probability of exceedance	[m]
IM	Inclinometer	[-]
LAT	Lowest astronomical tide	[m]
LCV	Lowest conceivable value	[-]
LEPP-MC	Linear elastic perfectly plastic with a MC failure criterion	[-]
MC	Mohr Coulomb	[-]
MCC	Modified cam clay	[-]
Nap	Dutch reference level	[m]
NCS	Normal consolidation surface	[-]
SL	Surface level	[m]
SSC	Soft soil creep	[-]
TSP	Total stress path	[-]

Definitions of Key Terms

The following list contains a short explanation of the key terms used in this report. Notice that the definitions are presented in an alphabetic order.

Amorphous peat	Organic soil where the natural material is highly decomposed
Analytical model	A mathematical model that has a closed form solution
Anisotropic behaviour	The properties (strength, stiffness, permeability) are dependent on its orientation
Axisymmetric condition	A condition where two stresses are symmetrical to each other
Consolidation	Time-dependent deformation of soils resulting from the expulsion of water from the soil pores
Constitutive behaviour	Describes how a material responds to external loading
Creep (or secular strain)	Strain that develops with time under constant effective stress
Critical state	Stress state of continuous shearing at constant shear stress and constant volume
Critical state line (CSL)	Represent the failure state of soils in the critical state soil mechanics
Cross anisotropy	Soil properties and the soil response in the lateral directions are the same but are different from those in the vertical direction
Destructuration	Degradation of the bonds in the microstructure of a soil during plastic straining
Deterministic calculation	A calculation that requires precisely defined input values, while the actual values may be uncertain
Deviatoric loading	Loading that generates a shear stress in a soil mass
Deviatoric strain	Type of strain that occurs during shear loading
Dilantancy	Change of volume when it is distorted by shearing

Direct strain (or initial strain)	Elastic strain that immediately occurs after loading due to a change in effective stress
Drainage path	Longest path for a water particle to reach the drainage boundaries
Effective stress	Stress which is carried by the soil particles
Elastic materials	Materials that return to their original configuration after unloading
Empirical model	A model that is based on empirical observations rather than on mathematically describable relations
Excess pore water pressure	Pore water pressure in excess of the hydrostatic pore water pressure
Fibrous peat	Organic soil that mainly consists of partially decomposed fibrous material
Fitting	Comparison between the in-situ measurement and the predicted value
Groundwater	Water under gravity that fills the soil pores
Horizontal deformation	Deformation in lateral direction
Hydrodynamic period	The time to dissipate the excess pore pressures caused by an stress increment
Inclinometer	A tool that monitors the horizontal deformation
In-situ behaviour	Behaviour as observed in the field
Intrinsic time	Time required to load a soil to its current stress condition
Invariant	A parameter which is independent of the chosen axis system
Isotaches	Lines of equal strain rate
Isotropic behaviour	The properties (strength, stiffness, permeability) are independent on its orientation
Linear strain (Cauchy strain)	Ratio of change in dimension relative to their initial height

Natural strain (Hencky strain)	Ratio of change in dimension relative to their present height
Normally consolidated soil	A soil that has never experienced effective stresses greater than its current effective stress level
Numerical model	A mathematical model that uses a numerical stepping procedure to describe the highly non-linear behaviour of complex materials (for example those of soils)
Oedometer test	A laboratory test that is used to determine the stiffness parameters of a soil sample
Overconsolidated soil	A soil that has experienced effective stresses greater than its current effective stress level
Overconsolidation ratio (OCR)	Ratio between the actual stress and the preconsolidation stress
Piezometer	A tool that monitors the excess pore pressures
Plane strain condition	A condition where the strain in one or more directions is zero or small enough to be neglected
Plastic materials	Materials that do not return to their original configuration after unloading
Preconsolidation stress	Maximum effective stress that a soil was subjected to in the past
Pre-overburden pressure (POP)	Expresses the difference between actual stress and the preconsolidation stress
Probabilistic calculation	A type of calculation that explicitly accounts for uncertainties
Probability density function	A function of a continuous random variable that describes the relative likelihood to occur at a given point in the observation space
Probability of failure	The probability that a value will exceed the limit state
Reliability index	A relative measure of the current condition, which provides a qualitative estimate of the expected performance

Representative parameter	An average parameter value without the inclusion of (a) partial material factor(s)
Settlement	Deformation in the vertical direction
Settlement beacon	A tool that monitors the vertical deformation
Soil fabric	Structural arrangement of the soil particles
Spatial variability	A material property that exhibits different values at distinctive locations
Stress path	Graphical representation of the stress development of a soil particle in the underground
Taylor series technique	An technique that uses a series expansion to estimate the value of particular function
Three sigma rule	A method to define the standard deviation in cases where the amount of available data is sparse
Total stress	Stress which is carried by the soil particles, the liquids and gases in the voids
Triaxial test	A laboratory test that is used to determine the strength parameters of a soil sample
Variation coefficient	Normalized measure that indicates the dispersion of a probability distribution
Viscous materials	Materials that behave like a (thick) fluid during loading
Wick drain	A prefabricated drainage strip that consists of a plastic core and is surrounded by a geotextile jacket
Yield surface	Surface that separates stress states that produce elastic responses from stress states that produce plastic responses

1.   Introduction and Problem Description

This thesis is about the modelling of horizontal soil deformations. A general introduction to the subject is given in section 1.1. The general introduction will be used to describe the phenomena and the troubles caused by excessive lateral deformations. Section 1.2 explains the relevance of this research, and indicates why the current prediction of lateral deformations is fairly poor. On the basis of the previous sections a problem description, main objective and several research questions can be formulated in section 1.3. To demarcate the scope section 1.4 puts a number of constraints to confine the size of this research. Finally, a guideline is given for the structure of the report, and the research approach will be elaborated in more detail.

1.1.   General introduction

Embankments are among the most ancient forms of civil engineering construction, but are also among the most relevant today. Embankments are required in the construction of roads, dikes, airport runways and railway works. Historically, the placing of these structures has preferred sites of good geotechnical quality, in order to reduce the technical problems and thus the cost associated with their construction (Leroueil *et al.*, 1990). However, during the last decades socio-economic and political considerations have forced the use of sites of lower quality, referring to instable and highly compressible subsoils. In spite of the copious experience with this type of construction, the construction of embankments on compressible soils still poses many delicate problems. Most of these problems are related to stability and deformation. This research concentrates on the latter and especially on the horizontal component of deformation as shown in figure 1. Notice that horizontal deformations are just like the vertical deformations composed of three components, which are: initial deformation, deformation due to consolidation and deformation due to creep. Remark that the deformations due to creep is also called secular deformation (Buisman, 1940). Furthermore, it is important to state the components are not consecutive processes, because creep deformations take place during all stages of construction.
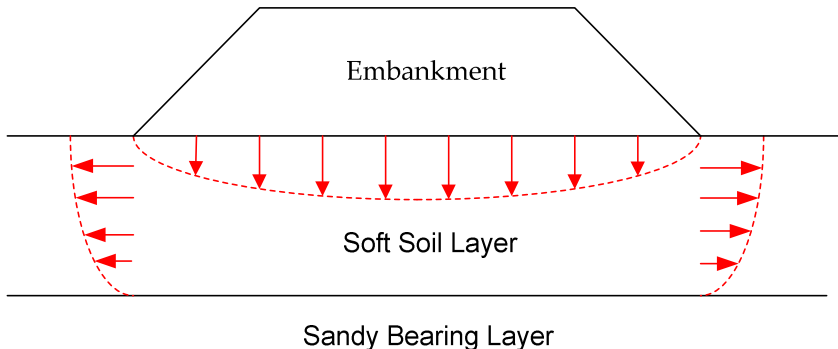
Figure 1 – Schematic deformation behaviour of an embankment on soft soil

The initial deformation is the elastic response as a result of a change of effective stress in the soil, and is mostly small compared to the time-dependent consolidation and creep deformations. According to Folkes and Crooks (1985) the amount of horizontal soil

deformations is dependent on a number of factors; which are the ratio between horizontal and vertical stresses, compressibility, density and stress history of the soil. This thesis focuses on the deformation behaviour of normal consolidated clays and peaty soil deposits. It is well known that these soils have a large compressibility, relatively low density and limited stress history. For this reason, the expected horizontal deformations are expected to be larger than for overconsolidated clays or granular materials. Notice that the lateral deformations in granular materials can still be significant if the density of the material is sufficiently low. However, the deformation behaviour of granular materials is not considered here.

Large horizontal deformations could have an adverse effect on piles, cables and ducts, which are located in the vicinity of the embankment construction. These horizontal displacements cause additional forces and moments on for instance a pile foundation, which could subsequently result in damage to the foundation and structure above (Jeong *et al.*, 2004). For this reason, the magnitude of the horizontal deformations should be restricted, especially in the neighbourhood of deformation sensitive structures. Notice that the number of documented cases in practice where horizontal deformations have resulted in problems are limited. In spite of that a couple of cases are found where horizontal soil deformations have created problems. Some of them are discussed in the remainder of this section.

A case study where horizontal deformations assumed to be the main problem was reported by Stermac *et al.* (1968). He and his fellows noticed unusual lateral deformations near several bridge abutments in Quebec Canada. Through these lateral movements the rocker bearings were not able to properly transfer the loading of the bridge to the pile foundation anymore. This caused multiple severe cracks in the asphalt layer of the bridge.

An exceptional case has been discussed by Fellenius and Johansson (1972) where piles of a building have buckled due to excessive lateral soil movements (see figure 2). The accident happened in Huddinge near Stockholm where a surcharge loading caused large horizontal movements in the soft clay, which has an undrained shear strength of about 8.5 kPa. It is important to state that the buckling of the piles did not occur instantaneously, but several years after the placement of the surcharge loading. It is therefore likely that consolidation and creep deformations have resulted in the failing of the piled structure.
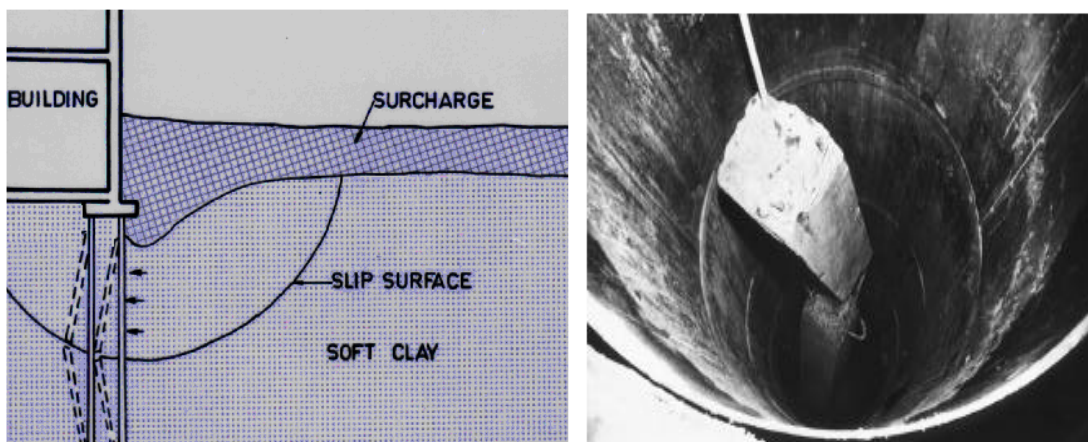
Figure 2 – Problem illustration and example of a ruptured pile (Fellenius and Johansson, 1972)

Another example of the excessive horizontal deformation was observed near a railway track in Rotterdam during the 1970s. Figure 3 shows that the construction of an embankment near the railway has caused a substantial bend in the original straight railway track. This indicates that the occurred horizontal deformation is likely to be related to failure. According to Marche and Chapuis (1973) it is possible to link the amount of horizontal deformations to the factor of safety used in stability analyses.
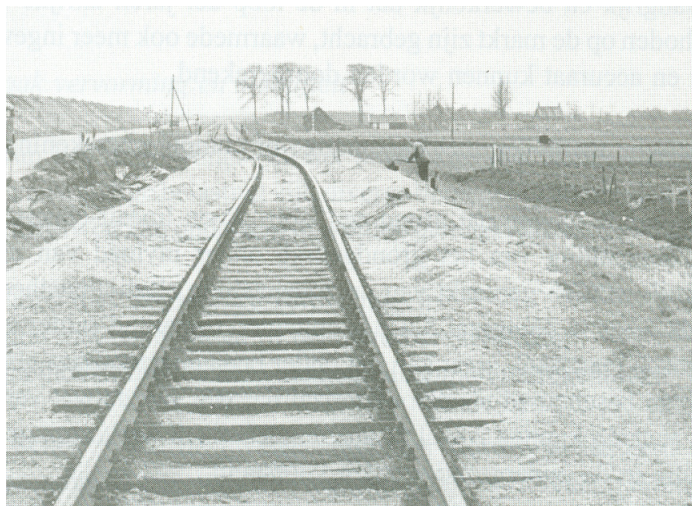
Figure 3 – Excessive horizontal deformation of a railway near Rotterdam (Termaten et al., 1992)

More recently, in 2006 the concrete track of the HSL railway near The Hague, which was founded on pile foundation, has experienced a horizontal deformation of 30 mm (Maas and Wuite, 2006). For normal railway tracks this magnitude of horizontal deformation is not a serious problem, but for high speed railway tracks more stricter margins are prevalent. The lateral movements were caused by the peaty soil deposit under an embankment, which was located adjacent to the concrete track. Subsequently, these movements increased the forces and moments in the pile foundation. To prevent any additional horizontal deformation a sheet pile wall of 800 m had been installed, otherwise the horizontal deformations could increase further to an unacceptable value of 80 mm. The sheet pile wall and the repair measurements have resulted in a loss of about 10 million Euros.

In the last two decades several initiatives have been made to improve the performance of an embankment constructed on a soft soil deposit (among others: Ladd *et al.*, 1994; Gaberc, 1999; Sánchez-Alciturri *et al.*, 1999; Rowe *et al.*, 2001; Long and O'Riordan, 2001; Larsson and Mattsson, 2003). These embankments were built to gain a better insight into the behaviour of soft soils during embankment loading. Some of them are discussed in more detail in paragraph 2.1. During the construction of these embankments the settlements, pore pressures and horizontal deformations have been monitored. The general tendency is that settlements can be estimated with a reasonable accuracy; while the prediction of the excess pore pressures and horizontal deformation is mostly very poor. So it is fair to say that the design and construction of embankments on soft soils is still a challenge.

1.2.   Relevance of this research

The previous case descriptions show that the development of horizontal soil deformation is still not sufficiently understood. A recent literature study by Mestat (2001) underlines this statement. He analyzed 44 cases dating back from 1972 till 2001 where predicted and measured deformations are compared with each other. The results were worrying, because the relative error at the end of construction was on average 50% with maxima rising up to 250%. Therefore it seems that the conventional models are not yet able to satisfactorily describe horizontal soil displacements. It is doubtful that these differences between predicted and measured values in the field can be attributed entirely to one factor. According to Poulos (1972) the main reasons for the discrepancy between predicted and measured are as follows. Note that the inclusion of the Poisson's ratio is eye-catching. In contrast to the other factors the Poisson's ratio is a model parameter while the others are related to soil characteristics.

- The difficulty of estimating the Poisson's ratio
- Anisotropy of the soil
- Non linear stress-strain behaviour of the soil
- Non homogeneity of the soil
- Incorrect assumptions, i.e. the stiffness determination of the embankment

The main question remains why these models fail to incorporate ground behaviour correctly. In the last decades several instrumented embankments have been constructed on soft soils to improve the understanding of the field behaviour (Ladd *et al.*, 1994; Rowe *et al.*, 2001; Feddema *et al.*, 2009). However, it still appears to be difficult to include all relevant aspects of soft soil behaviour into the model simulations. Most of the currently available models do not acknowledge several of the factors mentioned above. For example, the analytical models of Van IJsseldijk and Loof assume linear elastic behaviour of the soft subsoil. Next to that it supposes that the soft soil layer is completely homogeneous and that the reaction to the foundation load is fully undrained (υ=0.5). Even the prevailing constitutive models in Plaxis, like Modified Cam Clay and Hardening Soil, use a simple isotropic framework for the prediction of horizontal soil deformations. Therefore, it seems to be attractive to use empirical models. For instance, the one formulated by Bourgens and Mieussens (1979), because it indirectly contains the highly non-linear stress-strain behaviour and the anisotropic character of the natural soils. A main disadvantage of the empirical models remains that a limited insight is gained into the physical processes related to the determination of these deformations.

However, during the last decade significant progress has been made in the development of numerical models. Some of these developments relevant for the prediction of horizontal soil deformations are discussed in this section. For example, the development of the viscoplastic Soft Soil Creep model (Vermeer and Neher, 2000). The main difference with the conventional elastoplastic models is that irreversible strains are not described as plastic strains but as viscoplastic strains. Through this adjustment irreversible strains could only emerge when a physical time increment applied. This has the benefit that strains under constant effective stress could be included.

Despite the inclusion of creep strains in the Soft Soil Creep model, the prediction of the horizontal displacements is still not very satisfying (Neher *et al.*, 2001). To improve the result Wheeler (2003) suggested to use an anisotropic elastoplastic model called S-Clay1, which is an extension of the critical state models (Schofield and Wroth, 1968). This model includes a rotational hardening law to account for the influence of plastic anisotropy. The initial tests have been performed on various soft Finnish clays. The results of the triaxial tests were compared with the Cam Clay model and the S-Clay1 model (Karstunen and Koskinen, 2008). The preliminary results indicated that the yield stresses and plastic strains are significantly better predicted by the anisotropic S-Clay1 model than by Modified Cam Clay model. The inclusion of anisotropic soil behaviour is also plausible in-situ, because of the platy shape of the soil particles, deposition process and consolidation history of most soft soils. Recently, an additional enhancement has been proposed by Leonie *et al.* (2008). This model could simulate anisotropy as well as creep behaviour under an embankment, which makes it more suitable for the prediction of horizontal soil deformations in the long-term.

The S-Clay1 model and the Anisotropic Creep model are user-defined models in the finite element program Plaxis, this means that they are not commercially available yet. For this reason, an additional validation of these anisotropic models will be desirable. In this thesis the anisotropic and isotropic models will be compared with in-situ measurements of two real field cases. However, before a definite judgement can be made about the additional value of these anisotropic models, a first order Taylor series approach is used to gain insight into the sensitivity of the various parameters used in the calculation (Duncan, 2000). If this sensitivity analysis is omitted, it will be troublesome to judge which model is the most suitable for predicting horizontal soil displacements.

1.3. Problem definition, main objective and research questions

In the previous sections the importance of an improved prediction of the horizontal soil deformations has been emphasised. In the current engineering practice it is not unusual to predict horizontal deformations with a method which neither accounts for creep and anisotropy. In the last years several researchers (Whittle, 1993; Koskinen *et al.*, 2002; Karstunen *et al.*, 2006) have shown that neglecting creep and anisotropy in soft soils could result in a mediocre prediction of the vertical and horizontal deformations.

The problem definition of the research has been formulated below. Note that the problem definition is stated quite generally in order to indicate the involvement of numerous aspects in the modelling of horizontal soil deformation.

The conventional models for the assessment of horizontal soil deformations fail to incorporate essential soil features, and underexpose the uncertainties involved in the parameter estimation.

As a result, the main objective is formulated as follows:

To improve the insights into the constitutive behaviour of soils related to the determination of the horizontal soil deformations. This should ultimately improve the quality of the model predictions.

To reach this main objective a number of research questions should be answered. These are summed up below:

- What is the influence of a stress path on the amount of horizontal soil deformation?
- How is creep simulated in the constitutive models of Plaxis?
- Under which circumstances are the empirical and analytical models still useful?
- What is quality of the predictions obtained with the constitutive models in Plaxis?
- Which degree of uncertainty can be expected in the horizontal soil deformation prediction?
- Which soil features could be included to improve the present state of the art models even further?

1.4. Scope of the research

The scope of the research on horizontal soil deformation is bound by a number of constraints:

- Horizontal deformations are mainly analyzed for soft soil deposits, therefore the focus is on normal and lightly overconsolidated clays and peaty soils with OCR values smaller than 2.
- Analysis is restricted to embankment related problems, excavations are not included in this thesis
- Loading conditions are considered static, while dynamic or cyclic loading conditions are not part of the analysis
- Interaction of the soil with structures is not envisaged
- Temperature effects on the strength and stiffness of soils are not analysed
- Bonding and destructuration of soils are not included
- The calculations are performed for 2D plane strain situations (this assumption is usually valid for embankments, because the strain in one of the main directions is nearly zero)

In short, the focus of this thesis is on the determination of horizontal soil deformations in soft soils caused by static loading conditions. As already mentioned the uncertainties around the predictions could be substantial, errors of about 50% and more are not uncommon in the geotechnical practice (Mestat, 2001). The research therefore deliberately concentrates on horizontal displacements and not on the interaction processes, because a poor prediction of the lateral deformations will also result in an incorrect assessment of the forces and moments on for example a pile foundation.

Remark that this list of constraints does not imply that dynamic loading situations, temperature effects, bonding and destructuration of soft soils are not worth investigating. It is still important to investigate the effects of these phenomena on the horizontal deformation behaviour of soft soils. However, due to the restricted time span of this thesis, these aspects should be considered in additional research work.

1.5.   Research approach and structure of the report

The approach for this research is based on sequencing steps (see figure 4). The structure of the report is analogous to these steps. The steps taken in this research are:

- Making a literature study on soft soil behaviour   (chapter 2)
- Analyzing the state of the art models   (chapter 3)
- Elaboration of the two case studies   (chapter 4)
- Drawing conclusions and recommendations   (chapter 5)

Chapter 2	*Chapter 3*	*Chapter 4*	*Chapter 5*
Literature on soft soil behaviour	State of the art models	Case studies	Conclusions & Recommendations
Topics: - Field behaviour - Stress paths - Consolidation - Creep - Anisotropy	Types: - Empirical models - Analytical models - Numerical models	Cases: - Abcoude, the Netherlands - Brass, Nigeria	Highlights: - Main results - Uncertainties - Topics for further research

Figure 4 – Structure of the thesis report

The emphasis of this thesis is on analyzing the state of the art models and on the comparison with the field measurements of the considered case studies. The literature study is nonetheless important to gain a proper insight into the physical processes related to the determination of horizontal soil deformations.

Chapter 2 outlines the basic knowledge that is required for the analysis of horizontal soil displacements. The chapter starts with a description of field behaviour of soft soils subjected to an embankment loading. To describe this field behaviour, four test embankments with different soft soil characteristics will be discussed. This is needed to obtain sufficient insight in the deformation behaviour of soft soils at various locations under the embankment. The next paragraph deals with stress paths, because a well-considered examination can only be made when a good understanding of the prevalent stress paths is obtained. Subsequently, the distinctive theories of consolidation and creep are discussed. These theories are required for the determination of the time-dependent deformations. Chapter 2 closes with a discussion about anisotropic soil behaviour in natural soft soils.

An analysis of the state of the art models is carried out in chapter 3. It starts with a presentation of the empirical model proposed by Bourgens and Mieussens (1979). Furthermore, the analytical models of Van IJsseldijk and Loof are explained, which are based on the theory of elasticity (De Leeuw, 1963). The numerical models are investigated with the FE program Plaxis 2D version 9 (Brinkgreve and Broere, 2008). A 2D schematisation is possible, because only plain strain conditions are considered. The constitutive models which are considered are: Linear Elastic Perfectly Plastic with a Mohr Coulomb failure criterion (Smith and Griffiths, 1982), Modified Cam Clay (Roscoe and Burland, 1968), Soft Soil Creep

(Vermeer and Neher, 1999), S-Clay1 (Wheeler *et al.*, 2003) and Anisotropic Creep (Leonie *et al.*, 2008). The last two material models are user-defined models. The Linear Elastic Perfectly Plastic with a Mohr Coulomb failure criterion is considered as a reference model, which is frequently used as first order model in geotechnical applications. The choice for the Modified Cam Clay and Soft Soil Creep is explainable, because S-Clay1 and Anisotropic Creep model are derived from these models.

In chapter 4 two case studies have been worked out. The first case deals with the construction of an embankment near the existing A2 highway in Abcoude the Netherlands. The subsoil at this location consists of a thick peaty soil deposit underlain by firm Pleistocene sand layer. Horizontal soil deformations caused by this new embankment affect the information gantries founded on piles, which are located among both embankments. The pile foundation will endure an additional forces and moments due to horizontal soil deformations. Therefore various inclinometers are installed to monitor the magnitude of the horizontal soil deformation (see Appendix 3). The second case treats the embankment construction for a LNG export facility in Brass Nigeria. The subsoil at this location consists of soft clay layers interrupted by various thin sand layers. During the embankment construction five inclinometers are frequently monitored to get an impression of the development of the horizontal displacements with time. For both case studies the field measurements are compared with the simulation results of the considered models.

This thesis ends with the conclusions and recommendations. This chapter tries to give an answer to the various research questions and discusses to what extent the main objective is reached (conclusions). It also discusses what is still missing and what topics need additional research (recommendations). The current chapter and final chapter 5 can be considered as a summary of this thesis.

2.   Literature on Soft Soil Behaviour

This chapter reviews the literature on soft soil behaviour. As already mentioned in the previous chapter, the thesis concentrates on normal or lightly consolidated clays and peaty soil deposits. For a meaningful study on horizontal soil deformation it is necessary to gain sufficient knowledge about the physical processes related to these types of soils. The first topic deals with an evaluation of a number of test embankments on various soft types of soils. During and after the construction of these test embankments, the deformations and pore pressure were frequently monitored to obtain an idea about the constitutive behaviour of soft soils. The next section elaborates on an analysis of stress paths. A sufficient understanding of stress paths is required to make a well-considered choice about the state of the art models analyzed in chapter 3. In section 2.3 the theories on consolidation and creep will be discussed. This is necessary because time-dependent behaviour plays a major role in the determination of horizontal soil deformations. In the last section of this chapter a discussion can be found on the anisotropic behaviour of natural soils. Notice that anisotropic behaviour of soils is mostly ignored in the current modelling practice; the geotechnical engineers usually use isotropic models as Modified Cam Clay or Soft Soil Creep to simulate horizontal displacements. Finally, it is important to realize that real soil behaviour is much more complex than the discussed theories. The intention here is to include the most significant processes, so that real soil behaviour is approached as close as possible.

2.1.   Evaluation of field behaviour

In this paragraph a critical evaluation is given about the field behaviour of soft soils subjected to an embankment loading. Such an evaluation is very helpful for the interpretation of the results obtained in the case studies of Abcoude and Brass. For the evaluation of field behaviour, four test embankments will be discussed that have been frequently monitored with respect to the settlements, horizontal deformations and pore pressures. Notice that the selected test embankments are constructed on different soft soils, which is done deliberately to examine the effect of different types of soft soil on the development of pore pressures and deformations.

The first field case is the 11.0 m high embankment for the interstate highway 95, which is constructed during the sixties and is located in Saugus Massachusetts (Ladd *et al.*, 1994). Piezometers, settlements rods and inclinometers were used during construction and after construction for an additional period of 4 years to monitor the in-situ performance of the embankment. The subsoil at this location consists of 40 m thick layer of Boston blue clay. The compressibility of this clay is not extremely high, because CR values of about 0.3 were observed. However, the vertical and horizontal permeability of the clay is quite low, in the order of 10^{-8} cm/s, which indicates that Boston blue clay is a fairly homogeneous clay.

The next case is the Bricor test embankment that has been constructed near the existing A16 highway during the late 1980s (Feddema *et al.*, 2009). The embankment is constructed in multiple stages, and has a final height of almost 6.0 m. The subsoil consists of various clay and peaty soil layers, which have a total thickness of approximately 15.0 m. The monitoring

of this case is limited to the construction phase. There are barely measurements available after construction of the embankment. For this reason, no judgement can be made about the long-term deformation behaviour of this embankment.

The third case is a test embankment that is constructed on a soft compressible organic clayey silt in Sackville New Brunswick (Brisbois, 1999; Rowe *et al.*, 2001). This test embankment was part of the testing program of the highway between Moncton in New Brunswick and Amherst in Nova Scotia, which was constructed during the early 1990s. The test embankment was constructed prior to the roadway construction to gain better insight into the behaviour of organic clayey silt. In contrast to the cases in Saugus and Bricor this test embankment has been constructed to failure within 25 days, while the other cases monitored the deformation behaviour over a much longer period. It is therefore expected that the stress path is different from the other embankments that are constructed close to the K_0-condition.

The last case that is considered is a test embankment that is constructed in Athlone for the highway between Dublin and Galway in Ireland (Long and O'Riordan, 2001). This test embankment has been constructed in multiple stages during 1986 till 1988. The principal objectives of this test embankment were to assess the compressibility and consolidation properties of the soft clay layers, which extend over a depth of at least 8.0 m. Vertical and horizontal deformation were monitored long after the construction of the embankment. Note that the last measurements were taken in 1997, which is about 9 years after construction.

The remainder of this paragraph discusses the results of the considered test embankments in more detail.

2.1.1. *Saugus test embankment constructed on Boston Blue Clay*

For the extension of the Interstate Highway I-95, which is located about 20 km north of Boston Massachusetts, it was decided to construct a 11.0 m high test embankment to gain more insight into the behaviour of the thick layer of Boston blue clay (Ladd *et al.*, 1994). The construction of this test embankment started in the late 1960s and lasted for 1.5 years. To monitor the performance several piezometers, settlement rods and inclinometers were installed under and adjacent to the embankment. The monitoring started after the first construction stage and stopped 4 years after the end of construction. As a result, the total monitoring period compromised approximately 4.7 years. The in-situ measurements were compared with the model simulations of the finite element program Abaqus, which simulated the Boston Blue Clay with the Modified Cam Clay and MIT-E3 material model. The MIT-E3 model has some similarities with the S-Clay1 model, because it also able to simulate anisotropic behaviour with a rotational hardening rule. More information of this model can be found in Whittle (1993). However, before presenting the outcome of the measurements and the results of the model simulations, the subsection starts with brief description of the ground conditions and the manner the embankment is constructed.

Description of ground conditions
The subsurface conditions at the test section were determined from borings and a number of field instruments. From these measurements, it appeared that the underground at the test

location in Saugus Massachusetts, mainly consisted of Boston Blue Clay. The total soil profile is shown in table 1. The mean water table is located at 0.8 m above mean sea level.

Table 1 – Soil profile at Saugus test location

Soil Type [-]	Top of Layer [m +AMSL] [1]	Bottom of Layer [m +AMSL]	Thickness [m]
Peat	1.5	0.0	1.5
Marine Sand	0.0	-3.0	3.0
Boston Blue Clay	-3.0	-44.0	41.0
Glacial Till	-44.0	-50.0	6.0
Shale	-50.0	OD [2]	-

[1] AMSL is above mean sea level

[2] OD is observed depth

However, for the assessment of pore pressures and deformations only the Boston Blue Clay layer is of interest, because the compressible peat layer is removed during construction. The stress history of Boston blue clay layer is presented in figure 5. The findings indicate that the preconsolidation stress varies significantly over the depth of the layer. For this reason, it was chosen to divide the clay layer in 12 sublayers. Each sublayer has of course different OCR, but also distinctive compressibility and permeability values have been assigned. Furthermore, figure 5 shows that the first 5.0 meters of the clay layer are highly overconsolidated. The preconsolidation stress is not exceeded even after incorporation of the full embankment load. Nevertheless, observe that there is a significant scatter in the oedometer measurements. To include this uncertainty, two distinctive stress path profiles have been posed.
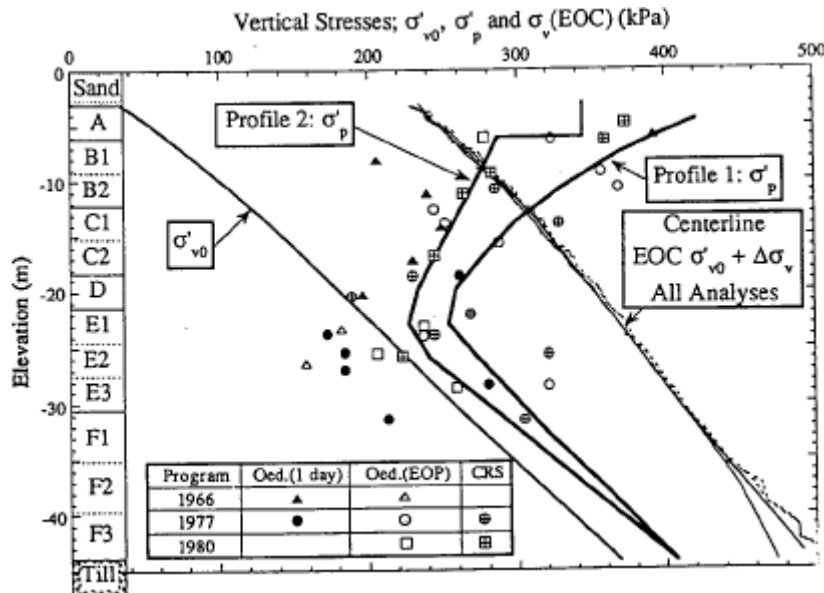
Figure 5 – Stress history of the Boston Blue Clay (Ladd et al., 1994)

For the determination of the consolidation and permeability parameters of the various sublayers, an extensive laboratory program has been performed; which contains incremental oedometer tests, constant rate of strain oedometer tests, and oedometer tests on both vertical and horizontal specimens. Tests in the upper crust usually produced a CR values about 0.1 to

0.3 and permeabilities in the order of 10^{-8} m/s. While tests in the lower part of the clay layer (i.e. below -20 m AMSL) often had much larger compressibility, CR values of 0.4 to 0.5 were found. Also the permeability of the lower Boston blue clay can be a factor 10 lower.

Construction of the embankment
The test embankment was constructed in three stages. In stage 1 the peat layer is replaced by sand. The filling process continued till 2.75 m above mean sea level, and was performed during construction day 92 till 123. After the application of the first stage the piezometers, settlement rods and inclinometers were installed. During construction stage 2, which started 6 months after the first stage, the embankment was heightened to 11.0 m above mean sea level. The total construction time of the second construction stage was about 5.3 months. The final stage 3 to a height of 12.2 m above mean sea level was applied in 22 days after a waiting time of 4,5 months.

Results and discussion
Ladd *et al.* (1994) presents a detailed comparison of the in-situ measurements of the pore pressure, settlement and horizontal deformation with the model simulations. As already indicated, the dominating layer with respect to pore pressures and deformations is the Boston Blue Clay layer. This clay layer is simulated with Modified Cam Clay model and MIT-E3 model. Notice that these elastoplastic models do not include creep. The other soils, such as the fill material and the marine sand, use a much simpler elastoplastic model.

The piezometer measurements show very small excess pore pressure in the Boston Blue Clay close to the upper and lower drainage boundaries. However, piezometers near the centre of the layer typically show less than 20% of excess pore pressures dissipation 4 years after construction of the test embankment. Another observation is that the pore pressures remain quite low in the upper crust of the Boston Blue Clay. The reason why these pore pressures remain so low is probably due to the overconsolidated state of the clay in this region (Raymond, 1972). Furthermore, the observations show that the excess pore pressures are fairly well predicted with the considered models.

One consistent observation for the settlements is that the model predictions underestimate the in-situ settlements in the upper part of the Boston blue layer after the end of construction. There is much better agreement between predictions and measurements at the middle and bottom of the clay layer. An explanation for the poor prediction in the upper Boston Blue Clay layers is possibly related to the uncertainty of the compressibility parameters, which is also shown in figure 5.

All inclinometers measure progressive outward horizontal displacements at all elevations in the Boston blue clay throughout the entire monitoring period. Figure 6 shows that the inclinometers at the toe of the embankment record the largest horizontal soil movements. For instance, figure 6 shows the predictions with the Modified Cam Clay model for two profiles with different stress histories. The observations shows that the model simulations with Modified Cam Clay model also show a slight lateral spreading during consolidation.
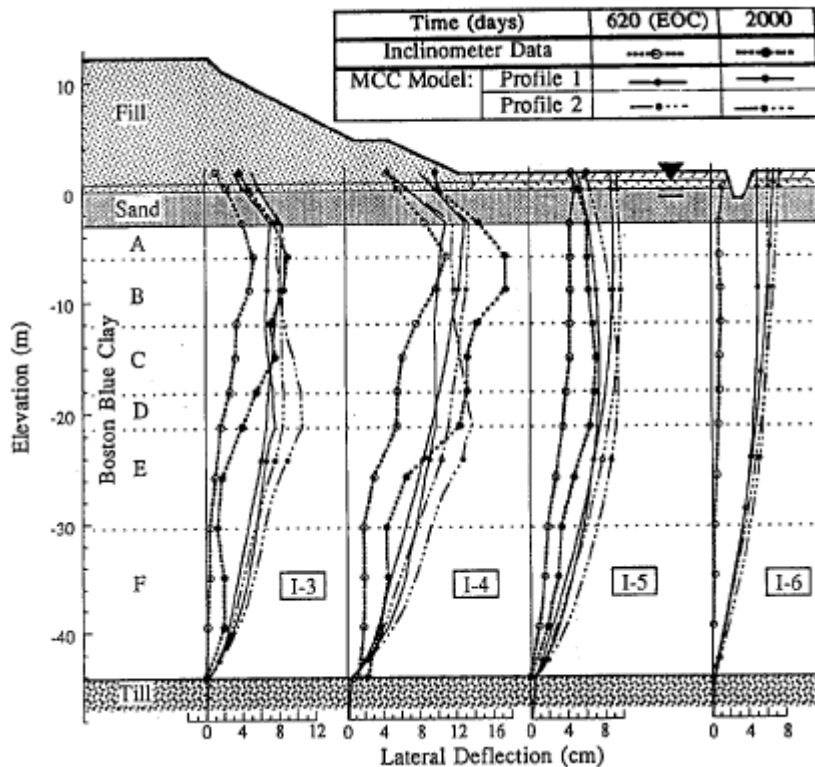
Figure 6 – Comparison of MCC predictions and measured lateral deflections (Ladd et al., 1994)

The MIT-E3 model, which accounts for anisotropic yielding, nicely predicts continued lateral spreading during consolidation that agrees reasonably well with the measured data. This may be an indication that creep effects are not the only major factor during consolidation of the Boston Blue Clay as previously suggested by Borja *et al.* (1990).

2.1.2. *Bricor test embankment constructed on a layered profile of peat and clay layers*

During the end of 1980s an investigation started with the goal to improve the accessibility of the Randstad near Rotterdam (Feddema *et al.*, 2009). Part of this investigation was the construction of a test embankment to study the properties of the clayey and organic soil layers more into detail. The test embankment with vertical drainage was constructed close to the Highway A16 near the Brienenoord Bridge. The total height of the embankment was almost 6.0 m, and the construction process was divided into 14 stages. Furthermore, the monitoring equipment was used to measure the pore pressures, settlements and horizontal deformations. According to Feddema *et al.* (2009) no comparison could be made between the measured pore pressure and the simulated pore pressures, because the exact distance between the piezometers and the drains were not known. It was also not possible to examine the long-term behaviour of the soft soils, because the monitoring program stopped 1.5 years after construction.

The in-situ measurements were compared with the results of the finite element program Plaxis, which used the viscoplastic Soft Soil Creep model to simulate time-dependent behaviour of clayey and peaty soil layers. Again, before presenting the in-situ measurements and the results of the model simulations, this subsection begins with brief description of the ground conditions and some notes about the way the embankment is constructed.

<u>Description of ground conditions</u>
For the description of the ground conditions use has been made of borings and cone penetration tests. These measurements have been used to determine the soil profile, which is presented in table 2. Notice that the water table at this location is slightly below surface level.

Table 2 – Soil profile at Bricor test location

Soil Type [-]	Top of Layer [m +Nap] [1]	Bottom of Layer [m +Nap]	Thickness [m]
Clay	-1.5 to -2.1	-2.2 to -3.4	0.1 to 1.9
Holland peat	-2.2 to -3.4	-4.0 to -5.2	0.6 to 3.0
Clay	-4.0 to -5.2	-5.9 to -6.2	0.7 to 2.2
Holland peat	-5.9 to -6.2	-6.6 to -6.9	0.4 to 1.0
Clay	-6.6 to -6.9	-13.0 to -14.0	6.1 to 7.4
Basis peat	-13.0 to -14.0	-15.6 to -17.0	1.6 to 4.0
Pleistocene sand	-15.6 to -17.0	OD [2]	-

[1] Nap is Dutch reference level related to the water level in the river IJ in Amsterdam
[2] OD is observed depth

Table 2 shows that the subsoil at the test location is very heterogeneous till a depth of -15.6 to -17.0 m Nap. The findings indicate that the subsoil has a layered profile of clay and peaty soil layers. Significant vertical and horizontal deformations are expected during and after the construction of the embankment. To examine the soil properties of each layer sufficiently, a large number of laboratory test have been performed, such as incremental oedometer tests and triaxial tests, have been performed.

The oedometer tests revealed that the OCR of the first peat and clay layer are highly overconsolidated, the OCRs are respectively 8.6 and 5.4. The remaining soft soil layers have an OCR varying from 1.5 to 2.5. In addition, the oedometer test results were also used to assess the compressibility. For the clay layers λ^* values varying between 0.09 till 0.15 are found. This parameter has to be used as input parameter in the Soft Soil Creep model. To find the corresponding CR value, the λ^* values have to be multiplied with the natural logarithm of 10. This results in CR values ranging between 0.2 and 0.3 for clayey soils. The organic soils have a higher compressibility, because the λ^* values are about 0.13 for Basis peat and 0.19 for Holland peat. This leads to CR values of respectively 0.3 and 0.45.

Furthermore, the critical state values of the strength parameters are deduced from triaxial tests. Relatively high friction angles are found for organic soils, angles of 40° and more are not unusual. The lightly overconsolidated clay layers have much lower critical state fiction angles; the angle varies between 25° and 30°. However, the highly overconsolidated clayey upper layer has a friction angle that is about similar to the organic soils.

<u>Construction of the embankment</u>
The Bricor test embankment was constructed in 14 stages. The total height of the embankment was almost 6.0 m, which means that the thickness of each construction stage was about 0.5 m. The first construction stage was executed in November 1988. After this stage vertical drainage was installed with a centre to centre distance of 1.75 m. Notice that the monitoring devices were already installed several months earlier. The last construction

stage was applied in April 1990. According to Feddema *et al.* (2009) the waiting period between the stages was on average 1.0 to 1.5 month. Furthermore, to guarantee the stability of the embankment, use has been made of lateral berms on both sides of the embankment.

Results and discussion

The results of the comparison between the in-situ measurements and the model simulations are presented in this subsection. The clay and organic soil layers use the Soft Soil Creep model to describe the soil behaviour. The other materials, such as the embankment fill and the Pleistocene sand are modelled with the Hardening Soil model. Moreover, it should be noted that the comparison between measured and simulated could only be made during the construction phase till 1.5 years after construction. It is thus not possible to evaluate the long-term deformation behaviour of these soft soils.

The settlement beacons indicate that the settlement at the end of construction has a value of 1.75 m under the centre of the embankment and 1.20 m under the lateral berms. The last settlement measurement dates back to November 1990, the settlement under the centre of the embankment was at that time 2.10 m and 1.25 m under the lateral berms. The model simulations fit closely with the in-situ measurements, except at the toe of the embankment. At this location the modelled settlements are significantly overestimated. These differences is attributed to the heterogeneity of the underground, because the thickness of the soft soil layers varies significantly at the test location (see table 2).

The inclinometer measurements have been performed at the toe of the embankment and the toe of the lateral berm. At the end of construction (April 1990) the maximum lateral deformations at these locations were respectively 0.55 m and 0.35 m. Figure 7 shows the comparison between the in-situ horizontal soil deformations and the simulated horizontal soil deformations at the toe of the embankment for a number of moments in time.
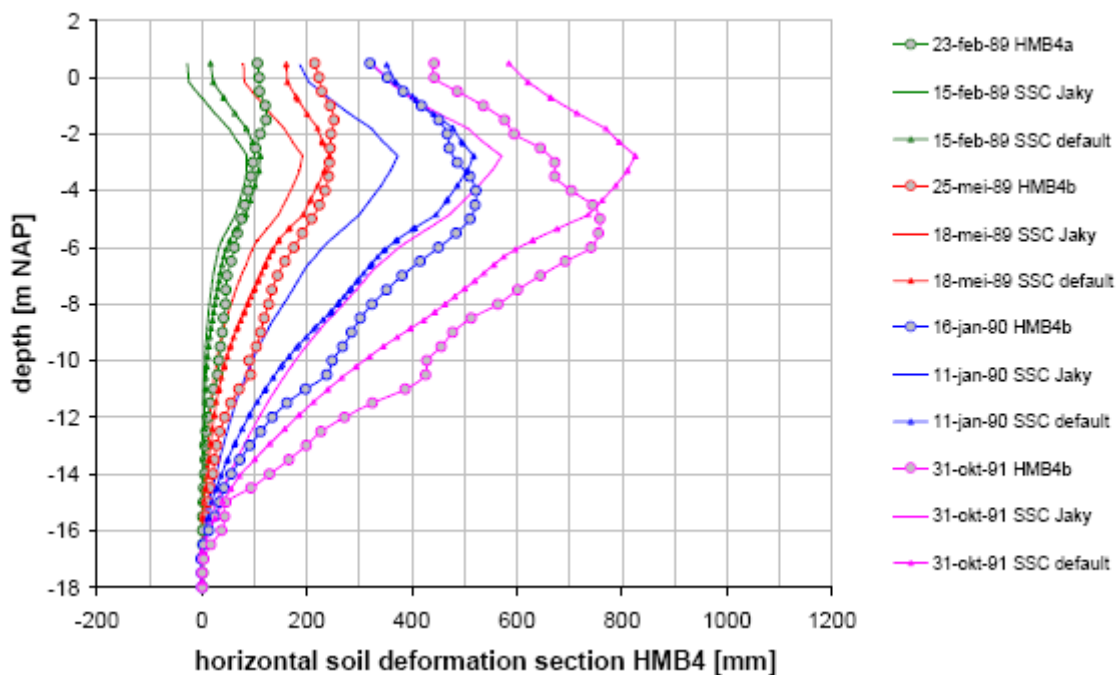
Figure 7 –Horizontal deformation profiles under the toe at Bricor (Feddema et al., 2009)

The graph presents the measurements of inclinometer HMB4 and the results of Soft Soil Creep (SSC) simulations. The subscripts Jaky and default indicate the way in which the normal consolidated value of the lateral earth pressure coefficient has been determined. According to Jaky the K_0^{NC} is only dependent on the friction angle as shown in formula 1.

$$K_0^{NC} \approx 1 - \sin \varphi' \tag{1}$$

In the default condition the K_0^{NC} value is analytically derived from an oedometer condition by Brinkgreve (1994). This is possible because the K_0^{NC} value and the slope of the critical state line M are interrelated. The relationship between these parameters is shown in formula 2.

$$M = 3 \cdot \sqrt{\frac{\left(1 - K_0^{NC}\right)^2}{\left(1 + 2K_0^{NC}\right)^2} + \frac{\left(1 - K_0^{NC}\right) \cdot \left(1 - 2.v_{ur}\right) \cdot \left(\lambda^* / \kappa^* - 1\right)}{\left(1 + 2K_0^{NC}\right) \cdot \left(1 - 2v_{ur}\right) \cdot \left(\lambda^* / \kappa^*\right) - \left(1 - K_0^{NC}\right) \cdot \left(1 + v_{ur}\right)}} \tag{2}$$

The findings indicate that the lightly overconsolidated clay and peat layers generate the largest horizontal soil deformations. However, the horizontal movements are suppressed by the highly overconsolidated crust. The comparison between the Soft Soil Creep model and the in-situ measurements seems reasonable. Notice that the fitted default values match closer to the in-situ measurements than the simulations performed with empirical relation of Jaky (see figure 7). For example, the difference between the last in-situ measurement and the model simulations with a default value of K_0^{NC} or Jaky are respectively 10% and 25%. Finally, it is striking that the horizontal displacements in the soft soils at Bricor are much larger than the horizontal displacements measured in the Boston blue clay. A possible explanation for this discrepancy is related to the difference in stress history. The Boston blue clay is highly overconsolidated in the first 15 m below surface level, while the soft soils under the Bricor test embankment do not have a significant stress history.

2.1.3. *Sackville test embankment constructed on an organic clayey silt*

Soft organic clayey silt deposits are found in many parts of Canada, also in New Brunswick where several road construction projects have been initiated in the early 1990s. An example of such a project is the widening of the Trans-Canada highway between Moncton and Amherst. An instrumented test embankment was constructed in Sackville prior to the roadway construction to evaluate the performance of the organic clayey silts (Brisbois, 1999; Rowe *et al.*, 2001). This test embankment contains a geotextile reinforced section and an unreinforced section, this thesis only describes the unreinforced section. In comparison to the other considered test embankments, the Sackville test embankment was loaded to failure. This means that the stress path is different, because it progresses to the critical state, while the stress paths of the other test embankments progress near the K_0-line. Furthermore, it is important to mention that the embankment was constructed in such a way that failure could only take place on the northern side, because the other sides were stabilized with lateral berms. The final remark before the ground conditions and the construction aspects are described is that this case study only presents in-situ measurements; no attention is paid to model simulations.

<u>Description of ground conditions</u>

The test embankment is situated in a tidal salt marsh. The soil profile is presented in table 3, and is based on borehole logs. It shows that the subsoil consisted of several types of clayey silts. In which the organic clayey silt is the most susceptible for large vertical and horizontal deformations. Notice that the clay crust and the stiff clayey silt are both largely overconsolidated. As a result, it is expected that the development of pore pressures and deformations is limited in these layers.

Table 3 – Soil profile at Sackville test location

Soil Type [-]	Top of Layer [m +SL] [1]	Bottom of Layer [m +SL]	Thickness [m]
Clay crust	0.0	-1.2	1.2
Organic clayey silt	-1.2	-3.6	2.4
Sandy clayey silt	-3.6	-4.2	0.6
Organic clayey silt	-4.2	-10.0	5.8
Stiff clayey silt	-10.0	OD [2]	-

[1]   SL is surface level

[2]   OD is observed depth

To examine the soil properties an extensive number of field and laboratory test have been performed. For example, vane tests were performed to assess the undrained shear strength of the soft soils. Monitoring wells and piezometers were used to determine artesian water pressure and the permeability of the various layers. Incremental oedometer tests were used to assess the compressibility and the stress history of the clayey silt layers.

From the vane data it appeared that the soil strength is variable at shallow depths above 4.0 m below surface level. The undrained shear strength of the unreinforced section varied between 30 kPa to 40 kPa, which is approximately 25% higher than the reinforced section. Based on this information, it was considered appropriate to arrange the sections in such an order that the stronger soil was beneath the unreinforced section, thereby minimizing the difference in fill thickness required to fail the two sections. Notice that only the undrained shear strength is reported, because the embankment is constructed to failure within a month. It is therefore expected that the soil response will be close to undrained.

The piezometer and monitoring well measurements were used to evaluate the permeability of the clayey silt layers. These measurements show that the clayey silt has a permeability in the order of 10^{-7} to 10^{-8} m/s. However, the permeability of the organic clayey silt layers is generally one order of magnitude greater.

The incremental oedometer test results suggest that there is a sharp difference in compressibility between the organic clayey silt layers and the clay crust on top. The OCR of the organic silt layer varies between 1.0 to 1.5, while the OCR of the overconsolidated clay was in all cases higher than 3.5. It is noted that the CR has a value of approximately 0.3 for the organic silts. If this value is compared with the organic soil layers of the Bricor case, it can be concluded that the CR value of these organic silts is not extremely high. It is therefore expected that the horizontal soil displacements are lower than those reported in Bricor.

Construction of the embankment

The construction process of the Sackville test embankment is divided into 4 stages as shown in figure 8. The graph shows that fill thickness was increased to 1.3 m, 2.25 m and 3.4 m during the first, second and third construction stage. In the last construction stage, it was rapidly built to failure in a period of 3 days. Figure 8 shows that the total pressure cell readings correspond to the measured embankment thicknesses as obtained from the settlement plates.
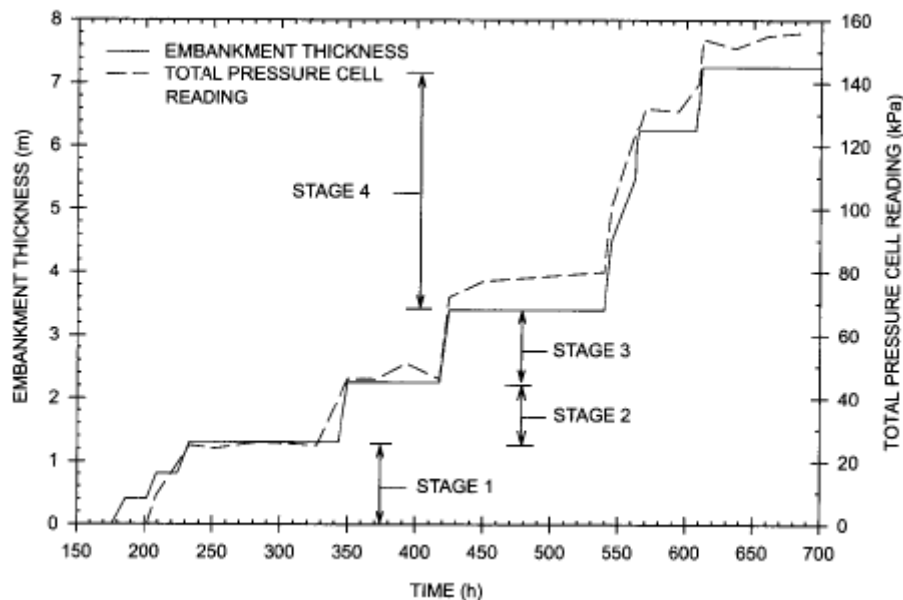
Figure 8 – Construction process of the Sackville test embankment (Rowe et al., 2001)

The piezometers, settlement plates, inclinometers and total pressure cells were installed three months before the start of construction. The field instrumentation was several times monitored prior to construction until its initial performance was considered to be satisfactory and zero readings were ensured. During construction these devices were monitored at least twice a day, but more frequently in the final stage when there was evidence of rapid soil movement.

Results and discussion

The instrumentation and field performance of the unreinforced section of the test embankment constructed at Sackville New Brunswick has been described (Rowe *et al.*, 2001). This test section behaved elastically during the first, second and third construction stage. In the last stage of the embankment construction, the embankment height was rapidly increased until failure occurred at a fill thickness of 6.25 m. The observed soil behaviour during this stage was of a viscoplastic type. Note that no classical abrupt failure was encountered during the construction of this embankment.

The piezometer measurements show a direct increase of excess pore pressure as result of the addition of fill material, but they also continued to raise between the different construction stages. This rise is not in line with the expectations, because you should expect a decline between the construction stages. However, a possible explanation could be that there is a gradual destructuration at the end of construction that results in a generation of excess pore

pressures between the stages. Another plausible explanation that could have resulted in the continued increase of excess pore pressures is the time dependent development of deviatoric strains. Furthermore, it is observed is that the pore pressures slowly develop during the first stages, but very rapidly increase as the fill was raised from 3.4 m to 6.25 m. According to Leroueil *et al.* (1985) this typical behaviour could be attributed to the initially overconsolidated state of the soft subsoil at the early stages. After the preconsolidation stress the pore pressures develop considerably, which is an indication of normal consolidated soil behaviour. The corresponding Δp/Δu ratios are about 1.0 in the overconsolidated state, while the Δp/Δu ratio is approximately 0.8 to 0.9 when the soil becomes normal consolidated again.

This distinction is also visible in figure 9, where the development of horizontal soil deformations is presented near the toe of the embankment for various moment in time. The findings indicate that the horizontal soil deformations are limited up to an embankment thickness of 3.4 m. This reflects the essentially elastic response of the soft subsoil. When the embankment thickness is raised from 3.4 m to 5.0 m the horizontal displacements increase with 250%. After a embankment thickness of 5.0 m the inclinometers could no longer be monitored due to a blockage at 3.5 m below ground surface. According to Rowe *et al.* (2001) this blockage is an indication of a failure zone at this depth. However, it is also possible that this blockage occurred due to a too large difference in horizontal displacement between the organic clayey silt and sandy clayey silt layer.
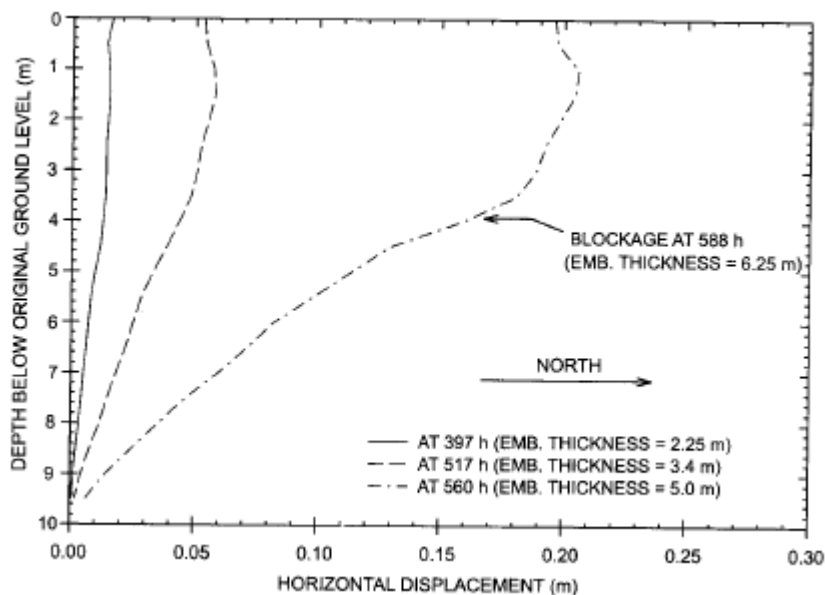
Figure 9 – Horizontal deformation profiles at the toe of the Sackville test embankment

The settlement plates measurements indicate that the settlements were relatively small, less than 0.2 m, after the second construction stage. However, when the embankment thickness was further raised the settlement rate exponentially increased until failure occurred.

2.1.4. Athlone test embankment constructed on very soft clays

To complete the construction of the new bridge over the Shannon River in the late 1980s, approach embankments of 8.6 m were required above the marshland of Athlone in the Irish midlands (Long and O'Riordan, 2001). The new bridge was necessary to improve the traffic

flow on the N6 road between Dublin and Galway. The approach embankments are situated on very soft glacial lake clay and highly compressible organic clays. The geotechnical properties of these soft soils were intensively analyzed during the site investigation. However, there remained a significant amount of uncertainty, which complicates an accurate determination of the soil parameters. For this reason, it was decided to construct two test embankments prior to the actual works, which were known as the main and subsidiary test embankments. The principal objective of the main trail was to assess the compressibility and consolidation parameters of the soft subsoil. For the subsidiary embankment a failure was induced, because the objective was to determine the strength characteristics of the subsoil stratum. In addition, during construction of the actual embankments 6 cross sections were defined to monitor the pore pressures, settlements and lateral deformations.

The findings presented in this section show some of the site investigation results and monitoring measurements during construction for the real embankment and test embankments. Again, this case study only presents field measurements; no attention is paid to model simulations.

Description of ground conditions

The soil profile as shown in table 4 is based on a group of shell and auger borings. The groundwater table at the test location seldom drops more than 1.0 m below ground level. A typical seasonal variation between 0.4 m to 1.0 m in groundwater level is observed. Notice that the presented soil profile is not fixed; some variations in layer thickness are possible, especially for the organic clay and laminated clay.

Table 4 – Soil profile at Athlone test location

Soil Type [-]	Top of Layer [m +SL] [1]	Bottom of Layer [m +SL]	Thickness [m]
Peat	0.0	-1.5	1.5
Marl	-1.5	-2.2	0.7
Organic clay	-2.2	-6.0	3.8
Laminated clay	-6.0	-10.8	4.8
Glacial till	-10.8	OD [2]	-

[1] SL is surface level

[2] OD is observed depth

In addition to the classification testing an extensive laboratory and field testing programme has been performed; which included incremental oedometer tests, constant head tests, rising head tests, vane tests and piezocone testing.

The incremental oedometer tests were used to analyse the compressibility and the stress history of the soil. The compressibility ratio CR for the deformation sensitive soil layers are on average 0.48, 0.36, 0.40 and 0.14 for respectively the peat, marl, organic clay and the laminated clay. From the measurements it also appeared that the preconsolidation stress in the complete soil profile, except the glacial till, is slightly higher (+ 5.0 to 10.0 kPa) than the prevailing soil stresses. This means that the OCR values are close to unity.

The permeability was investigated for the organic clay and the laminated clay using borehole constant head tests and rising head tests. For the organic clay the coefficient of permeability reduced with increasing stress from about 7.0 x10^{-9} m/s at 30 kPa to 1.0 x10^{-9} m/s at 60 kPa. The results of the laminated clay is more scattered, but an average the permeability has a value of 2.0 x10^{-9} m/s. If these values are compared with the previous cases, it can be observed that the permeability values of the Athlone clays are quite low.

The undrained shear strength is measured with vane tests. The data obtained from these tests resulted in a very unusual strength profile, because the undrained shear strength in the organic clay falls from 16 kPa on top to about 8 kPa at the base of the layer. For the laminated clay layer the shear strength initially decreases from 8 kPa to approximately 4 kPa before increasing again to approximately 10 kPa towards the base of the layer. When the undrained shear strength results are compared with other well-researched sites on clayey soil, for example those at Bothkennar near Edinburgh in Scotland. Nash *et al.* (1992) found out that the most striking difference with the Athlone clays is the lack of evidence of overconsolidation. An increase in shear strength with depth is found for the Bothkennar clays, but such a finding is not obvious for the Athlone clays. However, it is possible that the strength values obtained at Athlone are obfuscated by rate of vane rotation or the disturbance effects due to vane insertion. These results should therefore be interpreted with suspicion.

Construction of the embankment
The construction of both main and subsidiary embankment is not well reported in Long and O'Riordan (2001). However, it is known that the main test embankment was constructed in stages till a height of 8.6 m above ground surface, and that new stages were only applied if the factor of safety was at least 1.25. The total construction process covered a period of almost 2 years. This seems quite long, but one has to be aware that the measured shear strengths were very limited during construction as already explained. The subsidiary test embankment has been constructed to failure in a couple of days. Failure occurred at a fill thickness of about 3.0 m. The observed failure surface was non-circular, with at least half of its length in the laminated clay.

Results and discussion
The results of the in-situ measurements for both test embankments, which are located north of the town of Athlone, are presented. These test embankments were constructed to gain more insight into the strength and deformation behaviour of the soft underground near the Shannon River.

The maximum settlement under the centre of the main test embankment is 2.6 m 1 year after the end of construction. The settlement at the toe of the embankment has a value of approximately 1.0 m. A detailed analysis revealed that almost half of the settlement occurred in the peat and marl strata. The organic clay and the laminated clay contributed each with percentage of respectively 28% and 20% (Long and O'Riordan, 2001).

The piezometer measurements were used to obtain the pore pressure coefficient B that represents the ratio between the excess pore pressure increment to the vertical effective stress increment (Skempton, 1954). For a correct use of this data, it has to be corrected for

settlement effects. The organic clay has a B ratio close to 1.0 under the main test embankment. However, lower values are obtained for the laminated clay, the B ratio varies in this layer between 0.5 and 0.8. These lower values are probably due to the laminated structure, which allowed more rapid drainage. In the subsidiary trail the B values for the organic clay remained between 0.8 and 1.0 and exceeded 1.0 as failure of the embankment was approached. A rapid increase of the parameter B was also observed for the Sackville test embankment close to failure.

The maximum lateral movements have been plotted as a ratio of the maximum settlements in figure 10 for both test embankments and two cross sections of the actual embankment. Note that section E is located at the west bank of the Shannon River, while section F is located at the east bank. From the site investigation it appeared that the thickness of the organic clay and laminated clay is significantly greater at the west bank than at the east bank.
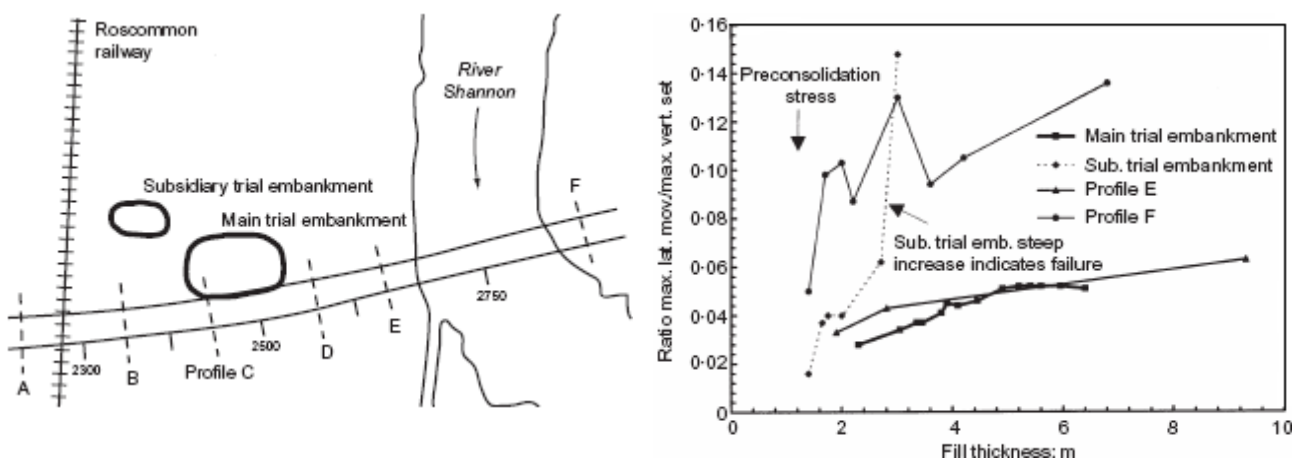
Figure 10 – Site layout and ratio of lateral to vertical deformations for the Athlone test embankment

The findings show that the average ratio between lateral and vertical deformations is about 0.05 for profile E and the main trail, but higher ratios are found for profile F and the subsidiary trail. It is not surprising that the lower values occur at the west bank, where the combined thickness of the soft soils is largest, and thus settlement is highest. However, it is important to stress that these ratios are not completely in line with the other published data. For example, Tavenas *et al.* (1979) showed that this ratio was about 0.16 for embankment constructed on clayey soils. This is significantly higher than that was recorded at Athlone. A possible explanation for these low values is due to the presence of organic layers.

2.2. Stress path analysis

A stress path presents the stress development of a soil particle in the underground. A difference could be made between the total stress path (soil particles + pore pressures) and the effective stress path (only soil particles). The course of a stress path determines the response of a soil to a foundation load, which could then be used to assess the development of deformations within the subsoil. It is therefore essential to consider the stress paths in relation to their application and their capability to match the prevalent soil behaviour. In this thesis soft soils under embankment loading are considered. Examples of such stress paths

are given of the last subsection of this paragraph. With a proper knowledge about these stress paths a good decision can be made for the types of models selected in the next chapter.

For an embankment loading the average effective stress and the deviator stress are increasing with time. However, the relation between horizontal effective stress, vertical effective stress and shear stress are different for distinctive stress points in the soil. Figure 11 shows that there are roughly three distinct loading situations in a soil layer under an embankment, which are triaxial compression, simple shear and triaxial extension.
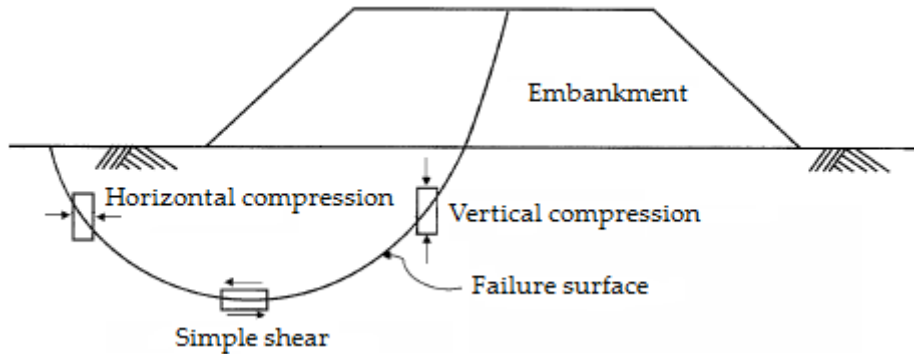
Figure 11 – Stress conditions under an embankment (Zdravković et al., 2002 after Bjerrum, 1973)

At the centre of the embankment the soil is subjected to vertical compression ($\Delta\sigma_v > \Delta\sigma_h$). The shear stress is increasing in the direction of the toe of the embankment, where the maximum can be found exactly under the toe of the embankment ($\Delta\sigma_v = \Delta\sigma_h$). When moving further away from the embankment the stress condition changes from shearing to horizontal compression ($\Delta\sigma_v < \Delta\sigma_h$). For convenience the stress paths are mostly presented using the stress invariants of Lambe (1967) or Roscoe *et al.* (1958). The meaning of these representations are discussed in subsection 2.1.2. Next to these representations a global description of stresses is given, and the stress paths of a soft soil subjected to an embankment loading are presented.

2.2.1. Stress description and the effective stress concept

Stresses in a soil mass are the result of self weight and external forces. In reality there are many types of external forces which could influence the stress state in a soil; examples are the load of a foundation slab or a load due to snow. Stress states can be described by the Cartesian system (x, y and z) or the cylindrical coordinate system (r, θ and z). In this research the stress states are exclusively represented with the Cartesian system. A Cartesian stress tensor is shown in formula 3.

$$\sigma = \begin{bmatrix} \sigma_{xx} & \sigma_{xy} & \sigma_{xz} \\ \sigma_{yx} & \sigma_{yy} & \sigma_{yz} \\ \sigma_{zx} & \sigma_{zy} & \sigma_{zz} \end{bmatrix} \tag{3}$$

When there are only normal stresses and no shear stresses in the system, the stress tensor can be described with formula 4.

$$\sigma = \begin{bmatrix} \sigma_1 & 0 & 0 \\ 0 & \sigma_2 & 0 \\ 0 & 0 & \sigma_3 \end{bmatrix}$$

(4)

The σ_1, σ_2 and σ_3 are the principle stresses. Conventionally, $\sigma_1 > \sigma_2 > \sigma_3$, where σ_1 is the major principle stress, σ_3 is the minor principle stress and σ_2 the intermediate principle stress. The described stress concept is only valid for continuous media. In reality the soil body is composed of discrete particles, where the properties vary widely between neighbouring crystals. However, for general engineering purposes, it is convenient to ignore this molecular nature, and to describe the soil on a macroscopic level (Valliappan, 1981).

For saturated soils Terzaghi (1943) has shown that the response of the soil to given a disturbance is controlled by the effective stress, which is defined as the difference between total stress and pore water pressure. Formula 5 presents the concept in matrix form.

$$\begin{bmatrix} \sigma'_{xx} & \sigma_{xy} & \sigma_{xz} \\ \sigma_{yx} & \sigma'_{yy} & \sigma_{yz} \\ \sigma_{zx} & \sigma_{zy} & \sigma'_{zz} \end{bmatrix} = \begin{bmatrix} \sigma_{xx} & \sigma_{xy} & \sigma_{xz} \\ \sigma_{yx} & \sigma_{yy} & \sigma_{yz} \\ \sigma_{zx} & \sigma_{zy} & \sigma_{zz} \end{bmatrix} - \begin{bmatrix} u & 0 & 0 \\ 0 & u & 0 \\ 0 & 0 & u \end{bmatrix}$$

(5)

The formula above shows that pore water pressures cannot sustain shear. As a result, the soil particles have to resist all the shear forces. Accumulated experience of the effective stress principle confirms that in nearly all circumstances the behaviour of soils is controlled by the effective stresses (Skempton, 1984).

2.2.2. Stress path representations

In most geotechnical problems the state of stress varies with time. For this reason, to get a proper overview of the stress history a visualization of the stress path is highly desirable. Several types of representations have been proposed. In this research the representation of Lambe (1967) and Roscoe *et al.* (1958) will be used for the stress path representation. Note that the stress representations make use of stress invariants; this means that they are independent of the axis system.

These stress representations are linked to the principle axes of stress and hide the orientation of these principle axes. This does not pose any constraint on the interpretation of triaxial and plane strain tests, because in these tests the principal directions are fixed. It can place a constraint in several geotechnical problems, where rotations of principle axes do occur (Leroueil *et al.*, 1990). For example, Symes *et al.* (1988) indicate that rotation of principle axes has a significant effect on the behaviour of soils. Therefore, one should be aware of the limitations associated with these representations of stress paths and the way to interpret them accordingly.

Lambe's representation

In the stress representation of Lambe (1967) the Mohr circle could be completely defined with stress invariants s and t as shown in figure 12. The effective stress circle can be deduced from the total stress circle by a horizontal translation which equals the pore water pressures. It should be noted that Lambe originally used symbols p' and q instead of s' and t, but these latter symbols have been chosen in order to avoid confusion with the invariants suggested by Roscoe *et al.* (1958).
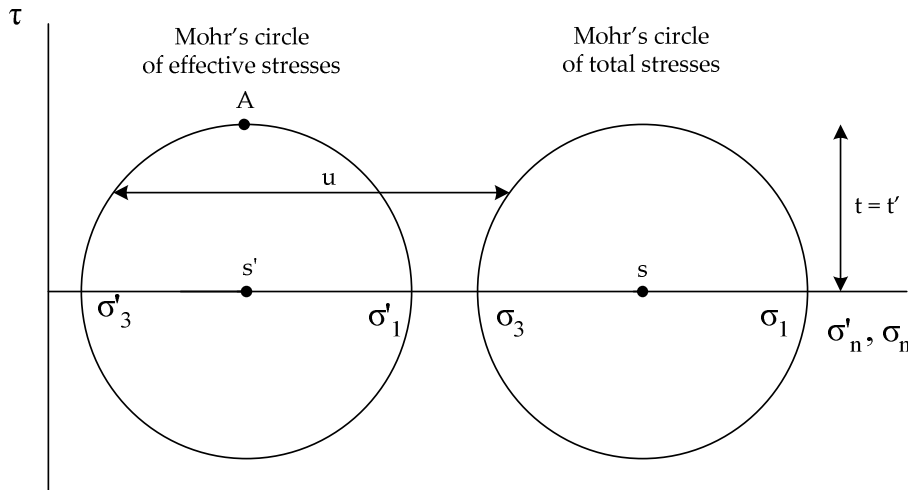
Figure 12 – Mohr diagram for presenting two-dimensional stress states

The s and t variables are presented in formulas 6 and 7.

$$s' = \frac{\sigma_1' + \sigma_3'}{2} = s - u \tag{6}$$

$$t = t' = \frac{\sigma_1' - \sigma_3'}{2} \tag{7}$$

Lambe suggested that a state of stress in a soil should be represented by point A with the stress invariants s' and t. As a state of stress at a particular point varies, so will point A move in s' and t space in order to describe the corresponding stress path.

Roscoe's representation

Roscoe is one of the founding fathers of the Cam Clay theory. The basic principle of this theory is that all stress paths reach on a critical state line, where the effective stress, void ratio and shear strength remain constant (Schofield and Wroth, 1968). For the description of stress paths in a triaxial apparatus the stress variables p and q were defined (Roscoe *et al.*, 1958). Just like the s and t variables p and q are also independent of the axis system.

The p and q variables for triaxial condition are shown in formulas 8 and 9.

$$p' = \frac{\sigma_1' + 2 \cdot \sigma_3'}{3} = p - u \tag{8}$$

$$q = q' = \sigma_1 - \sigma_3 \tag{9}$$

A change in p indicates a volume change in the soil. In an undrained situation there are no volume changes, while in a drained situation there are volume changes to be expected. The q represents the shear stresses in the soil. So, in an isotropic loading condition the Δq should be zero. Furthermore, the pore pressures affect only the mean stress p. The effective stress state can be deduced from the total stress state by a translation of magnitude u parallel to the normal stress axis (see figure 12).

2.2.3. *Stress paths in soft soils subjected to an embankment loading*

Current methods for predicting the response of soft soils to surface loading are often unsuccessful; this is partly due to an incorrect incorporation of stress paths. Ladd *et al.* (1994) emphasizes the importance of a correct incorporation of the stress history for the prediction of lateral displacements. A proper determination of the total stress path (TSP) and the effective stress path (ESP) are therefore highly desirable to accurately predict the strains before and after yielding. Figure 13 shows a qualitative development of the total and effective stress path for an embankment constructed on a slightly overconsolidated soft soil layer. Notice that in reality the distinction between undrained deformation and deformation due to consolidation is not so strict. However, this interaction is so complicated that it is assumed here for the convenience of analysis that each type of deformation occurs separately (Matsuo and Kawamura, 1977). Furthermore, it is stressed that the exact course of the effective stress path is dependent on a number of factors, for example the imposed stress level, drainage conditions and rate of construction.
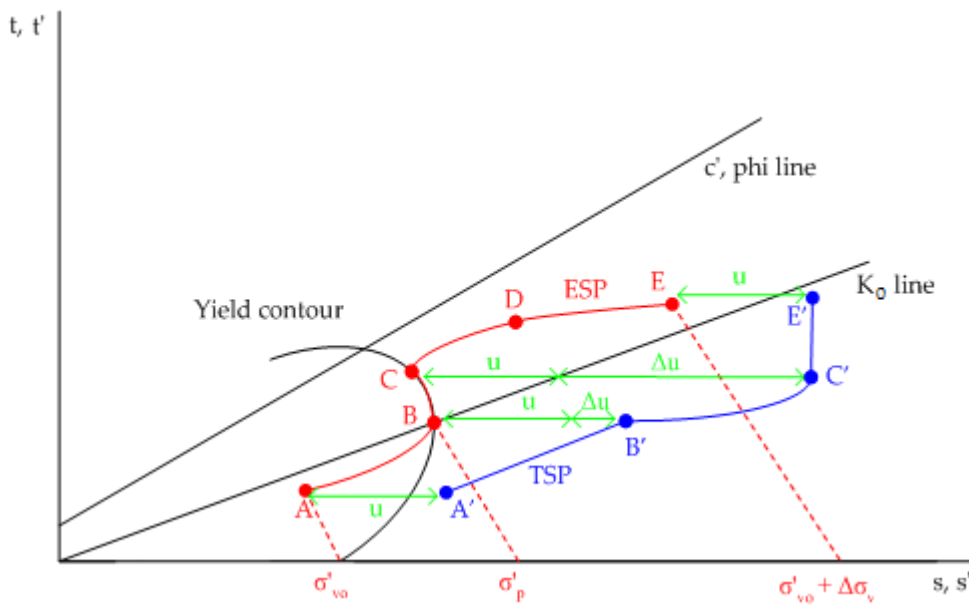
Figure 13 – Schematic overview of the TSP and ESP under an embankment (Leroueil et al., 1990)

The first phase of the effective stress path A to B is the initial quasi-elastic response, which relates to the overconsolidated state of the soil. The consolidation process in this phase takes place quickly and a limited amount of excess pore pressure could develop (small Δu). Conventionally, this phase is mostly ignored by custom models; they assume fully

undrained behaviour as the first loading response (Tavenas and Leroueil, 1980). Having passed the preconsolidation stress (point B), the stress path follows an undrained state of plastic shearing, where the stress path follows the yield contour. The stress invariant s stays in this phase almost equal, this means that the soil mass is volume preserving, which is typical for undrained behaviour. Furthermore, notice that during undrained shearing large excess pore pressures could develop (high Δu). After the undrained response, in phase C to D the consolidation process takes place, which leads to an increase of the vertical effective stresses in time due to the dissipation of excess pore pressures. The end of the consolidation process is represented by point E, in this point all excess pore pressure have been dissipated.

The advocated effective stress path development can also be recognized in the relationship between horizontal deformations at the toe of the embankment and vertical settlements under the centre of the embankment. Figure 14 shows this typical relation between horizontal and vertical displacements. Note that this relation is based on a large number of embankments which have been founded on a soft soil (Leroueil *et al.*, 1990).
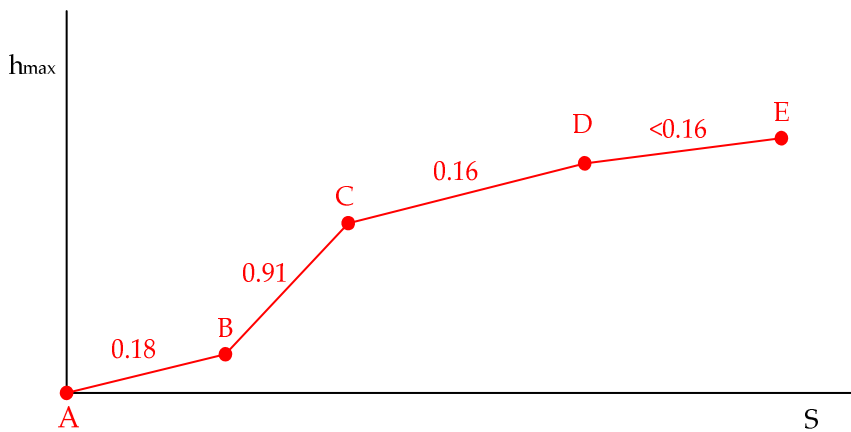
Figure 14 – Relation between horizontal deformation at toe and settlements under centre embankment

The findings show that during the initial phase A to B hardly any horizontal movements could occur at the toe of the embankment. In this phase the effective stress path stays very close to the K_0-line (see figure 13). Notice that a K_0 stress condition corresponds in general to zero horizontal strain, which is about similar to an oedometer sample that is confined in the lateral directions. Tavenas *et al.* (1979) analyzed 21 embankments of many geographical origins; this has resulted in a set of relations for the discussed phases.

Formula 10 is used to determine the maximum lateral displacements in the reconsolidation phase A to B.

$$h_{\max;rc} = \left(0.18 \pm 0.09\right) \cdot S_{rc} \tag{10}$$

When the subsoil behaves normally consolidated again, the horizontal displacements increase almost at the same level as the vertical settlements. This relation is presented in formula 11.

$$h_{\max;un} = \left(0.91 \pm 0.2\right) \cdot S_{un} \tag{11}$$

During the consolidation phase C to D the horizontal displacement develop less fast. The progress of horizontal displacement during consolidation can be estimated with equation 12.

$$h_{\max;co}(t) = \xi \cdot S_{co}(t) \tag{12}$$

The ξ is a function of the embankment width, embankment slope, thickness of soft soil deposit and the factor of safety of the embankment. However, in most cases parameter had a value of approximately 0.16. For the determination of ξ the prevalent factor of safety appears to be of utmost importance, because a fast progress of the lateral displacements indicates a low factor of safety (Marche and Chapuis, 1974; Matsuo and Kawamura, 1977). Notice that this equation is valid till 50% of consolidation, after this period (phase D to E) creep start to play a significant role in the development of lateral movements. Stewart's work (1996) suggests that the horizontal displacements are decreasing with time for consolidation degrees above 50%. However, no definite judgement can be made, because of the sparse amount of data available. Another remark is that these relations could only be used for clays and silts, for organic soils alternative relations should be used (Long and O'Riordan, 2001).

2.3. Theories and models for time-dependent deformations

A large part of the horizontal deformations in soft soils are time-dependent. These deformations consist of a consolidation and a creep part. The consolidation deformations are the result of dissipation of excess pore pressures due to the embankment loading. Deformations under a constant effective stress are known as creep. The mechanism that causes creep deformation is still not fully understood (Leroueil *et al.*, 1985; Floquet, 2006). It seems reasonable that creep deformations are the result of the gradual readjustment of soil grains in a more stable configuration. Another explanation of creep deformations is that they are caused by a very slow drainage of water from the micro-pores to the macro network (Berry and Poskitt, 1972). For a better understanding of the time-dependent deformations the existing theories and models are discussed in this paragraph.

However, before elaborating on the different theories some important aspects and definitions are discussed. For instance, the continuity equation, which is the starting point of all consolidation theories (Gibson *et al.*, 1967). A continuity equation is a differential equation that describes the transport of a conserved quantity. It explains roughly that the total amount inside a region can only change by the amount that passes in or out of the region through the boundary. The differential form of the continuity equation is given in formula 13.

$$\frac{\partial \rho}{\partial t} + \nabla(\rho \cdot u) = 0 \tag{13}$$

The application of this equation to saturated soils can be illustrated with figure 15, where a typical flow regime under an embankment during consolidation is given. The non-uniform embankment load produces excess pore pressures, which flow with time to the drainage boundaries. It should be noted that there is always a certain influence from the horizontal water flow on the rate of deformations, especially in the outer parts of the embankment. The deformations in these parts therefore become somewhat larger and occur more rapidly than

those calculated with the classical one-dimensional consolidation theory of Terzaghi (Larsson *et al.*, 1997). For this reason, to determine the horizontal deformations at the toe of the embankment, it is desirable to account for at least two dimensions. Extension to more dimensional consolidation could be done with the theory of Biot (1941).
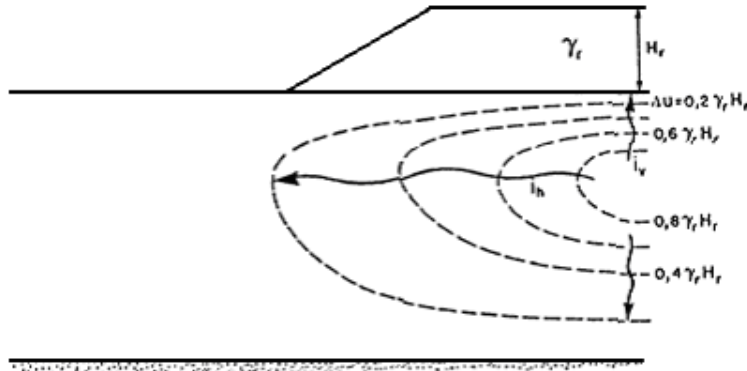
Figure 15 – Typical flow regime during consolidation under an embankment (Leroueil et al., 1990)

It is important to state that the current theories and models often describe axisymmetric conditions during shearing and isotropy during consolidation. In nature, most soils are subjected to a plane strain loading or three-dimensional loading conditions, and the consolidation behaviour is K_0. This means that anisotropy is subjected to the soil structure, because the soil properties are no longer the same in all directions (more information about anisotropy is given in section 2.4). The consequence of K_0 behaviour is that the normal consolidation line is shifted to the left in comparison to the isotropically consolidated soil, because the mean effective stress p' for a K_0-consolidated soil is not equal to the vertical effective stress as shown in formula 14.

$$p' = \frac{1 + 2.K_0}{3} \cdot \sigma_z'$$
(14)

The K_0-consolidated soil requires a lower mean effective stress to achieve the same void ratio as an isotropically consolidated sample. So, when analyzing a theory or the results of a model simulation one has to be aware of the assumptions made.

Another important aspect for the development of horizontal deformations with time is the magnitude of shear strains at the toe of the embankment. Tavenas *et al.* (1979) shows that for a slow embankment construction, the deformations are mainly caused by volumetric strains. Other factors that reduce the relative importance of shear strains are the slope of the embankment, the safety factor of embankment and the width of the embankment in proportion to the thickness of the soft soil layer. According to Leroueil *et al.* (1990) shear strains could be ignored if the safety factor of the embankment is higher than 1.3. However, for fast embankment constructions it is likely that shear deformations cannot be disregarded. Landva and La Rochelle (1982) reported cases for embankments on Escuminac peat were 30% of the deformations are the result of shear deformations. An example of such an embankment is presented in figure 16. Notice that the mechanism of excessive shear deformations has some similarities with the phenomenon of squeezing.
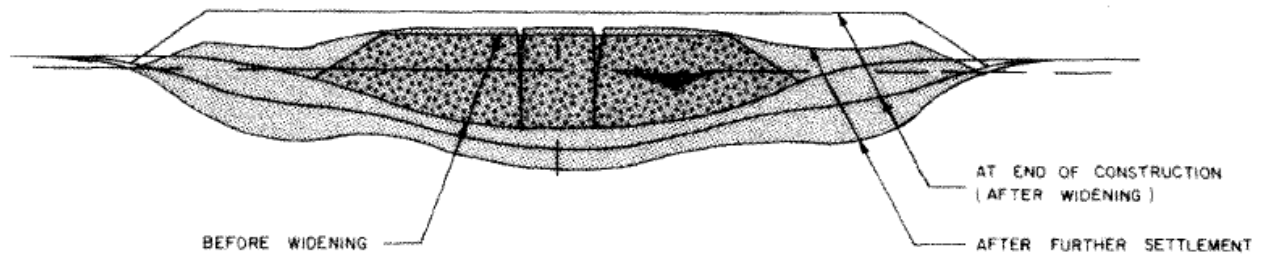
Figure 16 – Embankment with excessive shear deformations (Landva and La Rochelle, 1982)

Furthermore, for peaty soils a distinction has to be made between amorphous granular peat and fibrous peat, because the time-dependent behaviour is totally different (MacFarlane, 1969). The amorphous peats are nearly in line with the behaviour of clays in compression. For these types of soils the particles have mainly a colloidal size and the majority of pore water is absorbed around the soil structure. On the contrary, fibrous peats have a much more open structure, because the organic material is only partially decomposed. Most of the water occurs as free water rather than viscous adsorbed water. In such peats, the consolidation process cannot be governed by a sequential expulsion of interparticle and intraparticle void water (Landva and La Rochelle, 1982). For this reason, the time-dependent response will be significantly different from the amorphous peats and clayey soils. This different behaviour becomes even more clear in the experimental relationships between void ratio, effective pressure and permeability as shown in figure 17.
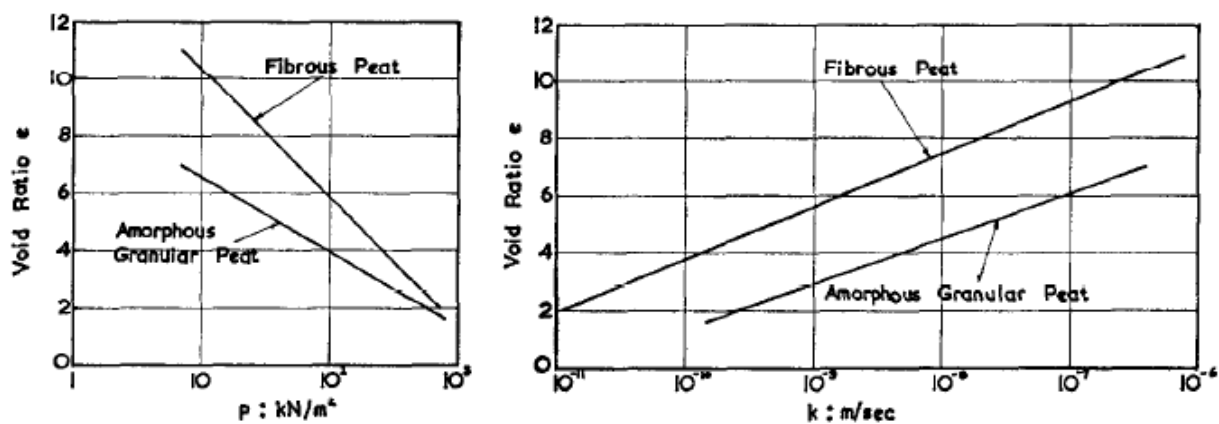
Figure 17 – Relations between void ratio, effective pressure and permeability (Berry and Poskitt, 1972)

The most striking difference is the larger compressibility of the fibrous peats. Figure 17 also shows that the initial void ratio of the fibrous peat is mostly larger than the void ratio of the amorphous granular peat.

The remaining part of this paragraph starts with a brief description of the pioneers of the consolidation and creep theory. Subsequently the end of primary (EoP) and the elasto-viscoplastic (EVP) model formulations are discussed. These model formulations are also known as theorem A and theorem B (Ladd *et al.*, 1977). It is remarkable that even after so many years of discussion, there is still a disagreement among some researchers about which theorem is valid.

2.3.1. *Pioneers of consolidation and creep theory*

In this subsection the most important researchers of the consolidation and creep theory are briefly discussed. Notice that it is not the intention to be all-embracing, but to capture the most important developments in the time-dependent behaviour of soft soils. The discussion covers the following key developments:

- Terzaghi's classical consolidation theory (1923)
- Buisman's log time relationship (1932)
- Taylor and Merchant's creep formulation (1940)
- Šuklje's isotaches concept (1957)
- Bjerrum's times lines and equivalent time concept (1967)

Terzaghi's classical consolidation theory

The classical theory for one-dimensional consolidation was development by Terzaghi (1923). This theory still forms the basis for several time-dependent soil models. Terzaghi validated his theory with a number oedometer tests, which is tool where small samples were step-wise loaded until all excess pore pressures have been dissipated. According to Leroueil *et al.* (1990) the full dissipation process usually lasts for several hours, but in extremes cases it can take 24 hours. However, notice that the theory of consolidation proposed by Terzaghi has a number of assumptions, which are summed up below:

- Strains are one-dimensional and remain small
- Soil is homogenous and saturated
- Particles of soil and pore fluid are incompressible
- Flow of the pore fluid is according to Darcy (see formula 15)

$$v = k \cdot i \tag{15}$$

- Permeability is constant
- Linear relation exist between the void ratio and the effective stress (see formula 16)

$$\partial e = -m_v \cdot \partial \sigma_v' \tag{16}$$

- Soil exhibits no viscosity

Using the first five assumptions permits the consolidation equation to be written in the form of formula 17.

$$\frac{\partial e}{\partial t} = \frac{k.(1+e)}{\gamma_w} \cdot \frac{\partial^2 u}{\partial z^2} \tag{17}$$

This equation expresses the fact that the rate of change in void ratio at a given instant depends on the permeability and the form of the excess pore pressure isochrone, but not on the compressibility of the material.

When the last two assumptions are incorporated, and the applied stress is assumed to be constant, the equation turns into the form of formula 18.

$$\frac{\partial u}{\partial t} = \frac{k.(1-e)}{\gamma_w.a_v} \cdot \frac{\partial^2 u}{\partial z^2}$$ (18)

The first right part of the differential equation has been called the coefficient of consolidation, and is represented with symbol c_v (see formula 19).

$$\frac{\partial u}{\partial t} = c_v \cdot \frac{\partial^2 u}{\partial z^2}$$ (19)

This differential equation can be solved with the finite difference technique or the Fourier series. The solution for the consolidation equation is usually presented graphically, for example in figure 18 as a relation between the average degree of consolidation versus the time factor. Notice that the cases A till D correspond to different initial excess pore pressure distributions and drainage conditions. The time factor is defined with formula 20.

$$T_v = \frac{c_v \cdot t}{H^2}$$ (20)
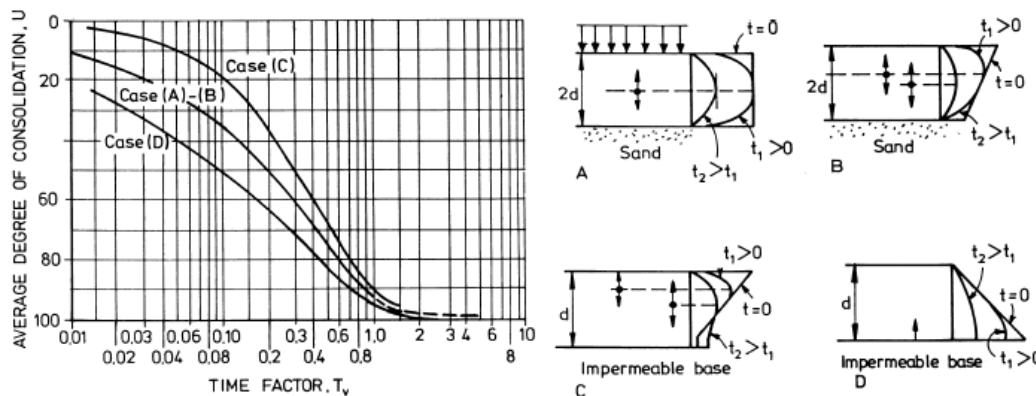
Figure 18 – Relation between time factor and average degree of consolidation (Larsson et al., 1997)

It is clear that the assumptions necessary for the development of Terzaghi's solution are not fully in agreement with the real physical behaviour of a consolidating bed of soft soil. According to Leroueil and Tavenas (1980) this solution is only a crude approximation of the in-situ behaviour. Some of the limitations are summed up below:

- Theory is only applicable for relatively small strains, while in reality strains could reach values of 50% for peaty soils as shown by Landva and La Rochelle (1982)
- Conditions are rarely one-dimensional in practice, in general the flow is at least two dimensional, and therefore more rapid consolidation can be expected
- Theory assumes that the coefficient of consolidation is equal during loading and unloading, while this coefficient is not a constant in reality (Dykstra *et al.*, 2009)
- Other significant implication is that straining will stop after dissipation of excess pore water pressures

Later publications have tried to improve the one-dimensional consolidation theory of Terzaghi (1923). For example, Gibson *et al.* (1967) removed the limitation of small strains and also the changes in soil compressibility and permeability were taken into account. Due to the inclusion of these factors the coefficient of consolidation as shown in formula 19 changes into the expression as shown in formula 21.

$$c_f = -\frac{k(e)}{\rho_f} \cdot \frac{(1+e_0)^2}{1+e} \cdot \frac{\partial \sigma'}{\partial e}$$

(21)

Note that the ρ_f in this formula is the fluid density. It is important to realize that this equation is not a constant, except for some specific cases. As a result, analytical techniques are not sufficient anymore, and numerical techniques are needed to solve the equation of one-dimensional consolidation.

Buisman's log time relationship
In 1932 Keverling Buisman, who was a professor in soil mechanics at the Delft University of Technology, found that the deformation pattern of soft soils in a consolidation test did not approach a constant final value, but that the deformations continued very long. This means that the tail of a deformation curve is not horizontal. On a logarithmic scale the secular deformations can be represented by an inclined straight line as shown in figure 19.
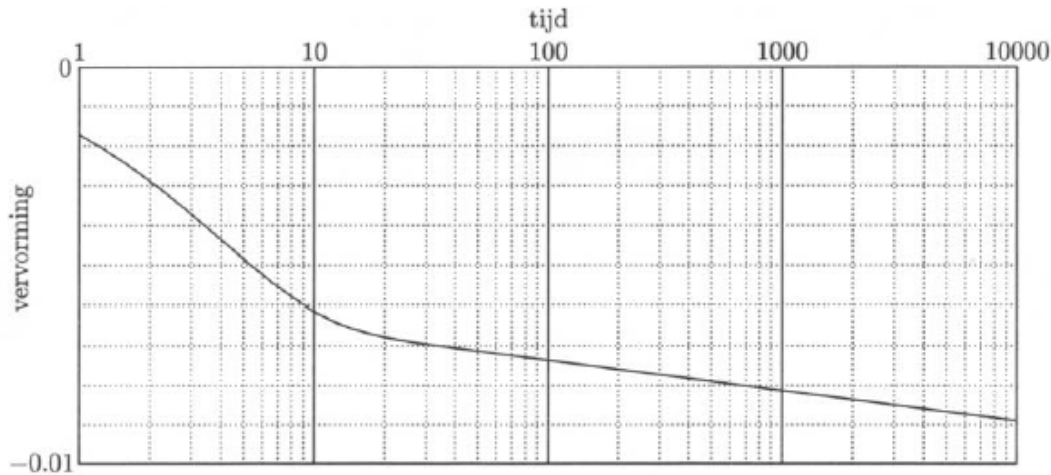
Figure 19 – Secular effect simulated in a consolidation test (Buisman, 1940)

During the first international congress on soil mechanics at Harvard in Cambridge Massachusetts in 1936, he wrote the equation for primary and secondary strain in the form of formula 22.

$$\varepsilon = -\sigma' \cdot \left[\alpha_p + \alpha_s \cdot \log\left(\frac{t}{t_0}\right) \right]$$

(22)

In which the subscripts p and s refers to primary and secondary. Furthermore, notice that the magnitude of the primary and secondary strains depend on the applied load. This may suggest that the relation between stress and strain is linear, which in general is not the case. Therefore, the coefficients α_p and α_s depend upon the applied stress and the stress history.

From a theoretical point of view formula 22 is somewhat peculiar, because when time is extended to infinity the strain would become larger than the thickness of the considered sample. However, the performance of this formula is still useful for common time spans in civil engineering.

<u>Taylor and Merchant's creep formulation</u>
The model formulation by Taylor and Merchant has become well-known, because it was the first attempt to relate creep and instant deformation with deformation due to dissipation of excess pore pressures (Christie, 1964). The theory gave a reasonable description of the phenomenon of secondary compression, which at least provides a partial explanation of the discrepancies that have been observed between full-scale measurements compared to the estimates based on Terzaghi's theory. The equation which was used to describe the combined phenomena is presented in formula 23.

$$\frac{de}{dt} = \frac{\partial e}{\partial t} + \frac{\partial e}{\partial p'} \cdot \frac{dp'}{dt} \tag{23}$$

In which e and p' represent the void ratio and vertical effective stress. The first term on the right describes the creep and the second term reflects the contribution of the direct strains. According to Christie (1964) the creep strains can also be represented with formula 24.

$$\frac{\partial e}{\partial t} = -\mu(CD) \tag{24}$$

The distance between C and D is shown in figure 20, where the distance is a measure for the rate of secondary compression. The μ is a constant, which Taylor and Merchant call the coefficient of secondary compression. In addition, the line A to G describes the initial deformations and the line A to B represents the maximum deformation inclusive creep.

Figure 20 – e versus p relationship for a single pressure increment (Christie, 1964)

<u>Šuklje's isotaches concept</u>
In 1957 professor Šuklje proposed the isotache model in which the compressibility of soft soils is strain rate dependent during both primary and secondary consolidation. In contrast to the conventional models, the isotache model assumes that primary consolidation and secondary compression are not two separate processes, occurring respectively before and after the dissipation of excess pore pressures (Larsson *et al.*, 1997). Šuklje was the first to suggest that the behaviour of soft soil in one-dimensional compression is governed by a unique relation between effective stress, void ratio and rate of change in void ratio as shown in formula 25.

$$R\left(\sigma_v^{'}, e, \frac{\partial e}{\partial t}\right) = 0 \tag{25}$$

The isotache concept is illustrated more clearly in figure 21. This figure shows that Šuklje assumed a parabolic excess pore pressure isochrone. On the basis of this assumption the relations between stress, void ratio and rate of change in void ratio could be specified. Moreover, the model also accounts for the fact that time-dependent deformations are influenced by the thickness of the clay layer, permeability and drainage conditions.
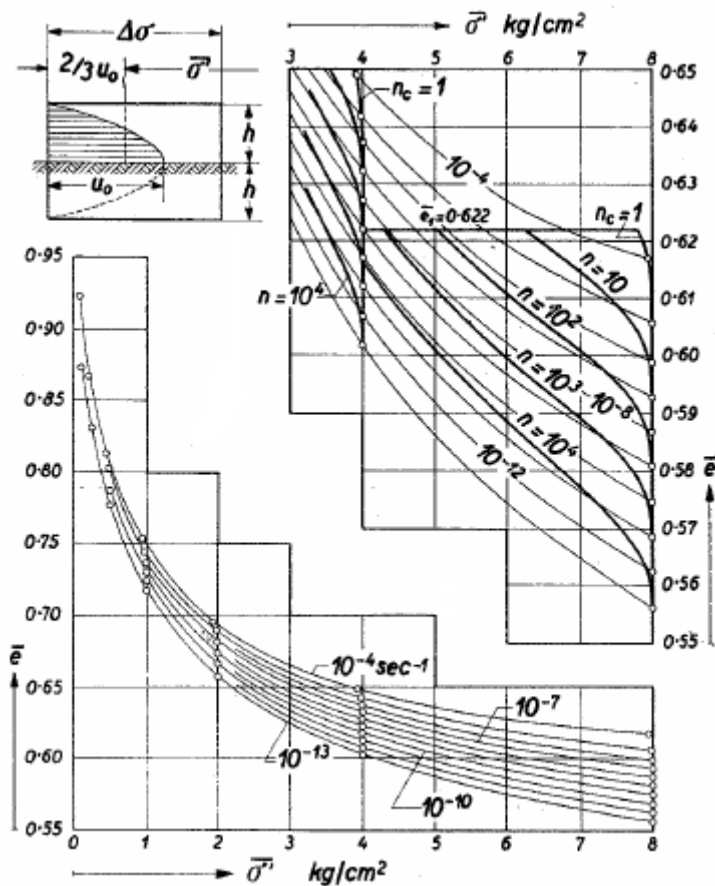
Figure 21 – Isotache concept (Šuklje, 1957)

The lines of equal strain rate are called "isotaches". Šuklje was the first person in soil mechanics who used this term. The stress-strain path can be extrapolated to thicker soil layers with an approximate method. The n is the ratio between real thickness in the field

versus thickness of the sample in the laboratory. Due to this scaling effect, the stress-strain paths of thicker samples are positioned lower in figure 21. Another important notion is the effect of creep in a previous loading step on a new loading step, because it initially decreases the deformation of the new step (Šuklje and Majes, 1989).

The isotache approach proposed by Šuklje is the dominating concept of the models presented over the last 20 to 30 years. Laboratory tests and well documented case histories tend to confirm the validity and the applicability of the model during both primary and secondary consolidation (Leroueil, 2006). Furthermore, Šuklje and Majes (1989) show that the isotache approach can be smoothly implemented into numerical computer programs. For these reasons, a large number of the current models are based on this concept (Garlanger, 1972; Leroueil *et al.*, 1985; Yin and Graham, 1992; Imai, 1989; Den Haan, 1994).

Bjerrum's time lines and equivalent time concept
Bjerrum was director of the Norwegian Geotechnical Institute from 1951 to 1973. He acknowledges that there was a lack of clarity about the distinction between primary and secondary consolidation. Therefore, to remove this lack of clarity the definitions instant compression and delayed compression were postulated (see figure 22). The instant compression occurs simultaneously with the increase in effective pressure and causes a reduction in void ratio (Bjerrum, 1967). The delayed consolidation is independent of the effective stress; it is only affected by the elapsed time. In fact, these new terms clearly describe the reaction of a soft soil with respect to the effective stress. According to Bjerrum (1967) the hydrodynamic period is insignificant for delayed compression at constant effective stress, due to the relatively low rate of volume change. On the contrary, the hydrodynamic period completely governs the magnitude of deformation during instant compression.
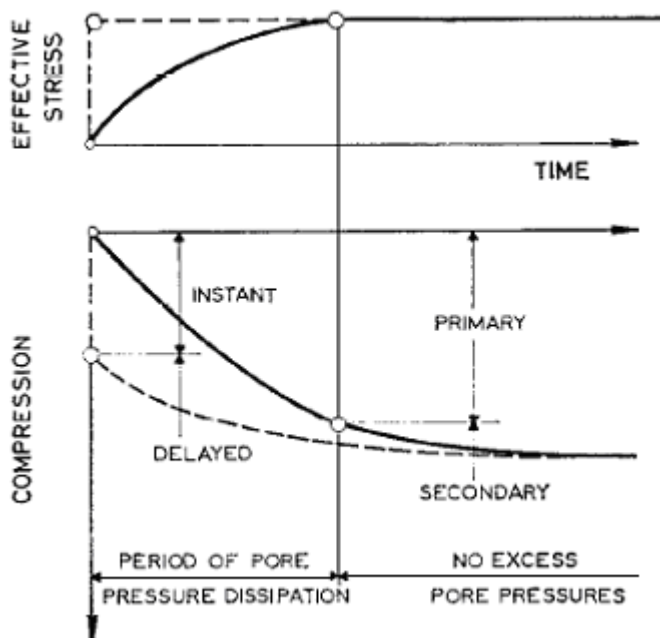
Figure 22 – Definition of instant and delayed compression (Bjerrum, 1967)

These definitions are the basis for the conceptual model presented in figure 23. This model is formulated in a similar fashion to the Šuklje isotache approach, which also assumes that

primary consolidation and secondary compression are not dividable into separate processes. Consequently, the constitutive relationship of Bjerrum's model (see formula 26) is closely related to Šuklje's model (see formula 25).

$$R\left(\sigma_v^{'}, e, t\right) = 0 \tag{26}$$

The only difference between the models is that Bjerrum's model is based on time lines, while Šuklje's model uses lines of equal void ratio. However, it is possible to convert times lines into isotaches. For example, Janbu (1969) defined the term time resistance, which relates a reference time to a particular strain rate. Also Tavenas *et al.* (1978) indicates that a specific strain rate can be easily linked to a single time line. Notice that the relation between isotaches and time lines is not fixed, but dependent on the type of soil. Furthermore, it should be emphasized that Bjerrum's model is primarily intended for deformations that have developed in a geological perspective of time. This means that the model is perfectly suitable to explain the apparent overconsolidation in natural soils due to geological ageing, and to make clear why deformations may occur under structures in spite of the fact the apparent preconsolidation has not been exceeded (Larsson *et al.*, 1997). In practise, the engineer designs structures for time periods of 50 to 100 years, while the model is actually intended to describe deformations from a geological perspective of time. However, from a conceptual point of view this model is still useful to explain the basic principles behind the compression of soils.
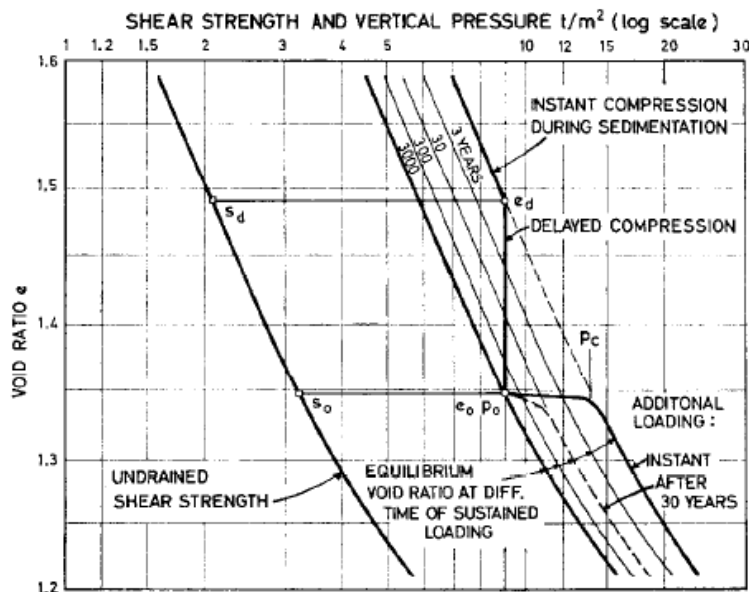
Figure 23 – Compressibility and shear strength of clay exhibiting delayed compression (Bjerrum, 1967)

Figure 23 presents the relationship between void ratio, shear strength and vertical pressure. It can be seen that a soil reacts stiff at the instant compression line, and that the delayed compression takes place at constant vertical pressures. In addition, the model also includes time-dependent increase of shear strength, because the relation between shear strength and the apparent preconsolidation pressure is assumed to remain the same. Notice that this is also the case when the apparent preconsolidation pressure is increased by time-dependent deformations at constant vertical pressure (Larsson and Mattsson, 2003).

2.3.2. *End of primary (EoP) model formulations*

An important question in the time-dependent behaviour of soils is whether or not creep acts as a separate process from consolidation. Ladd *et al.* (1977) postulated two extreme hypotheses, which are:

- Hypothesis A: secondary compression takes place after the primary consolidation. The end of primary (EoP) curve is unique. This means that no creep takes place until almost all pore water pressures have been dissipated.
- Hypothesis B: secondary compression already takes place during primary consolidation. It assumes that some sort of structural viscosity is responsible for creep, which starts already in the primary consolidation phase.

The meaning of these hypotheses for a laboratory and an in-situ condition is graphically shown in figure 24, where the vertical strain is plotted against the logarithms of the vertical effective stress and time. Hypothesis A shows a clear distinction between deformation due to dissipation of excess pore pressure and deformation under constant effective stress. For hypothesis B the strain curve bends immediately due to creep behaviour of the soil. For the first hypothesis the difference between laboratory curve and the in-situ curve can be explained with the quadratic layer thickness effect (Jamiolkowski *et al.*, 1985). In addition, for hypothesis B, the figure show that it is possible that the in-situ curve joins the laboratory curve after some time, which is the result of the generation of creep strains that already start in the primary phase. Notice that the visualization in figure 24 is not fully correct, because hypothesis B should be curved instead of a straight line in the ε_v versus σ_v' plot.
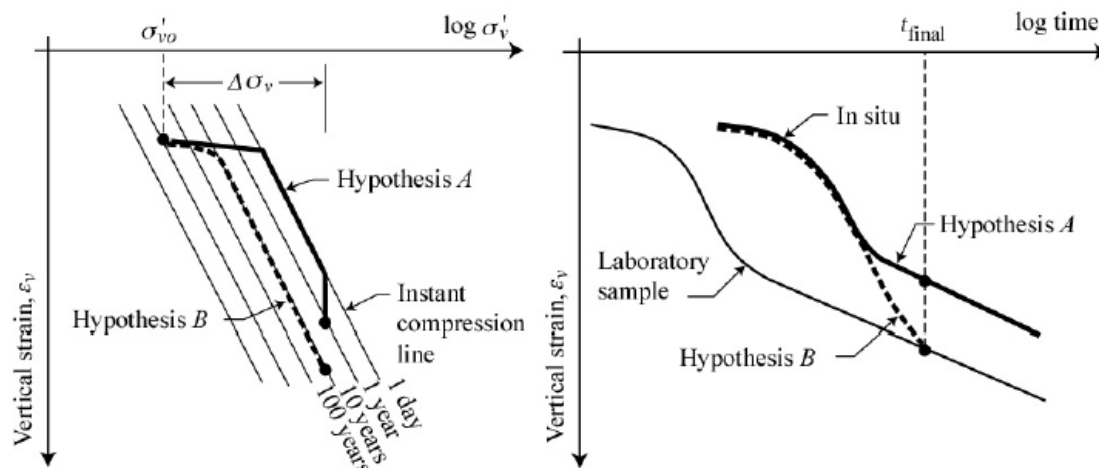
Figure 24 – Consolidation of clay according to hypotheses A and B (Leroueil, 2006)

Mesri and co-workers are supporters of hypothesis A, where deformation due to dissipation of excess pore pressures and creep deformation are seen as distinctive constitutive processes (Mesri and Godlewski, 1977). According to this theory creep deformation is the result of different physical processes, such as the re-orientation of soil particles and distortion of the diffuse double layer. If this strict separation is assumed, it is possible to define a unique EoP curve, which is independent of the duration of the primary consolidation stage. The uniqueness of the EoP is demonstrated in figure 25 for San Francisco Bay Mud. This figure shows the results of three laboratory samples with different heights subjected to the same loading conditions. The considered samples resulted in nearly the same curve, which

indicates that the relation between the void ratio and the vertical effective stress could be independent of the duration of the primary consolidation stage. If this EoP relation is assumed to be valid, it becomes easy to translate a laboratory sample to a field condition.
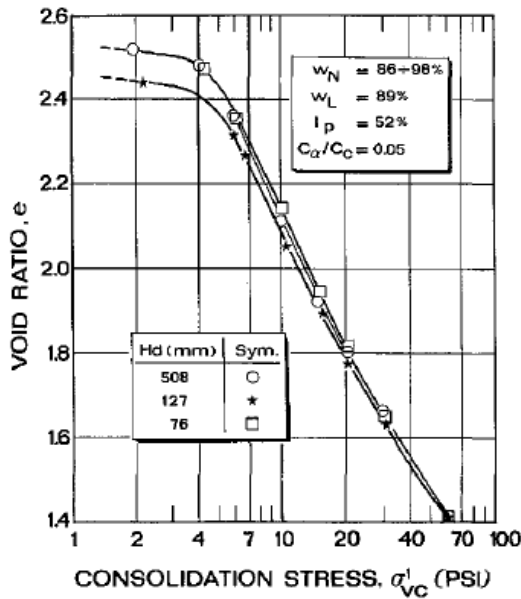
Figure 25 – End of primary curves for San Francisco Bay Mud (Jamiolkowski et al., 1985)

According to Mesri *et al.* (1997) the secondary compression can be determined from an empirical relationship between C_α/C_c. This unique relationship exists for all natural soils, and holds true at any time, effective stress and void ratio during secondary compression (Mesri and Godlewski, 1977). For clays, the C_α/C_c value is equal to 0.04 ±0.01, but is higher for organic soils. Notice that the primary compression index C_c denotes the slope of e versus the logarithm of σ'_v relationship throughout both recompression and compression ranges. According to Mesri and Vardhanabhuti (2005) the magnitude and behaviour of C_α with time is directly related to the magnitude and development of C_c with effective vertical stress. In general, the secondary compression index C_α remains constant, decreases, or increases with time. The size of this value is dependent on the current effective stress and the stress history of the soil. In the case where the current effective stress level equals the preconsolidation pressure, the C_α increases significantly due to the transition from recompression to compression (Mesri *et al.*, 1997). However, if the vertical effective stress is beyond two times the preconsolidation pressure the slope of the EoP curve gradually decreases with stress. According to Terzaghi *et al.* (1996) the cause of this decline can be found in the decreasing permeability of the soil with increasing values of vertical effective stress. However, for most practical purposes the secondary compression index can be assumed to be a constant value with time.

The interrelationship between primary consolidation and secondary compression can also be expressed mathematically. The most general constitutive equation for one-dimensional consolidation is given in formula 27.

$$\frac{de}{dt} = \left(\frac{\partial e}{\partial \sigma'}\right)_t \cdot \left(\frac{\partial \sigma'}{\partial t}\right) + \left(\frac{\partial e}{\partial t}\right)_{\sigma'} \qquad (27)$$

In which the term $(\partial e/\partial\sigma')_t$ represents the compressibility of the soil structure with effective stress, and combined with $(\partial\sigma'/\partial t)$ it describes the void ratio decrease with time associated with an effective stress increase. The other term $(\partial e/\partial t)_{\sigma'}$ represents the compressibility of the soil structure with time, which actually describes the creep action. This equation can be integrated to obtain the change in void ratio as shown in formula 28.

$$\Delta e = \int_0^t \left[\left(\frac{\partial e}{\partial \sigma'} \right)_t \cdot \left(\frac{\partial \sigma'}{\partial t} \right) + \left(\frac{\partial e}{\partial t} \right)_{\sigma'} \right] dt \tag{28}$$

If the EoP theory is assumed where separate and independent mechanisms control $(\delta e/\delta\sigma')_t$ and $(\delta e/\delta t)_{\sigma'}$ equation 25 can be rewritten into formula 29 (Mesri and Choi, 1985).

$$\Delta e = \int_0^{t_p} \left[\left(\frac{\partial e}{\partial \sigma'} \right)_t \cdot \left(\frac{\partial \sigma'}{\partial t} \right) + \left(\frac{\partial e}{\partial t} \right)_{\sigma'} \right] dt + \int_{t_p}^t \left(\frac{\partial e}{\partial t} \right)_{\sigma'} dt \tag{29}$$

The time span for zero till t_p represents the primary consolidation stage; during this stage the term $(\delta\sigma'/\delta t)$ is not equal to zero and $(\delta e/\delta t)_{\sigma'}$ is assumed to be negligible. It is important to state that there is no proper scientific proof for this assumption. The time beyond t_p is the secondary compression stage, in which the term $(d\sigma'/dt)$ is zero. A graphical sketch of these stages is shown in figure 26. Notice that the separated integral will inevitably leads to a discontinuity in the e versus t curve.
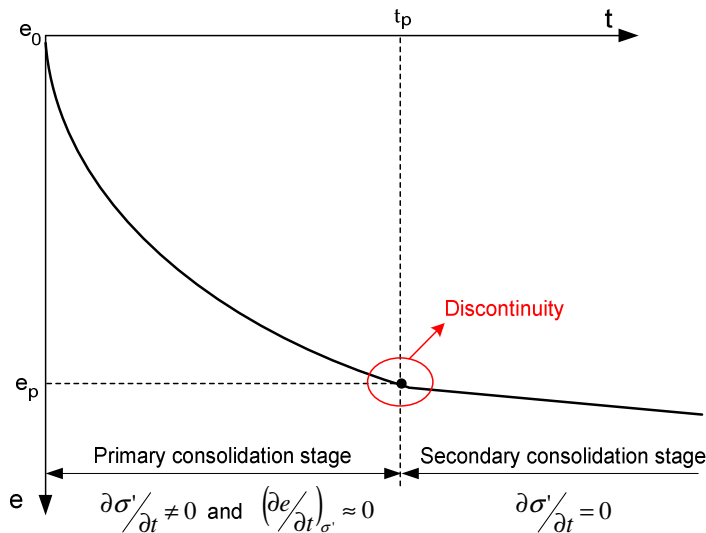
Figure 26 – Consolidation stages (Mesri and Choi, 1985)

This mathematical formulation has been implemented in the program Illicon, which was developed at the University of Illinois during the 1980's. This program has been used to back calculate the measured settlements of the Skå Edeby test embankment (Terzaghi *et al.*, 1996)

In spite of the seemingly good results considerable amounts of criticism have been expressed on the mathematical formulation of the EoP theory (Schiffman *et al.*, 1987; Kabbaj *et al.*, 1988; Imai, 1989; Leroueil, 2006). According to Schiffman *et al.* (1987) and Imai (1989) the mass

balance is not completely satisfied, which was claimed to be satisfied by Mesri and Godlewski (1977). In addition, Kabbaj *et al.* (1988) examined the performance of four test embankments, and concluded that the in-situ vertical strain is larger than the vertical strain measured in the laboratory. This indicates that the EoP concept is not fully correct, and that the in-situ soil behaviour is not completely in line with hypothesis A. The strain rate dependency during primary consolidation and secondary compression is also emphasized by Leroueil (2006) as presented in figure 27. The findings show that the strain rates observed in-situ vary from 10^{-8} to 10^{-10} s^{-1}, while the laboratory strain rates range from 10^{-5} to 10^{-8} s^{-1}.
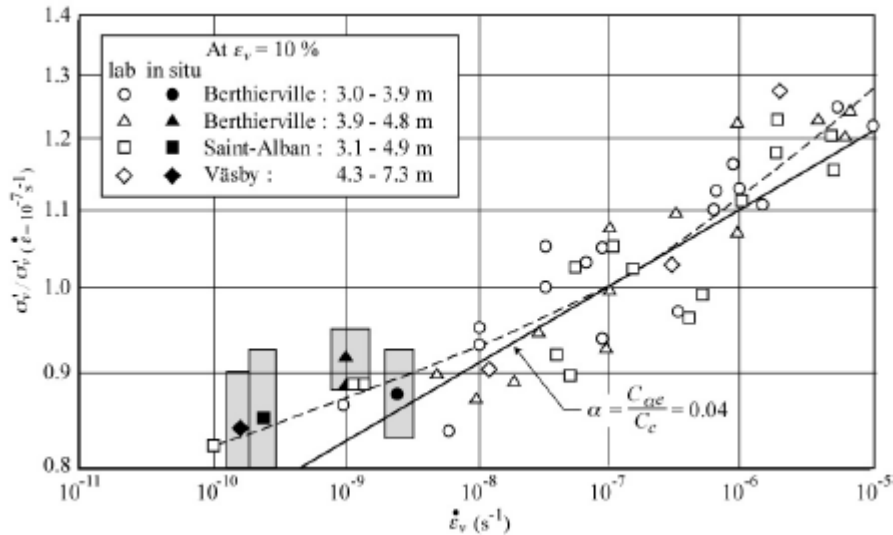
Figure 27 – Normalized stress-strain rate relations at a strain of 10% (Leroueil, 2006)

Probably due to the simplicity of the EoP principles, this concept is still quite often used in the daily geotechnical practice. However, in the academic practice the EoP concept is barely advocated, and elasto-viscoplastic (EVP) model formulations are much more accepted. Some of them will be discussed in the next subsection.

2.3.3. Elasto-viscoplastic (EVP) model formulations

The elasto-viscoplastic (EVP) modelling concept indicates that there is a significant development of creep deformation during primary consolidation, which implies that the stress-strain curves obtained in-situ are different from those obtained in laboratory. The deformation measured at the end of primary consolidation is smaller in-situ than the measured values from oedometer tests (Kabbaj *et al.*, 1988). This behaviour is in line with what Ladd *et al.* (1977) calls hypothesis B as discussed at the beginning of subsection 2.3.2.

The separated formulation of primary consolidation and secondary compression caused significant confusion. Mesri and co-workers have assumed that the excess pore pressures dissipate during the primary consolidation phase, and creep only occurs in the secondary compression phase (Ladd *et al.*, 1977; Jamiolkowski *et al.*, 1985; Mesri and Choi, 1985). In these models it is difficult to define the transition time from consolidation to creep; is it for 95%, 99% or 100% degree of consolidation. If 100% is chosen creep will almost not exist, which is not likely for most soft soils. This vagueness is emphasized by Landva and La Rochelle (1982), they state that it is barely possible to distinguish between primary and

secondary consolidation. In the EoP theory the mechanisms consolidation and creep are treated as different constitutive phenomena. This is the crucial difference with the EVP model formulations (Leroueil *et al.*, 1985; Kabbaj *et al.* (1988); Yin and Graham, 1994; Kim and Leroueil, 2001). Notice that these elasto-viscoplastic model formulations are particular cases of the isotache model proposed by Šuklje (1957). The term isotache refers to a constitutive relationship between vertical effective stress, strain (or void ratio) and strain rate (or rate of change in void ratio) as shown in formula 30.

$$R\left(\sigma_v^{'}, \varepsilon, \partial\varepsilon/\partial t\right) \ or \ \left(\sigma_v^{'}, e, \partial e/\partial t\right) = 0 \tag{30}$$

Originally, Šuklje (1957) described the isotaches in terms of void ratios, while the more recent isotache models use a strain formulation (Leroueil *et al.*, 1985; Den Haan, 1994). The benefit of the strain formulation is that the problem of initial void ratio differences on experimental results has been removed. However, the strain variant is equivalent to the void ratio variant, and the relation between strain and void ratio is shown in formula 31.

$$\varepsilon = \frac{\partial e}{1 + e_0} \tag{31}$$

The EVP model formulations assume that the rate of strain with respect to time at any state point (σ'_v, ε_v) can be expressed as the sum of an elastic strain rate component and a viscoplastic strain rate component as shown in formula 32.

$$\partial\varepsilon_v/\partial t = \partial\varepsilon_v^e/\partial t + \partial\varepsilon_v^{vp}/\partial t \tag{32}$$

The elastic and viscoplastic components are graphically presented in figure 28. The figure shows a clear distinction between elastic and viscoplastic strains by means of a kink at the preconsolidation pressure. Notice that the viscoplastic strains are the result of volume changes due to excess pore water dissipation and viscous soil behaviour (Kabbaj *et al.*, 1986).
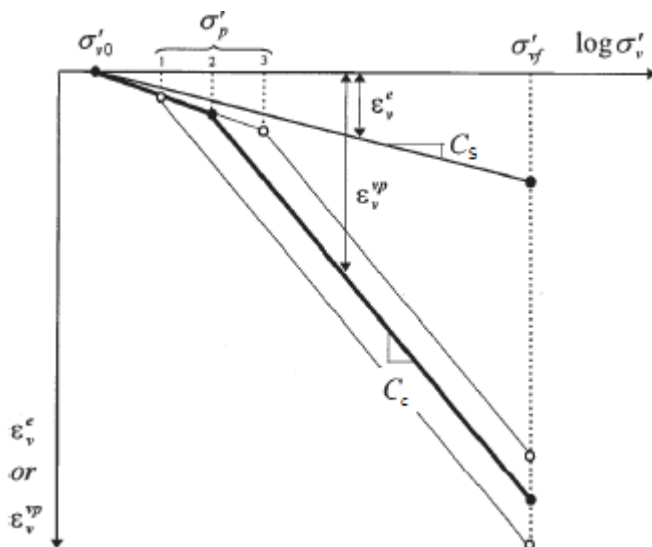
Figure 28 – Stress strain relation (Kim and Leroueil, 2001)

The total strain can easily be obtained by integration of equation 32 as shown in formula 33.

$$\varepsilon_v = \int_0^t \left(\frac{\partial \varepsilon_v^e}{\partial t} + \frac{\partial \varepsilon_v^{vp}}{\partial t} \right) dt \tag{33}$$

As a result of the elasto-viscoplastic model formulation the integral does not have to split up into a primary consolidation and secondary consolidation integral. This is in glaring contrast to the EoP model formulation as shown in formula 29.

The remaining part of this subsection elaborates on two popular isotache model formulations. The first model is the isotache model proposed by Leroueil *et al.* (1985); this model concentrates mainly on the development of the viscoplastic strains. This model is therefore principally suitable to describe compression in the normally consolidated region (Kim and Leroueil, 2001). The other elasto-viscoplastic model which is presented is the a,b,c isotache model developed by Den Haan (1994). An important difference between the considered models is that the latter has a natural strain formulation, while the first applies a linear strain formulation.

Isotache model proposed by Leroueil and co-workers
To analyze the effects of strain rate and viscoplastic strain on the consolidation process of natural soils, Leroueil *et al.* (1985) proposed a non-linear viscoplastic model in which viscoplastic behaviour is controlled by a unique relationship between effective stress, strain and strain rate. The model can be considered as a particular case of the isotache model proposed by Šuklje (1957). This model is described by two curves, one giving the variation of the preconsolidation pressure with the rate of strain, and the other plots the vertical strain against the vertical effective stress normalized with respect to the preconsolidation pressure at the particular strain rate. Once these curves are known for a given soil, any relation between stress, strain and strain rate can be easily reconstructed as shown in figure 29.
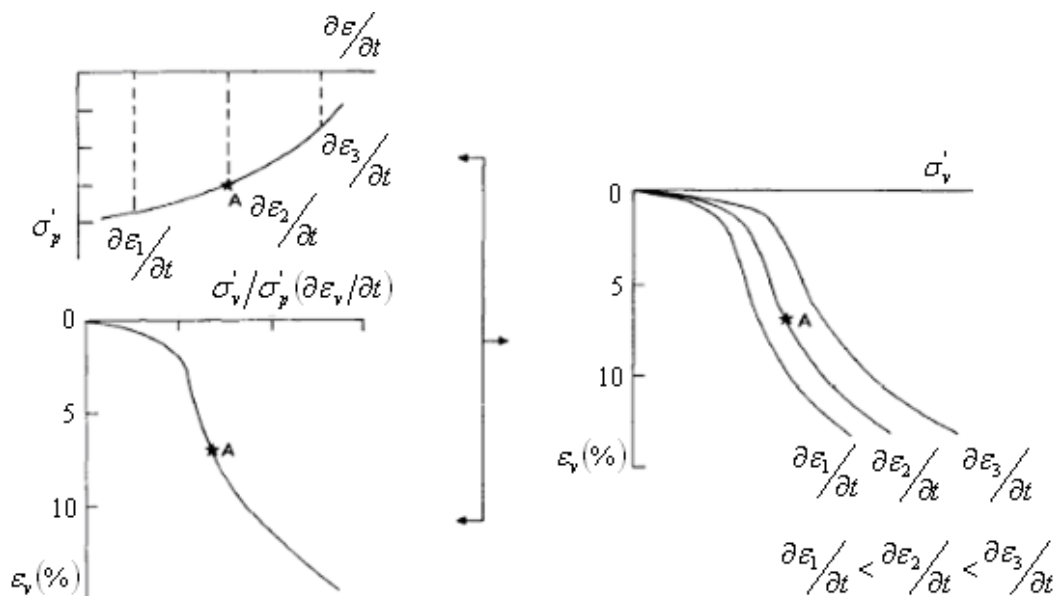
Figure 29 – Suggested rheological model for natural clay (Leroueil et al., 1985)

Figure 29 shows that the isotaches are written in terms of strain, and give a description of the complete compression curve. The isotaches are normalized for the preconsolidation stress, which implies that they are dependent on the rate of strain. The findings also indicate that a higher strain rate results in a higher vertical effective stress, which seems to be consistent with the expectations. The model was first applied to a variety of laboratory tests (long-term creep tests, multi-stage loading tests and relaxation tests). This investigation has shown that the observed behaviour matches closely with the proposed rheological model (Leroueil *et al.*, 1985; Kabbaj *et al.*, 1986). Figure 30 shows an example for St. Césaire clay from Quebec Canada. The results indicate a unique relationship between stress, strain and strain rates, which are usually encountered in laboratory.
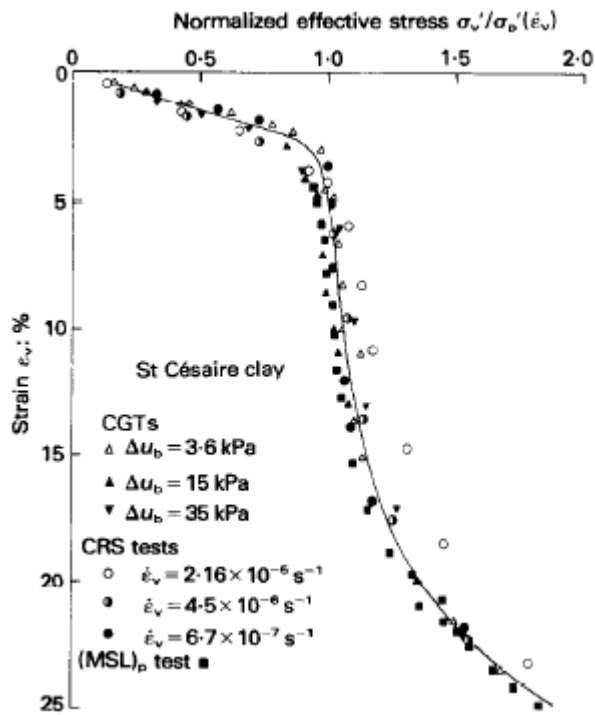
Figure 30 – Normalized σ′ᵥ versus εᵥ relationship for St. Césaire clay (Leroueil et al., 1985)

However, the findings indicate that for unusual strain rates of 2.16 10^{-5} s^{-1} and higher; the unique relation between stress, strain and strain rate is not applicable anymore. Two plausible explanations are possible. Firstly, due to the natural variability of the soil (i.e. variations in water content and grain size distributions). Secondly, due to thixotropic hardening that could occur at these high strain rates (Leroueil *et al.*, 1985).

The experimental data presented above is a confirmation that the rheological behaviour of natural clays can be described by formulas 34 and 35.

$$\sigma_p^{'} = f\left(\frac{\partial \varepsilon_v}{\partial t} \right) \tag{34}$$

$$\frac{\sigma_v^{'}}{\sigma_p^{'}} = g\left(\varepsilon_v \right) \tag{35}$$

In which function f indicates that the preconsolidation pressure is dependent on the rate of vertical strain. The function g is used to advocate that there is a relationship between the ratio of stresses and vertical strain. Once these two relationships are known for a given soil, any relation between stress, strain and strain rate can be easily reconstructed. Moreover, these equations can be combined (see formula 36) to obtain the general rheological as proposed by Leroueil *et al.* (1985).

$$\partial \varepsilon / \partial t = f^{-1}\left(\sigma_v' / g(\varepsilon_v) \right)$$ (36)

This formula can also be used directly in numerical models to analyse consolidation problems of various natural soft soils (Kim and Leroueil, 2001). It should be kept in mind that this rheological model has a limitation at high strain rates. However, this should not be a problem in practise, because the strain rates observed in the field are in most cases much lower than the rates used in the laboratory as shown in figure 27.

Isotache model proposed by Den Haan

The a,b,c isotache model also describes a unique relationship between vertical effective stress, strain and rate of strain (Den Haan, 1994). The total strain can be obtained by adding the direct rate of strain with the secular rate of strain. These terms are similar to the instant and delayed compression that are proposed by Bjerrum (1967). They are believed to be more accurate than the terms primary consolidation and secondary compression as used in the EoP theory, because these refer to consecutive processes.

Before the principles of the a,b,c isotache model are discussed, the subsection starts with the isotache formulation of Yin and Graham (1989; 1994). If this model is properly understood, it will become easier to comprehend the principles behind the isotache model proposed by Den Haan (1994). It is important to state that the Yin and Graham's model uses the concept of equivalent times, while Den Haan uses isotaches that refer to a particular rate of secular strain. Both concepts are interrelated, which means that an equivalent time can be translated to a unique secular rate of strain. Larger equivalent times are associated with smaller rates of secular strain. The equivalent time is thus a mathematical tool used for scaling creep strains. An illustration of the equivalent time lines concept is given in figure 31. The figure shows that the rate of secular strain is bounded by a limit time line; at this line the creep strains are equal to zero. In a more recent publication Yin *et al.* (2002) replaced the logarithmic secular strain function for a hyperbolic secular strain function. In that case a limit time line definition is not required, because a hyperbolic function asymptotically converges to an end value. Furthermore, the instant time line and reference time line are analogous to the κ and λ line used in the critical state theory (Roscoe *et al.*, 1958; Schofield and Wroth, 1968). The κ line is used to describe the elastic strains, which is comparable to the direct strain used in the a,b,c isotache model. The λ line is used to describe plastic strains. Notice that this line does not incorporate any viscosity yet.
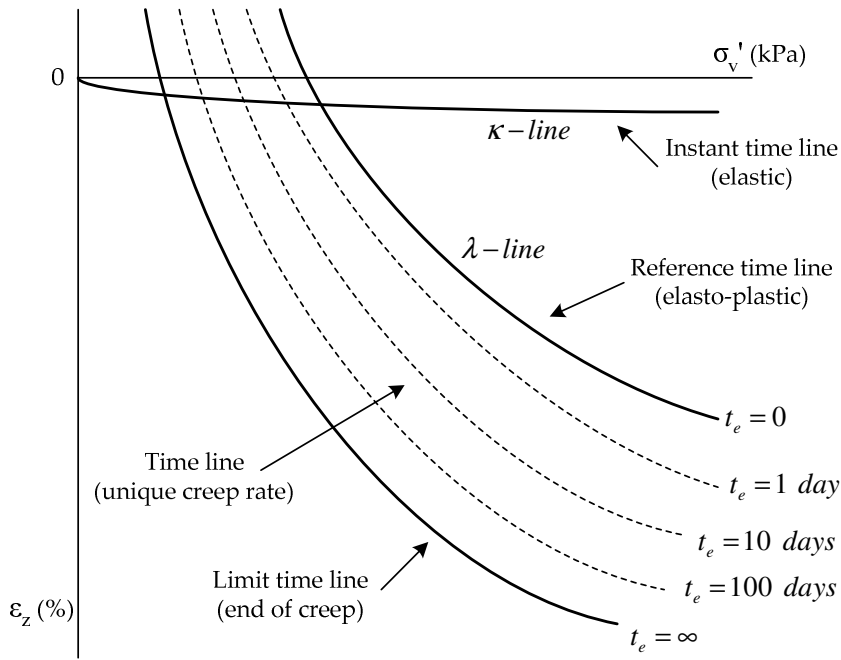
Figure 31 – Illustration of the equivalent time lines concept (Yin and Graham, 1994)

The principles of the a,b,c isotache model are graphically given in figure 32. In this figure the direct strain and the secular strain are plotted against the vertical effective stress. The direct strain is due to changes in effective stress, while the secular strain is progressing with time. The graph shows that the lines of equal rate of secular strain are called isotaches, which are approximately similar to the equivalent time lines of Yin and Graham (1994). Also observe that the reference rate of secular strain is linked to the preconsolidation stress.
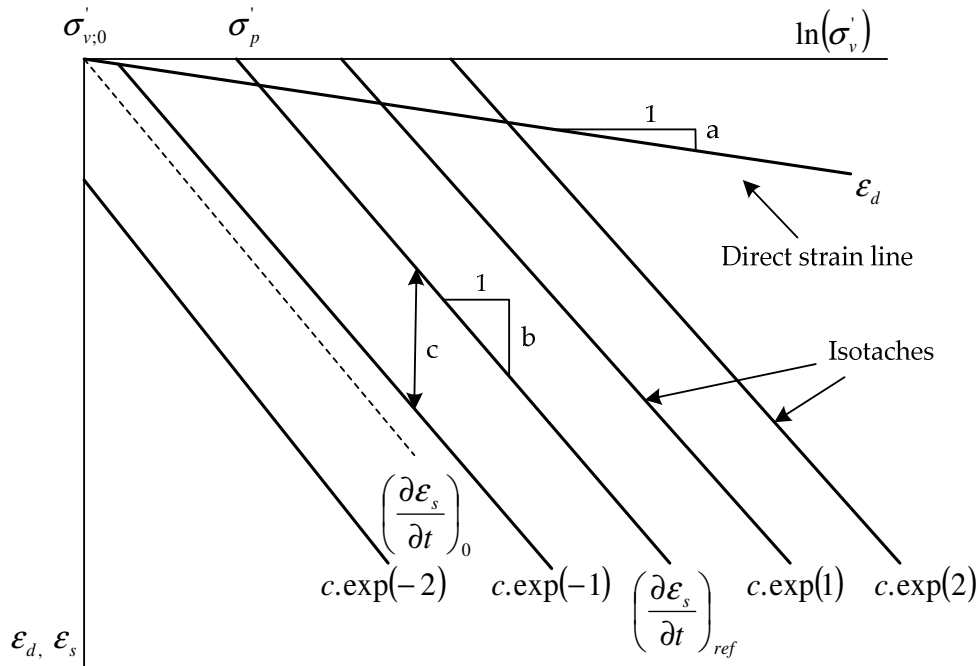
Figure 32 – Principles of the a,b,c isotache model (Den Haan, 1996)

The mathematical formulation of the direct strain and secular strain are based on Den Haan and Sellmeijer (2000). The direct strain is obtained from the change in vertical effective stress as shown in formula 37. The rate of direct strain, which is the derivative of direct strain, is presented in formula 38.

$$\varepsilon_d = a \cdot \ln\left(\sigma_v' \Big/ \sigma_{v;0}'\right) \tag{37}$$

$$\dot{\varepsilon}_d = \frac{a}{\sigma_v'} \cdot \frac{\partial \sigma_v'}{\partial t} \tag{38}$$

In which a and $\sigma_{v;0}'$ represent respectively the direct compression index and the initial vertical effective stress.

The secular strain and the secular rate of strain are given in formulas 39 and 40. Notice that formula 39 has a stress component but also a time dependent component.

$$\varepsilon_s = (b-a) \cdot \ln\left(\sigma_v' \Big/ \sigma_{v;0}'\right) - c \cdot \ln\left(\dot{\varepsilon}_s \Big/ \dot{\varepsilon}_{s;0}\right) \tag{39}$$

$$\dot{\varepsilon}_s = \dot{\varepsilon}_{s;0} \cdot \left(\sigma_v' \Big/ \sigma_{v;0}'\right)^{\frac{b-a}{c}} \cdot \exp\left(-\varepsilon_s \Big/ c\right) \tag{40}$$

Soil parameters b and c are representing the secular compression index and the coefficient of rate of secular compression. The initial rate of secular deformation can be related to a fixed reference rate at reference value of stress. For the reference rate of initial rate of secular strain Den Haan (2001) uses ratio between c and τ_{ref}. The τ_{ref} is the reference intrinsic time that would be required to obtain the present compression; this is mostly assumed to be 1 day, referring to the oedometer test with loading steps of 24 hours. Servais (2006) shows that it is convenient to use the preconsolidation pressure as reference value of stress. Through this assumption the ratio of stresses simplifies to 1/OCR. As a result, equation 40 can be rewritten into formula 41.

$$\dot{\varepsilon}_s = c \Big/ \tau_{ref} \cdot \left(1 \Big/ OCR\right)^{\frac{b-a}{c}} \cdot \exp\left(-\varepsilon_s \Big/ c\right) \tag{41}$$

The total strain or total rate of strain can be easily found when the direct strain and secular strain are added up. In addition, in the preceding derivations the strain formulations have been used without an explicit definition. Den Haan (1994) uses a natural strain formulation, which is also known as Hencky strain. Natural strains are determined by taking the incremental deformation relative to the present height. Conventionally, most models use a linear strain formulation, which is attributed to Cauchy. Examples of models that use a linear strain formulation are the Bjerrum model (1967, 1973) and Yin and Graham (1989, 1994). The strains are in this case calculated with respect to their initial height. It is important to state that all these models are isotache models, which should produce nearly similar results when

the right parameters are used. However, the strain formulations tend to deviate at large volumetric strains as shown in figure 33. It shows the results of an oedometer test on a Holocene peat sample from the A2 road widening project. This sample had an initial water content of 800% and a bulk density of 9.6 kN/m³.
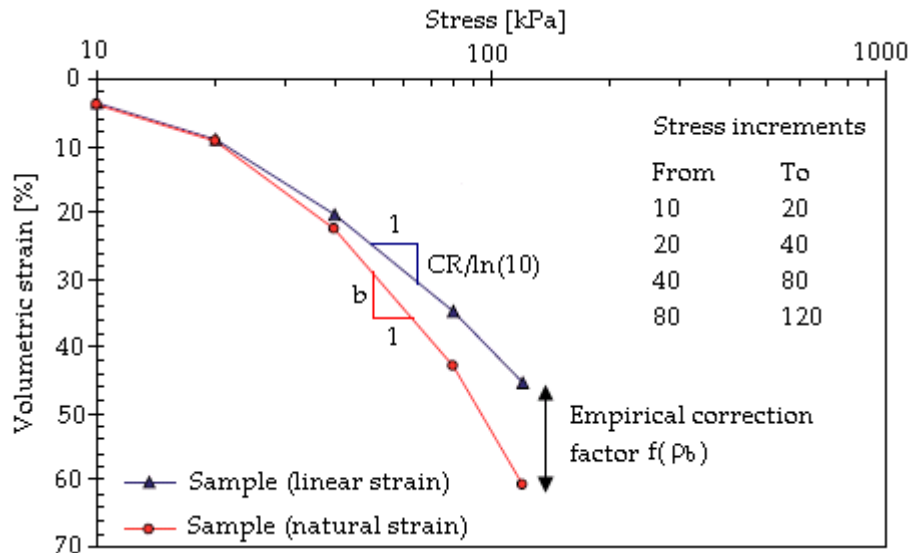
Figure 33 – Stress-strain curve with a linear and a natural strain formulation (Dykstra et al., 2009)

The figure above shows that the difference between linear and natural strains becomes significant for strains larger than 20%. In practice the strains are often smaller than 20%. In this range the stress-strain relations for both formulations follow nearly a similar path. However, for very soft clays and highly compressible peats it is possible that the strain reaches a value of 50% or even more (Landva and La Rochelle, 1982). In such a situation the slope difference between linear and natural strains becomes significant. The question arises then which strain formulation is the most appropriate for describing large strains (ε>20%). Dykstra *et al.* (2009) indicates that both strain formulations have different limitations. The linear strain formulation allows strains larger than 100%, while the natural strain allows void ratios to be become infinitely small. This means that no definite answer can be given for the most suitable strains formulation for large strains. More information about the conversion from a linear strain parameter CR to natural strain parameter b and vice versa is given in paragraph 3.3.3. Notice that an empirical correction factor is required to correct for the slope difference, which is related to the bulk density (more info is given in section 3.3.3).

2.4. Anisotropic behaviour of natural soft soils

Many soft soil strata have been deposited over areas of large lateral extent, and the deformations they have experienced subsequent to deposition have been essentially one-dimensional. The consequence is that material properties are different in the horizontal and vertical directions (Lings *et al.*, 2002). This means that the behaviour of natural soil departs significantly from isotropy, where the soil response is assumed to be independent on the orientation of the principal stresses. Anisotropy refers thus to any directional dependence in a material property. The anisotropic soil behaviour affects material properties such as strength, stiffness and permeability. Their anisotropy is believed to come from the micro-

structure of soils, including their particle arrangements, void distributions and nature of contact between particles (Atkinson *et al.*, 1990). These features reflect the soils origin and depositional and post-depositional environments. According to Zdravković and Jardine (2001) it would not be possible to predict ground movements or pore water pressure generation accurately, without accounting for anisotropy in the modelling of soil behaviour.

Constitutive soil models developed in the last 30 years have mainly considered soil to be isotropic; these models assume the strength, stiffness and permeability parameters to be similar in any direction. Anisotropic models have been rarely used because the input parameters are difficult to obtain, which is actually the result of the inability of the conventional laboratory equipment to investigate such behaviour (Zwanenburg and Barends, 2005). However, recent developments, such as the hollow cylinder apparatus and the axial shear apparatus enable us to investigate soil behaviour more into detail, so that the anisotropic parameters can be determined in a consistent way (Molenkamp and Heshmati, 1998; Zdravković and Jardine, 2001).

In relation to the subject of this thesis, to improve the prediction of horizontal deformations, it seems necessary to include the anisotropy of soils. According to Tavenas *et al.* (1979) anisotropic behaviour should be included, especially during the consolidation stage, to increase the predictability of the long-term horizontal deformations. An example of the effect of anisotropy on the undrained shear strength under an embankment is shown in figure 34.
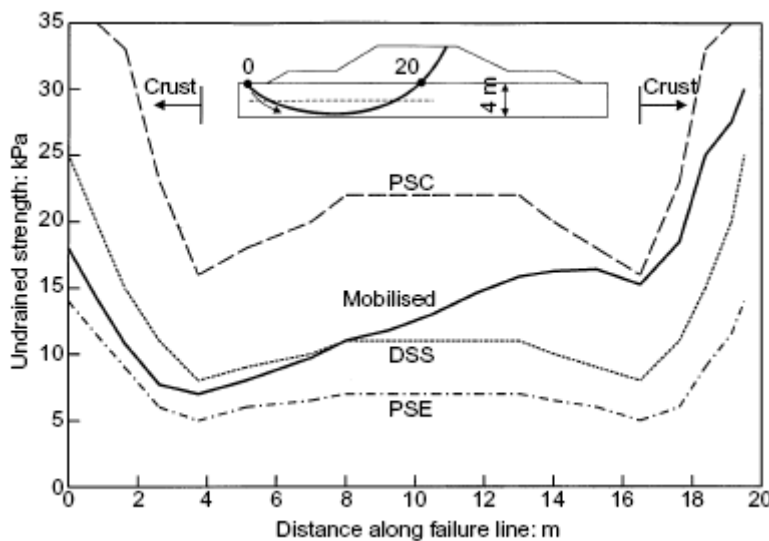
Figure 34 – Mobilized and available undrained strength along failure surface (Zdravković et al., 2002)

The abbreviations PSC, DSS and PSE represent the undrained shear strength under plane strain compression, direct simple shear and plane strain extension. It can be concluded that different stress conditions result in distinctive undrained shear strength distributions. The mobilized shear strength distribution does not follow a particular stress condition, because the embankment imposes large rotations of the principle stresses in the foundation soil. This mobilized undrained shear strength distribution confirms thus that the subsoil is highly anisotropic. The remaining part of this paragraph discusses the effects of anisotropy in strength, stiffness and permeability on the behaviour of soils. The paragraph closes with a short discussion on how anisotropy can be implemented in the models.

2.4.1. *Effects of anisotropy in strength, stiffness and permeability on the behaviour of soils*

As emphasized in the introduction, anisotropy seems to be an important feature in the description of natural soft soils. It starts with a discussion of the effects of anisotropy on the strength parameters. Notice that the effects are evaluated on the drained strength but also on the undrained strength. The subsequent part deals with the effects of anisotropy on the stiffness parameters. Zwanenburg and Barends (2005) explain that the incorporation of stiffness anisotropy is especially important in peaty soils. This is due to the fibrous nature of peat; a difference can be expected in the directions parallel and perpendicular to the fibres. Finally, the effects of anisotropy on the permeability of natural soft soils are analyzed. For most natural soft soils the permeability in vertical and horizontal directions are not the same. This was already recognized by Lumb and Wong (1971); they stated that the drainage in horizontal direction is generally more rapid than in the vertical direction.

Anisotropy and strength
In the 6th Rankine lecture Bishop (1966) already shows that the undrained shear strength was dependent on the principal stress directions. This paper shows that different values are found in the undrained shear strength for the direct shear test and the triaxial compression test. According to Bishop (1966) these differences overshadow refinement in our methods of analysis, and are an indication that we might need to rethink about the way we determine the undrained shear strength. The strength parameters should be evaluated with the correct orientation, or empirical factors have to be applied to the strength results obtained from the conventional laboratory tests.

An extensive investigation of the effect of strength anisotropy on the behaviour of embankments on soft grounds was performed by Zdravković *et al.* (2002). They investigate the test embankments built on soft Champlain clay deposits, which are located in eastern Canada. The laboratory experiments indicate that the magnitude of the undrained shear strength is dependent on the orientation of the major principle stress. For example, the undrained shear strength in a triaxial compression test was significantly higher than in a direct simple shear test. This strength anisotropy is mainly the result of the difference in orientation of the major principal stress to the vertical when the soil is sheared. Zdravković and Jardine (2001) describe the orientation to the vertical with angle α. Most soils exhibit maximum strength when α is equal to zero, and decays as α increases. Therefore, the triaxial compression strength (α=0°) is significantly higher than the simple shear strength ($\alpha\approx45°$). However, the directional dependent stress-strain behaviour cannot be investigated in detail using the conventional laboratory equipment. A more suitable device as already mentioned is the hollow cylinder apparatus, which is capable to measure α continuously between 0° and 90° (Hight *et al.*, 1997). This allows a wide range of engineering problems to be analyzed that could not be simulated with triaxial or plane strain devices completely. Figure 35 shows the results of four soil samples, which are tested in the hollow cylinder apparatus. The abbreviations KSS, HK, HRS and HPF4 stand for a mixture clay-silt-sand, clay-sand, sand and dense silt. These experiments reveal that all considered soils have a strong relation with angle α, which implies that they are strongly anisotropic.
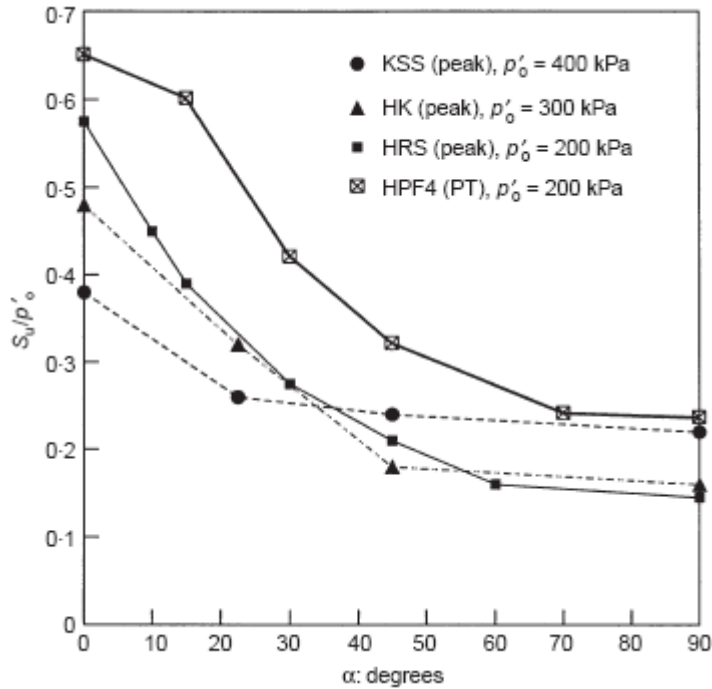
Figure 35 – Anisotropy of the undrained shear strength for 4 K₀-consolidated soils (Hight et al., 1997)

In addition, Nishimura (2005) explained the difference in strength anisotropy between the effective strength parameters and total strength parameters for London clay. The findings were remarkable, because no significant differences were observed in the effective strength parameters ϕ' and c' for vertical and horizontal cut specimens in triaxial compression. However, large differences were observed for undrained shear strength c_u. Nishimura (2005) concluded therefore that the strength anisotropy of London clay was solely the result of the pore water pressure behaviour. The same conclusion could be drawn from the data obtained by Yimsiri (2001), who also conducted a series of triaxial compression tests with vertically and horizontally cut specimens on a number of clayey soils.

Anisotropy and stiffness
For a more accurate calculation of the horizontal soil deformations in natural soft soils, it is desirable to incorporate the stiffness in anisotropy, because the difference between vertical and horizontal stiffness could be significant. For example, Nishimura (2005) shows that the ratio between the vertical and horizontal Young's moduli varied between 1.1 and 2.0 for London clay. A higher stiffness ratio was reported by Lings *et al.* (2000) for Gault clay, which is lightly overconsolidated clay located near Cambridge. They performed several triaxial tests on horizontally and vertically cut samples, and found vertical to horizontal stiffness ratios of approximately 4.0. Both investigations indicate that the stiffness of soft soils is anisotropic. However, it is important to state that the investigation of Lings *et al.* (2000) was only valid for small strains.

Zwanenburg and Barends (2005) have investigated the stiffness anisotropy in peaty soils. They show that there are three optional causes for peat to behave anisotropic. First is the anisotropy due to the structure of peat. The stiffness in the main fibre direction differs from the stiffness perpendicular to the fibres, because it is assumed that the fibres are mainly orientated in the horizontal plane. Notice that this is also known as structural anisotropy.

The second is a load-induced anisotropy. Since peat is a soft and compressible material, the stiffness depends on the stress level or even on the rate of compression. For this reason, a large axial compaction increases the rate of anisotropy considerably. The third option originates from a difference in loading and unloading conditions. When a sample is reloaded after an unloading step, the soil reacts differently in horizontal and vertical direction than during a virgin loading.

Material models that include anisotropic behaviour are not commonly available in the daily geotechnical practise. It is plausible that the stiffness properties of most natural soft soils have at least some degree of anisotropy. For instance, in peaty soils the horizontal stiffness increases faster during compaction than the vertical stiffness, which is mainly the result of the radial pre-stressing of the fibres (Zwanenburg and Barends, 2005). However, in literature, there are some models which simulate anisotropic soils behaviour with cross-anisotropy (Lumb and Wong, 1971; Nishimura, 2005). This means that the soil properties and the soil response are the same in the lateral directions, but different from those in vertical direction. Notice that this assumption reduces the complexity substantially, because to fully describe anisotropic behaviour 21 elastic constants are needed, while cross-anisotropy only requires 5 elastic constants (Graham and Houlsby, 1983).

Anisotropy and permeability
For almost all natural soft soils there is a considerable difference in the horizontal and vertical permeability. In extreme cases, Beckwith *et al.* (2003) indicate that the horizontal permeability of a bog peat could be hundred times larger than the vertical permeability. Therefore, it seems to be clear that the direction and quantity of the groundwater flow differs markedly from that in isotropic and homogeneous media. More evidence for anisotropy in permeability is pointed out by Lumb and Wong (1971) for a circular footing on a layer of clay. Figure 36 shows that significant errors can occur when anisotropy is ignored in the permeability parameters. A limitation of this model is that the soil stiffness is assumed to be a constant value, while in reality the stiffness is expected to increase during consolidation.
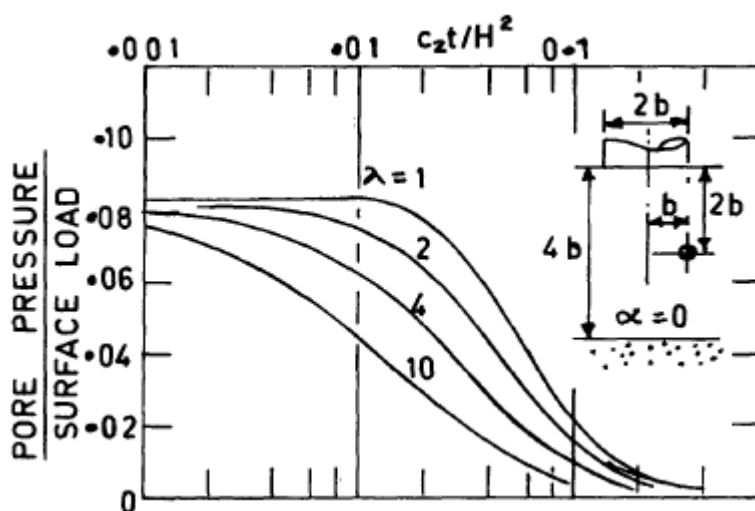
Figure 36 – Effect of anisotropy at a point off axis (Lumb and Wong, 1971)

The λ parameter gives the relation between the vertical and horizontal permeability. For example, a λ of 10 means that the horizontal permeability is 10 times larger than the vertical

permeability. For an isotropic soil λ is equal to one. Figure 36 shows that different λ ratios have a large impact on the dissipation curve. This implies that the vertical and horizontal permeabilities have to be measured, except in extreme cases where λ is much larger than 10.

When a natural soft soil is assumed to be anisotropic, the differential equation for one-dimensional consolidation of Terzaghi (1923) has to be extended to a more dimensional differential equation of Biot (1941), which is shown in formula 42.

$$\frac{\partial u}{\partial t} = c_x \cdot \frac{\partial^2 u}{\partial x^2} + c_y \cdot \frac{\partial^2 u}{\partial y^2} + c_z \cdot \frac{\partial^2 u}{\partial z^2} \tag{42}$$

Notice that the consolidation coefficient has a direct relation with the permeability as shown in formula 43. This relation is also valid for the lateral directions. It is important to mention that the calculation of Lumb and Wong (1971) is based on cross-anisotropy, which means that the horizontal components c_x and c_y are assumed to be equal to each other.

$$c_z = \frac{k_z \cdot E_z}{\gamma_w} \tag{43}$$

An important aspect in the anisotropy of permeability is presented in figure 37, which shows a thin layer of highly decomposed peat between layers of poorly decomposed peat.
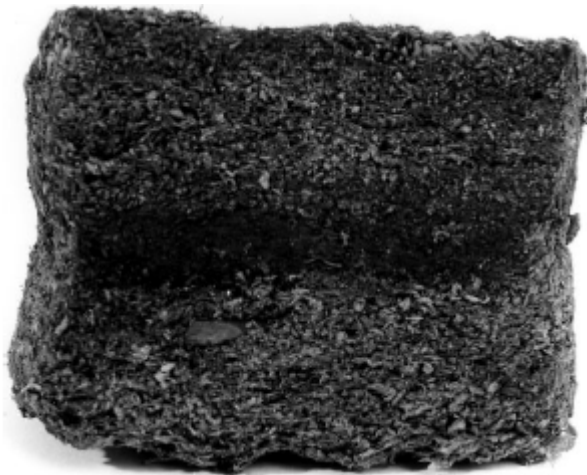
Figure 37 – A peat sample with layers of varying degrees of decomposition (Beckwith et al., 2003)

It is likely that if the permeability had been measured for each recognizable layer separately, the degree of anisotropy would have varied considerably. In this case, the thin decomposed layer dominates the permeability of the whole sample. It appears therefore that anisotropy in soft soils, at least in some circumstances, is scale dependent.

2.4.2. *Implementation of anisotropy in geotechnical modelling*

The implementation of anisotropy in geotechnical modelling could be done in various ways. According to Nishimura (2005) there are three approaches to express anisotropy in a soil model. Firstly, a pragmatic approach in which the strength, stiffness and permeability parameters of an isotropic model are varied depending on the principal stress direction. For example, when the horizontal soil deformations have to be determined at the toe of the embankment, simple shear tests should be used for the determination of the parameters (see figure 11). Notice that the material properties would be overestimated with triaxial test parameters, which is mainly the result of a difference in orientation of the major principal stress to the vertical when the soil is sheared. Secondly, the critical state models can be extended with an anisotropic bounding surface. The concept has been applied in a series of constitutive models, examples are MIT-E3 and S-Clay1 (Whittle, 1993; Wheeler *et al.*, 2003). The majority of these models assume elliptic or logarithmic spiral yield surfaces rotated in the q and p space. In which the rotated yield surface is simulated with a kinematic hardening law, representing the evolution of anisotropy during plastic straining (McGinty *et al.*, 2009). An illustration of such a model is shown in figure 38. However, it is important to state that the use of these models is restricted to normal and lightly overconsolidated soils, because anisotropy in the elastic stage is not incorporated. An important reason to ignore anisotropic elastic behaviour is the complexity of measuring the anisotropic elastic parameters in the laboratory (Karstunen, 2005). When these models are still applied to heavily overconsolidated soils (OCR>4), such as London clay, one of the potential problems is the overestimation of the shear strength (Whittle, 1993). Nevertheless, Koskinen *et al.* (2002) show that for normal and lightly overconsolidated soils the shear strength can be well fitted with a rotated yield surface.
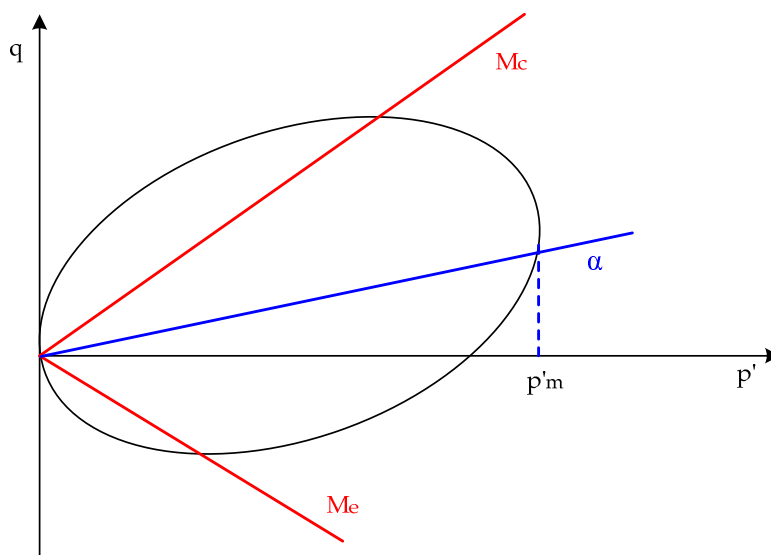
Figure 38 – Anisotropic bounding surface in rotational hardening models (Nishimura, 2005)

Thirdly, anisotropic soil behaviour could be modelled with a multi-laminate framework. The framework was originally developed for describing a brittle material with flaws, which are simulated as planes of weaknesses. The essence of this concept is to regard the general 6 degrees of freedom stress-strain relationship of a soil element as an assemblage of strain-

strain relationships of reduced degrees of freedom. For instance, the multi-laminate model by Pande and Sharma (1983) describe the stress-strain relationship of soil by integrating stress-strain relationships along several planes in the three-dimensional space. Anisotropy may be simulated by varying the strength and stiffness parameters for each plane. The main benefit in comparison to the anisotropic bounding surface models is that there is no need for a rotational hardening law, so less parameters are required. The major drawback of the multi-laminate mechanism model is that it requires a considerable consumption of computer memory, because the state parameters need to be stored for each plane (Karstunen, 2005).

In this thesis, only the first and second approach are considered to express anisotropy in natural soft soils, because those are implementable in the finite element program Plaxis 2D. The first approach is applied in the parameter determination of the Linear Elastic Perfectly Plastic model with a Mohr Coulomb failure criterion, Modified Cam Clay model and Soft Soil Creep model. The other models, S-Clay1 and Anisotropic Creep belong to the second approach. Both approaches will be used to determine the horizontal soil deformations adjacent to embankments.

3.   Analysis of the State of the Art Models

For the prediction of horizontal displacements that develop during and after the construction of an embankment various models are currently available. The need for such models has arisen from observations that show the detrimental effect of lateral deformations on the performance of a structure. The chapter starts with a description of the model of Bourgens and Mieussens (1979), which is an empirical model that is based on 32 embankments constructed on a variety of clayey soils. Paragraph 3.2 elaborates on the analytical model formulations of Van IJsseldijk and Loof. These models have only found there roots in the Dutch geotechnical practice; outside the Netherlands the models of Van IJsseldijk and Loof are seldom used. It is important to state that there are more analytical proposals internationally. However, as far as the author knows, the focus of the other analytical models, for example the one of Stewart *et al.* (1996), has been mainly on the interaction processes with a pile foundation. These models take the uncertainty in the prediction of the lateral movements for granted. Moreover, the content of this research is predominantly on soil behaviour and not on the behaviour of the affected structure. The discussion is therefore restricted to the model of Van IJsseldijk and Loof. In the next paragraph a short description is given about the finite element program Plaxis 2D V9. This numerical program calculates stresses and strains with a coupled system of partial differential equations. The paragraph continues with a discussion about a number of material models, which can be incorporated in the considered finite element program. In this discussion, most attention will be paid to the user-defined anisotropic models S-Clay1 (Wheeler *et al.*, 2003) and Anisotropic Creep (Leonie *et al.*, 2008). The chapter closes with a comparison of the considered models, and a simple reliability method to evaluate the sensitivity of the parameters on the simulated results.

3.1.   Empirical models

In several cases the horizontal soil deformations below and adjacent to embankment are difficult to predict accurately with analytical and numerical models. A lot of models have failed, because they were based on the assumption that the soil response is undrained throughout construction and truly drained after construction. According to Tavenas and Leroueil (1980) these models ignore the effect of the initial quasi-elastic response in the overconsolidated state of the soft soil. As a result, the lateral displacements are significantly overpredicted when fully undrained behaviour is assumed during the whole construction period. Another reason for the poor prediction of the lateral deformations is that horizontal soil behaviour is affected by a number of complicating factors, which are not easily included in the analytical or numerical models. For example, it is difficult to incorporate the highly non-linear stress-strain behaviour and the anisotropy of a soft soil (Poulos, 1972). Good predictions are often found with empirical models, because the complex factors are implicitly included. The empirical model that is discussed in the remaining part of this paragraph is the model proposed by Bourgens and Mieussens (1979). They analyzed 32 field cases, and on the basis of those results a practical design method is suggested for the determination of horizontal soil deformations. Finally, it is important to mention that this model is only valid close to the toe of an embankment.

3.1.1. Bourgens and Mieussens

In the model of Bourgens and Mieussens (1979) the total horizontal soil displacement is a summation of an initial part and a consolidation part. The most important parameters for the determination of the horizontal displacements are summed up below, and are also presented graphically in figure 39.

- Relation between the thickness of the soft soil layers (D) and the average width of the embankment (B)
- Relation between the distance of the crest till the toe of the embankment (L) and the distance between crest till the location where the horizontal displacements have to be determined (X)
- Undrained shear of the subsoil (c_u)
- Relation between undrained shear strength of the top layer (c_{us}) and undrained shear strength of the soft soil layers underneath (c_u)
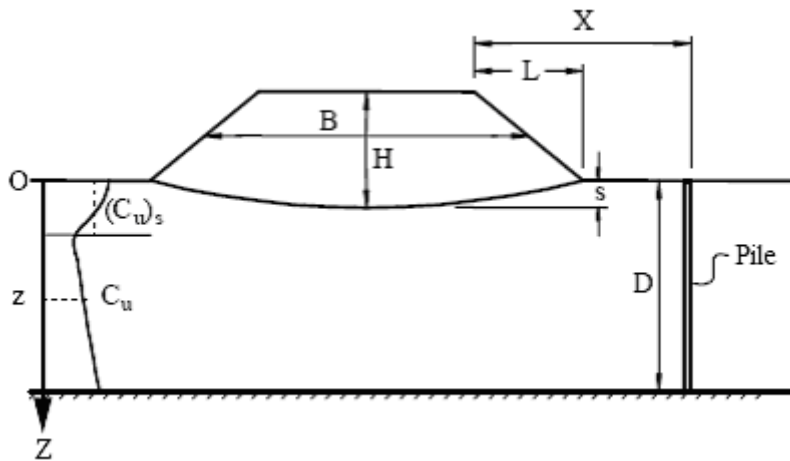
Figure 39 – Parameters used in the Bourgens and Mieussens model (Bourgens and Mieussens, 1979)

For the determination of the maximum initial horizontal displacements the safety factor of the embankment has to be calculated with formula 44. This formula calculates the safety factor for the undrained situation, because during the initial stage of construction the pore pressures are not dissipated yet. The relation between the factor of safety and the horizontal displacements is not new, because Marche and Chapuis (1974) already used it for controlling the stability of an embankment.

$$FS = \frac{(\pi + 2) \cdot c_u}{\gamma_{dry} \cdot H} \tag{44}$$

This formula requires the undrained shear strength from vane tests. If these tests are not available, the relation posed in formula 45 should be used (Ladd, 1991).

$$c_u = 0,22 \cdot \sigma_v' \cdot OCR^m \tag{45}$$

Parameter m gives an indication of the stress dependency of the soil, which is approximately 0.5 for sandy soils and 1.0 for soft soils.

Bourgens and Mieussens (1979) plotted the safety factors for all field cases against the dimensionless movement factor, which is the ratio between the maximum initial horizontal deformation and the thickness of the soft soil layer. The results are presented in figure 40 for various ratios of X/L.
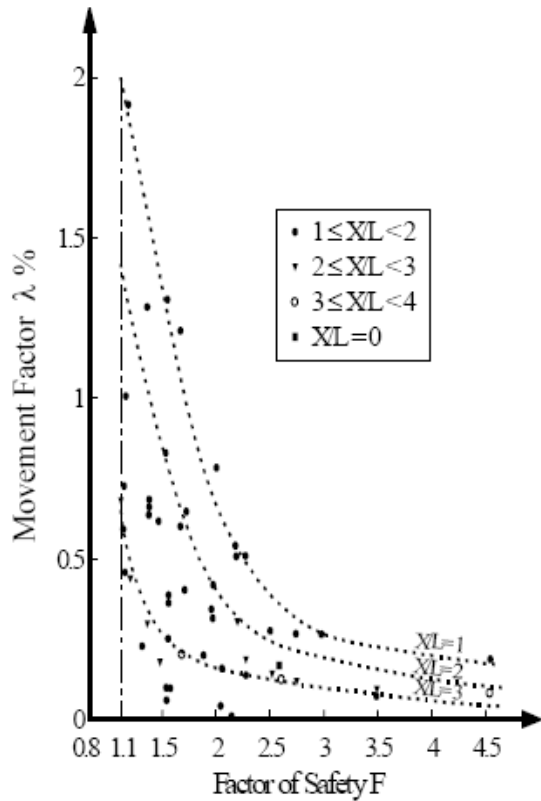
Figure 40 – Graph to determine the initial lateral deformations (Bourgens and Mieussens, 1979)

If the factor of safety and the X/L values are known the movement factor can be easily determined for the graph. Subsequently, the maximum initial horizontal displacements can be calculated with formula 46.

$$h_{max;i} = D \cdot \lambda \tag{46}$$

Moreover, the results presented in figure 40 are in line with the expectations, because when the movement factor increases the factor of safety decreases. The largest movement factor is often obtained when the safety factor approaches the critical value of one.

The maximum horizontal displacements during consolidation are calculated with a relation proposed by Tavenas *et al.* (1979). This relation as shown in formula 47 connects the maximum horizontal displacement during consolidation with the settlements at the centre of the embankment. Notice that this equation is only valid for approximately the first 5.0 years of consolidation, after this period the time-dependent lateral deformations seem to decrease. Additional restrictions are that the safety factor of the embankment should be above 1.3, X/L ratios smaller than 2.25 and the D/B ratios smaller than 0.25.

$$h_{max;c} = 0.16 \cdot (S_{tot} - S_{el}) \tag{47}$$

Formula 47 shows that the consolidation settlement can be found when the elastic settlement is subtracted from total settlement at a particular time. Furthermore, it is possible to specify the horizontal deformations due to consolidation for higher D/B ratios. The consolidation deformation has to be multiplied with 1.1 for D/B ratios between 0.25 and 0.6. For D/B ratios higher than 0,6 it is advised to multiply the consolidation deformation with a factor 1.2.

In summary, the maximum horizontal soil deformation can be calculated with formula 48.

$$h_{max;tot} = \lambda \cdot D + 0.16 \cdot (S_{tot} - S_{el}) \cdot f_{D/B} \tag{48}$$

Furthermore, Bourgens and Mieussens (1979) propose three normalized curves, which are shown in figure 41, to describe these distributions with depth. The first curve should be used when the entire soft subsoil stratum is normally consolidated. If the stiffness of the compressible layers is relatively uniform with depth, it is advised to use the second curve. The last curve should be used when an overconsolidated clay crust is present below surface level. The mathematical formulations for these curves are given in formulas 49, 50 and 51.

$$(1) \quad y = 1.83Z^3 - 4.69Z^2 + 2.13Z + 0.73 \tag{49}$$

$$(2) \quad y = 3.42Z^3 - 6.37Z^2 + 2.14Z + 0.81 \tag{50}$$

$$(3) \quad y = -2Z^3 + 1.5Z + 0.5 \tag{51}$$

With these equations it is possible to determine the horizontal deformation at each depth. Notice that these distributions are only valid close to the toes of an embankment.
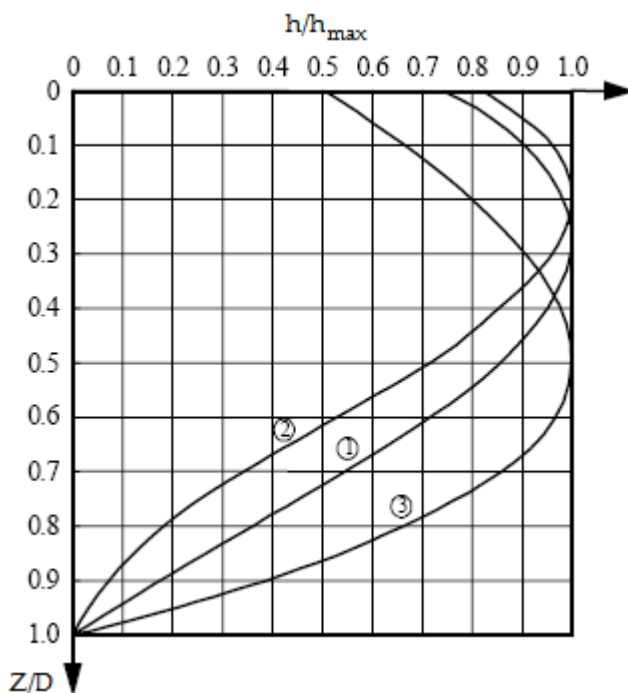
Figure 41- Horizontal deformation distributions with depth (Feddema et al., 2009)

The model of Bourgens and Mieussens has according to Feddema *et al.* (2009) two significant limitations. Firstly, the proposed equation for the prediction of the horizontal displacements due to consolidation is only valid close to the toe of the embankment. Secondly, it is not possible to give an indication of the long-term horizontal deformations (> 5 years).

3.2. Analytical models

The analytical models Van IJsseldijk and Loof simulate horizontal soil behaviour with the volume preserving linear elastic theory originally developed by Jürgenson (1934). The response to embankment loading is therefore fully undrained. According to Tavenas and Leroueil (1980), this assumption could lead to significant overestimations. The considered models ignore the initial quasi-elastic response, which relates to the overconsolidation state of soils. Notice that this behaviour is graphically shown in figure 14 with stress path stage A to B. However, due to its simplicity, the model is still used as a first indication for the prediction of horizontal soil behaviour.

Next to the assumptions of fully undrained and linear elastic soil behaviour, more simplifications are made in the models of Van IJsseldijk and Loof. For instance, the model is restricted to two-dimensional loading situations, and only one soft soil layer could be incorporated in the calculation scheme. This means that it is not possible to simulate layered soil profiles. Furthermore, it is considered that the stiffness of the deep foundation layer (i.e. sandy or rocky material) is infinite.

The original formulation of Van IJsseldijk and Loof is created in 1955 in the laboratory of Grondmechanica Delft. De Leeuw (1963) converted these analytical models into normalized tables for terrace and strip loading situations. The difference between a terrace and strip loading situation is shown in figure 42.
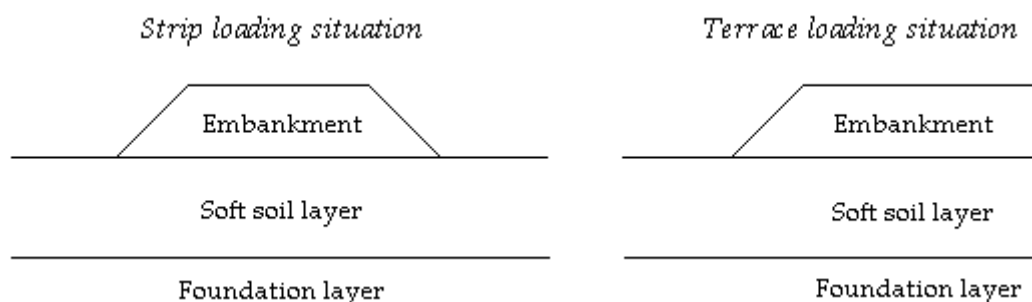
Figure 42 – Considered loading situations in the models of Van IJsseldijk and Loof (De Leeuw, 1963)

The normalized quantities that are used in the tables of De Leeuw are presented in formulas 52 and 53. With these normalized quantities the horizontal soil stress and horizontal soil deformation can be easily calculated for each location under an embankment.

$$\sigma_{xx}/q \tag{52}$$

$$\left(E/h.q\right) \cdot u \tag{53}$$

The E of formula 53 represents the elasticity modulus of the soft soil layer. This modulus is often determined from the predicted total settlement (S_{tot}) under the centreline of the embankment as shown in formula 54.

$$E = 1,25 \cdot \frac{q \cdot h}{S_{tot}}$$

(54)

This approach was also applied in the initial design of the abutment structures of the Betuwe Route (Havinga, 1995).

3.2.1. Van IJsseldijk

The analytical model of Van IJsseldijk simulates one soft soil layer that is subjected to an embankment loading. The model assumes that the stiffness of the soft soil is uniform over the depth of the layer. Figure 43 shows a graphical schematisation of the model for a terrace loading situation.
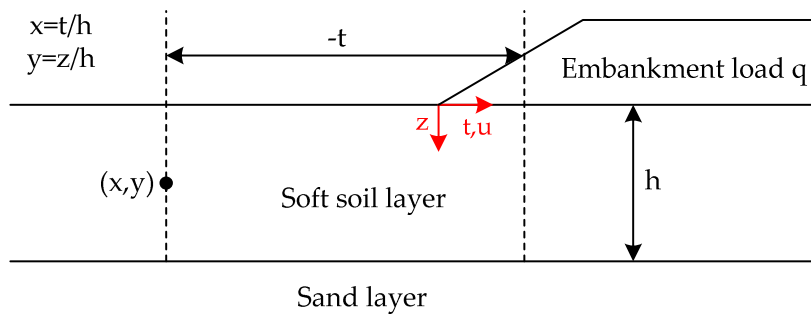
Figure 43 – Modelling horizontal soil deformations according to Van IJsseldijk

For the determination of the normalized quantities (as expressed in formulas 52 and 53) at a particular point (x,y), the values t and h have to be known. The t value is the lateral distance between the considered point till half of the slope of the embankment, and h is the thickness of the soft soil layer. Subsequently, the dimensionless values x and y are used in the tables of De Leeuw (1963) to read off the normalized quantities. For the Van IJsseldijk case, the tables are shown in Appendix 1. However, to ultimately determine the increase of horizontal stress σ_{xx} and the increment in horizontal soil deformation u, the normalized quantities have to be multiplied with respectively the embankment load q and the soft soil thickness multiplied by the embankment load divided by the elasticity modulus (h.q/E).

3.2.2. Loof

The analytical model of Loof also simulates one soft soil layer that is subjected to an embankment loading. However, in contrast to the model of Van IJsseldijk the main difference is that this model includes an infinitely stiff, but flexible, rigid top layer (Hoefsloot, 2008). This results in different boundary conditions at y=0 for both models. In the case of Van IJsseldijk the horizontal soil stress must be zero, while for Loof the horizontal soil deformation requires to be zero at this location. It is evident that this rigid top layer restricts the development of horizontal deformations in the subsoil. The graphical schematisation of the Loof model is presented in figure 44.
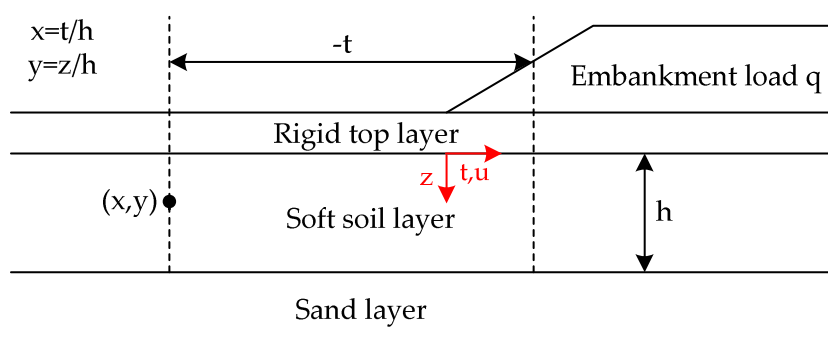
Figure 44 – Modelling horizontal soil deformations according to Loof

The assumption of an infinitely stiff, but flexible, rigid top layer is of course an idealization of real soil behaviour, which makes the analytical formulation a lot easier. These stiff layers could be a highly weathered clay crust or just a dense sandy layer. The amount of horizontal soil deformation that could develop in these soils is limited, and is often negligible with the quantity that could develop in the soft soil layer. For this reason, it is fair to neglect the rigid top layer in the analysis of horizontal soil deformations. Furthermore, the procedure for the determination of the normalized quantities is similar to the model of Van IJsseldijk. The tables of De Leeuw (1963) for the Loof case are presented in Appendix 2. Notice that the x value in the normalized tables extends till plus or minus 4, while for Van IJsseldijk this value extends till plus or minus 8. This emphasizes the diminishing effect of the rigid top layer on the development of horizontal soil deformations under an embankment.

3.3.   Numerical models

A first indication of horizontal soil deformation is often obtained with an empirical or an analytical model. These models are useful in the early design stage to gain insight into the influence of the various parameters on the amount of horizontal deformation. In general, it is not practical to use numerical techniques in this stage, because the values of the geotechnical properties of the subsoil are mostly largely unknown. However, if the geotechnical engineer has a sufficient experience with numerical techniques and is familiar with the local soil conditions, it is probably more efficient to use numerical techniques directly. For a less experienced engineer it is advised to start with simple empirical or analytical models. Later in the design stage when an extensive site investigation has been performed, it could be desirable to use numerical models. With such a model it is possible to gain more insight into the response of soft soils subjected to an embankment loading. The considered numerical models in this paragraph are based on the finite element (FE) technique. The most popular FE packages internationally are Sage-Crisp, Cesar-Rosalie, Plaxis and Abaqus (Mestat, 2001). In this thesis the FE package Plaxis is used, because this one is available at Boskalis.

The FE program Plaxis is available in 2D and 3D. This program is capable to simulate deformation and stability analyses for various types of geotechnical applications. In this thesis, Plaxis 2D version 9 will be used, because the embankments considered in the case studies are assumed to be plane strain. The 2D assumption is allowed, because the cross section of the embankment is more or less uniform over a certain length perpendicular to the cross section. Plaxis solves like any other FE program boundary value problems with a set of partial differential equations. This set of equations is used to describe the displacement field

as well as the pore pressure field for a saturated or a partially saturated soil. However, to solve the partial differential equations, it is first needed to discretise the considered area in a number of regions of arbitrary shape; these regions are also known as the finite elements (Hughes, 2000). The local discretisation inside the finite elements is described with shape functions, which have a particular degree of interpolation. The FE program Plaxis applies standard 15 node triangular elements and 4th order shape functions to approximate the pore pressure and the displacement field. A numerical integration technique is subsequently used to find the solutions of these differential equations.

A limitation of Plaxis is that the excess pore pressures are not coupled with the stress history for a soil that is modelled as an undrained material. The simulations in Plaxis indicate that the generated excess pore pressures are similar before and after the preconsolidation pressure. However, the piezometers under the test embankment in Saint-Alban illustrate that there is a difference in excess pore pressure generation during the initially overconsolidated state and the primary consolidation stage (Leroueil *et al.*, 1990). The measurements show that $\Delta u/\Delta \sigma$ ratio varies from 0.4 to 0.6 in the initially overconsolidated stage, while the $\Delta u/\Delta \sigma$ ratio is about equal to 1.0 during primary compression. Plaxis ignores this distinction, and predicts therefore too much pore pressures in the initially overconsolidated state. It is important to state that this deviation increases for soils which are more overconsolidated. Nevertheless, the soils treated in this research have a small OCR or POP value, which implies that the error remains relatively low.

In addition, FE programs use material models to simulate the stress-strain behaviour of soils. It is important to realize that material models are at best approximations of real soil behaviour. In general a material model is considered to perform better if more aspects of soil behaviour are incorporated. The following categories of material models for soils are possible with increasing complexity: isotropic linear elastic, isotropic non-linear elastic, isotropic elastoplastic without strain hardening, isotropic elastoplastic with strain hardening, isotropic elasto-viscoplastic with strain hardening, anisotropic elastoplastic with strain hardening, and anisotropic elasto-viscoplastic with strain hardening.

During the last decades the most heavily used material model is the Linear Elastic Perfectly Plastic with a Mohr Coulomb failure criterion, but recent advantages in numerical modelling have provided an impetus for the development of more sophisticated constitutive models (Smith and Griffiths, 1982). However, most material models assume that strain increments consist of an elastic strain component and a plastic strain component. The elastic material behaviour is often modelled with Hooke's law (see formula 55).

$$
\begin{bmatrix} \dot{\sigma}'_{xx} \\ \dot{\sigma}'_{yy} \\ \dot{\sigma}'_{zz} \\ \dot{\sigma}'_{xy} \\ \dot{\sigma}'_{yz} \\ \dot{\sigma}'_{zx} \end{bmatrix} = \frac{E}{(1+v)\cdot(1-2v)} \cdot \begin{bmatrix} 1-v & v & v & 0 & 0 & 0 \\ v & 1-v & v & 0 & 0 & 0 \\ v & v & 1-v & 0 & 0 & 0 \\ 0 & 0 & 0 & \tfrac{1}{2}-v & 0 & 0 \\ 0 & 0 & 0 & 0 & \tfrac{1}{2}-v & 0 \\ 0 & 0 & 0 & 0 & 0 & \tfrac{1}{2}-v \end{bmatrix} \cdot \begin{bmatrix} \dot{\varepsilon}_{xx} \\ \dot{\varepsilon}_{yy} \\ \dot{\varepsilon}_{zz} \\ \dot{\gamma}_{xy} \\ \dot{\gamma}_{yz} \\ \dot{\gamma}_{zx} \end{bmatrix}
\tag{55}
$$

This simple law only requires the elasticity modulus and the Poisson's ratio as model parameters. It is important to state that this law is the basis of most higher order models. For the description of irreversible strains elastoplastic models use the formulation presented in formula 56. However, a clear distinction has to be made between associated plasticity and non-associated plasticity. For associated plasticity the plastic potential function is equal to the flow rule, while this function is different for non-associated plasticity. An example of a model that uses associated plasticity is the Modified Cam Clay, and Linear Elastic Perfectly Plastic with Mohr Coulomb failure criterion is example of a non-associated model. Notice that the magnitude of the plastic strains is determined with the plastic multiplier λ.

$$\dot{\varepsilon}^p = \dot{\lambda} \cdot \frac{\partial g}{\partial \sigma'} \qquad (56)$$

For a creep model irreversible strains during primary loading are described by viscoplastic strains. The amount irreversible strain is not dependent on whether a stress path reaches the flow contour or not, but on the ratio between actual stress and the preconsolidation stress.

For perfect plasticity the position of the yield contour is static during plastic straining. However, if hardening or softening rules are incorporated in the material model, the flow contour is not fixed in time anymore. To describe hardening or softening the flow function requires at least one state parameter. Notice that hardening is mostly used to simulate non-linear soil behaviour during the primary loading stage (Muir Wood, 1990). There are three types of hardening discussed; which are compaction hardening, friction hardening and kinematic hardening. With compaction hardening a cap is situated on the yield contour to limit the elastic range, this is useful for compressive stress paths in soft soils. The preconsolidation stress is mostly used as state parameter to describe the translation of the cap with increasing compression. Friction hardening is applied to simulate the decreasing stiffness with increasing deviatoric loading. In this case it is practical to use the mobilized friction angle as state parameter. If the maximum friction angle is reached the deviator strain will go to infinity. The last type of hardening that is considered here is kinematic hardening. A distinguishing characteristic of kinematic hardening is that the flow contour changes from orientation, which leads to extra plastic strains. A model which uses such a hardening rule is S-Clay1, this model uses state parameter α to describe the degree of plastic anisotropy in a soil (see figure 38). Finally, softening behaviour reduces the strength of soils, which leads to a smaller yield contour. An example of softening behaviour is the fracturing of cohesive ties in soft soils due to large shear loads. Leroueil *et al.* (1979) uses the term destructuration to describe the fracturing process of natural soils.

In this thesis five material models are applied in Plaxis to predict the lateral deformations under and adjacent to embankments. The models that are considered here are the Linear Elastic Perfectly Plastic with a Mohr Coulomb failure criterion, Modified Cam Clay, Soft Soil Creep, S-Clay1 and Anisotropic Creep. The last two models are user-defined, which means that they are not commercially available in Plaxis. These models are programmed in the Fortran language, and can be implemented as a dynamic link library in the FE program Plaxis (Wiltafsky, 2003). The next subsections pay attention to the description of the material models. Notice that these descriptions will emphasize on the modelling of horizontal soil deformations.

3.3.1. *Linear Elastic Perfectly Plastic with Mohr Coulomb failure criterion*

The Linear Elastic Perfectly Plastic (LEPP-MC) model uses Hooke's law and the Mohr Coulomb failure criterion to describe elastic and plastic behaviour respectively. Somewhat confusing, in Plaxis this model is called Mohr Coulomb, which actually only represents the plastic part of the model. In this thesis the full term LEPP-MC is used to avoid confusion. In geotechnical engineering the LEPP-MC model is often used as first approximation for the description of in-situ soil behaviour. The principles of the model are presented in figure 45. The figure shows that there is sharp transition between elastic and plastic strains. It is important to emphasize that plasticity is equal to failure in this model.
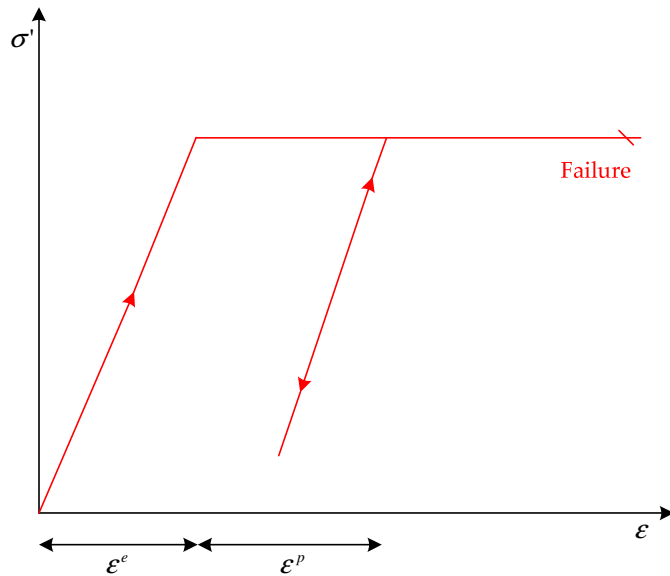
Figure 45 – Basic principles of the LEPP-MC model

In order to evaluate whether or not plasticity occurs six Mohr Coulomb yield criterions are postulated, which are only functions of stress. Plastic yielding takes place when the yield function above zero (Brinkgreve and Broere, 2008). An example of a yield criterion is presented in formula 57.

$$f = \tfrac{1}{2} \cdot \left(\sigma_3^{'} - \sigma_1^{'} \right) + \tfrac{1}{2} \cdot \left(\sigma_3^{'} + \sigma_1^{'} \right) \cdot \sin \varphi' - c \cdot \cos \varphi' \tag{57}$$

Notice that a perfect plasticity model is a model with fixed yield surface. In order words the yield function is fully defined by model parameters and not affected by plastic straining. The magnitude of the plastic strain is proportional to the derivative of the yield function as shown in formula 56. According to the classical plasticity theory (Hill, 1950) the same yield functions are used to describe plastic strains (f=g). This means that the plastic strain can be represented as a vector perpendicular to the yield surface. However, if associated plasticity is used the plastic strains are significantly overestimated. To prevent this overestimation non-associated plasticity functions have to be defined. In this case the plastic potential functions are not equal to the yield functions anymore (see example in formula 58).

$$g = \tfrac{1}{2} \cdot \left(\sigma_3^{'} - \sigma_1^{'} \right) + \tfrac{1}{2} \cdot \left(\sigma_3^{'} + \sigma_1^{'} \right) \cdot \sin \psi - c \cdot \cos \psi \tag{58}$$

Formula 58 shows that the dilatancy angle is adopted in stead of the friction angle to describe the plastic strains. This choice leads to a smaller amount of plastic strains, because the dilatancy angle is always lower than the friction angle. Notice that the cohesion, friction angle and dilatancy angle are used for the description of plasticity. Furthermore, the stress states within the yield surface are predicted with Hooke's law, and are therefore fully elastic. The required parameters for Hooke's law are the modulus of elasticity and Poisson's ratio as shown in formula 55. To complete the description, figure 46 shows a visualization of the full Mohr Coulomb yield criterion in principal stress terms. Notice that hexagonal cone is presented for a friction angle of 30° and zero cohesion.
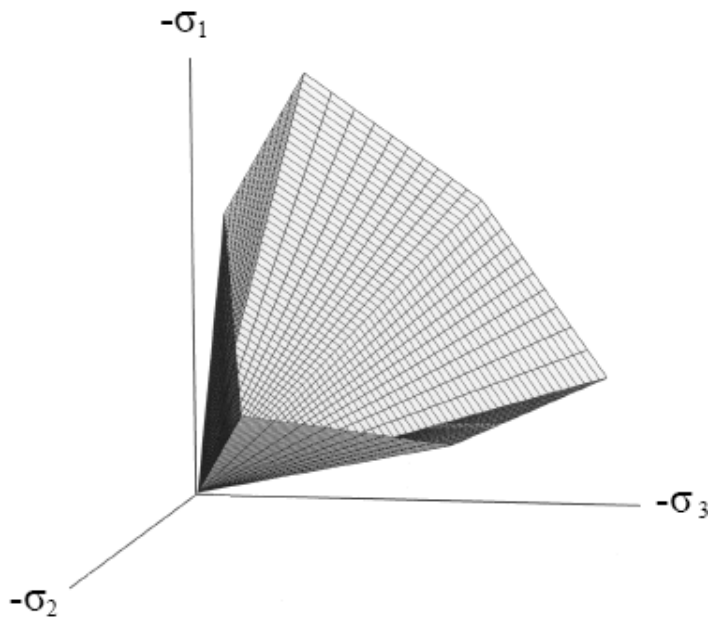
Figure 46– Complete yield surface in principal stress space (Smith and Griffiths, 1982)

For the modelling of horizontal soil deformations under or adjacent to embankment it is important to consider the expected stress paths. As shown in figure 11 there are three distinctive stress conditions under an embankment. For example, under the centre of the embankment the vertical stress increase (σ_1) is higher than the horizontal stress increase (σ_3), while under the toe of an embankment the vertical stress increase (σ_1) is about equal to the horizontal stress increase (σ_3). At some distance away the toe of the embankment the horizontal stress increase (σ_3) exceeds the vertical stress increase (σ_1). It is therefore possible that different yield functions become active at different places under the embankment. The stress in the other lateral direction (σ_2) can easily be deduced from Hooke's law and a plain strain assumption as shown in formula 59.

$$\sigma_2 = v \cdot (\sigma_1 + \sigma_3) \tag{59}$$

Finally, the LEPP model does not have a cap to restrict the elastic area. For certain stress paths this limitation could lead to a significant underprediction of the strains. In extreme situations the strains will remain elastic for infinitely high compressive stresses, which is for instance the case in isotropic compression. This model should only be considered as a rough estimation of real soil behaviour.

3.3.2. *Modified Cam Clay*

The original formulation of the Cam Clay model is developed during the late 1950s at the University of Cambridge (Roscoe *et al.*, 1958). The mathematical formulation of the Cam Clay model is based on the critical state soil mechanics (CSSM) theory. After the introduction of the original Cam Clay model the qualifier "modified" has been added, because there was no complete satisfaction about the formulation of the flow rule (Roscoe and Burland, 1968). In contrast to the LEPP-MC model, this model uses a hardening rule to describe the relation between the increase of preconsolidation pressure and the development plastic volumetric strains. This leads to an increase of the yield contour during plastic straining. Furthermore, a central aspect of this theory is that all soils fail on a unique line in p' and q space, which is also known as the critical state line (CSL). If a soil reaches the CSL the void ratio remains constant, this means that no hardening or softening behaviour occurs anymore. It is also important to mention that the CSL is not a physical boundary as the Mohr Coulomb failure criterion. For example, for a highly overconsolidated soil it is possible that the stress path crosses the CSL till the initial yield contour is reached.

The roots of the critical state theory are based on the work of Hvorslev (1937). He showed that the peak shear stress at failure of a soil is a function of the effective normal stress and the void ratio. A similar assumption is also used by Roscoe and Burland (1968) as starting point, because it assumes that there is a logarithmic relation between the effective stress and the void ratio during isotropic compression. These relations are presented in formulas 60 and 61 for respectively primary loading and unloading / reloading. In which parameters λ and κ represent the primary compression index and recompression index.

$$e_{pl} = e_0 - \lambda \cdot \ln\left(\frac{p'_{pl}}{p'_{pc}} \right) \tag{60}$$

$$e_{ur} = e_0 - \kappa \cdot \ln\left(\frac{p'_{ur}}{p'_{pc}} \right) \tag{61}$$

In the primary loading stage plastic strains are generated, which lead to an irreversible reduction of the void ratio. To describe these strains a flow rule has been proposed to give the relation between volumetric plastic strains and deviatoric plastic strains. The suggested formulation is presented in equation 62.

$$\frac{\varepsilon_p^p}{\varepsilon_q^p} = \frac{\partial g/\partial p}{\partial g/\partial q} = \frac{M^2 - q^2/p^2}{2q^2/p^2} \tag{62}$$

The Modified Cam Clay (MCC) assumes associative plasticity, and integration will lead to the yield function as shown in formula 63.

$$f = \frac{q^2}{M^2} + p' \cdot \left(p' - p'_c \right) \tag{63}$$

The yield surface (f=0) is an ellipse in p' and q space. Notice that the yield surface is the boundary of the elastic stress states. Stress paths within this boundary respond elastically, whereas stress paths outside this boundary react plastically. A visualization of the yield surface of the MCC model is presented in figure 47. The figure shows that the shape of the ellipse is dependent on slope M and the preconsolidation stress of the soil sample. The formula for the M parameter in triaxial compression is presented in formula 64.

$$M = \frac{6 \sin \varphi_{cv}'}{3 - \sin \varphi_{cv}'} \tag{64}$$
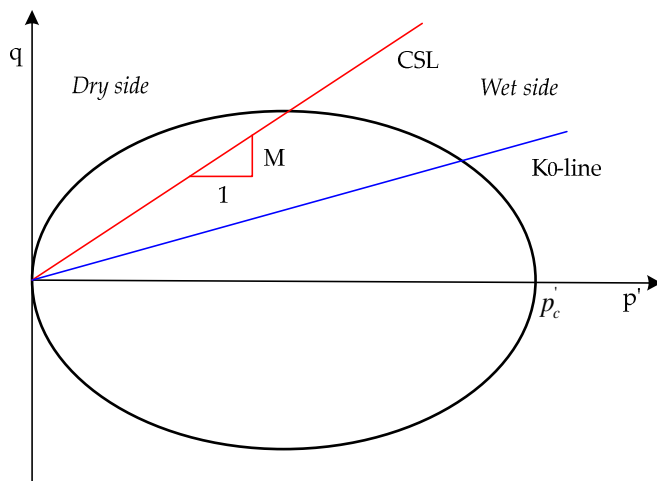
Figure 47– Yield surface of the MCC model in p'and q space (Muir Wood, 1990)

The increase of the yield surface is modelled with a cap hardening rule. This model uses the increase of preconsolidation pressure to simulate the generation of plastic volumetric strains as shown in formula 65. In this case, parameter ν represents the specific volume of the soil.

$$\partial \varepsilon_p^p = \frac{\lambda - \kappa}{\nu} \cdot \frac{\partial p_c}{p_c} = \frac{\lambda - \kappa}{1 - e} \cdot \frac{\partial p_c}{p_c} \tag{65}$$

In this thesis only normal and lightly overconsolidated soils are treated, which means that the stress paths will remain at the wet side of the CSL. For highly overconsolidated soil it is possible that a stress path reaches the yield contour at the dry side of the CSL. As a result, softening behaviour has to occur to return the stress path to the CSL again. According to Brinkgreve and Broere (2008) softening should be prevented, because it is a numerical instable process. Without special regularization techniques, softening behaviour can lead to mesh dependency and convergence problems of the iterative procedures in a FE program. In addition, it is well known that stress paths at the dry side will lead to an overestimation of the strength, because the q values become unrealistically high. However, these problems are not troublesome for the soils considered in the case studies, due to the fact that they are usually located at the wet side. The explained principles are clarified in figure 48. This figure presents the ESP for a drained and an undrained lightly overconsolidated soil subjected to a triaxial loading. The figure also shows that the ESP of a drained triaxial test approaches the CSL with a straight line. The difference with the undrained triaxial test is that the stress path

starts vertical, because the elastic volumetric strains are zero during undrained loading. Outside the elastic region plastic strains will occur. Note that plastic strains are compensated by elastic expansion, which leads to a decline of the effective pressure. The expansion is needed to satisfy the undrained condition that the sum of the volumetric strains has to be equal to zero. Failure (F) occurs when the ESP reaches the CSL. For this reason only the ESP is presented and the TSP has been omitted in figure 48.
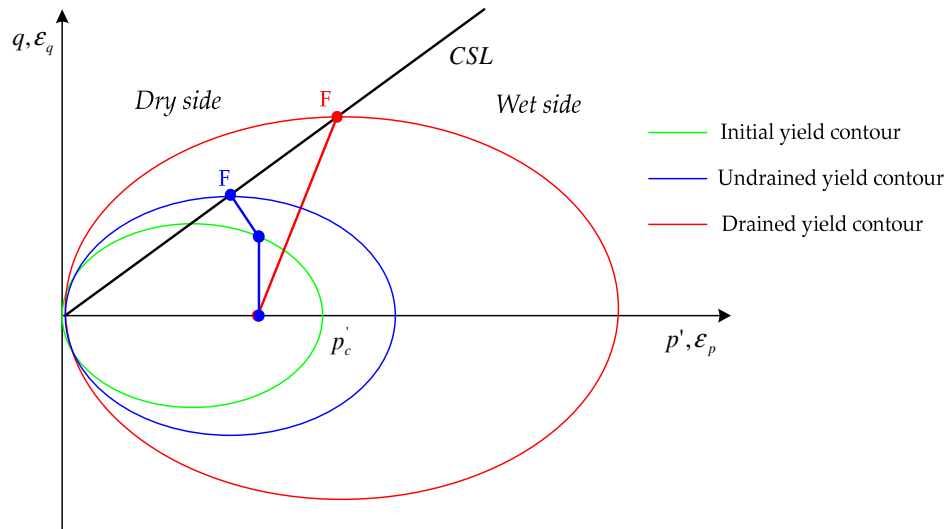
Figure 48 – Drained and undrained behaviour during triaxial testing on lightly overconsolidated soils

A number of case studies presented in literature show that the long-term lateral deformations are significantly overestimated with the MCC model (Neher *et al.*, 2001; Brinkgreve, 2004). The main reason why the lateral deformations are too high is the result of the associative flow rule. There are several suggestions to improve the prediction of the lateral deformations. For example, a kinematic hardening law could be used to include anisotropy. Another option is to apply a non-associative flow rule to reduce magnitude of plastic strains (Ladd *et al.*, 1994).

3.3.3. *Soft Soil Creep*

The Soft Soil Creep (SSC) model is an isotropic model, which is closely related to the one dimensional isotache theory and uses some principles of the MCC model. The additional feature of this model is that irreversible strains can develop under constant effective stress, because the formulation is based on viscoplasticity and not on elastoplasticity. This strain generation is in contrast with the elastoplastic models LEPP-MC and MCC that only generate strains when the stress state is altered. For the description of the creep strains a new stress measure named p^{eq} is adopted as shown in formula 66 (Vermeer and Neher, 1999). This measure influences the size of the ellipse, and correspondingly the development of creep strains. Notice that the ellipses are almost analogous to the ones proposed in the MCC model as introduced by Roscoe and Burland (1968).

$$p^{eq} = p' + \frac{q^2}{M^2 \cdot p'}$$
(66)

This isotropic model is extended to a general K_0-consolidated condition, which is generally observed in the field. In such a situation the stress components in the lateral directions have to be multiplied with factor K_0^{NC}, which leads to the formulation presented in formula 67.

$$p^{eq} = \sigma_1' \cdot \left(\frac{1 + 2K_0^{NC}}{3} + \frac{3 \cdot \left(1 - K_0^{NC}\right)^2}{M^2 \cdot \left(1 + 2K_0^{NC}\right)} \right) \tag{67}$$

The compressibility parameters adopted in the SSC model are λ^*, κ^* and μ^*, where the superscript * denotes modified. These parameters are defined in terms of volumetric strain, while the original Cam Clay parameters κ and λ are defined in terms of void ratio. The additional parameter μ^* is the modified creep index, which determines the time-dependent behaviour in the long-term.

These parameters can be incorporated into a linear strain framework, but also in a natural strain framework. If a linear strain framework is used in Plaxis the CR, RR and C_α have to be divided by ln10 to obtain the modified compressibility parameters. It is also possible to use these parameters in an updated mesh analysis, which is based on natural strain framework. However, an empirical correction factor that is related to the bulk density should be applied to correct for the slope difference, which is already illustrated figure 33. An example is presented in formula 68 for the modified compression index. Notice that the correction factor varies from 1.1 for clayey soils to 1.6 for peaty soils.

$$\lambda^* = \frac{CR}{\ln 10} \cdot f(\rho_b) \tag{68}$$

On the other hand, the a,b,c isotache parameters of Den Haan (1994) can also be used as input parameter for the calculations in Plaxis. Notice that the a,b,c parameters require an updated mesh analysis, because they are based on a natural strain formulation. The stiffness parameters λ^* and μ^* are equal to isotache parameters b and c. It is also possible to use the isotache parameters of Den Haan (1994) in a linear strain framework. Formula 69 shows that the same empirical correction factor is required to the correct the slope difference.

$$\lambda^* = \frac{b}{f(\rho_b)} \tag{69}$$

The remaining isotache parameter a is not equal the modified parameter κ^*. A stiffness factor is used to convert a into κ^*. The result is shown in formula 70 (Servais, 2006).

$$\kappa^* = \frac{\left(1 - v_{ur}\right) \cdot \left(1 + 2K\right)}{\left(1 + v_{ur}\right)} \cdot a \tag{70}$$

The K value represents the earth pressure coefficient, which is not a constant value during reloading and primary loading. However, for the sake of simplicity an average value of K is often assumed to obtain a constant κ^* value. In the daily practice κ^* is often assumed to be equivalent to 2a (K and v_{ur} are respectively 1.0 and 0.2).

The SSC model is based elasto-viscoplasticity, which means that the total strain rate is summation of the elastic strain rate and the creep strain rate (see formula 71). Notice that this formula is presented in a differential form, because it will be used for transient and continuous loading problems (Vermeer and Neher, 1999).

$$\dot{\varepsilon} = \dot{\varepsilon}^e + \dot{\varepsilon}^c \tag{71}$$

The irreversible strains only occur when a physical time increment is applied. This means that it is not important if a stress point reaches the yield contour. What matters is the distance between the current equivalent stress and the equivalent preconsolidation stress. In mathematical terms the creep function can be expressed with formula 72.

$$\dot{\varepsilon}^c_p = \frac{\mu^*}{\tau} \cdot \left(\frac{p^{eq}}{p^{eq}_{pc}} \right)^{\frac{\lambda^* - \kappa^*}{\mu^*}} \tag{72}$$

This formula only describes the development of volumetric creep strains. The SSC model is therefore still incomplete, because soft soils also exhibit deviatoric creep strains. For introducing general creep strains, it is assumed that the creep strain is simply a time-dependent plastic strain. With this assumption it becomes possible to adopt a flow rule, which gives the relation between volumetric and deviatoric creep strains. The plastic potential function g is defined with p^{eq} (see formula 66).

These principles are visualized in figure 49. This figure shows that the slope of the CSL and the equivalent effective stress p^{eq} determine the shape of the yield contour, and therefore the ratio between volumetric and deviatoric creep strains. These creep strains are determined with an associative flow rule (i.e. irreversible strains perpendicular on the yield contour). In addition, it uses a Mohr Coulomb criterion to prevent stress states on the dry side of the CSL.
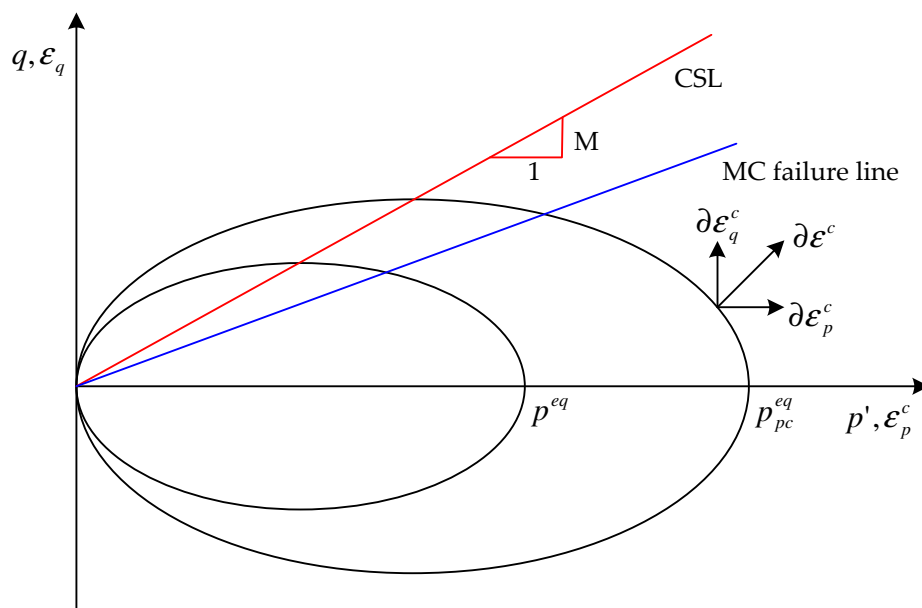
Figure 49 – Creep ellipses in p' and q space (Vermeer and Neher, 1999)

During the construction of an embankment the soft foundation soil often becomes normal consolidated again. This means that the value of p^{eq} increases till the equivalent preconsolidation pressure. When the value of p^{eq} is close or equal to the equivalent preconsolidation the creep strains increase very quickly, because exponent $(\lambda^*-\kappa^*)/\mu^*$ has generally a value of approximately 20. Furthermore, the change of the preconsolidation pressure is described with a hardening law as shown in formula 73.

$$p_{pc}^{eq} = p_{pc;0}^{eq} \cdot \exp\left(\frac{\varepsilon_p^c}{\lambda^* - \kappa^*}\right) \tag{73}$$

The elastic strains are determined with Hooke's law, which is essentially based on isotropic elasticity (see formula 55). Vermeer and Neher (1999) show that the recoverable strains for an oedometer like condition can be defined with formula 74.

$$\dot{\varepsilon}^e = \kappa^* \cdot \frac{\dot{p}'}{p'} = \kappa^* \frac{1+\nu_{ur}}{1-\nu_{ur}} \cdot \frac{1}{1+2K_0} \cdot \frac{\dot{\sigma}_1'}{\sigma_1'} \tag{74}$$

For a proper functioning of the SSC model, a thorough attention should be paid to the determination of the sensitive parameters M and K_0^{NC}, because they have a significant effect on the amount of horizontal deformations. Brinkgreve (2004) presented a case study where a 5,0 m high embankment was constructed on a 10.0 m thick layer of clay. Four calculations where performed with different OCR and M values. The results showed that distinctive M values could result in large differences in vertical and horizontal deformation. For example, M values of 0.99 and 1.36 resulted in a difference of 0.55 m in lateral deformation over a time period of 3 years. Notice that these M values are not arbitrary chosen, because the first is based on friction angle (see formula 64), and the second uses the Plaxis definition that is based on K_0^{NC} (see formula 2). Figure 50 shows the relationship between M and K_0^{NC} for a common compressibility ratio and a common elasticity constant.
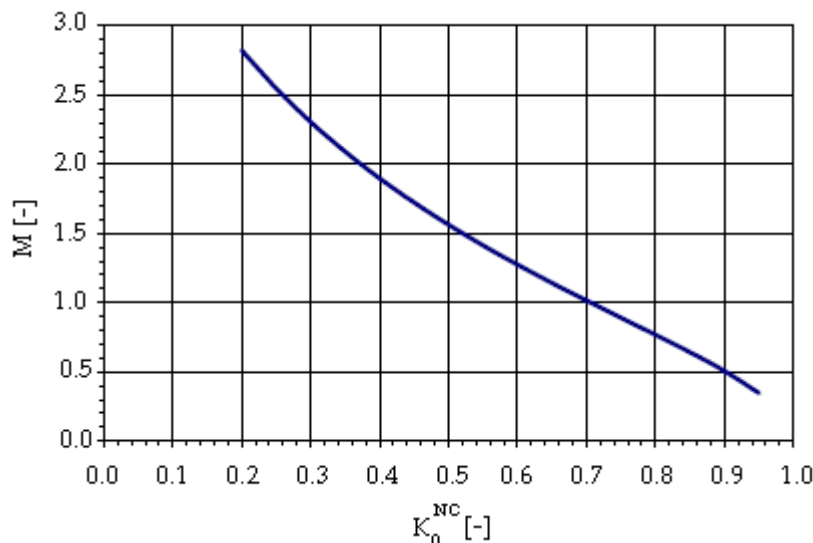
Figure 50 – Relation between M and K_0^{NC} for $\lambda^*/\kappa^* = 4{,}0$ and $\nu_{ur} = 0{,}15$

The input parameters should preferably be obtained from a K_0-CRS oedometer test, because the relation presented in formula 2 is valid for one-dimensional compression at a constant rate of strain in the normal consolidated range. These conditions are similar to the last part of the K_0-CRS oedometer test. It is not advised to use Jaky's rule of thumb, especially in the case of peaty soils and organics clays, because they underestimate the value of M (Den Haan and Feddema, 2009). The cause of this underestimation lies predominantly in the determination of the friction angle, which is frequently determined from standard oedometer and triaxial tests. For example, in the Dutch geotechnical practise it is customary to cut the friction angles off at strain values of 2% to 5% (Feddema *et al.*, 2009). This leads to conservative value of the friction angle, and as a consequence to unrealistic high values for K_0^{NC}, which corresponds to large horizontal soil deformations.

3.3.4. S-Clay1

The S-Clay1 model is an extension of the conventional critical state models. The extension compromises a rotational hardening law that accounts for plastic anisotropy in soft clays, which causes the yield contour to be sheared. Notice that the extent of shearing gives an indication of the degree of anisotropy. Unlike many anisotropic elastoplastic models that are published previously (Banerjee and Yousif, 1986; Whittle, 1993); the suggested rotational hardening rule of the S-Clay1 model includes dependence on the plastic volumetric strain increments but also on plastic shear strain increments. This is in contrast to most other anisotropic models, because they only incorporate the plastic volumetric strain increments in the rotational hardening rule. The rotational hardening rule in the S-Clay1 model has been validated by a number of case studies. Figure 51 shows some results of the validation of the simulated yield curve with the measured yield points for Bothkennar and Mexico City clay.
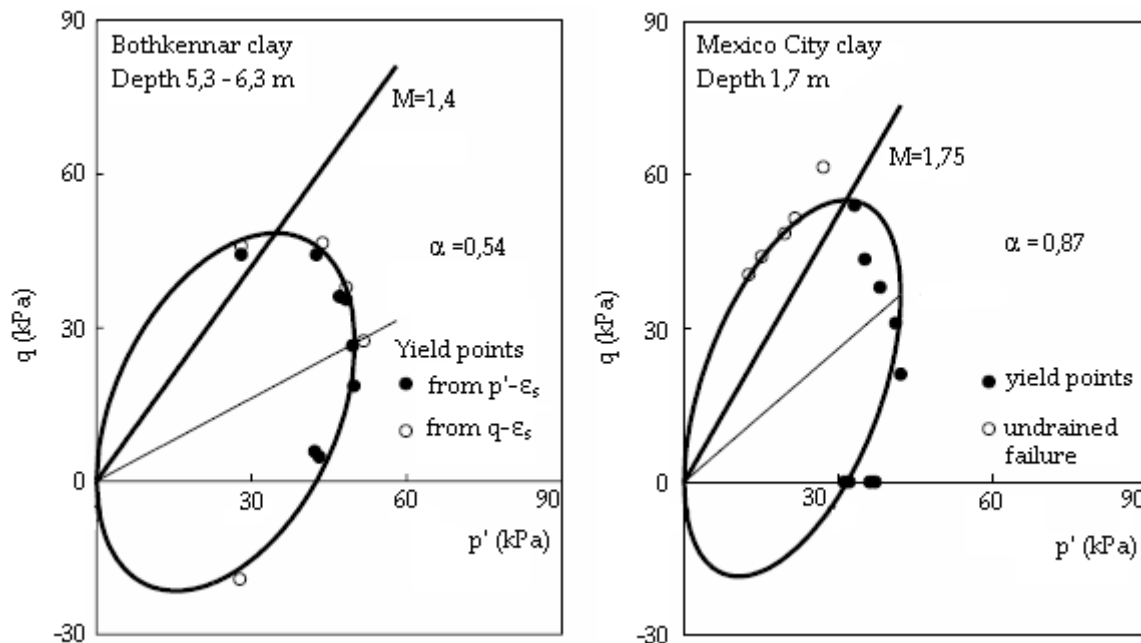
Figure 51 – The initial yield curves for Bothkennar clay and Mexico City clay (Wheeler et al., 2003)

The figure shows that the yield points are nicely described by the simulated yield curve as suggested by Wheeler *et al.* (2003). However, according to Krenn *et al.* (2003) the accurateness

of the rotational hardening law is highly dependent on the ratio q/p'. If the ratio is high, which indicates that the soil is close to the CSL, the post-yield volumetric strains are significantly underestimated. It is believed that the underestimation of the plastic strains is caused by the effect of destructuration. On the other hand, for lower q/p' ratios the post-yield strains are reasonably predicted by the S-Clay1 model. This indicates that the effect of destructuration is most pronounced when the soil is close to failure. In addition, the effect of bonding and destructuration is also dependent on the sensitivity of the soil (Karstunen and Koskinen, 2004). For Murro clay (S_t=10.5) the inclusion of destructuration resulted only in a small improvement of the horizontal soil deformations, although for Vanttila clay (S_t>50) the destructuration could lead to significantly higher horizontal deformations. However, the embankments considered in the this thesis are not subjected to loading situations close to the CSL, and the sensitivity of the examined soft soils is expected to be low. For this reason, the simulations in the next chapter are restricted to S-Clay1 model, which does not include the effect of destructuration.

The anisotropic models that have been proposed in the past require a significant number of additional parameters. For example, the model proposed by Pestana and Whittle (1999) that includes for anisotropy, small strain non-linearity and hysteresis. This model needs a considerable amount of non-standard testing to determine the model parameters. Karstunen and Koskinen (2008) advocate that several features are not important for normally or lightly overconsolidated soft soils, which means that there are much simpler anisotropic formulations possible. The presented S-Clay1 model is deliberately kept as simple as possible. In comparison to the parameters of the MCC model, the S-Clay1 model requires just two additional parameters (β and μ) associated with the rotational hardening rule. All soil constants, except parameter μ, can be obtained from the results of standard triaxial tests and oedometer tests. Furthermore, it is emphasized that the S-Clay1 model only considers plastic anisotropy, because plastic deformations are likely to be dominating in normally and lightly overconsolidated soft soils. Elastic anisotropy is not included, because it will increase the complexity of the model enormously. To fully describe elastic anisotropic behaviour 21 elastic constants are needed. However, most models that describe elastic anisotropy assume isotropy in the lateral planes (cross anisotropy); the amount of elastic constants is then reduced to 5 (Budhu, 2007). Also no attempt has been made to model the non-linearity for the small strain stiffness. Again, this is in the interest of simplicity, and is justified by the fact that this non-linearity is mainly important for heavily overconsolidated clays, where realistic modelling of the non-linearity at small strains is often of crucial importance (Wheeler *et al.*, 2003). For the S-Clay1 model elastic behaviour is described with the same isotropic relation as in the MCC model (see formula 61). However, the assumption of isotropic elastic behaviour inside the yield curve implies that the S-Clay1 model is mainly suitable for embankment related problems. It is not suitable for analyzing excavation problems, where most of the subsoil follows an unloading stress path.

The yield surface of the S-Clay1 model in principal stress space is a sheared ellipse as shown in figure 52. Notice that this representation is only valid for simplified stress conditions like a triaxial test. For general stress states the invariants p' and q cannot be used, and anisotropy has to be expressed with a dimensionless second order tensor, which is also known as the fabric tensor. The basic principles for the generalization are reported in Karstunen (2005).
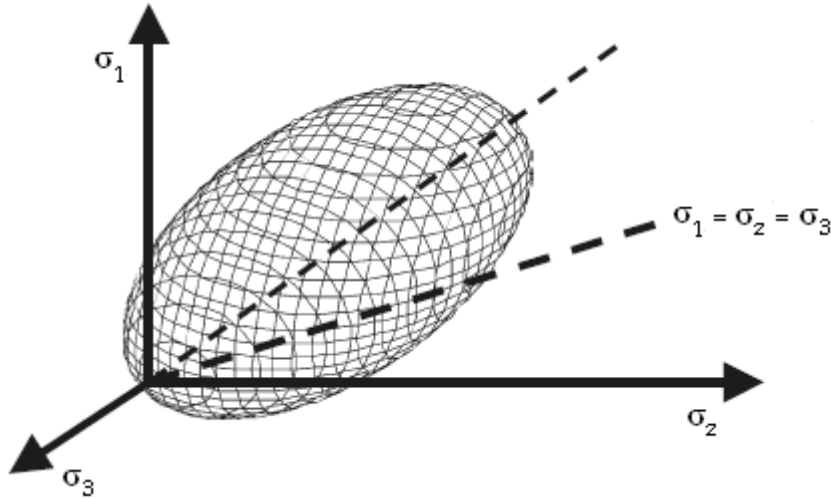
Figure 52 – Yield surface of the S-Clay1 model in a 3D stress space (Karstunen and Koskinen, 2008)

The formulas presented in this section are only valid for triaxial test conditions. This choice has been adopted to make it easier to explain the main principles behind the S-Clay1 model, without the complicating matrixes for the various vectors and tensors.

The mathematical formulation of the yield function is given in formula 75. In which the value of α is a measure for the degree of plastic anisotropy in a soil. If α is equal to zero, the soil behaviour is isotropic and similar to the yield surface in the MCC model. The state variable p'_m is the maximum value of p' on the sheared ellipse (see also figure 38).

$$f = \left(q - \alpha \cdot p'\right)^2 - \left(M^2 - \alpha^2\right) \cdot \left(p'_m - p'\right) \cdot p' = 0 \tag{75}$$

The plastic strain increments are determined with an associative flow rule as suggested by Wheeler *et al.* (2003). This appears to be a reasonable approximation for natural clays with an inclined yield surface. Notice that for the sake of simplicity an associative flow is very desirable, because the numerical implementation will be much easier. The mathematical formulation of the flow rule is presented in formula 76.

$$\frac{\partial \varepsilon_q^p}{\partial \varepsilon_p^p} = \frac{2 \cdot \left(q/p' - \alpha\right)}{M^2 - \left(q/p'\right)^2} \tag{76}$$

The S-Clay1 model incorporates two hardening rules. The first is a cap hardening law, which is assumed to be solely related to the plastic volumetric strain. Notice that this hardening rule is equivalent to the one proposed in the MCC model. The second is a rotational hardening rule that describes the change of inclination of the yield curve, which is produced by plastic straining. The proposed form of this hardening rule is shown in formula 77.

$$\partial \alpha = \mu \cdot \left(\left(\chi_p \left(q/p'\right) - \alpha\right) < \partial \varepsilon_p^p < \beta \cdot \left(\chi_q \left(q/p'\right) - \alpha\right) \cdot \left\{\partial \varepsilon_q^p\right\}\right) \tag{77}$$

The χ parameters are the target values of anisotropy, because it restricts state variable α to a maximum. The χ expressions can be determined from the experimental data obtained by Näätänen and Lojander (2000). They suggest the following χ relations in formulas 78 and 79.

$$\chi_p(q/p') = \frac{3 \cdot (q/p')}{4} \tag{78}$$

$$\chi_q(q/p') = \frac{q/p'}{3} \tag{79}$$

The soil constant β controls the relative effectiveness of the plastic shear strains and plastic volumetric strains in rotating the yield curve. For the modelling of horizontal deformations plastic shear strains are mostly dominating. This means that the overall target value for α will be closer to target value χ_q. Furthermore, the Macaulay bracket on the plastic shear strain increment ensures that the model remains sensible when the plastic shear strains become negative during yielding at the dry side of the CSL. Omission of the Macaulay bracket would mean that α would diverge from the target values χ, which will lead to numerical instability (Wheeler *et al.*, 2003). However, it is important to emphasize that the S-Clay1 model is not intended to be used at the dry side of the CSL. The model predictions at this side are likely to be inaccurate. The last parameter that requires special attention is μ. The model parameter μ controls the rate at which α progresses towards its current target value. Unfortunately, it is not possible to suggest a simple and direct method for determining this parameter. The only solution is to perform model simulations with different values of μ, and then compare these simulations with the observed behaviour to select the most appropriate value. In practice, this procedure is mostly not feasible. For this reason, Zentar *et al.* (2002) suggested that the value of μ for a soft soil will normally lie between $10/\lambda$ to $15/\lambda$. Karstunen and Koskinen (2008) used this empirical relation, and concluded that the model simulations are not particularly sensitive for changes in μ.

In addition, the initial value of state variables α_0 and p'_{m0} have to be assigned to specify the initial size and inclination of the yield curve. The state variable α_0 is determined from the K_0 condition, which implies that the ratio between shear strains and volumetric strains is equal to 2/3 (Wheeler *et al.*, 2003). When this ratio is combined with the flow rule as expressed in formula 76, the initial yield inclination corresponding to K_0 compression can be postulated as shown in formula 80. Budhu (2007) indicated that the effective stress ratio q_0/p'_0 for K_0 condition is determined with formula 81.

$$\alpha_0 = \frac{(q_0/p'_0)^2 + 3 \cdot (q_0/p'_0) - M^2}{3} \tag{80}$$

$$q_0/p'_0 = \frac{3 \cdot (1 - K_0)}{1 + 2.K_0} \tag{81}$$

The maximum stress on the initial yield curve p'_{m0} is calculated by fitting the yield function as presented in formula 75 with the maximum measured stress point, using independent derived M and α_0 values for specifying the shape of the curve. Furthermore, the model parameter β can also be estimated from the K_0 condition. Wheeler *et al.* (2003) suggested the following analytical relation (see formula 82).

$$\beta = \frac{3}{8} \cdot \frac{4M^2 - 4 \cdot \left(q_0/p_0'\right)^2 - 3 \cdot \left(q_0/p_0'\right)}{\left(q_0/p_0'\right)^2 - M^2 + 2 \cdot \left(q_0'/p_0'\right)} \tag{82}$$

Finally, some words about the accuracy of the predictions with the S-Clay1 model. Yin and Karstunen (2008) show that the S-Clay1 model is able to reduce the horizontal deformations during and after construction. Whereas the isotropic MCC model significantly overestimates the amount of lateral deformation (Brinkgreve, 2004). The improved prediction with this model is mainly attributed to the rotational hardening law. So, when the inclination of the yield curve increases, the magnitude of the volumetric plastic strain increments decreases, which ultimately leads to a lower lateral deformations.

3.3.5. *Anisotropic Creep*

The Anisotropic Creep (AC) model is very recently developed by Leonie *et al.* (2008). This model is an extension of the isotropic viscoplastic SSC model, because it accounts for anisotropy during viscoplastic straining. To incorporate this type of anisotropy a rotational hardening rule has been incorporated, which is nearly similar to the one suggested by Wheeler *et al.* (2003) in the S-Clay1 model. As a result, the model predictions of the S-Clay1 model should be identical to the AC model at very low strain rates. An example of such a situation is presented in Leonie *et al.* (2008), where the undrained shear strength is similar for Haney clay in triaxial compression when the strain rate of the AC model was set to 0.05% per hour. An additional confirmation that the ellipses of the MCC model are not suitable for modelling the behaviour of natural soils appears from the experimental evidence shown in figure 53. A better match could be obtained with the proposed rotational hardening rule, which leads to a skewed yield surface.
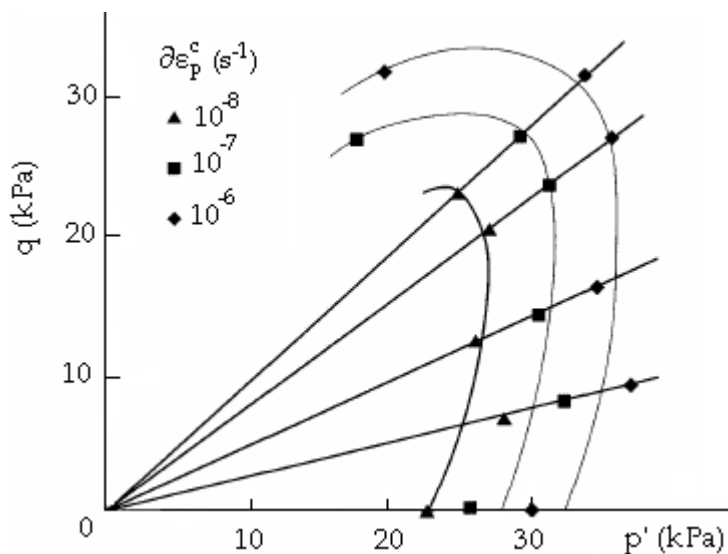
Figure 53 – Yield contours for different volumetric creep strain rates (Boudali, 1995)

Before going into detail about this model, it is important to state that the AC model is not the same as the EVP-SClay1 model as proposed by Yin and Karstunen (2008). Because the latter is based on the classical overstress theory of Perzyna (1963), while the AC model used an extended version of this overstress theory. According to the classical overstress theory the

total strain rate is composed of an elastic and an viscoplastic strain rate component. The elastic strain rates are simply calculated with Hooke's law as already presented in formula 55. The viscoplastic strain rates are determined with an associative flow rule with respect to the dynamic loading surface. The mathematical formulation for the viscoplastic strain rate is shown in formula 83.

$$\dot{\varepsilon}_{ij}^{vp} = \mu \cdot \{\Phi(F)\} \cdot \frac{\partial f_d}{\partial \sigma_{ij}'}$$

(83)

In which parameter μ is the viscoplastic multiplier, which determines the magnitude of the viscoplastic strains. The function Φ(F) is the overstress function representing the difference between the dynamic loading surface and the static yield surface. Again, the Macaulay bracket indicates that the function is zero for negative values and has a value for positive values. Furthermore, the ∂f$_d$ is the viscoplastic potential function that determines the direction of the viscoplastic strains. The difference with the extended version, which is used in the AC model, is that creep strains can also develop in the initially overconsolidated state. However, be aware that the creep strain rate is decreasing with increasing value of OCR, and almost negligible at OCR values higher than 1.3. Due to the incorporation of creep strains in the elastic region a smooth transition is obtained between the mainly elastic region and the viscoplastic region; this is more realistic for natural soils than an abrupt kink that is normally simulated by the classical overstress models (Leonie *et al.*, 2009).

A visualization of the anisotropic creep ellipses in p' and q space is shown in figure 54. Notice that the representation in stress invariants p' and q is only possible if the soil is assumed to be cross-anisotropic, which means that there is no rotation in the principal stress direction of the lateral planes.
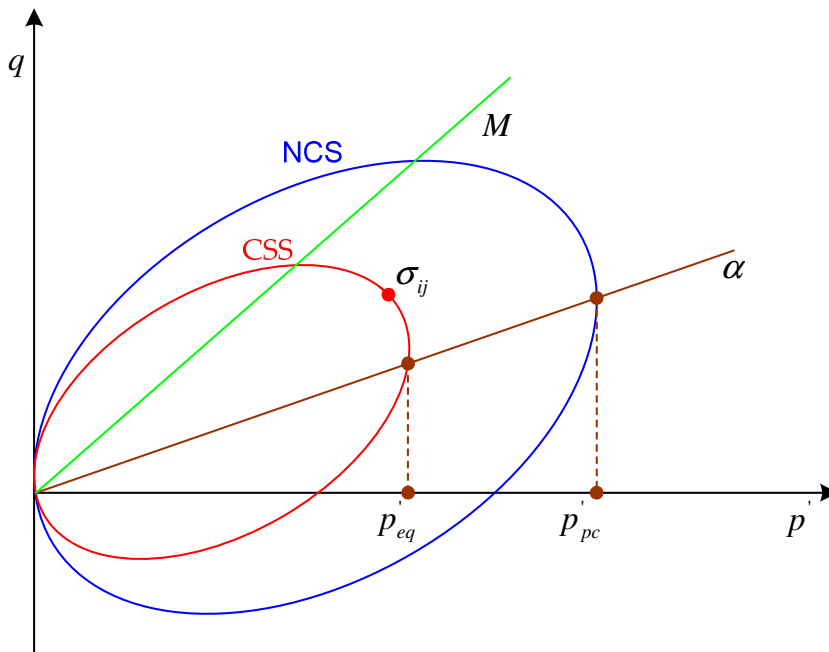
Figure 54 – Anisotropic creep ellipses in p' and q space (Leonie et al., 2008)

The biggest rotated ellipse of figure 54 defines the normal consolidation surface (NCS). The intersection of the vertical tangent to the ellipse with the p' axis is the isotropic effective preconsolidation pressure p'$_{pc}$. The size of this sheared ellipse increases with the volumetric creep strains according to the hardening rule presented in formula 84.

$$p'_{pc} = p'_{pc;0} \cdot \exp\left(-\frac{\varepsilon^c_p}{\lambda^* - \kappa^*}\right)$$

(84)

The other ellipse represents the current stress surface (CSS), on this surface the actual effective stress σ'$_{ij}$ can be found. The intersection of this curve with the horizontal axis is the so-called equivalent mean stress p'$_{eq}$. Notice that equivalent mean stress can be regarded as an isotropic measure of the current stress. The mathematical formulation of p'$_{eq}$ is given in formula 85.

$$p'_{eq} = p' + \frac{(q - \alpha \cdot p')^2}{(M^2 - \alpha^2) \cdot p'}$$

(85)

When the sheared ellipses of the CSS and the NCS are overlapping (p'$_{eq}$ = p'$_{pc}$), the soil is in a normal consolidated state. The ratio between p'$_{eq}$ and p'$_{pc}$ could therefore be used as indicator of the overconsolidation ratio. However, the symbol OCR* is used, because OCR is referring to the vertical overconsolidation ratio. The scalar quantity α in equation 85 acts like a rotational hardening parameter, and its evolution is governed by the rotational hardening rule proposed in formula 86.

$$\partial \alpha = \omega \cdot \left[\left(\frac{3q}{4p'} - \alpha \right) \cdot \partial \varepsilon^c_p + \omega_d \cdot \left(\frac{q}{3p'} - \alpha \right) \cdot \left\{ \partial \varepsilon^c_q \right\} \right]$$

(86)

The soil constants ω and ω_d control the rotation rate of the ellipse. Both parameters are related to basic soil parameters, and do not require any calibration. The shear rotation parameter ω_d is similar to the parameter β in the S-Clay1 model (see formula 82). Whereas parameter ω controls the absolute rate in which the NCS rotates with viscous straining. Leonie *et al.* (2008) shows that parameter ω can be estimated with formula 87. It is important to state that ω is closely related to μ in the S-Clay1 model, so their order of magnitude should be about similar. The outcome of the substitution is presented in formula 86. If ω parameter is set to zero means that the NCS remains in its initial rotated state. Notice that the parameter α_0 represents the initial inclination of the ellipse, and is formulated analogous to the S-Clay1 model (see formula 80).

$$\omega = \frac{1}{\lambda^*} \cdot \ln \frac{10M^2 - 2\alpha_0 \omega_d}{M^2 - 2\alpha_0 \omega_d}$$

(87)

The volumetric creep strain rates are deduced from the one-dimensional creep model proposed by Vermeer *et al.* (1998). The mathematical formulation for general states of stress and strain is presented in formula 88.

$$\dot{\varepsilon}_p^c = \frac{\mu^*}{\tau} \cdot \left(\frac{1}{OCR^*} \right)^{\frac{\lambda^* - \kappa^*}{\mu^*}} \tag{88}$$

Next to the volumetric component a natural soils also has a deviatoric component. To determine the deviatoric creep strain the same assumption has been adopted as in the SSC model, which means that the creep strain is simply considered as a time-dependent plastic strain. With this assumption it becomes possible to adopt a flow rule, which gives the relation between the volumetric and the deviatoric creep strains. The result of the adopted flow rule is presented in formula 89.

$$\frac{\partial \varepsilon_q^c}{\partial \varepsilon_p^c} = \frac{\partial p_{eq}'/\partial q}{\partial p_{eq}'/\partial q} = \frac{2 \cdot (q/p' - \alpha)}{M^2 - (q/p')^2} \tag{89}$$

This paragraph concludes with a short discussion about the simulations performed with the AC model. For example, Leonie *et al.* (2008) performed a number of model simulations with the SSC model and the AC model, and compared these with the outcomes of the triaxial compression and extension tests. The results show that the isotropic ellipses of the SSC model overestimate the value of K_0^{NC}, which leads to a significant overestimation of the horizontal soil deformations. Whereas the results of the AC model show a more realistic prediction of K_0^{NC}, which is due to the incorporation of the rotational hardening rule that includes the effect of anisotropy. Furthermore, one of the scarce real applications of the AC model is the embankment construction on Venice lagoon silts as presented by Berengo *et al.* (2008). They show that the match between the simulated lateral deformation and the observed lateral deformation is improved, especially in the long-term where the viscous effects become significant. However, a limitation of the AC model is that large creep strains can even develop in soft soils with OCR values close to unity and in-situ stresses only; this is of course not very realistic (Karstunen, 2010). However, since embankment loading is considered in this thesis, which would turn the soil in a normal consolidated state anyway. For this reason, this limitation is not regarded as a serious obstacle.

3.4. Evaluation of the considered models

Before the case studies are presented in the next chapter, the considered models are first subjected to a thorough evaluation. This is necessary to obtain a good overview of the capabilities of the different models. It starts with a comparison between the empirical, analytical and numerical models. The comparison describes the amount of parameters required for each model, and pays extra attention to the parameters that are important for the modelling of horizontal soil deformations. It also explains the different aspects of soil behaviour that are incorporated in each model. Furthermore, the limitations of the considered models are described. In the second paragraph an extended version of the reliability method of Duncan (2000) is presented to assess the reliability of an embankment. This extension includes the point-to-point variability of natural soils, which is also known as the spatial variability (Vanmarcke, 1977). Notice that the spatial averages have a smaller standard deviation than the corresponding point standard deviation obtained from laboratory or field tests. The reliability method of Duncan (2000) inclusive spatial variability

gives insight into the sensitivity of the parameters, which is required for the prediction of the horizontal soil deformations. If such a method is omitted, it will be troublesome to judge which model is the most suitable for predicting these displacements. In general, anisotropic models require more input parameters; these extra parameters bring more uncertainty in the analysis, in particular when the input parameters are roughly estimated. Furthermore, the reliability method of Duncan (2000) is based on the first two terms of the Taylor series expansion technique. This means that linear approximations are made to determine the sensitivity at a particular point. Such an analysis can be interpreted as a rough approximation to assess the reliability of a geotechnical structure. The outcome of the method proposed is a reliability index β, which can be related to a probability of failure. More information about the method is given in the second subsection of this paragraph.

3.4.1. *Comparison between models and their limitations*

In this subsection the considered models are discussed in relation to their capability to predict horizontal deformations. It seems to be obvious that the quality of the prediction is improved when more aspects of real soil behaviour are included in the simulation. This suggests that more sophisticated are the method of choice for determining the magnitude of the lateral deformations. However, these models require in general a larger amount of input parameters. If the accuracy of the input parameters is mediocre, the prediction of the lateral deformation will also be doubtful. In that case, it is prudent to use less advanced models that require less uncertain input parameters. This means that the decision for a particular model should not be solely based on the degree of sophistication, but also on the quality of the laboratory test and in-situ measurements. It is therefore highly desirable to compare these models with each other, and to discuss their limitations. After this discussion, the reader should have a better understanding when to use which type of model.

Table 5 in this subsection presents the properties of the considered models. It includes the empirical model of Bourgens and Mieussens (1979), analytical models of Van IJsseldijk and Loof (De Leeuw, 1963), numerical model LEPP with Mohr Coulomb failure criterion (Smith and Griffiths, 1982), numerical model MCC (Roscoe and Burland, 1968), numerical model SSC (Vermeer and Neher, 1999), numerical model S-Clay1 (Wheeler *et al.*, 2003), and the numerical AC model proposed by Leonie *et al.* (2008). This table shows the amount of input parameters that are needed for the considered models, but also the distinctive aspects of soil behaviour that are incorporated. The table confirms that the most sophisticated numerical model, the AC model, describes more aspects of real soil behaviour, but on the other hand it also requires a large amount of input parameters. Notice that the empirical model of Bourgens and Mieussens (1979) should include the effect soil anisotropy. However, the way is unknown, which means that the additional value is limited. It is not possible to examine the contributions of each aspect of soil behaviour individually. In practice, it is often not necessary to determine which soil feature is the most dominant. However, in this academic exercise it is desirable to know which soil feature is essential in the determination of the horizontal soil deformations.

Table 5 – Properties of the considered models

Model	Type	Input Parameters		Aspects of Soil Behaviour						
[-]	[-]	[No.]	A	B	C	D	E	F	G
Bourgens & Mieussens	Empirical	γ_{dry}, c_u, OCR, S_{tot}, S_{el} and $f_{D/B}$ (5 or 6)	x	x			x	x	
Van IJsseldijk & Loof	Analytical	B, t, h, q and S_{tot} (5) [1]	x						
LEPP with MC criterion	Numerical	γ_{sat}, k_x, k_y, E_{oed}, ν, c and φ'_{cv} (7) [2]	x	x					
MCC	Numerical	γ_{sat}, k_x, k_y, M, POP, ν_{ur}, φ'_{cv}, c, e_0, λ and κ (11)	x	x		x			
SSC	Numerical	γ_{sat}, k_x, k_y, K_0^{NC}, POP, ν_{ur}, φ'_{cv}, c, λ^*, κ^*, μ^* (11)	x	x	x	x			
S-Clay1	Numerical	γ_{sat}, k_x, k_y, M, POP, ν_{ur}, φ'_{cv}, c, e_0, λ, κ, μ and β (13) [3]	x	x	x	x		x	
AC	Numerical	γ_{sat}, k_x, k_y, M, OCR, ν_{ur}, φ'_{cv}, c, λ^*, κ^*, μ^*, ω and ω_d (13)	x	x	x	x		x	

[1] The modulus of elasticity can be determined from load q, soft soil thickness h and total settlement S_{tot}

[2] The dilatancy angle ψ is assumed to be zero for the considered soft soils

[3] The μ in S-Clay1 is a rotational hardening parameter, while parameter μ^* in SSC and AC represents the modified creep index

The symbols A till G represent the distinctive aspects of soils behaviour, and are explained in the summation presented below.

A. Represents the ability to simulate elastic behaviour
B. Represents the ability to simulate consolidation
C. Represents the ability to simulate creep behaviour
D. Represents the ability to simulate soil hardening
E. Represents the ability to simulate anisotropy during elastic straining
F. Represents the ability to simulate anisotropy during plastic straining
G. Represents the ability to simulate bonding and destructuration

The empirical model of Bourgens and Mieussens (1979) is based on 32 embankments situated on various clayey subsoils. This model is only valid close to the toe of an embankment. Notice that at this location the lateral deformations are expected to be the largest. Table 5 shows that this model requires 5 or 6 parameters, because $f_{D/B}$ is only needed when the ratio between the thickness of the soft subsoil and width of the embankment is larger than 0.25. The parameters γ, OCR and c_u are needed to determine the safety factor of the embankment. In particular the value of the undrained shear strength c_u has a significant influence on the magnitude of the horizontal deformations. The remaining settlement parameters S_{tot} and S_{el} have an effect on the magnitude of the horizontal deformation due to consolidation. Recently, Feddema *et al.* (2009) applied the model of Bourgens and Mieussens (1979) for a number of embankments, and compared the results with the in-situ measurements. These results indicated that the model performs quite well, because the difference between simulated and measured value about 30%. However, on the condition that the creep does not play a significant role and that the safety factor is above 1.3 during construction.

The analytical models of Van IJsseldijk and Loof simulate horizontal soil behaviour with a volume preserving linear elastic theory. According to Tavenas and Leroueil (1980), this assumption leads to significant deviations compared to the measurements obtained in-situ. Furthermore, it is not possible to simulate a layered soil profile, because the model assumes that the subsoil is uniform. Feddema *et al.* (2009) analyzed the same cases with the analytical models of Van IJsseldijk and Loof, and concluded that the simulations with these models are of moderate quality. The average difference between measured and simulated has a minimum value of about 50%. A main reason why the difference is so large is presumably due to the assumptions made (uniform soil profile, undrained behaviour etc), which differs significantly from the in-situ soil behaviour. It is therefore not advised to use this model, unless the model assumptions practically fit the case conditions.

The first numerical model that is considered is the linear elastic perfectly plastic model with a Mohr Coulomb failure criterion (LEPP-MC). The assumption of perfect plasticity implies that the yield function is completely defined by the input parameters and not affected by plastic straining. The quality of the prediction with this model is to a large extent dependent on the stiffness E and the Poisson's ratio ν. If the stiffness during primary compression is selected, it is possible that the horizontal deformations are overestimated. However, it is also not prudent to apply the reloading stiffness, because the horizontal deformations will then be significantly underestimated. A significant handicap of the model is that it cannot handle different stiffness values for different stress states in a single calculation. In addition, Brinkgreve and Broere (2008) show that the Poisson's ratio seems to be essential for the modelling of horizontal soil deformations, because the relation between horizontal and vertical stresses is solely determined by this parameter as shown in formula 90.

$$K_0 = \frac{\sigma_h'}{\sigma_v'} = \frac{\nu}{1-\nu} \tag{90}$$

Note that Poisson's ratio is a pseudo elastic constant in the LEPP-MC model, and not a pure elastic constant as in the other numerical models. That is the reason why the subscript ur has been omitted for this model in table 5.

Finally, Brinkgreve (2004) shows that the model simulations with this model are not very realistic, because the results show inward lateral deformations due to elastic compaction in the consolidation phase. The key issue here is to take sufficient plastic shear deformation into account. However, to incorporate these irreversible deformations at least one hardening law is required to ensure that the horizontal deformations increase during consolidation.

The Modified Cam Clay (MCC) model was introduced by Roscoe and Burland (1968). This theory assumes that there is a logarithmic relation between effective stress and void ratio during isotropic compression. In contrast to the LEPP-MC model, the MCC model includes a hardening law to include the development of plastic volumetric strains. Another difference is that the MCC uses an associative flow rule to describe plastic strains in stead of a non-associative flow rule. For the sake of simplicity this assumption is very desirable, because the numerical implementation will be much easier. However, the consequence of this is assumption is that the horizontal deformations are significantly overestimated, when these values are compared with the in-situ measurements (Neher *et al.*, 2001). In addition, the most important parameters that affect the magnitude of the lateral deformation are the slope of the critical state line M. Notice that the largest lateral deformations were obtained for a low M value. It is also important to mention that the Poisson's ratio v_{ur} is a pure elastic parameter, which is only important inside the yield contour. For this reason, this model parameter does not play a dominant role in the normal consolidated range, and is therefore not of special importance when mainly normal consolidated clays are considered.

The next numerical model that is considered is the Soft Soil Creep (SSC) model, which is extension of the MCC model (Vermeer and Neher, 1999). The additional feature of this model is that it includes irreversible strain under constant effective stress, because the formulation is based on viscoplasticity instead of elastoplasticity. However, it is also likely that the SSC model overestimates the horizontal deformations, because it uses an associative flow rule. The input parameters of the SSC model are almost identical compared to the MCC model, the only difference is that SSC uses an extra compressibility parameter μ^* that includes creep strains. For a proper functioning of the SSC model, a thorough attention should be paid to the determination of the sensitive parameters K_0^{NC} and μ^*. Notice that the M parameter is not based on the friction angle as in the traditional critical state theory, but on the K_0^{NC} parameter (see formula 2). According to Brinkgreve (2004) these parameters have a significant effect on the amount of horizontal soil deformations under an embankment.

The fourth numerical model is the user-defined model S-Clay1, which includes a rotational hardening law to account for anisotropy during plastic straining. Wheeler *et al.* (2003) show that this model simulates yield stresses significantly better than the isotropic models. The simulations with this model require a just few additional parameters, while other anisotropic models, for example the model of Pestana and Whittle (1999) require much more additional parameters. The parameter that has a large effect on the amount of horizontal displacements is again the parameter M, because it determines the height of the ellipse and it influences the initial inclination of the yield contour. Another important input parameter is β, because it controls the relative effectiveness of the plastic strains in rotating the yield curve. Initial calculations with the model show that the incorporation of the rotational hardening law improves the prediction of the horizontal displacements substantially (Yin and Karstunen, 2008). An large improvement is that the overestimation is drastically reduced, especially

during the construction phase of an embankment. In the long-term when the creep becomes important, the S-Clay1 model seems to underestimate the lateral deformations. This is logical because this anisotropic model does not include creep.

The last numerical model is the user-defined Anisotropic Creep (AC) model, which is recently proposed by Leonie *et al.* (2008). This model is a combination of the SSC model and the S-Clay1 model. It is therefore more suitable than the S-Clay1 model to make long-term prediction. A desirable feature of this model is that creep strains are also generated during the initially overconsolidated state, because it applies an extended version of the overstress theory of Perzyna (1963). Table 5 the AC model requires a relatively large amount of parameters. The difference with the anisotropic S-Clay1 model is that an extra parameter is needed to simulate creep behaviour. Notice that parameter M and ω_d (= β in S-Clay1) are also essential parameters in the determination of the horizontal soil deformations. Initial calculations with the AC model are already made by Berengo *et al.* (2008) for an embankment on Venice lagoon silts. The results indicated that this model is suitable to simulate the lateral deformations, especially in the long-term when creep becomes important.

3.4.2. *Simple method to evaluate the reliability of deformation predictions*

The last part of this chapter is devoted to the description of a simple method to evaluate the reliability of deformation predictions. The results of this analysis give an indication of the combined effects of the uncertainties. In addition, it also provides a logical framework for choosing proper maximum horizontal deformation values, which are appropriate for the involved degree of uncertainty and the consequences of failure. Most reliability methods apply the reliability concepts to the ultimate limit state, for example to judge the reliability of the factor of safety. Only a small amount of the reliability methods are suitable to evaluate the reliability of a deformation prediction to assess the serviceability limit state. According to Zhang and Ng (2005) the calculation of the serviceability limit state is still generally based on deterministic approaches. This is not judicious because the deterministic approach gives no insight into the degree of uncertainty involved.

In this thesis, an extended version of the reliability method proposed by Duncan (2000) is used, which can be applied for both limit states. This extension version incorporates the point-to-point variability of natural soils (Vanmarcke, 1977), which is also known as the spatial variability. The inclusion of the spatial variability is essential, because the point estimates obtained from the field and laboratory testing overestimate the variability of the spatial average. For this reason, Lo and Li (2007) propose a reduction factor to account for the scale effect in the estimates of the standard deviations.

This reliability method is based on the Taylor series expansion technique. The considered method of Duncan (2000) only uses the first two terms of the Taylor series to estimate the sensitivity of the parameters, and assumes that the geotechnical parameters are not correlated with each other. The ultimate result of the analysis is a reliability index, which can be used as relative measure of confidence in the ability of a structure to perform its function in a satisfactory manner. It is noted that the reliability analysis is only performed for the soft soil layers, because these layers are expected to have a large effect on the magnitude of the horizontal soil deformations. The other soils, such as the embankment fill and the stiff soil

layers, are not expected to have significant effect; these layers are only modelled with respect to their mean value. Reliability analysis often use the term probability of failure to judge the performance of a structure. Formula 91 shows how the reliability and the probability of failure are related.

$$P = 1 - R \tag{91}$$

According to Kamien (1995) the term probability of failure should be replaced for the probability of unsatisfactory performance, because the event whose probability is described is not necessarily a catastrophic failure. For example, if one pile in a pile foundation has failed due to excessive lateral deformation, does mostly not imply that the complete building above will collapse. However, it is possible that some cracks occur in the building, which is of course unsatisfactory but not catastrophic. Notice that the remainder of this subsection concentrates on the description of the consecutive steps that are need to be followed.

The first step of the reliability method is the calculation of the lateral deformation with the most likely values of the parameters. Notice that the most likely values are the mean values of the lab and field data. The result of this calculation is the HD_{MLV} value. The next step is to estimate the standard deviations of the uncertain parameters. For a correct determination of the standard deviation two sources of uncertainty have to be included. Firstly, the uncertainty produced in the estimation of the average value. Secondly, the uncertainty caused by spatial variability. Lo and Li (2007) combined these sources of uncertainty in one equation as shown in formula 92.

$$\sigma_{net} = \sqrt{\frac{1}{N} + \Gamma^2} \cdot \sigma_{point} \tag{92}$$

In which N and Γ^2 represent respectively the number of independent sample points and the variance reduction factor for spatial averaging over the prescribed zone. The Γ^2 is a variance reduction factor due to the fact that its value is always less than unity. Notice that the evaluation of Γ^2 is usually complicated, because the variation of the soil property with depth is mostly not available. In practice, formula 93 is often applied to estimate the variance reduction factor (Vanmarcke, 1977). It shows that the variance reduction factor is dependent on the size of the failure domain L and the scale of fluctuation δ over that domain.

$$\Gamma^2 \approx \frac{\delta}{L} \tag{93}$$

A large scale of fluctuation implies that the soil property is slowly varying within a large distance, and gives a smooth variation within the soil profile. On the other hand, a small value of δ signifies that the soil property fluctuates rapidly around the average. Li (1989) determined the δ value for a number of clayey soils, and concluded that the scale of fluctuation is mostly smaller than 0.5 m. The other parameter L is the length of the failure domain; for the modelling of horizontal soil deformations it represents the thickness of the soft soil layers.

The standard deviation of the point values can be determined by various methods. The most appropriate method is mainly dependent on the amount of data available. The statistical way as shown in formula 94 is not always possible, because the amount of available data could be too limited.

$$\sigma_{point} = \sqrt{\frac{\sum(x_i - \bar{x})^2}{N-1}} \tag{94}$$

Another method to determine the point standard deviation is the three-sigma rule, which is especially suitable in situations where the amount of data is sparse. This rule of thumb uses the fact that 99.73% of all values of a normally distributed parameter fall within three standard deviations from the average. The three-sigma rule can therefore be used to estimate the standard deviation by estimating the highest conceivable value (HCV) and the lowest conceivable value (LCV) of an uncertain parameter, and then dividing the difference by six as shown in formula 95.

$$\sigma_{point} = \frac{HCV - LCV}{6} \tag{95}$$

However, Baecher and Christian (2003) indicate that the three-sigma rule is not correct, because people tend to overestimate LCV and underestimate HCV of a limited data set. This leads to smaller standard deviations, and subsequently higher reliability indexes. The reason for this behaviour is that people put too much faith in the results obtained from a small number of observations (Folayan *et al.*, 1970). A solution to account for this uncertainty is to reduce the denominator of the three-sigma rule as shown in figure 55. The figure shows that for a sample size of 20, the value of the denominator is still less than four.
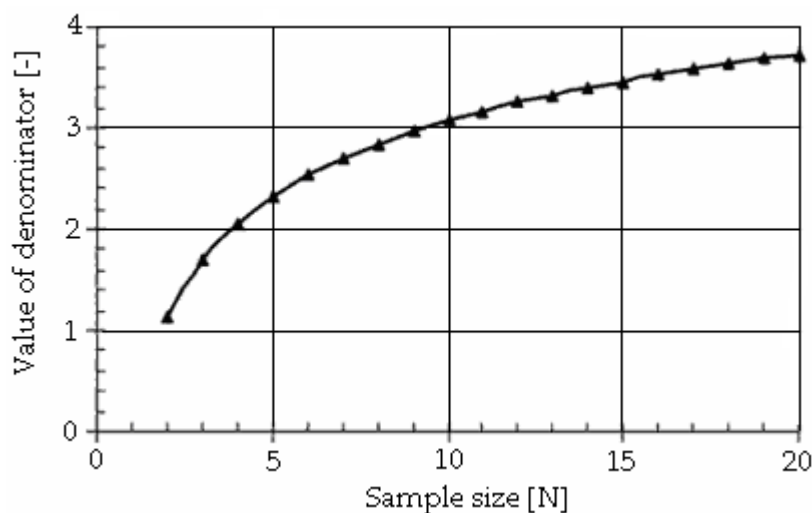
Figure 55 – Value of the denominator as function of the sample size (Baecher and Christian, 2003)

In addition, it is advised to compare the obtained point deviations with the published values in literature (Kulhawy, 1992; Lacasse and Nadim, 1997). Nevertheless, it is important to use judgement when using the standard deviations from published sources, and to consider as

well as possible the degree of uncertainty in the particular case at hand. When the values of N, Γ^2 and σ_{point} are known the net standard deviation can be calculated from formula 92.

The third step contains multiple computations of the horizontal deformation with each parameter increased by one standard deviation and subsequently decreased by one standard deviation, while all other parameters remained equal to their mean values. The sum of all computations can be used to determine the coefficient of variation (see formula 96). Notice that the value ΔHD_n represents the difference in horizontal deformation for the particular parameter, which is increased and decreased by one standard deviation.

$$CV = \frac{\sqrt{\left(\left(\frac{\Delta HD_1}{2}\right)^2 + \left(\frac{\Delta HD_2}{2}\right)^2 + \left(\frac{\Delta HD_n}{2}\right)^2\right)} + |\varepsilon|}{HD_{MLV}}$$

(96)

Formula 96 is based on the Taylor series technique, and assumes that all parameters are independent of each other. In reality several geotechnical parameters do have a degree of dependency, but for the sake of simplicity they are assumed to be independent. The magnitude of the ΔHD components give an insight into the sensitivity of the parameters. If the value is high, it means that the simulated horizontal deformation is very sensitive for changes in the considered parameter. On the other hand, if the value is low, the predicted horizontal deformation is rather insensitive for changes of the parameter. Furthermore, the model uncertainty is incorporated with factor ε that accounts for the difference between the prediction and in-situ observation. The vertical bars indicate that ε is an absolute value, which implies that this factor is always positive. If this factor is omitted, the highest variation coefficient would be obtained for the higher order models (i.e. S-Clay1), because these models require the highest amount of (uncertain) input parameters.

The last step is the determination of the reliability index and the corresponding probability of unsatisfactory performance. To determine the reliability index Duncan (2000) assumes a lognormal distribution of the horizontal deformation values. The mathematical formulation of this index is presented in formula 97. The value $HD_{x\%}$ is the horizontal deformation that is related to a certain probability of exceedance and HD_{MLV} indicates the most likely horizontal deformation, which is already determined in the first step.

$$\beta = \frac{\ln\left(\frac{HD_{x\%}}{HD_{MLV}} \cdot \sqrt{1 + CV^2}\right)}{\sqrt{\ln\left(1 + CV^2\right)}}$$

(97)

According to Duncan (2000) the lognormal distribution is a reasonable approximation. However, there is no irrefutable proof that the horizontal deformation values are really lognormally distributed. The reason why it is often used in the engineering practice is that the probability density function is zero for negative values. This is nice feature, because negative values of the horizontal displacement near an embankment are not very unrealistic. An example of a lognormal probability density function is presented on the next page in figure 56.
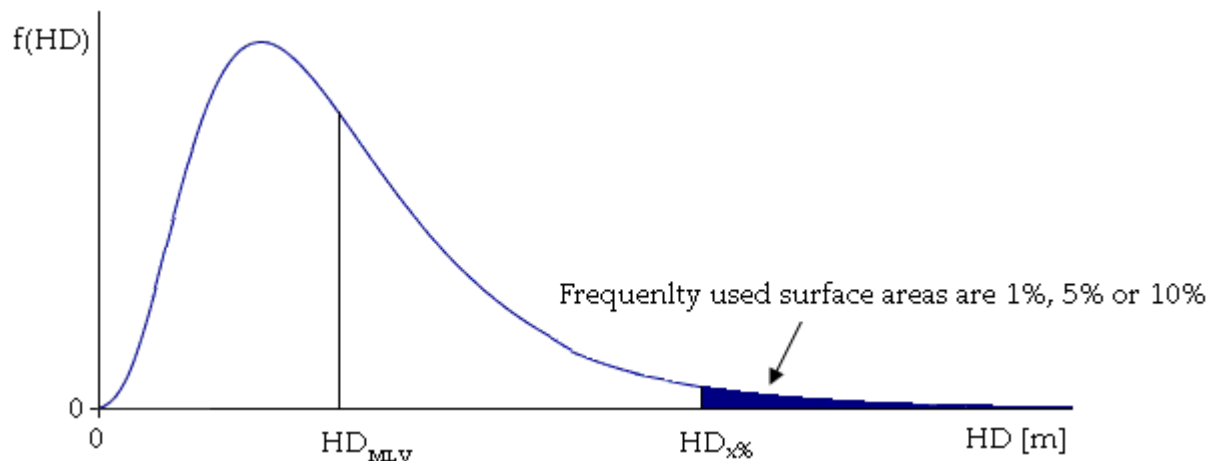
Figure 56 – Example of a lognormal probability density function

The obtained reliability index can be converted to a reliability value with the cumulative standard normal distribution. For example, this could be done with the statistical function NORMSDIST in Excel. The corresponding probability of unsatisfactory performance can easily be determined from formula 91.

Furthermore, it is interesting to know what reliability index is considered to be acceptable. To answer this question one has to bear in mind that a reliability index is a relative measure to assess the current condition of a geotechnical structure, it only provides a qualitative estimate of the expected performance. Embankments with relatively high reliability indices will be expected to perform their function well. On the contrary, embankments with low reliability indices will be expected to perform poorly. Kamien (1995) suggested indicative target reliability values for geotechnical structures in general (see table 6). Notice that these values are indicative, and should preferably be determined for each project separately.

Table 6 – Indicative target reliability values (Kamien, 1995)

Expected Performance Level [-]	β value [-]	P [1] [%]
High	5.0	3.0×10^{-5}
Good	4.0	3.1×10^{-3}
Above average	3.0	1.3×10^{-1}
Below average	2.5	6.2×10^{-1}
Poor	2.0	2.3×10^{0}
Unsatisfactory	1.5	6.9×10^{0}
Hazardous	1.0	1.6×10^{1}

[1] Notice that a probability of 1.6×10^{1} means that 16 of the 100 structures will result in damage

If the target reliability is not reached, more attention should be paid to the accuracy of the uncertain parameters. It is advised to perform additional testing for the most sensitive parameters, which are the parameters with the highest ΔHD values. This should result in a decrease of the coefficient of variation, and correspondingly to an increase of the reliability index. Finally, it is noted that the embankments in Abcoude and Brass that are analyzed in the next chapter will use this reliability technique to judge the reliability of the predictions.

4.   Case Studies

In this chapter the state of the art models are compared with in-situ measurements obtained from two case studies. Notice that these in-situ measurements were not used during the calibration of these models. The validation is especially desirable for the user-defined models S-Clay1 (Wheeler *et al.*, 2003) and Anisotropic Creep (Leonie *et al.*, 2008), because these models are not commercially available in Plaxis. The first case study deals with the construction of a new road embankment near the existing A2 highway in Abcoude the Netherlands. The construction of this new road embankment caused lateral deformations in the soft subsoil. These lateral deformations affect the piles in the foundation of the information gantries, which are located next to the existing road embankment. The other case study is an embankment construction for a LNG export facility in Brass Nigeria. The subsoil at this location consists of soft clay layers, which are interrupted by several thin sand layers. Horizontal deformations were not measured to evaluate the affect on a nearby structure, because the LNG export facility is located in a remote area. The reason why these deformations are measured for this project is to monitor the stability during construction. The embankment construction of the Abcoude case started in the summer of 2007 and was completed in the spring of 2009. The embankment in Brass was constructed a lot faster, because the complete embankment was constructed in the second half of 2008. For both case studies in-situ measurements (settlement beacon data, pore pressure data, inclinometer data etc) were available from the start of construction till about a year after construction. As a result, it is not possible to compare the long-term behaviour of the embankments with in-situ measurements. Furthermore, it is important to state that both projects are situated in a deltaic area. A visualization of the project locations is given in figure 57.
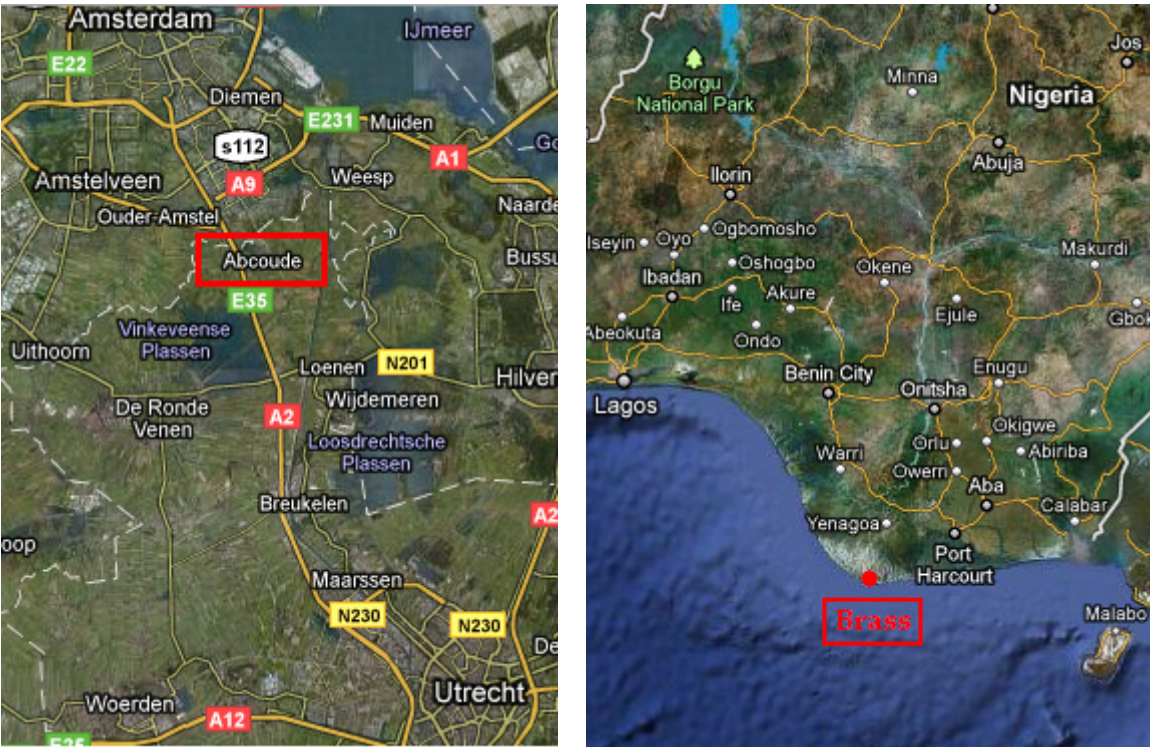
Figure 57 – Geographical location for both projects

The calculation procedure to determine the horizontal deformations will be similar for both case studies. The horizontal deformation profile will be calculated at various locations under the embankment. Suggested is to analyze the horizontal deformations at least at the crest and the toe of the embankment. If the inclinometer is not located at the crest or the toe an additional calculation is required to make a comparison between simulated and measured possible. It is also important to state that the model predictions are analyzed at several moments in time, so that an idea is obtained about the development in time. Notice that long-term comparisons are not possible, because the measuring equipment was removed shortly after construction. In addition, reliability calculations will be performed to assess the sensitivity of the parameters in the considered models. To keep the number of computations within limits, the reliability calculations are only performed for the deformation sensitive layers under the toe of the embankment.

The introduction closes with some notes about the numerical modelling with Plaxis. The simulation with the empirical and analytical models is very straightforward, and requires no further explanation. However, the modelling with a finite element program like Plaxis requires extra attention. For example, undrained behaviour can only be modelled with drained input parameters in a consolidation analysis. The pore pressures are indirectly incorporated into the stiffness matrix. Vermeer *et al.* (2009) shows that the simulations with undrained input parameters are unrealistic in a consolidation analysis. Another point of attention is that the embankments will be modelled with small strain analysis. Karstunen *et al.* (2006) show that an updated mesh analysis is mostly not necessary, because the results were only marginally different. Furthermore, the embankment is only modelled with simple elastoplastic models, because it is expected that horizontal deformations will be dominant in the soft subsoils. This is also advocated by Yin and Karstunen (2008); they show that embankments are dominated by the soft soil response, and are rather insensitive for the embankment parameters. It is finally noted that the dimensions of the model should be such that the boundaries do not have any effect on the results.

4.1. Abcoude – the Netherlands

The first case study is about the reconstruction of the A2 highway between Holendrecht and Maarssen. The goal of the reconstruction is to upgrade the existing A2 highway from three to at least five lanes, and with optional sixth lane. The project is highly needed because the road from Utrecht to Amsterdam as shown in figure 58 is heavily congested, especially in the rush hours. For this reason, Rijkswaterstaat (Department of Public Works) initiated a tender in 2005 to relieve the traffic between these cities. The main content of the work consisted of the reconstruction of the existing A2 highway into a one-directional five to sixth lane highway. For the other direction a new embankment is built adjacent to the existing highway. The A2 reconstruction project was tendered according to the principles of Design & Construct. In such a contract the contractor is responsible for both design and construction. This project was ultimately awarded to the consortium A2HoMa, which consisted of the contractors KWS, Boskalis and Mourik. This consortium proposed to construct the embankments with traditional construction techniques, like vertical drainage and extra surcharge height. The sand for the embankments between Holendrecht and Vinkeveen was transported with a

hydraulic pipeline system, which allows a large volume of sand to be transported in a relative short time span. An additional benefit of this construction method compared to the transport by trucks is that the hindrance to the traffic is significantly reduced. Furthermore, to control the deformation of the embankments a sophisticated monitoring program was adopted. A large number of settlements beacons were installed to control the vertical deformations, while the inclinometers were used to monitor the horizontal displacements.

The case study in this chapter deals with the influence of the new embankment on the information gantries. It is likely that these gantries founded on piles will be affected by horizontal displacements, because the soft soil deposit is compressed during the construction of the new embankment. A situation sketch of the highway reconstruction near Abcoude is presented in figure 58.
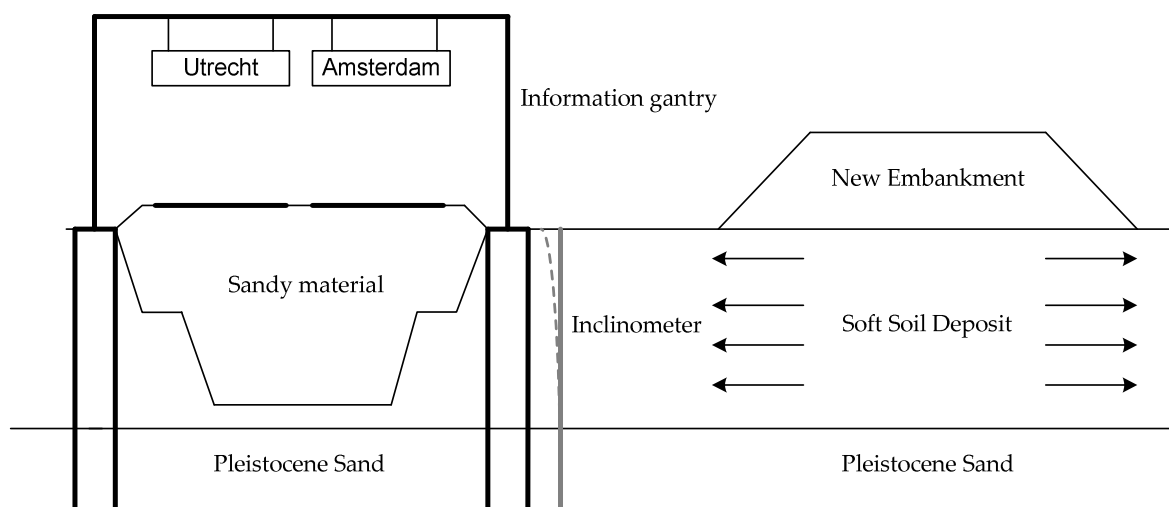
Figure 58 – Situation sketch of the highway reconstruction near Abcoude

The figure shows that the information gantries are located near the toes of the existing embankment in the soft soil deposit. The horizontal displacements caused by the construction of the new embankment increase the forces and moments in the piles of the foundation. When the maximum force in the pile foundation is exceeded the information gantry could collapse. In a traditional Construct contract the client would specify sheet pile structure around all information gantries to eliminate the risk completely. Fortunately, a Design & Construct contract leaves more room for alternative solutions. The involved geotechnical engineers had the feeling that a sheet pile structure around each information gantry was not completely necessary from a structural point of view. For this reason, several calculations were performed with the analytical model of Van IJsseldijk to obtain a rough estimate of the horizontal displacement. If the predicted horizontal displacement exceeded a value of 5.0 cm a sheet pile structure was installed from the beginning. In cases where the maximum calculated horizontal displacement was close to the critical value of 5.0 cm an inclinometer was installed to monitor the horizontal soil deformations on a frequent basis. An overview of all installed inclinometers is presented in Appendix 3. If the maximum value of 5.0 cm was exceeded a sheet pile structure was put into place to prevent any additional lateral deformations. This approach appeared to be cost-effective compared to the traditional Construct contract, because only 25% information gantries required a sheet pile structure in stead of all information gantries (Te Boekhorst and Nguyen, 2007). However, the comparison

between analytical model predictions and the in-situ measurements was at best moderate. The results indicate that the horizontal soil deformations are generally overestimated with the analytical model of Van IJsseldijk (De Leeuw, 1963). The main reason for the large difference between measured and predicted is presumably the result of the assumptions made (uniform soil profile, undrained behaviour etc), which differs markedly from in-situ soil behaviour. To improve the model prediction near the information gantries, the horizontal soil deformations are analyzed in this thesis with the empirical model of Bourgens and Mieussens (1979) and five numerical models in Plaxis with a varying degree of sophistication. This case study concentrates on inclinometer IM-17, which is located near the village Abcoude. The geographical locations of the inclinometers are shown in Appendix 3. Next to the presentation of the model predictions, attention is also paid to the description of the ground and hydrological conditions, geometry and construction of the embankment, and the parameter selection for the considered models.

4.1.1. *Description of ground and hydrological conditions*

The subsurface conditions near Abcoude are determined from a number of borings and cone penetration tests. These measurements show that the soft subsoil consists of a thin clay layer and a thick layer of Holland peat. The Holland peat is local organic soil that is mainly found in the western part of the Netherlands. According to the definition of MacFarlane (1969) this peat is best classified as a fibrous peat, because a large amount of vegetation is still visible. For the prediction of the horizontal soil deformations the clay and the peat layer are both important, because these soft soil layers have oedometer stiffness below 2 MPa at a reference stress of 100 kPa.

Underneath the soft soil layers a stiff Pleistocene sand layer is found. This layer has high strength and stiffness values, which is the result of several ice ages during the Pleistocene epoch. The reliability of the deformation predictions are therefore mainly dependent on the stiffness properties of the clay and peat layer, because realistic changes in the stiffness properties of the Pleistocene sand are not expected to change the total amount of horizontal soil deformation significantly. The complete soil profile is presented in table 7.

Table 7 – Soil profile at the considered location near Abcoude

Soil Type [-]	Top of Layer [m +Nap] [1]	Bottom of Layer [m +Nap]	Thickness [m]
Clay	-2.5	-4.1	1.6
Holland peat	-4.1	-8.0	3.9
Pleistocene sand	-8.0	-12.0	-

[1] Nap is Dutch reference level related to the water level in river IJ in Amsterdam

This table shows that the thickness of the soft subsoil is 5.5 m. The Holland peat layer is dominating, because it is more than 2.5 times thicker than the clay layer. The hydrostatic water level in the polder is -3.3 m Nap, which is just 0.7 m under surface level. However, this level is not decisive, because the artesian water pressure in the Pleistocene sand reaches a height of -2.7 m Nap, which is almost equal to surface level.

4.1.2. Geometry and construction

The embankment near the considered information gantries was constructed in four stages as shown in figure 59. This data is obtained from a settlement beacon that was located in the centre of the embankment. The figure shows that the total amount of sand that has been placed is about 7.2 m, and the average height of the construction stages is about 1.8 m. According to the specification the waiting period for each extra meter should be at least one month (Turnhout *et al.*, 2006). This condition was most critical for the second construction stage, because 1.5 m was applied after 53 days. It is important to state that such a condition was required to guarantee the stability of the embankment.

Figure 59 also shows that the settlement immediately after the last construction stage was 2.17 m. The settlement process stabilizes at a value of 2.50 m at the end August 2008. Notice that the settlements development from August 2008 till the removal of the beacon in April 2009 is marginal (+/- 0.03 m). This additional amount of settlements can be attributed to creep.
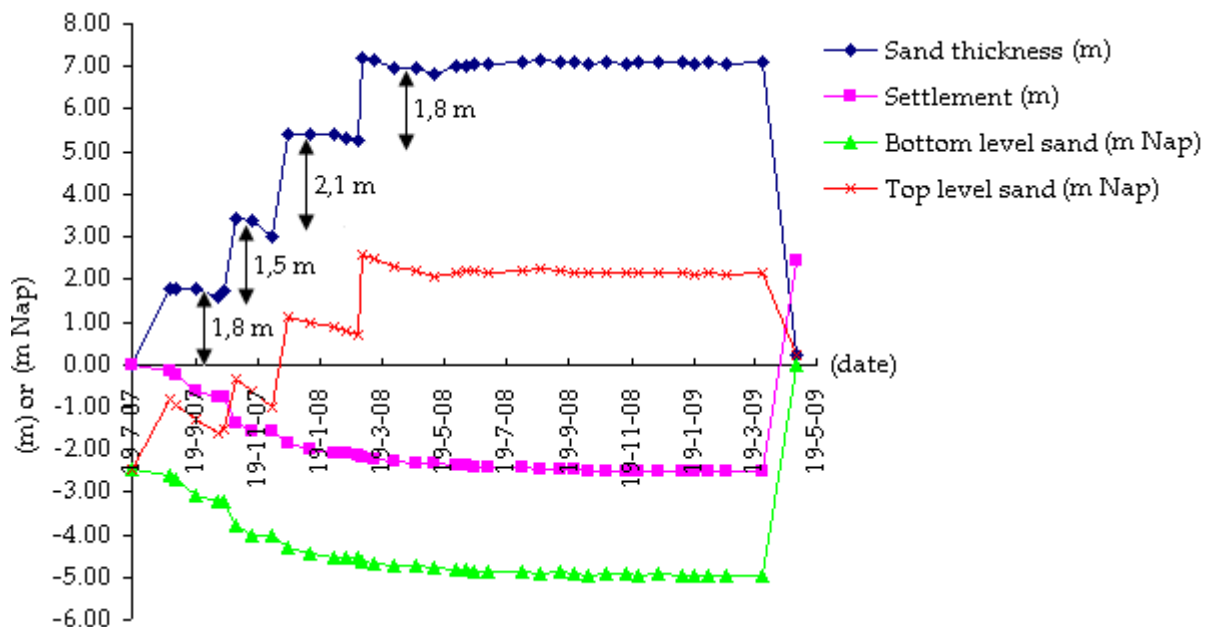
Figure 59 – Settlement beacon data obtained from the centre of the embankment

To speed up the consolidation process vertical drains have been installed immediately after the first construction phase till a depth of -7.0 m Nap in a triangular pattern with a centre to centre distance of 1.0 m.

During the construction period the embankment is raised under a slope of 1:1.5. This means that for every 1.0 m in height, the translation in horizontal direction is at least 1.5 m. According to Ladd *et al.* (1994) the slope of the embankment plays an important role in the development of horizontal displacement, because the slope is indirectly related to the safety factor of the embankment. For example, Bourgens and Mieussens (1979) show that a low safety factor will result in higher amount of horizontal deformation at the toe of the embankment. The geometry of the embankment is graphically presented in figure 60.
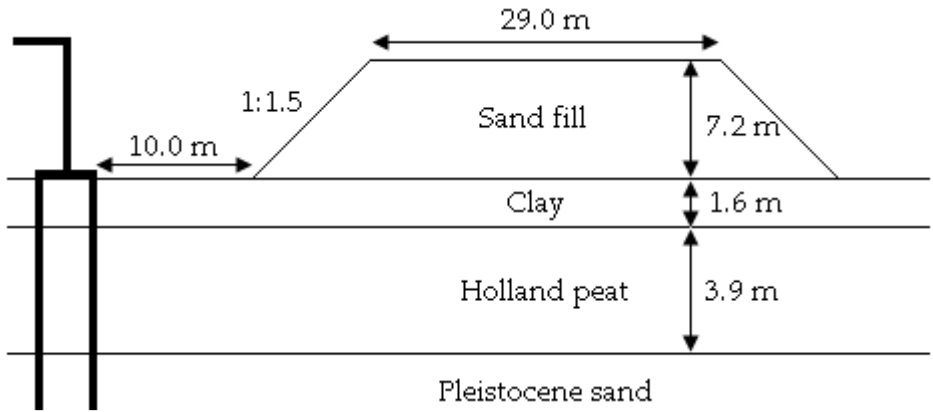
Figure 60 – Geometry of the embankment (not on scale)

The figure shows that the distance between the toe of the new embankment and the considered information gantries is about 10.0 m. The model predictions will therefore be made at the crest and the toe of the embankment, but also at the location of the inclinometer that the located next to the information gantry.

4.1.3. *Parameter selection of considered models*

The geotechnical properties that are required as input parameters for the considered models are presented in this subsection. The subsoil at the considered location consists of a clay layer on top and a thick Holland peat layer underneath. The performed laboratory measurements indicate that the soil properties are highly variable. This is illustrated in figure 61, which shows the water content measurements for both soft soils at various locations across the project trace.
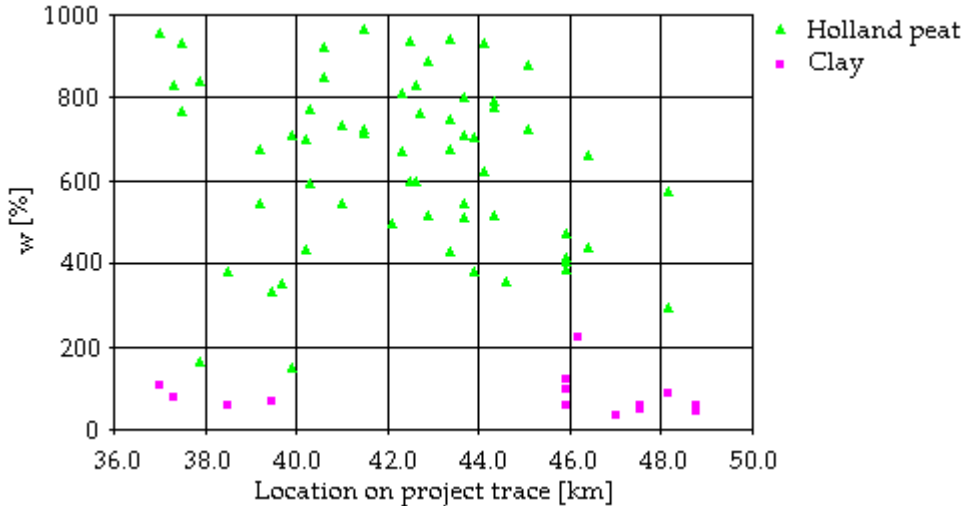
Figure 61 – Water content measurements at various locations across the trace

This figure shows that there is no particular trend in the water content measurements. It is therefore valid to assume that the soil samples belong to one test population. A large benefit of this assumption is that the data set becomes large enough to calculate the mean and standard deviation with conventional statistical methods. Table 8 shows the representative

parameters for clay and Holland peat. These parameters were determined from the project database, which contained various laboratory measurements carried out by Fugro and Mos.

Table 8 – Geotechnical parameters for clay and Holland peat

Parameter	Unity	Clay		Holland peat	
		Mean	σ_{point}	Mean	σ_{point}
$\gamma_{in\text{-}situ}$	[kN/m³]	15.9	0.53	9.4	0.92
CR	[-]	0.14	0.01	0.41	0.09
CR/RR	[-]	7.0	-	7.0	-
CR/C$_\alpha$	[-]	20.0	-	14.0	-
E_{oed} [1]	[kPa]	1635	159	586	156
c_v	[m²/s]	$8.24 \cdot 10^{-8}$	$1.04 \cdot 10^{-7}$	$2.4 \cdot 10^{-7}$	$3.2 \cdot 10^{-7}$
φ'_{cv} [2]	[°]	26.4	4.0	32.8	5.0
c	[kPa]	2.1	2.0	5.3	4.3
c_u	[kPa]	26.5	4.0	13.1	5.3
POP	[kPa]	16.6	8.5	19.8	5.1
e_0	[-]	1.9	0.8	5.5	2.6
k_v	[m/day]	$4.2 \cdot 10^{-5}$	$5.4 \cdot 10^{-5}$	$3.5 \cdot 10^{-4}$	$4.7 \cdot 10^{-4}$
k_h/k_v	[-]	1.5	-	10.0	-
K_0^{NC}	[-]	0.61	0.09	0.46	0.06
ν_{ur}	[-]	0.20	-	0.20	-

[1] Oedometer stiffness is determined for a reference stress level of 100 kPa

[2] Critical state value of the effective friction angle is estimated from CU triaxial test results; a direct determination was not possible because the friction angles were cut off at 5% strain

This table shows that the in-situ weight (i.e. combination of organic material, water and gas) of Holland peat is very low, even lower than the volumetric weight of water. The measured compressibility values for Holland peat are comparable with the values obtained for the peat layer at Bricor (Feddema *et al.*, 2009). On the other hand, the compressibility of the clay layer is comparable with the laminated clays in Athlone (Long and O'Riordan, 2001). A graphical representation of the compression ratios, which are plotted against the in-situ volumetric weights, is given in figure 62.
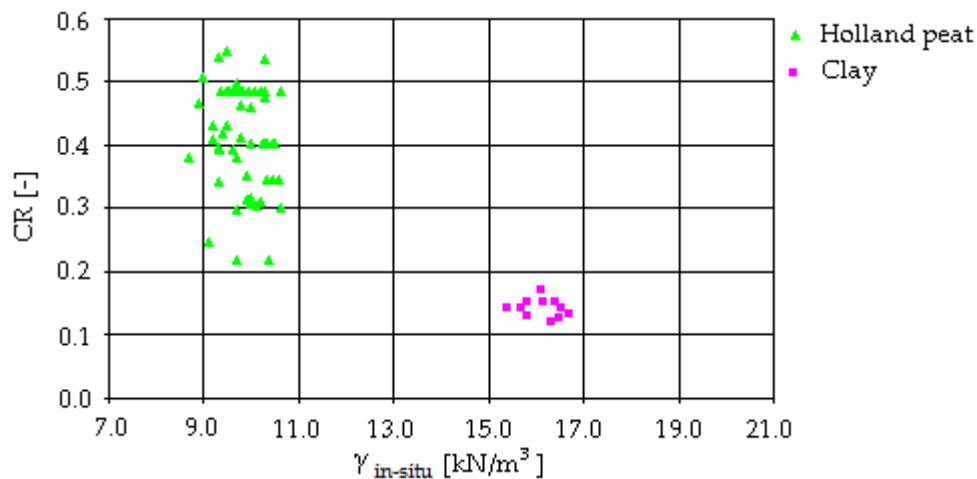
Figure 62 – Compression ratio plotted against the in-situ volumetric weight

Another observation that can be made from table 8 is that the standard deviation is large for the consolidation coefficient as well as the permeability. Figure 63 illustrates the large standard deviation of the coefficient of consolidation for the clay and Holland peat layer. These consolidation coefficients were determined with the method of Taylor. Note that the findings indicate the consolidation coefficients increase with increasing density for the clay samples, while the Holland peat samples seems to be uncorrelated.
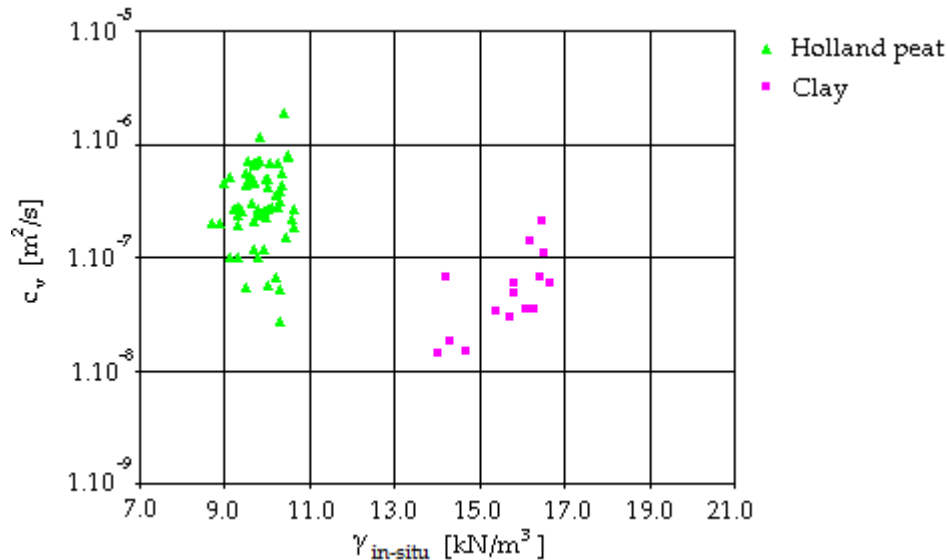
Figure 63 – Consolidation coefficient plotted against the in-situ volumetric weight

According to Duncan (2000) these observations are not strange, because the permeability generally has variation coefficients in the order of 100% to 250%. In addition, the void ratio of Holland peat is almost three times larger than the void ratio of the clay layer on top. These high void ratios are characteristic for fibrous peats, because the structure between the fibres is relatively open. When the permeability ($4.0 \cdot 10^{-9}$ m/s) and void ratio (5.5) are plotted in figure 17, the behaviour is in line with fibrous peat. Table 8 also shows that K_0^{NC} value of the clay layer is much higher than K_0^{NC} value of Holland peat. Den Haan and Feddema (2009) indicate that this difference can be attributed to the fibre structure of Holland peat.

Furthermore, the standard deviations could not be determined in statistical way for all parameters (see indications - in table 8). The three-sigma rule can be applied to determine the point values of the standard deviations. The results of this analysis are presented in table 9. It is important to emphasize that the values of HCV and LCV are at best rough estimations, and should not be interpreted as precise values.

Table 9 – Point values of the standard deviations for the remaining geotechnical parameters

Parameter	Soil	Unity	Mean	HCV	LCV	σ_{point}
CR/RR	Clay/Peat	[-]	7.0	10.0	4.0	1.0
CR/C_α	Clay	[-]	20.0	40.0	14.0	4.3
CR/C_α	Peat	[-]	14.0	25.0	10.0	2.5
k_h/k_v	Clay	[-]	1.5	3.0	1.0	0.5
k_h/k_v	Peat	[-]	10.0	50.0	5.0	7.5
ν_{ur}	Clay/Peat	[-]	0.2	0.4	0.1	0.05

Note that the presented point standard deviations are based on the traditional three-sigma rule, which uses a denominator of 6. Baecher and Christian (2003) advised to reduce the denominator in cases where the amount data is limited. However, in this case several empirical relations have been applied that give a reasonable estimation of the outer bounds of particular parameter (Vermeer *et al.*, 2009). If figure 56 of Baecher and Christian (2003) was applied, the denominator should have a value of approximately 2. This would definitely result in too large values of the point standard deviations.

The models in Plaxis require input parameters that are closely related to the parameters presented in table 8. For example, parameters λ^*, κ^* and μ^* are used instead of CR, RR, C_α. The alternative stiffness parameters λ^*, κ^* and μ^* are easily obtained by dividing CR, RR, C_α by the natural logarithm of 10. The calculations are performed with a small strain analysis, because the parameters are based on a linear strain formulation. The original Cam Clay parameters λ and κ are obtained when parameters λ^* and κ^* are multiplied by a factor $(1+e_0)$. Furthermore, the M values are based on parameter φ'_{cv}, except for the SSC model that uses a relation that is based on K_0^{NC}. The μ and β are the anisotropic parameters in the S-Clay1 model. These parameters are equivalent to the ω and ω_d of the AC model. The value of μ is based on the empirical relation proposed by Zentar *et al.* (2002), while the value of ω is determined from the empirical relation proposed by Leonie *et al.* (2008). The values obtained with these relations could be different. However, when these models are compared with each other, the values of μ and ω should be similar (Karstunen, 2010). In this case study these parameters are both determined with Zentar *et al.* (2002). Tables 10 and 11 present the mean and point standard deviations for the clay and the Holland peat layer.

Table 10 – Mean and point standard deviations for the alternative clay parameters in Plaxis

Parameter	Unity	Mean	HCV	LCV	σ_{point}
λ	[-]	0.174	0.189	0.162	0.005
κ	[-]	0.050	0.055	0.046	0.002
λ^*	[-]	0.060	0.065	0.056	0.002
κ^*	[-]	0.017	0.019	0.016	0.001
μ^*	[-]	0.003	0.004	0.002	0.0003
M	[-]	1.0	1.3	0.7	0.1
μ (or ω)	[-]	57.5	71.8	47.1	4.8
β (or ω_d)	[-]	1.4	1.8	1.0	0.1

Table 11 – Mean and point standard deviations for the alternative peat parameters in Plaxis

Parameter	Unity	Mean	HCV	LCV	σ_{point}
λ	[-]	1.157	1.411	0.904	0.085
κ	[-]	0.332	0.403	0.260	0.024
λ^*	[-]	0.178	0.217	0.139	0.013
κ^*	[-]	0.051	0.062	0.040	0.004
μ^*	[-]	0.013	0.016	0.010	0.001
M	[-]	1.3	1.6	1.0	0.1
μ (or ω)	[-]	10.8	13.0	8.6	0.7
β (or ω_d)	[-]	0.8	1.1	0.5	0.1

The parameters for the sand fill and Pleistocene sand are based on a deterministic analysis, because it is not expected that the magnitude of the horizontal soil deformation is strongly affected by these types of soils. Therefore, both sandy soils will be modelled in Plaxis with the elementary LEPP-MC model. The required geotechnical parameters for sand fill and the Pleistocene sand are presented in table 12.

Table 12 – Geotechnical parameters for the sand fill and Pleistocene sand

Parameter	Unity	Sand Fill	Pleistocene
γ_{dry}	[kN/m³]	17.0	18.0
γ_{sat}	[kN/m³]	19.0	20.0
k_y	[m/s]	1.0	1.0
k_x/k_y	[-]	1.0	1.0
E_{oed} [1]	[MPa]	15.0	50.0
ν	[-]	0.3	0.3
c	[kPa]	5.0 [2]	0.1
φ'	[°]	32.5	35.0
ψ	[°]	2.5	5.0

[1] Oedometer stiffness is determined for a reference stress level of 100 kPa

[2] A small fictitious cohesion is used to prevent numerical instability of the sand fill.

Notice that the values of these parameters are not based on laboratory results, but on empirical relations and experience (Vermeer *et al.*, 2009).

4.1.4. *Model predictions and comparison with in-situ measurements*

This subsection presents the predictions made with the empirical, analytical and numerical models. The maximum horizontal soil deformation will be calculated under the crest, the toe and at the inclinometer that is located 10.0 m outside the toe of the embankment. In addition, the horizontal soil deformations are calculated for various moments in time. For this case study it is chosen to carry out calculations after the 3rd construction stage, 4th (= last) construction stage, one year after the last construction stage and 25 years after the last construction stage.

However, the applicability of the model of Bourgens and Mieussens is limited to the toe of an embankment. This is due to the fact that the empirical relation for estimating the horizontal consolidation deformations is only valid near the toe of the embankment. Notice that the horizontal displacements 25 years after construction could not be determined as well, because the settlement beacon was removed 1.5 years after the last construction stage. The complete calculation is also not feasible for the analytical models. The horizontal soil deformation can only be determined immediately after third and last construction stage, because undrained soil behaviour is assumed. It is therefore not possible to account for time-dependent processes like consolidation and creep. Moreover, the analytical models Van IJsseldijk and Loof cannot handle lateral deformation under the crest of the embankment, because the predictions are unrealistic in this region.

Unfortunately, it was not possible to include model simulations of the AC model, because the available dll (ACM_MC.dll) is working properly. More information about the causes of the malfunctioning is presented in the discussion of this case study. In addition to the determination of the maximum horizontal deformation, the horizontal deformation profiles are presented for each model at the considered places and times. This makes it possible to compare the results of the considered models with each other, and to analyse the differences in more detail. This subsection concludes with a sensitivity analysis for the 2nd construction stage and the 4th construction stage at the toe of the embankment. After the sensitivity analysis, it becomes possible to evaluate the reliability of the predictions. In this thesis, an extended version of the reliability method proposed by Duncan (2000) will be used. More information about this method is given in section 3.4.2.

Before the results of the various models are presented, some general modelling aspects are discussed. In the model of Bourgens and Mieussens (1979) three normalized curves are proposed. The one that is used in this case study is number three, because this normalized curve includes the effect of a stiffer soft soil layer on top. The analytical models of Van IJsseldijk and Loof are modelled as a strip loading (see figure 42). If a terrace loading was selected the width of the embankment is assumed to be infinite.

Furthermore, to ensure relatively fast predictions with the FE program Plaxis, only half of the embankment is modelled. This is possible due to the symmetry of the embankment. Another important aspect is the simulation of vertical drains for an embankment that is modelled under plane strain conditions. For a correct simulation of the vertical drainage a correction has to be applied, because the consolidation behaviour around the vertical drain is essentially axisymmetric. Formula 98 is used here to correct the drain spacing B for plain strain conditions (Russell, 1992).

$$B = \frac{D}{2} \cdot \sqrt{\frac{3}{2} \cdot \left(\ln\left(\frac{D}{d_w}\right) - \frac{3}{4} \right)} \tag{98}$$

In which D is the diameter of the zone of influence and d_w is the equivalent diameter of the strip drain. In this case study, the real drains spacing is 1.0 m, which corresponds to a plane strain spacing of 0.9 m. In addition, mesh sensitivity studies were performed to confirm that the mesh was dense enough to give accurate results for all constitutive models concerned. The optimal mesh density for the stiffer soils appeared to be medium, while a fine mesh density was selected for the clay and Holland peat layer. Furthermore, each calculation phase uses a consolidation analysis to account for the time-dependent effects. Another point of attention is that the embankment should be modelled with a small strain analysis if linear strain parameters are used, while an updated mesh analysis should be used together with natural strain parameters. Simulations have been performed with both strain formulations, and resulted only in marginal differences. For this reason, it is decided to use a small strain analysis, because an updated mesh analysis is numerically more complex and requires considerably more calculation time.

Table 13 shows the predictions of the maximum horizontal soil deformations, which are simulated with mean values for the geotechnical parameters.

Table 13 – Maximum horizontal soil deformations predicted with mean values

Location [-]	Time [-]	B&M [cm]	Van IJ [cm]	Loof [cm]	LEPP-MC [cm]	MCC [cm]	SSC [cm]	S-Clay1 [cm]
Crest	3rd stage	-	-	-	8.3	14.4	14.6	11.3
	4th stage	-	-	-	12.6	12.6	10.7	10.9
	1 year after	-	-	-	12.8	13.9	20.9	12.4
	25 years after	-	-	-	13.0	14.1	31.4	12.5
Toe	3rd stage	36.1	70.3	36.5	10.1	20.6	23.1	18.3
	4th stage	41.2	82.0	42.5	17.0	27.4	26.1	23.7
	1 year after	46.8	-	-	17.3	27.7	34.8	24.3
	25 years after	-	-	-	17.6	28.1	58.3	24.8
Inclino-meter	3rd stage	-	23.8	1.1	1.8	3.3	2.9	2.5
	4th stage	-	27.7	1.3	2.6	3.7	3.4	3.5
	1 year after	-	-	-	1.8	4.4	3.6	3.6
	25 years after	-	-	-	1.7	4.5	5.2	3.7

Table 13 shows that the predicted horizontal displacements with the model of Bourgens and Mieussens (B&M) are structurally larger than the predictions with the constitutive models in Plaxis. Similar findings are observed for the analytical model Van IJsseldijk (Van IJ). This model generates much larger amount of horizontal deformation at the inclinometer location compared to other models. Another conspicuous observation is that most models, with exception of the LEPP-MC model, show a larger horizontal deformation at the crest after the 3rd stage than after the 4th stage. The explanation for this difference is probably related to the crest to toe distance, which is smaller after the 3rd construction stage. It is therefore likely that the horizontal deformations at the crest are influenced by the horizontal deformations at the toe, which are significantly larger as can be seen from table above. It is also concluded that the long-term predictions with the SCC model are significantly larger than the elastoplastic predictions. The increase of horizontal deformation is marginal in the long-term for the elastoplastic models. The LEPP-MC model predictions show even an inward movement during consolidation at the inclinometer location.

On the subsequent pages three graphs are presented where the horizontal displacements are plotted against depth. Figure 64 shows the horizontal deformations under the crest, while figure 65 presents horizontal deformations under the toe for the various moments in time. The predictions near the information gantry are inclusive the in-situ measurements, and are shown in figure 66. Notice that the predictions of Van IJsseldijk are not included, because horizontal deformations predicted with this model are much larger than the other models. If Van IJsseldijk was included into the figures, the differences between the other models would become undistinguishable.
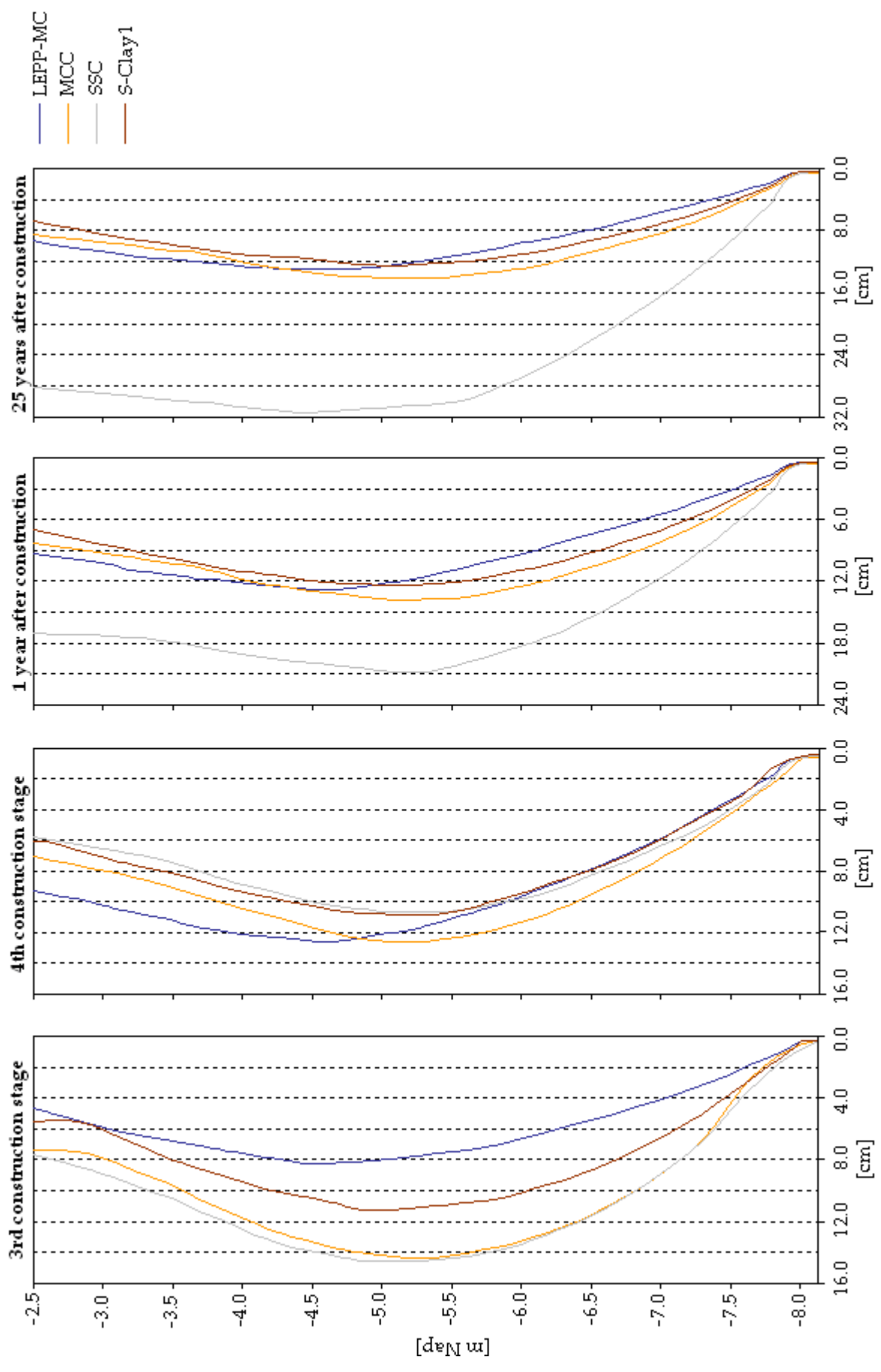
Figure 64 – Predicted horizontal deformation profiles under the crest of the embankment
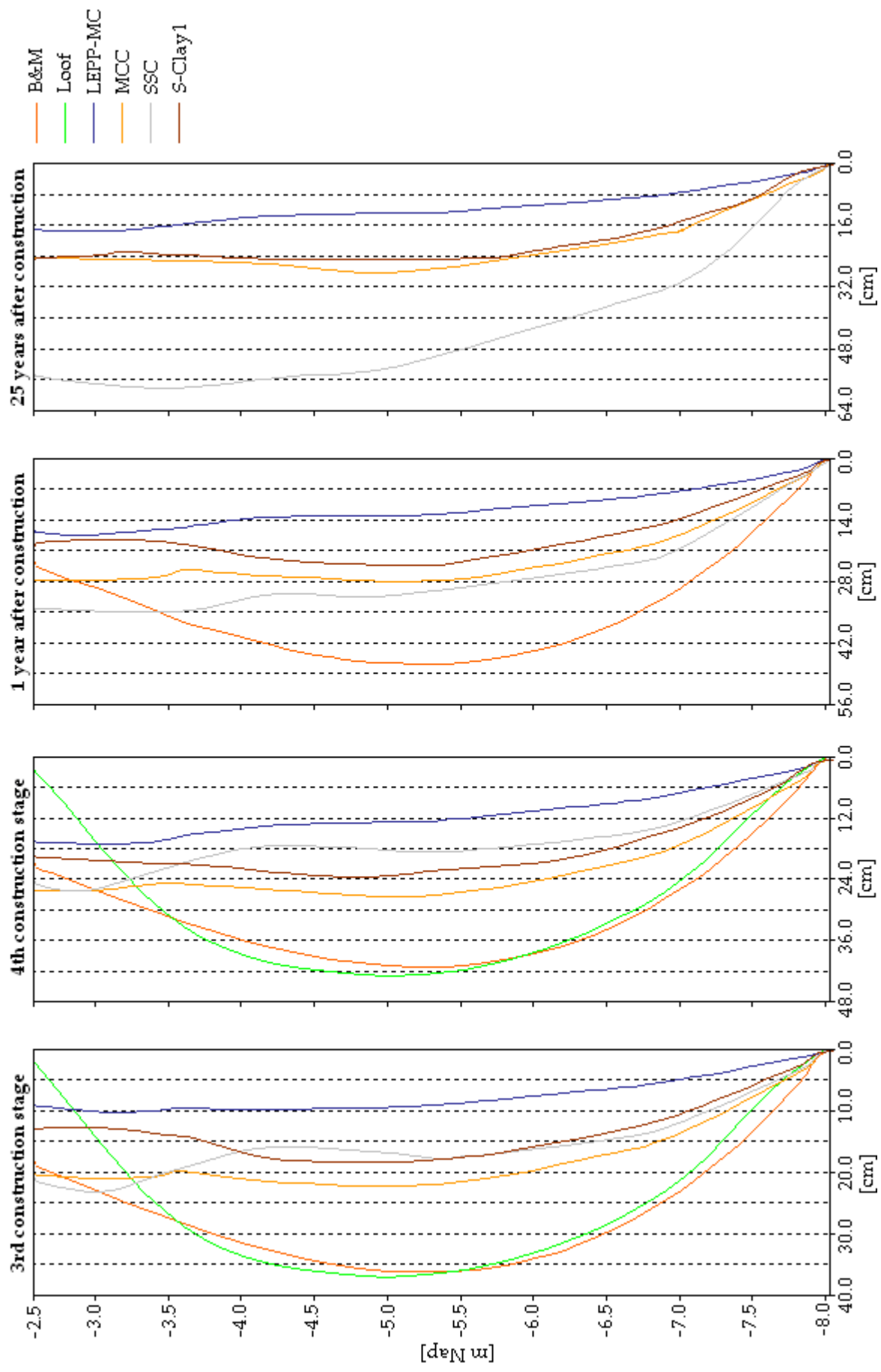
Figure 65 – Predicted horizontal deformation profiles under the toe of the embankment (exclusive the prediction of Van IJsseldijk)
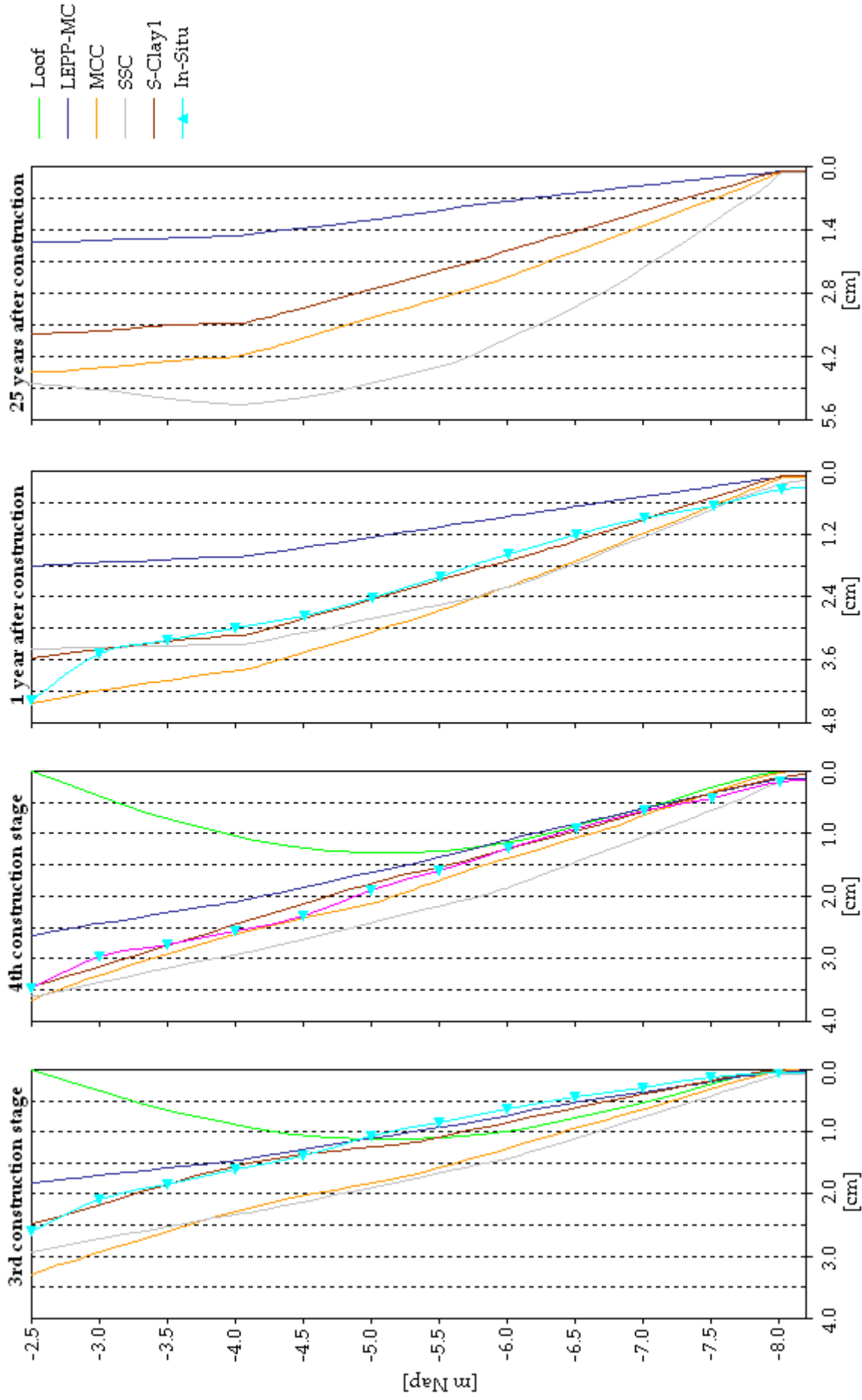
Figure 66 – Predicted horizontal deformation profiles at the inclinometer location (exclusive the prediction of Van IJsseldijk)

Figure 64 shows that the largest horizontal deformations are generated with the MCC and the SSC model. The horizontal deformations under the crest 25 years after construction are more than twice as high with the SSC model in comparison to the other models. The Plaxis output shows that the SSC model still generates excess pore pressures after construction, while the excess pore pressures decrease for the elastoplastic models. These additional excess pore pressures will dissipate, and will result in extra horizontal displacements. The shape of the horizontal deformation profiles is nearly similar to the ones reported profiles in Bricor (Feddema *et al.*, 2009) and Sackville (Rowe *et al.*, 2001). Furthermore, the location of the maximum horizontal deformation varies from -5.0 till -5.5 m Nap, which corresponds to the upper part of the peat layer.

Figure 65 shows the horizontal deformation profiles at the toe of the embankment. The findings indicates that the models of Bourgens and Mieussens and Loof have the tendency to predict more horizontal deformations than the constitutive models simulated in Plaxis. Note that the analytical model of Van IJsseldijk is not included in the graphs, because it predicts unrealistically large amount of horizontal deformation. The largest horizontal deformations in the long-term are again predicted with the SSC model. The lowest lateral deformations during all stages are simulated with the LEPP-MC model. Furthermore, during the 3rd and 4th construction stage the MCC and SSC model show that the largest horizontal displacements are observed in the clay layer on top. It is striking that the predictions with the S-Clay1 model are different, because the horizontal deformations in the clay layer remain limited. If the maximum horizontal deformation at the toe is relatively compared with the maximum horizontal deformation at the crest, it can be concluded the horizontal deformations are larger at the toe. The graphical output in Appendix 4 shows that the maximum horizontal deformations are observed a few meters inside the toe the embankment at the upper part of the Holland peat layer.

Figure 66 shows the horizontal deformation profiles at the inclinometer location, which is installed close to the information gantry. The in-situ measurements are included in the graphs after the 3rd construction stage, 4th construction stage and one year after construction. It is noted that the horizontal deformation profiles at this location are fundamentally different from the shapes observed at the crest and toe of the embankment. Furthermore, the findings indicate that the isotropic MCC and SSC models tend to overestimate the horizontal deformations. Similar findings were also reported by Neher *et al.* (2001). The best fits are definitely obtained with the S-Clay1 model, which uses a hardening law that accounts for anisotropy during plastic straining. This model predicts continued lateral spreading during consolidation that agrees nicely with the measured data. The results imply that creep may not be a major factor during and shortly after construction. Unfortunately, it was not possible to compare the in-situ measurements with the model predictions in the long-term. It is expected that the creep becomes more dominant a number of years after construction. In addition, the results 25 years after indicate that the maximum horizontal deformation is in most cases below the critical value of 5.0 cm, with exception of the SSC model that predicts a maximum horizontal deformation of about 5.2 cm. However, it is important to state that these model predictions are made with mean values. To gain more insight into the robustness of the predictions, simple reliability calculations are performed to evaluate the sensitivity of the parameters.

This subsection concludes with a number of reliability calculations. These calculations have been performed after the 2nd and 4th construction stage at the toe of the embankment. The first step of the reliability calculation is a sensitivity analysis where each model parameter is increased respectively decreased with one standard deviation. However, before a realistic sensitivity analysis can be performed, the standard deviations of the geotechnical parameters have to be converted from point to net values to account for spatial variability. The conversion from point to net values and the results of the sensitivity analysis are transferred to Appendix 5 to increase the readability of the main text. Notice that sensitive parameters have a large ΔHD value, and insensitive parameters have a small ΔHD value. The next step of the reliability calculation is the determination of the variation coefficient. This coefficient gives the relation between the total standard deviation and lateral deformations predicted with the mean values. To give an idea about the reliability of the predictions, the maximum horizontal deformation values that corresponds to respectively 5% and 1% probability of exceedance are given for the considered construction stages and distinctive models in tables 14 and 15.

Table 14 – Results at the toe of the embankment after 2nd construction stage

Model	$HD_{MAX;MLV}$	CV	$HD_{MAX;5\%}$	$HD_{MAX;1\%}$
[-]	[cm]	[%]	[cm] [1]	[cm] [2]
Bourgens & Mieussens	27.5	52.8	60.0	88.2
Van IJsseldijk	51.0	87.8	132.5	219.4
Loof	26.7	66.8	60.2	90.3
LEPP-MC	7.2	63.6	16.3	24.4
MCC	15.6	48.1	29.8	40.3
SSC	15.7	38.3	26.7	34.5
S-Clay1	13.1	26.3	19.4	23.1

[1] Maximum horizontal deformation at the toe that corresponds to 5% probability of exceedance
[2] Maximum horizontal deformation at the toe that corresponds to 1% probability of exceedance

Table 15 – Results at the toe of the embankment after 4th (= last) construction stage

Model	$HD_{MAX;MLV}$	CV	$HD_{MAX;5\%}$	$HD_{MAX;1\%}$
[-]	[cm]	[%]	[cm]	[cm]
Bourgens & Mieussens	41.2	47.3	77.9	105.1
Van IJsseldijk	82.0	81.9	205.5	331.5
Loof	42.5	56.6	87.9	124.9
LEPP-MC	17.0	63.7	37.4	55.2
MCC	27.4	43.8	49.9	66.1
SSC	26.1	29.7	40.4	49.0
S-Clay1	23.7	25.7	34.8	41.2

Table 14 indicates that the variation coefficient of the maximum horizontal deformation at the toe of the embankment after the 2nd construction stage varies roughly from 25% to 90%. The highest variation coefficients are obtained for Van IJsseldijk and the LEPP-MC model. Table 15 indicates that the variation coefficients after the 4th construction stage are somewhat lower. However, the variation coefficients of the empirical, analytical, LEPP-MC model are usually higher than 60%. The more sophisticated models in Plaxis (i.e. models that account

for soil hardening) have a significantly smaller coefficient of variation, something which is mainly the result of a lower model uncertainty (factor ε in formula 96). On the other hand, models like SSC and S-Clay1 generally have a higher parameter uncertainty, but this effect seems to be less dominant than the model uncertainty. Furthermore, the maximum horizontal deformations at the toe of the embankment which are related to 5% and 1% probability of exceedance correspond to β values of 1.6 and 2.3.

4.1.5. Discussion of results

This subsection discusses the predictions obtained with each model in more detail. Note that a comparison with the in-situ measurements is only possible at the inclinometer location, which is located 10 m outside the toe of the embankment. Furthermore, the results obtained with the AC model are not included, because it predicts much smaller lateral deformation and settlement compared to the in-situ measurements. To illustrate this underestimation a 1D settlement comparison is made for a 5.0 m thick layer of clay. The results of the AC model are compared with other elastoplastic and elasto-viscoplastic model formulations.

Bourgens and Mieussens
The discussion starts with the empirical model of Bourgens and Mieussens (1979). The horizontal deformations predicted with this model are larger than the predictions with the constitutive models simulated in Plaxis. However, it is important to mention that it was not possible to validate the predictions with in-situ measurements, because the model is only applicable at the toe of the embankment.

The possible explanation why the predicted horizontal deformations with this model are larger than the constitutive models simulated in Plaxis is likely to be caused by the empirical relation to determine the horizontal consolidation deformations. This empirical relation as proposed by Tavenas *et al.* (1979) appears to be too large. However, one has to be aware that this relation is based on the in-situ measurements of 21 embankments founded on a clayey subsoil. The analyzed embankments show a significant spread in the vertical to horizontal deformation ratios; the measurements indicate that the ratio varies from 0.03 to 0.32. The average value 0.16 is used in the model of Bourgens and Mieussens (1979). It is evident that this relation should be used with caution, especially for embankments situated on organic subsoils.

Van IJsseldijk and Loof
The predictions obtained with the analytical models Van IJsseldijk and Loof are of doubtful quality. Table 13 shows that the horizontal deformations predicted with these models are much larger when they are relatively compared with other models. In particular the model of Van IJsseldijk, which shows a maximum horizontal deformation value that is about three times larger than the constitutive models simulated in Plaxis. Loof tends to give better results, because the order of magnitude is at least more in line with the other models.

However, the in-situ measurements at the inclinometer location indicate that the horizontal deformation profiles predicted with both analytical models are incorrect (see figure 66). The in-situ measurements show that the maximum horizontal deformation is observed close to the surface level, while the largest horizontal deformation is observed for Van IJsseldijk and

Loof model in the upper part of the peat layer. Similar findings were reported by Peters and Steenbrink (2008) for the construction of the Oosterheemlijn in Zoetermeer. When these analytical models are studied in more detail, it is not surprising that these models show such aberrant behaviour. Both models assume that the soft subsoil responds in a fully undrained manner to embankment loading, something which is not observed in reality.

Linear Elastic Perfectly Plastic with a MC failure criterion

The first constitutive model that is simulated in Plaxis is the LEPP-MC model. The in-situ measurements indicate that the predicted horizontal deformations are significantly too low. However, the shape of the horizontal deformation profile is reasonably in line with what is measured in the field. In addition, the development of the horizontal soil deformations is highly unrealistic at the inclinometer location, because the LEPP-MC model predicts an inward movement during consolidation (see table 13). This inward movement is the result of elastic compaction during the consolidation period.

A large benefit of the LEPP-MC model is that the number of parameters is small. The more sophisticated S-Clay1 model requires nearly a double amount of input parameters. The sensitivity analysis for this model shows that the Young's modulus and the Poisson ratio have the largest influence on the magnitude of the horizontal deformation. Note that Poisson ratio in the LEPP-MC model is directly related to the K_0 value, which determines the ratio between horizontal and vertical stresses. It is therefore obvious that the Poisson ratio is an essential parameter in the calculation of the horizontal deformations.

Modified Cam Clay

The second constitutive model that is considered in Plaxis is the MCC model. In contrast to the LEPP-MC this model has the tendency to overestimate the horizontal deformations, especially during construction when creep does not play a dominant role. This is illustrated in figure 66, it shows that the predictions during and shortly after construction are larger than the in-situ measurements. This overestimation is well-known, and is already reported by several researchers. For example, Ladd *et al.* (1994) indicated that the horizontal deformations are usually overestimated with the MCC for the Saugus test embankment on Boston Blue Clay (see figure 6).

The sensitivity analysis shows that the M parameter, the void ratio and the POP are the most sensitive parameters of this model (see Appendix 5). A higher M value leads to stiffer soil behaviour. For this reason, when M is increased, the ratio between deviatoric and volumetric strains also increases. This means that the volumetric strain component gets lower, which logically results in a lower amount of the vertical and horizontal deformation.

Furthermore, formula 64 shows that M has a direct relation with φ'_{cv}. This implies that Holland peat has a higher M value, because the friction angle is significantly higher than the clay layer. The POP and void ratio influence the compressibility of a soil. As a result, when the POP is increased the soil responds will be stiffer. This should ultimately lead to a lower amount of deformations.

Soft Soil Creep

The third constitutive model that is used in Plaxis is the SSC model. Figure 66 shows that horizontal deformations predicted with model are larger than the horizontal deformations measured the field. During the construction period this model is comparable with the MCC model. The reason for this resemblance is that both models are essentially based on the critical state theory. It is therefore logical that both models yield nearly similar results in cases where time does not play an important role. After construction, when time component becomes important, the SSC model generates more horizontal deformations than the MCC model and other elastoplastic models. These additional horizontal deformations are the result of creep. As already indicated the validity of the long-term model prediction cannot be verified with in-situ measurements available in this case study, because the monitoring equipment was removed shortly after construction. However, Neher *et al.* (2001) showed for the Sackville and Skå Edeby test embankments that the SSC model tends to overestimate the long-term horizontal deformations at the crest as well as the toe of the embankment.

The results of the sensitivity analysis indicate that the friction angle, cohesion, K_0^{NC} value and modified creep index μ^* have a significant influence on the horizontal deformation. In the SSC model the K_0^{NC} value is directly related to parameter M (see formula 2) instead of the φ'_{cv} that mostly applied to determine the value of M. Note that a higher K_0^{NC} value results in a lower value of M, and consequently to higher horizontal deformations (see figure 50). In contrast to the MCC model, the SSC model applies a Mohr Coulomb failure criterion to limit the generation of plastic shear strains.

S-Clay1

The fourth constitutive model in Plaxis that is applied is the user-defined S-Clay1 model. As expected, the rotational hardening rule that accounts for plastic induced anisotropy reduces the amount of horizontal deformation. The results show that the predictions with the S-Clay1 model nicely fit with the in-situ measurements. These findings confirm that anisotropy plays at least an important during the early stage of consolidation. Unfortunately, it was not possible to compare the in-situ measurements with the long-term model simulations, because all inclinometers were removed shortly after the end of construction.

The parameters which have a significant effect on the horizontal deformation is parameter M, the void ratio, the POP and rotational hardening parameter β. The value of β is essential, because it controls the relative effectiveness of the plastic shear strains in rotating the yield curve. A higher value of β leads to a faster inclination of the yield curve, and consequently to lower horizontal soil deformations. The effect of other three sensitive parameters is already explained in the MCC model. This is logical because the S-Clay1 model is actually an anisotropic extension of the traditional critical state models (Roscoe and Burland, 1968).

Anisotropic Creep

The other user-defined model that is analyzed in Plaxis is the AC model, which is recently developed by Leonie *et al.* (2008). The AC model can be considered as a creep version of the S-Clay1 model, or as an anisotropic enhancement of the SSC model. This model should be able to simulate the behaviour of natural soils more elegantly, because it incorporates more features of real soil behaviour. However, the predictions obtained with this constitutive model are not very promising so far. When these predictions are compared with the in-situ

measurements it shows that both vertical and horizontal deformation are much lower than expected. To illustrate this underestimation, a 1D settlement comparison has been made for a 5.0 m thick clay layer. This clay layer is subjected to a loading of 100 kPa, and subsequently consolidation times of 10, 100 and 1000 days have been applied. The predictions are based on the clay parameters which have been reported in tables 8 and 10. Note that the settlement calculations are performed with a small strain analysis, because linear strain parameters have been used. The results of the calculations for the various moments in time are presented in table 16.

Table 16 – Predicted settlement comparison for various moments in time

Settlement / Model	Creep included [Y/N]	10 days [m]	100 days [m]	1000 days [m]
MSettle (NEN-Bjerrum) [1]	Y	0.08	0.20	0.52
SSC	Y	0.09	0.18	0.55
S-Clay1 (with rotation)	N	0.10	0.18	0.44
S-Clay1 (without rotation)	N	0.11	0.21	0.49
AC	Y	0.08	0.13	0.18

[1] Settlement calculation program developed by Deltares

Table 16 shows that the settlement of the considered models is nearly identical after 10 days. However, the difference of the AC model with the other constitutive models becomes significant after 100 days, and is even larger after 1000 days. It is surprising that the elasto-plastic S-Clay1 model predicts more settlements than the elasto-viscoplastic AC model that should include creep deformations. When the modified creep index μ^* of the AC model is multiplied with a factor 10, the settlement increases only with a few centimetres. As a result, it appears that the creep formulation is not well implemented in the currently available dll. Other important parameters, such as the stress history parameter OCR and rotational hardening parameter β do have a significant effect on the development of vertical and horizontal deformations. Unfortunately, it is not possible to investigate the creep formulation of this anisotropic model in more detail, because the Fortran codes were not available.

4.2. Brass – Nigeria

The second case study is about the construction of several embankments for a new liquefied natural gas (LNG) export facility in Brass Nigeria, which is located in the centre of the Niger Delta (see figure 57). Next to the projects Bonny and Olokola, the export facility in Brass is one of the large natural gas projects that are currently under construction in the Niger Delta. Large multinationals like Shell, Chevron, Exxon-Mobil and Total all have their stake in these projects. These projects are executed to satisfy the increasing demands for natural gas. Natural gas has multiple uses. For example, for the power generation of gas turbines, but is also used as cooking gas and it is an important feedstock for fertilizers.

The project in Brass compromises the construction of a condensate (CDS) tank, two liquefied patrol gas (LPG) storage tanks, and two LNG storage tanks as shown in figure 67. It is important to state that the two LNG tanks are situated on LNG tank area, while the two LPG tanks are situated on LPG tank area. The three embankment locations were all treated with traditional construction techniques, like surcharge and wick drains, to improve the soft subsoil under the tanks sufficiently. The embankment fill was applied in a traditional way with trucks and bulldozers. The surcharge and wick drains are required to reduce the amount of deformations after construction. Furthermore, the main contractor for the construction of this export facility is Overseas Bechtel. Boskalis Westminster is only a subcontractor that is responsible for the civil works onshore and some dredging works for a pipeline system.

Figure 67 – Site overview during construction inclusive the location of the inclinometers

To control the settlement, horizontal deformation and development of pore pressures a sophisticated monitoring program have been adopted. The total instrumentation consists of 20 settlements beacons, 5 extensometers, 5 inclinometers and an unknown number of piezometers have been placed. The settlement beacons are used to monitor the vertical deformations, but also to reconstruct the construction phasing. The extensometers were located at the top and bottom of the various clay layers to measure the relative contribution of each layer to the total settlement. The piezometers are embedded in the centre of each clay layer to measure the pore pressure during construction. In addition, the inclinometers are used as an early warning system for any potential slope failures, but they also give an indication whether the surcharge is being applied too quickly or not (Ballard, 2006). The

magnitude and development of horizontal displacements can thus be used as an effective tool to control the construction of embankments. Surprisingly, the client did not specify any strict criterion that relates to the amount and development of horizontal soil deformations.

For this project 5 inclinometers are installed close to the toes of the embankments as shown in figure 67. This case study concentrates on the in-situ measurements obtained with inclinometer IM-01, which is located on the east side of the CDS embankment. Notice that the distance between the CDS embankment and the LNG embankment is about 180 m. It is therefore assumed that the influence between CDS embankment and LNG embankment is negligible. The in-situ measurements will be compared with the five constitutive models simulated in Plaxis. Unfortunately, it is not possible to use the empirical and analytical models, because the subsoil is strongly layered. The applicability of these models is limited to an uniform soft soil layer, which is possibly overlain by a stiff soil layer. Apart from the presentation of the model predictions, attention is also paid to the description of ground and hydrological conditions, geometry and construction, and the selection of the parameters.

4.2.1. Description of ground and hydrological conditions

The subsurface conditions under CDS embankment are determined from boring 124 and cone penetration tests (CPTs) 133A, 134A and 135A. These boring and CPTs show a layered soil profile of sand and clay layers till depths of more than 100 m below surface level. However, for this analysis of horizontal deformations it is not necessary to evaluate the soil profile till these extreme depths, because the bottoms of the inclinometer rods are located at a depth of about -20 m LAT. In this case study, the depth of the soil profile is dependent on the installation depth of the wick drains, which are penetrated to a depth of circa -30 m LAT. Table 17 shows the relevant soil profile for this purpose (Peuchen, 2006).

Table 17 – Soil profile at the construction site in Brass

Soil Type [-]	Top of Layer [m LAT]	Bottom of Layer [m LAT]	Thickness [m]
Sand	3.4	-4.5	7.9
Sandy Clay	-4.5	-10.8	6.3
Sand	-10.8	-12.3	1.5
Soft Clay I	-12.3	-19.5	7.2
Sand	-19.5	-27.0	7.5
Soft Clay II	-27.0	-28.5	1.5
Sand	-28.5	-45.0	16.5

This table shows that the relevant soil profile exhibits three deformation susceptible layers. All these layers are fully saturated, because the free ground water level is located at a depth of 2.2 m LAT. The properties of the soft clay layers are quite consistent with each other, because the compressibility indices and overconsolidation ratios are nearly identical. However, the consolidation coefficient for the clay layer with designation soft clay II is twice as high compared to the clay layer with designation soft clay I (Dykstra, 2008). It was therefore necessary to make a clear distinction between these soft clay layers. More specific information about the parameters is reported in subsection 4.2.3. From boring 124 it appears

that the sand layers contain a small fraction of clay or silt. If these fractions are present, they seem to have a small influence on the drainage capacity, because the permeability is only slightly lower than clean sands (Budhu, 2007).

4.2.2. Geometry and construction

The embankments for the Brass project are constructed in a traditional way with surcharge and wick drains. The crest to crest distance of the embankments is about 20 m wider than the diameter of the storage tanks, which have a diameter of approximately 90 m. This large distance makes it possible to analyze the embankments under plane strain conditions. Furthermore, the embankments are raised under a horizontal to vertical ratio of 1.5. The loads imposed by the tanks are based on the analysis of SC-Solutions (Ballard, 2006). For the LNG and LPG an empty and total load of respectively 100 kPa and 250 kPa are reported. The CDS tank is a bit smaller; the empty and total load reaches values of respectively 80 kPa and 200 kPa. It is therefore evident that a large amount of surcharge is needed to prevent large deformations during the operational lifetime.

Figure 68 shows the planned project timeline for the site preloading and tank construction. This timeline shows that the installation of the work floor, wick drains and instrumentation will take about 3 months. Subsequently, the surcharge will be placed over a 3 month period, and the full surcharge will be maintained for another 6 months after the surcharge will be removed. The removal of the surcharge is also expected to take about 3 months. This is assumed to be equivalent to an effective preload period of 9 months. After the removal, the tanks will be constructed and tested in a time period of 30 months (2.5 years). At the end of the construction and testing of the tanks, the tanks will be filled with LNG or LPG for a service lifetime of 240 months (20 years).
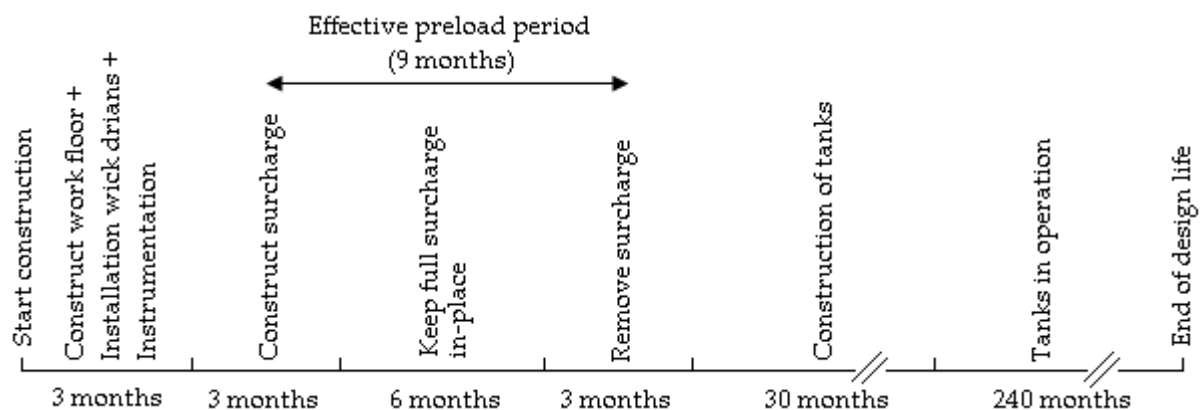
Figure 68 – Planned site preload and tank construction timeline (Ballard, 2006)

The real timeline during construction can be traced back from the settlement beacons that are located in the centre of the embankment. For the CDS embankment the results are obtained from SP1, which is graphically presented in figure 69. Notice that the construction sequence corresponds quite well with the planned phasing as described in figure 68. For example, the settlement beacon shows that the construction starts with a work floor. After the construction of the work floor a waiting period of approximately 100 days is observed. This period is partly used to install the wick drains in a triangular pattern with a centre to centre distance

of 1.5 m till a depth of -30.0 m LAT. The embankment construction from 3.5 m till 16,0 m consists of various small surcharge layers that have been applied in a time period of 45 days. Furthermore, the measurements indicate that the surcharge remains in-place for at least a time period of approximately 5.5 months. Figure 70 also presents the development of the settlement with time. It shows that after the last construction stage the settlement reaches a value of 1.29 m, and progresses further till a value of 1.52 m after 325 days.
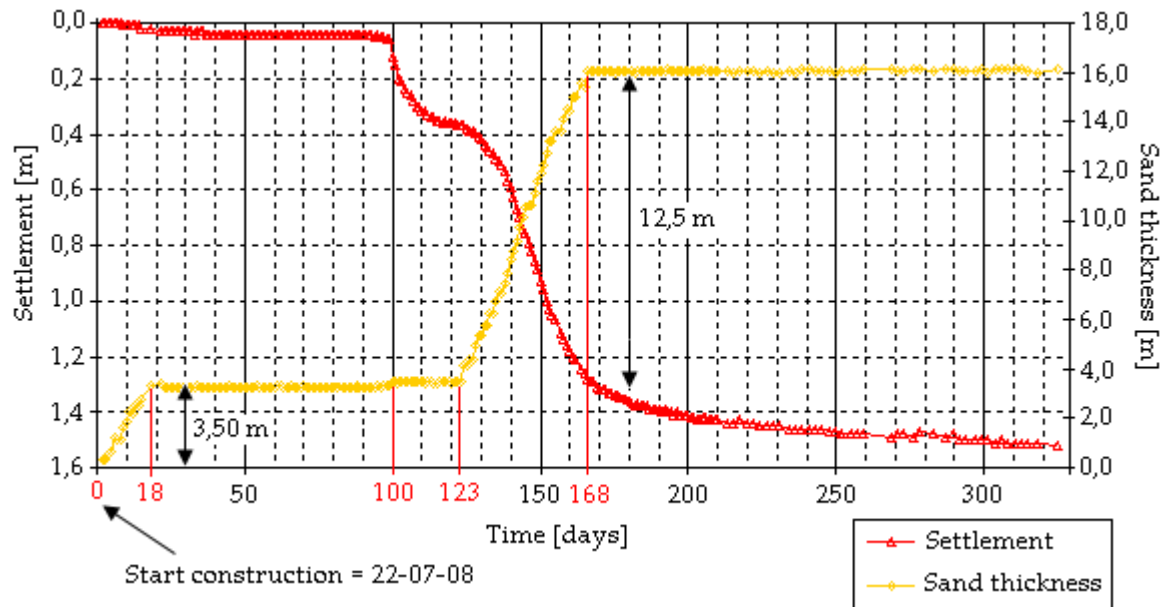
Figure 69 – Settlement beacon data obtained from the centre of CDS embankment

According to the planning approximately 13.5 m of surcharge had to be removed in the summer of 2009 to reach the design level of 4.5 m LAT, which corresponds to the bottom elevation of the tank base slab. However, due to some external circumstances the surcharge remained in place much longer. At this moment, it is expected that the surcharge will be removed at the end of 2010. It is important to mention that the load of the removed surcharge (+/- 225 kPa) is larger than the load of a full tank (+/- 200 kPa). This is a desirable situation, because the stress path remains on the recompression line, and less post-construction deformations will be expected.

4.2.3. *Parameter selection of considered models*

The geotechnical parameters that are required as input parameters for the considered models are presented in this subsection. The values of these parameters are principally based on a number of laboratory and field tests which are carried out by Fugro (Peuchen, 2006). If no specific laboratory or field information was available, empirical relations were applied. For example, parameter K_0^{NC} is determined from the empirical relation of Jaky (see formula 1). The boreholes and CPTs showed that the subsoil consists of a layered soil profile of multiple clay and sand layers. In this case study, only the upper two clay layers are of importance, because the bottom of the considered inclinometer is located at a depth of -21.6 m LAT. The relevant clay layers under the CDS embankment are the sandy clay and soft clay, which can be found at depths of -4.5 to -10.8 m LAT and -12.3 to -19.5 m LAT. These layers are expected to have the biggest influence on the quality of the horizontal soil deformation predictions.

However, before the sensitivity of these two clay layers can be assessed, table 18 presents the representative mean values for the sand fill, sand layers and clay layers (Ballard, 2006; Dykstra; 2008). Notice that there is no differentiation made between the geotechnical properties of the various sand layers. The variations are minor, and are not expected to have a significant effect on the horizontal soil deformations.

Table 18 – Mean values for the sand fill, sand layers and clay layers

Parameter	Unity	Sand Fill	Sand	Sandy Clay	Soft Clay I	Soft Clay II
k_v	[m/day]	1.0	$5.6 \cdot 10^{-3}$	$5.7 \cdot 10^{-6}$	$1.1 \cdot 10^{-5}$	$1.7 \cdot 10^{-5}$
k_h	[m/day]	1.0	$2.3 \cdot 10^{-2}$	$2.3 \cdot 10^{-5}$	$4.2 \cdot 10^{-5}$	$6.6 \cdot 10^{-5}$
γ_{dry}	[kN/m³]	16.7	17.9	-	-	-
γ_{sat}	[kN/m³]	17.2	19.3	15.9	16.2	16.3
K_0^{NC} [1]	[-]	0.50	0.41	0.54	0.56	0.59
ν_{ur}	[-]	0.2	0.2	0.3	0.3	0.3
CR	[-]	-	0.02	0.25	0.31	0.30
RR	[-]	-	$2.5 \cdot 10^{-3}$	$4.7 \cdot 10^{-2}$	$6.3 \cdot 10^{-2}$	$5.8 \cdot 10^{-2}$
CR/C_α	[-]	-	100.0	50.0	40.0	40.0
E_{oed} [2]	[MPa]	25.0	40.0	8.9	9.5	8.8
c_u	[kPa]	-	-	36.2	44.3	46.9
e_0	[-]	0.50	0.60	1.50	1.60	1.55
OCR	[-]	1.0	1.0	1.5	1.4	1.5
c_v	[m²/s]	$1.8 \cdot 10^{-2}$	$1.0 \cdot 10^{-4}$	$1.5 \cdot 10^{-8}$	$1.4 \cdot 10^{-8}$	$2.8 \cdot 10^{-8}$
φ'_{cv}	[°]	30.0	36.0	27.2	26.4	24.5
c [3]	[kPa]	5.0	0.1	1.1	2.1	2.4
ψ	[°]	2.5	5.0	0.1	0.1	0.1

[1] K_0^{NC} values are based on Jaky's formula

[2] Oedometer stiffness is determined for a reference stress of 100 kPa

[3] A small fictitious cohesion is used to prevent numerical instability of the sand fill

The table shows that the preconsolidation values remain quite low for all the considered clay layers, because the OCR values did not exceed a value of 1.5. The same trend is also observed for the other clay layers at greater depths (Dykstra, 2008). It is possible that significant horizontal deformations can develop at large depths due to these low preconsolidation pressures. Another observation that can be made from this table is that the CR/C_α ratios are quite large. For sandy clay a ratio of 50 is used, while the soft clays have a ratio of 40, while the general CR/C_α values for clays usually vary from 15 to 25 (Brinkgreve and Broere, 2008). It is noted that the original design calculations, which are performed by SC-Solutions fully ignored the creep behaviour (Ballard, 2006).

Table 19 presents the standard deviations for sandy clay and soft clay I. Notice that the parameters N and Γ^2 represent the number of independent sample points and the variance reduction factor for spatial averaging over the thickness of the soft soil layer. A precise determination of Γ^2 is not possible, because the complete picture of a soil property with depth is often unknown. However, Li (1989) indicates that the practical range of Γ^2 values usually varies between 0.1 and 0.5.

Table 19 – Standard deviations for the sandy clay and soft clay I

Parameter	Unity	Sandy Clay				Soft Clay I			
		σ_{point}	N	Γ^2	σ_{net}	σ_{point}	N	Γ^2	σ_{net}
k_v	[m/day]	$1.8 \cdot 10^{-6}$	13	0.2	$9.5 \cdot 10^{-7}$	$1.2 \cdot 10^{-6}$	19	0.2	$6.0 \cdot 10^{-7}$
k_h	[m/day]	$7.1 \cdot 10^{-6}$	13	0.2	$3.7 \cdot 10^{-6}$	$4.9 \cdot 10^{-6}$	19	0.2	$2.5 \cdot 10^{-6}$
γ_{sat}	[kN/m³]	0.43	6	0.1	0.22	0.37	38	0.1	0.13
K_0^{NC}	[-]	$3.8 \cdot 10^{-2}$	8	0.2	$2.2 \cdot 10^{-2}$	$4.1 \cdot 10^{-2}$	8	0.2	$2.3 \cdot 10^{-2}$
ν_{ur}	[-]	$5.0 \cdot 10^{-2}$	-	-	$5.0 \cdot 10^{-2}$	$5.0 \cdot 10^{-2}$	-	-	$5.0 \cdot 10^{-2}$
CR	[-]	$5.5 \cdot 10^{-2}$	6	0.2	$3.3 \cdot 10^{-2}$	$3.2 \cdot 10^{-2}$	38	0.2	$1.5 \cdot 10^{-2}$
RR	[-]	$9.0 \cdot 10^{-3}$	6	0.2	$5.4 \cdot 10^{-3}$	$7.0 \cdot 10^{-3}$	38	0.2	$3.3 \cdot 10^{-3}$
CR/C_α	[-]	5.0	6	0.2	3.0	5.0	26	0.2	2.4
E_{oed}	[MPa]	1.64	6	0.1	0.85	3.00	21	0.1	1.15
c_u	[kPa]	10.3	12	0.2	5.5	15.6	6	0.2	9.4
e_0	[-]	0.69	6	0.3	0.47	0.81	38	0.3	0.46
OCR	[-]	0.44	5	0.2	0.28	0.28	31	0.2	0.13
c_v	[m²/s]	$7.8 \cdot 10^{-9}$	13	0.3	$4.8 \cdot 10^{-9}$	$8.2 \cdot 10^{-9}$	19	0.3	$4.9 \cdot 10^{-9}$
φ'_{cv}	[°]	2.8	8	0.1	1.3	3.1	15	0.1	1.3
c	[kPa]	0.8	8	0.1	0.4	1.0	8	0.1	0.5

The constitutive models in Plaxis require alternative input parameters, which are easily determined from simple analytical expressions. Only the rotational hardening parameter µ is based on the empirical relation $10.0/\lambda$. This relation is proposed by Zentar *et al.* (2002). Note that the compressibility parameters are essentially linearizations of the stiffness parameters CR, RR and C_α. The results of this analysis are presented in table 20. More information about the derivation of the analytical expressions can be found in chapter 3.

Table 20 – Mean and net standard deviations for the Plaxis input parameters

Parameter [1]	Unity	Sandy Clay		Soft Clay I	
		Mean	σ_{net}	Mean	σ_{net}
λ	[-]	0.109	0.014	0.135	0.007
κ	[-]	0.041	0.005	0.055	0.002
λ^*	[-]	0.043	0.006	0.052	0.003
κ^*	[-]	0.016	0.001	0.021	0.001
μ^*	[-]	0.0009	0.0001	0.0012	0.0001
M	[-]	1.08	0.11	1.04	0.11
μ	[-]	91.7	7.7	74.1	6.2
β	[-]	0.60	0.15	0.64	0.16

[1] Notice that µ and β of the S-Clay1 model are equivalent to ω and ω_d of the AC model

The parameters for the sand fill and sand layers are based on a deterministic analysis, because it is not expected that the horizontal deformation is strongly affected by these sandy soils. However, for this case study the more advanced Hardening Soil model (Vermeer, 1978) is used for the sand layers, which are located between the various clay layers. The Hardening Soil model is more suitable to simulate distinctive stress paths, because it uses the oedometer stiffness (E_{oed}), triaxial stiffness (E_{50}) and unloading / reloading stiffness (E_{ur}) as input parameter. It is assumed that the value of the oedometer stiffness (see table 18) is similar to

the triaxial stiffness, while the unloading / reloading stiffness is assumed to be three times larger than the oedometer stiffness (Vermeer *et al.*, 2009). The possibility of more stiffness parameters as input value is an is advantage compared to the LEPP-MC model that includes only one stiffness parameter to simulate distinctive stress paths. If the LEPP-MC model was used for the simulation of the sand layers unrealistic unloading or reloading deformations would be obtained.

4.2.4. *Model predictions and comparison with in-situ measurements*

This subsection presents the results of the model predictions, and compares it with in-situ measurements obtained from inclinometer IM-01. It is suggested to analyze the maximum horizontal soil deformations under the crest, the toe and 10.0 m inside the toe of the embankment. Inclinometer IM-01 is located on the slope of the embankment, which means that the comparison could only be made 10.0 m inside the toe of the embankment. In addition, the horizontal deformations will also be assessed for various moments in time. It is proposed to carry out calculations for the last construction stage (till maximum sand height), ½ year after construction, after removal of the surcharge, and after the operational lifetime. Note that the model predictions can only be compared during and shortly after construction of the embankment, because all inclinometers were removed ½ year after construction.

Furthermore, it is important to mention that it is not possible to use the empirical model of Bourgens and Mieussens and the analytical models of Van IJsseldijk and Loof, because the composition of the subsoil is strongly layered. The applicability of these models is limited to a single or a number of soft soil layers, which are possibly overlain by a stiff soil layer. This means a layered soil profile can only be simulated with a FE program. In this case study, the FE program Plaxis 2D is used with different constitutive models to simulate the horizontal behaviour under embankments. The constitutive models that are considered are LEPP-MC, MCC, SSC and S-Clay1. Unfortunately, it was not possible to include model simulations of the AC model. An explanation of the malfunctioning of this model is given in the discussion of the previous case study. Apart from the determination of the maximum horizontal soil deformation, the horizontal soil deformation profile will be plotted for each model at the considered places and times. The subsection concludes with a sensitivity analyses after the last construction stage. The results of the sensitivity analysis will be used to assess the reliability of the model predictions, i.e. maximum horizontal deformations that correspond to a probability of exceedance of 1% and 5%.

The attention points for modelling in Plaxis are similar to the previous case study. However, some extra information is given about the simulation of wick drains in Plaxis 2D. When formula 98, which is used to correct the drain spacing for plain strain conditions, is plotted for different drain spacings some interesting features are discovered (see figure 70). The findings indicate that when the wick drain spacing is smaller than 1.5 m, the model spacing in Plaxis 2D under plain strain conditions is smaller. For example, a real spacing of 1.0 m corresponds to model spacing of 0.91 m. On the other hand, a plane strain model shows better drainage properties for spacings larger than 1.5 m, because the model spacing is larger than the real spacing. For this case study a centre to centre distance of 1.5 m has been adopted, and thus no correction factor is required.
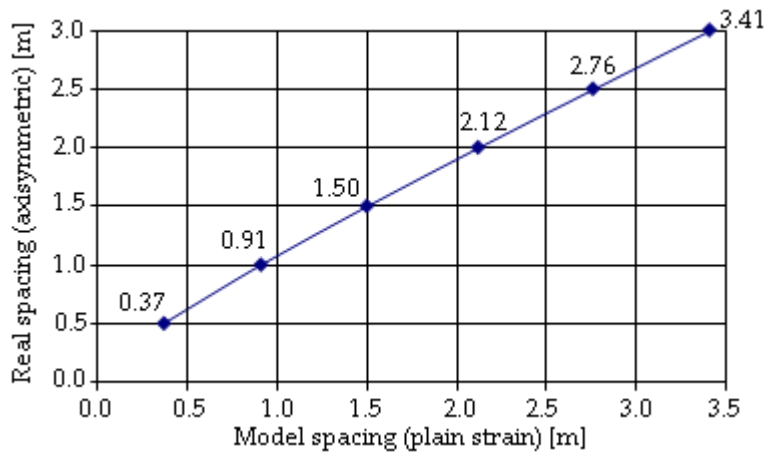
Figure 70 – Relation between real spacing and model spacing for wick drains

The results of the maximum horizontal soil deformations simulated with mean values of the geotechnical parameters for the considered models are presented in table 21.

Table 21 – Maximum horizontal soil deformations predicted with mean values

Location [-]	Time [-]	LEPP-MC [cm]	MCC [cm]	SSC [cm]	S-Clay1 [cm]
Crest	After last stage	8.5	13.8	11.1	11.0
	½ year after	8.3	14.7	14.1	11.6
	After removal	3.3	12.7	16.1	9.2
	End of design life	8.4	16.3	18.5	12.0
Toe	Last stage	9.2	17.4	14.7	12.7
	½ year after	9.0	18.6	18.7	13.0
	After removal	3.4	15.7	19.2	9.4
	End of design life	8.6	18.6	22.1	12.6
Inclinometer	Last stage	10.6	18.9	15.6	14.4
	½ year after	10.5	20.3	19.8	14.9
	After removal	3.7	16.8	20.0	10.8
	End of design life	9.7	20.0	23.1	14.5

Table 21 shows that the MCC model predicts the largest horizontal deformations after the last construction stage. When the consolidation process proceeds and creep becomes more important, the viscoplastic SCC model generates more horizontal deformation compared to the elastoplastic models. Furthermore, the findings show that the LEPP-MC predicts a small inward movement between the application of the last construction stage and ½ year after the last construction stage. Brinkgreve (2004) showed that this inward movement is not observed in reality. Another doubtful observation with the LEPP-MC model is that the predicted horizontal deformation is much lower after the removal of the surcharge than the other constitutive formulations. Notice that the horizontal deformation is reduced for about 60%, while the other elastoplastic models show reductions of approximately 20 to 30%.

On the next pages three graphs are presented where the horizontal deformations are plotted against depth. Figures 71, 72 and 73 show the horizontal deformations under the crest, the toe and at the inclinometer location for the considered moments in time.
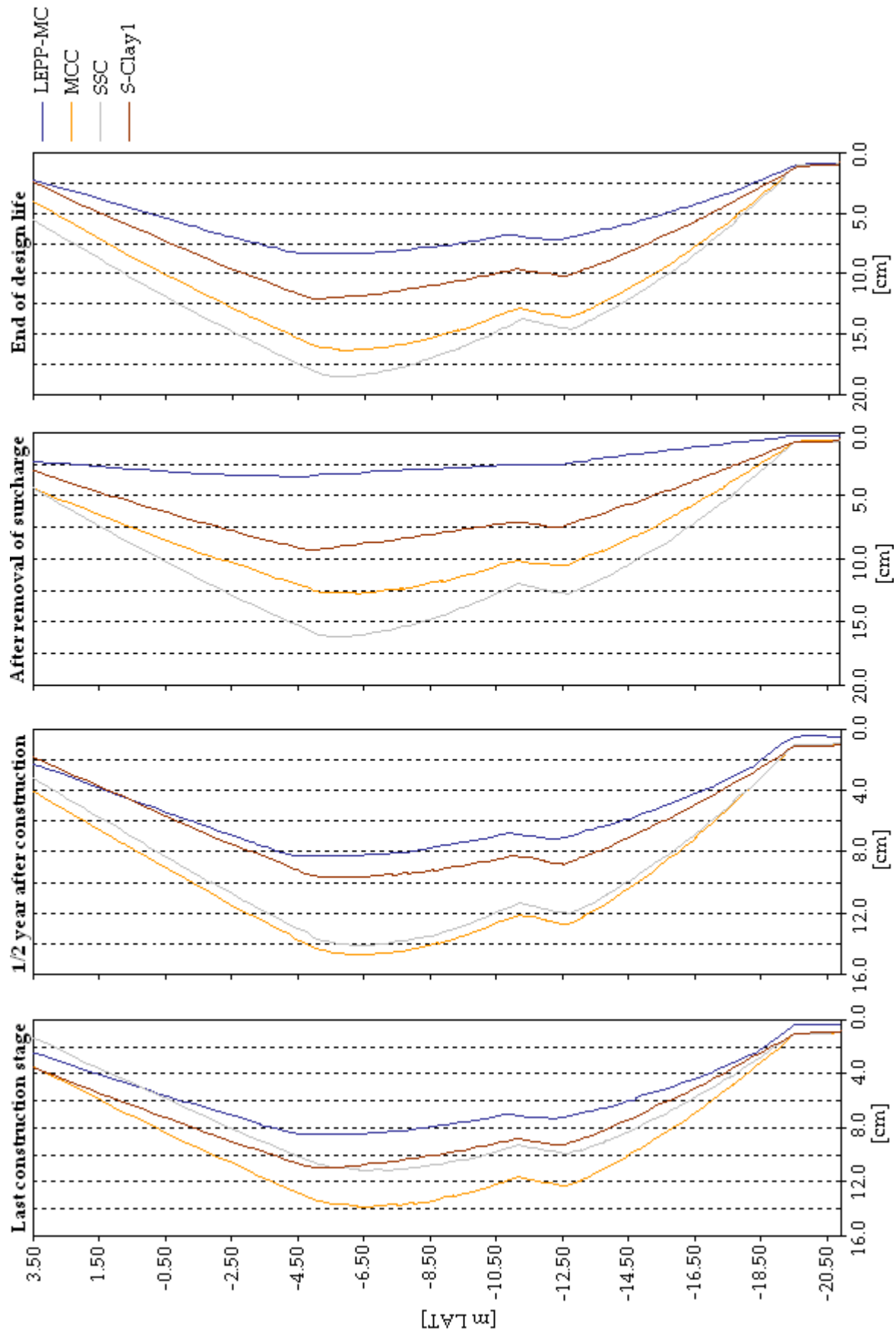
Figure 71 – Predicted horizontal deformation profiles under the crest of the embankment
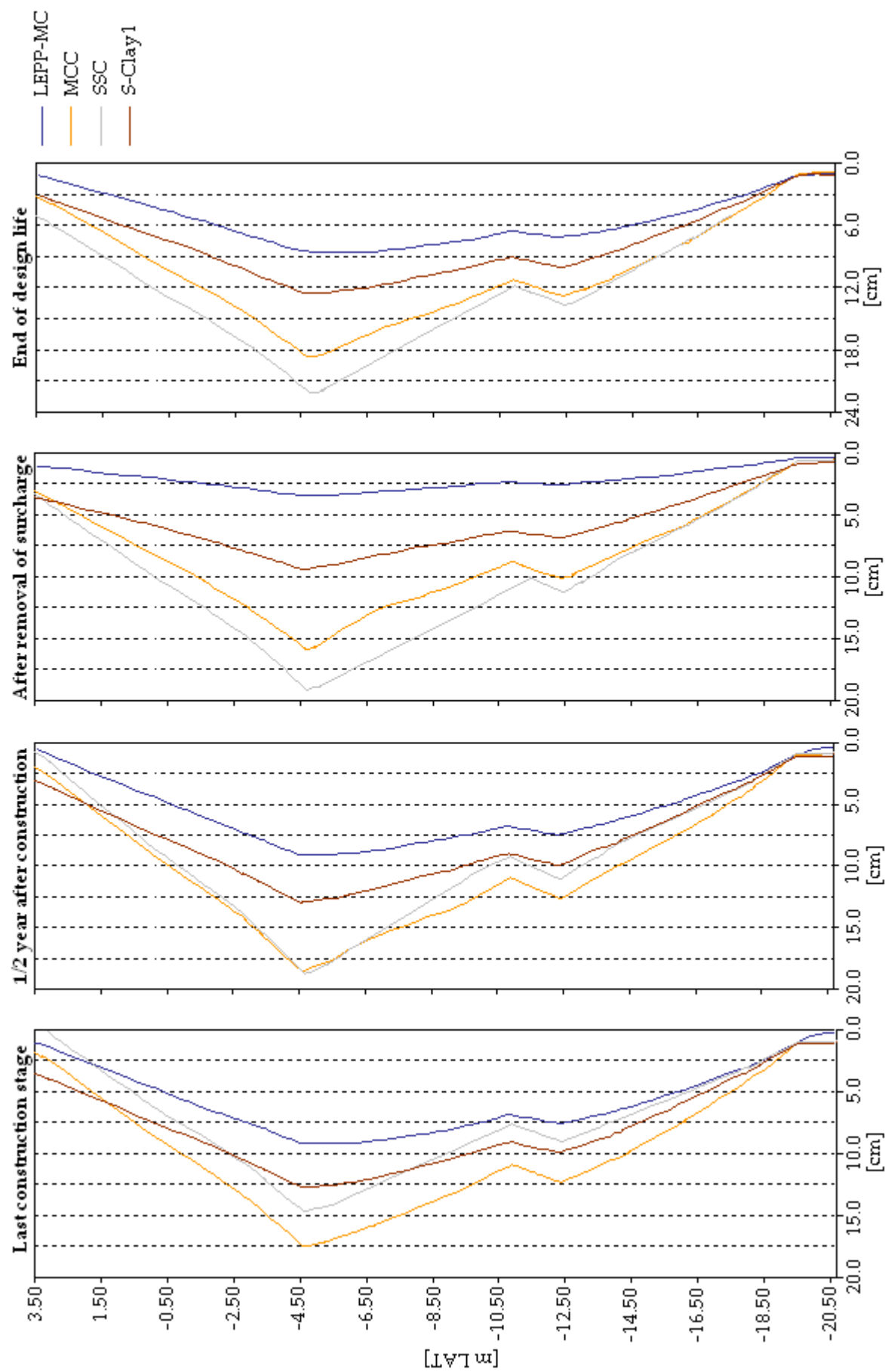
Figure 72 – Predicted horizontal deformation profiles under the toe of the embankment
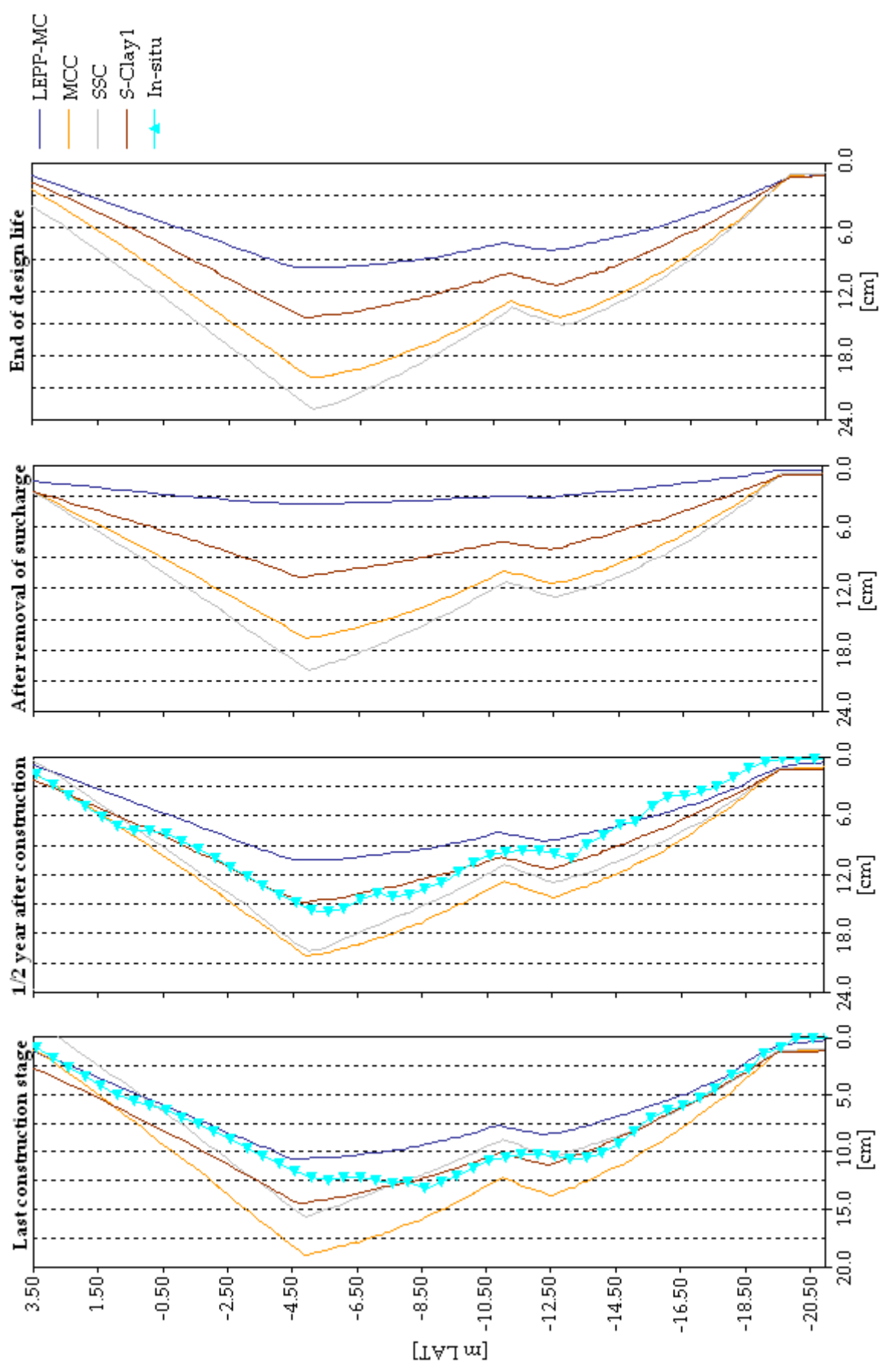
Figure 73 – Predicted horizontal deformation profiles at the inclinometer location

Figure 71 presents the development of horizontal deformation with depth under the crest of the CDS embankment in Brass Nigeria. The results show that MCC and SSC model predict the largest horizontal soil deformations. Notice that the maximum horizontal deformation is predicted in the upper part of the sandy clay layer at a depth of -6.5 m LAT. Furthermore, the reducing effect of the sand layer that is located between sandy clay and soft clay is clearly visible in the graphs for all constitutive models. Another conclusion that can be drawn from this figure is that the LEPP-MC model generally predicts lower horizontal deformations compared to the other models, especially after the removal of the surcharge. This is explainable because this model uses a single stiffness value as input parameter to represent various stress paths. In this case study the LEPP-MC model simulations are performed with the oedometer stiffness for primary compression. The other models use different stiffness values for primary compression and unloading / reloading. It is therefore logical that the rebound is much larger for the LEPP-MC model that uses a single stiffness value to represent multiple stress paths.

Figure 72 presents the horizontal deformation profiles at the toe of the embankment for four distinctive moments in time. The graphs indicate an sharp transitions between the various sand and clay layers, while the transitions at the crest are much more gradual. Next to that, the location of the maximum horizontal deformation is higher compared to the crest of the embankment. The graphs show that the maximum horizontal deformation is found at the top of the sandy clay layer, which is located at a depth of -4.5 m LAT. Another important observation is that the horizontal deformations predicted in the soft clay layer are 30 to 40% lower than sandy clay layer. This is explainable because the soft clay layer located deeper below surface level. According to the theory of Boussinesq (1885) the stress increase due to a load on top decreases quadratically with depth. As a result, smaller lateral deformations are expected at larger depths. Furthermore, the largest horizontal deformations in the long-term are again predicted with the SSC model. However, the difference is less pronounced than in the previous case study. The reason why this difference is less pronounced is presumably related to the higher CR/C_α ratio.

Figure 73 shows the horizontal deformation profiles at the inclinometer location, which is located 10 m inside the toe of the embankment. The graphical output of Plaxis shows that the maximum lateral deformations under an embankment are found close to the considered inclinometer (see Appendix 6). Note that the in-situ measurements are included after the last construction stage and ½ year after the last construction stage. It is not possible to compare the long-term predictions of the horizontal deformation with the in-situ measurements; all inclinometer were removed shortly after construction. However, the available measurements indicate that the best fits are obtained with the S-Clay1 model. The isotropic MCC and SSC model tend to overestimate the horizontal deformation under the slope of the embankment. Furthermore, the in-situ measurements also give an indication that the real soil profile is more complicated than the one assumed in table 17. For example, the in-situ measurements show that a small clay layer could be present a depth of 1.0 m LAT and a small sand layer at -16.0 m LAT. These findings give at least an indication that the real soil profile is probably more layered than was assumed. However, if the exact soil profile was known, it was still not desirable to include all these tiny layers in the geometry of Plaxis. When all these layers were included the calculation would be prone to numerical instability (Heeres, 2008).

This subsection concludes again with a number of reliability calculations, which are based on the extended version of the method of Duncan (2000). In this case study the reliability of the embankment is evaluated for the last construction stage at the toe of the embankment. These calculations start with a sensitivity analysis to assess the sensitivity of all geotechnical parameters. The results of this analysis can be found in Appendix 7. It is noted that the sensitivity is solely assessed for the sandy clay layer and the soft clay I layer, because the deeper clay layers were not monitored during construction. Finally, these findings can be used to determine the maximum horizontal deformation values which correspond to 5% and 1% probability of exceedance. The results of this analysis are reported in table 22.

Table 22 – Results at the toe of the embankment after the last construction stage

Model [-]	$HD_{MAX;MLV}$ [cm]	CV [%]	$HD_{MAX;5\%}$ [cm] [1]	$HD_{MAX;1\%}$ [cm] [2]
LEPP-MC	9.2	58.0	19.3	27.6
MCC	17.4	47.3	32.9	44.4
SSC	14.7	34.7	24.2	30.3
S-Clay1	12.7	24.9	18.5	21.8

[1] Maximum horizontal deformation at the toe that corresponds to 5% probability of exceedance

[2] Maximum horizontal deformation at the toe that corresponds to 1% probability of exceedance

This table shows that the variation coefficient after the last construction stage varies from roughly 25% to 60%. If these results are compared with table 15 (also at the toe and last construction stage), it is observed that the variation coefficients are of the same order of magnitude. Another consistent observation is that the variation coefficient is the highest for the LEPP-MC model, while the lowest value is found for the S-Clay1 model. It is important to emphasize that the lower variation coefficient of the more advanced models in Plaxis is mainly due to the lower model uncertainty. Figure 73 shows that the predicted horizontal deformation of the S-Clay1 model is nearly similar to the horizontal deformation measured from inclinometer IM-01, which means that model uncertainty is small for this model. On the other hand, the S-Clay1 model requires more (uncertain) input parameters, which leads to a higher parameter uncertainty (more ΔHD values in formula 96) compared to the LEPP-MC model that only needs a few input parameters (few ΔHD values). However, it appears that this effect is less dominant than the model uncertainty. The $HD_{MAX;5\%}$ and $HD_{MAX;1\%}$ values give an indication of the maximum horizontal soil deformation that could be expected when the different uncertainties are taken into account.

4.2.5. *Discussion of results*

This subsection discusses the results of the model predictions in more detail. This discussion is limited to the description of the constitutive models in Plaxis, because the empirical and analytical models are not able to simulate layered subsoils. Besides, the essential parameters of the sensitivity analysis will be discussed in more detail. Notice that a comparison with the in-situ measurements is only possible during construction and a ½ year after the end of construction at the inclinometer location. The considered inclinometer has a length of 24.0 m. It consists of 24 square steel sections (45.0x45.0x1.5 mm) of 1.0 m. It is also important to state that the connections are made with sockets, which are only welded on one side. This reduces the flexural rigidity of the steel rod, which makes it more suitable to follow the in-situ

ground movements. The bottom of the inclinometer is located at a depth of -21.6 m LAT, this implies that only the first two clay layers can be monitored (see table 17).

<u>Linear Elastic Perfectly Plastic with a MC failure criterion</u>
The first constitutive model that is simulated in Plaxis is the LEPP-MC model. Figure 73 shows that the predicted horizontal deformations are generally lower than the measured horizontal deformations during the construction of the embankment. On the other hand, the shape of the horizontal deformation profile is reasonably in line with the profile measured in-situ. The difference between the model predictions become significant after the removal of the surcharge. Unfortunately, no in-situ measurements are available to validate the model predictions. It is likely that this difference can be attributed to the single stiffness parameter, which is used to represent multiple primary loading stages but also an unloading and reloading stage. It is therefore not surprising that this model predicts much lower lateral deformation after the removal of the surcharge. Another striking observation is that the LEPP-MC model predicts an inward lateral movement towards the embankment during consolidation (see table 21), something which is caused by elastic compaction. According to Brinkgreve (2004) this inward movement is not realistic, and it is also not observed in-situ because the embankments show a smooth lateral spreading during consolidation.

The sensitivity analysis performed for the LEPP-MC model indicates that E_{oed} and Poisson ratio ν have a significant influence on the magnitude of the horizontal deformation. Notice that E_{oed} is the only stiffness parameter in this model. A higher value of the stiffness parameter E_{oed} leads to smaller horizontal and vertical deformations. The Poisson ratio is directly related the value of K_0 (see formula 90). The lateral earth pressure coefficient K_0 has an important influence on the ratio between the vertical and horizontal deformations.

<u>Modified Cam Clay</u>
The second constitutive model that is considered in Plaxis is the MCC model. In accordance with the previous case study the in-situ measurements indicate again that this model has the tendency to overestimate the horizontal deformations, especially during and shortly after construction. The main cause of this overestimation is related to the associative flow rule, which generates too much plastic volumetric strains. Figures 71, 72 and 73 show that the MCC model predicts the largest horizontal soil deformations during construction, while the viscoplastic SSC model exceeds the MCC model at the end of the design life. This is the result of the creep behaviour, which becomes more important after construction than during construction. However, the long-term difference between these critical state models is less explicit than in the first case study. This can be attributed to the relatively high CR/C_α ratios, which range from 40 for the soft clays to 50 for the sandy clay.

The sensitivity analysis made clear that the M and OCR have a large influence on the horizontal deformation prediction. These parameters both determine the shape of the yield contour, and consequently have an important effect on the amount of the plastic volumetric and plastic shear strains. When M increased with one standard deviation the yield contour becomes steeper, which consequently results in a stiffer soil response (i.e. lower amount of plastic volumetric strains). A higher OCR increases the size of the yield contour, which implies that the soil behaves longer in an elastic manner. This ultimately results in a lower amount of horizontal deformation.

Soft Soil Creep

The third constitutive model that is simulated in Plaxis is the SSC model. The SSC model is a viscoplastic extension of the MCC model. When the predictions made with this model are compared with the in-situ measurements, it can be concluded that the simulated horizontal deformations are usually too large (see figure 73). This creep model has the same problem as the MCC model, because it is again an isotropic model that generates too much volumetric strains, which is the result of the associative flow rule. A large advantage of the SSC model is that it predicts a continuous lateral spreading during consolation, something which is also observed from the inclinometer measurements. The lateral spreading is believed to be more realistic than the inward lateral movement as shown in the predictions with the LEPP-MC model. Similar conclusions are drawn for the Skå Edeby embankment in Sweden, where the horizontal soil deformations were monitored for approximately 20 years (Neher *et al.*, 2001).

In addition, the sensitivity analysis illustrates that the K_0^{NC} and OCR are crucial parameters for the determination of the horizontal deformations under an embankment. For the SSC model the K_0^{NC} is directly related to M, which determines the slope of the CSL. This is contrast to the other critical state models, these models determine M from the φ'_{cv} in triaxial compression. It is noted that M based on K_0^{NC} has value of 1.18 for sandy clay, while a value of 1.08 was found for M based on φ'_{cv}. Vermeer and Neher (1999) emphasize that a M value based on K_0^{NC} does not overestimate the strength and stiffness properties of a soil, because a Mohr Coulomb failure criterion is applied to prevent stress states at the dry side of the CSL

S-Clay1

The last constitutive model that is addressed is the user-defined S-Clay1 model, which is in fact an anisotropic extension of the MCC model. The predictions obtained with this model are of high quality, because excellent fits with the in-situ measurements are obtained. The results show that the predicted horizontal deformations are consistently lower than the predictions made with the isotropic critical state models. This is definitely the result of the rotational hardening, which rotates yield contour during plastic straining. Similar findings are reported by Koskinen *et al.* (2002) for the test embankment in Murro. It shows that the predictions with the S-Clay1 model perfectly matches with the in-situ measurements during construction and the first years after construction. However, the model prediction 5.0 years after construction shows that the in-situ horizontal deformations are underestimated with a few centimetres, something which is probably the result of creep. This is explainable because S-Clay1 model does not account for creep.

The sensitivity analysis shows again that M and OCR have a significant influence on the magnitude of the horizontal deformation. In addition, rotational hardening parameter β is important, because it determines the rotation of the yield curve during plastic straining. Appendix 7 shows that when β is increased with one standard deviation the maximum horizontal soil deformation already decreases with approximately 15%.

5.   Conclusions and Recommendations

In this thesis the predictability of the horizontal deformations resulting from an embankment construction on normal or lightly overconsolidated soft soils is subject of discussion. It is important to state that the interaction with structures, for example a pile foundation or a sewage pipe, is not considered. It deliberately focuses on the modelling of the (unhindered) horizontal deformations, because a poor prediction of these deformations would also result in an incorrect assessment of the forces and moments on adjacent structures.

Since the Roman age, embankments have been built on sites of good geotechnical quality, in order to reduce the technical problems and the cost associated with their construction. The construction of an embankment was predominantly a craft that was based on experience. However, during the last decades socio-economic and political considerations have forced the construction on less favourable subsoils. Less favourable implies that large vertical and horizontal deformations can be expected when embankments are situated on these types of soils. For this reason, more scientific approaches were required because the pure empirical knowledge was not sufficient anymore. It started with the development of analytical models to gain more insight into specific aspects of soil behaviour. These models require a closed-form mathematical expressions. As a result, to keep the expression solvable, it is evident that only a limited number of soil features can be incorporated. Nonetheless, the introduction of the Design & Construct concept calls for an update of the conventional models for predicting horizontal soil deformations, because in this concept there is a tendency to prescribe stricter functional requirements, which urges the need for more sophisticated models.

In the present engineering and academic practice a wide range of models are used to model the horizontal deformations under an embankment. The simplified analytical and empirical models on one side of the spectrum, and the user-defined FE models on the other side, while the conventional FE models are in the middle as shown in figure 74.
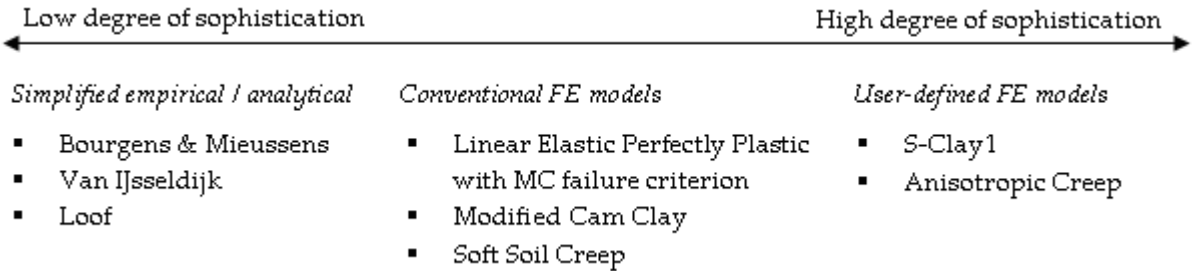
Figure 74 – Considered models which are used to predict the horizontal soil deformations

The models in figure 74 are used to simulate the horizontal deformations for two distinctive case studies. As far as possible, the predicted horizontal deformations were evaluated at the crest, the toe and outside the toe of the embankment at various moments in time. Unfortunately, the monitoring of the inclinometers stopped approximately a year after construction. This means that the quality of the model predictions cannot be validated with the in-situ measurements in the long-term.

When the predictions and the in-situ measurements of both case studies have been carefully analyzed, it becomes possible to elaborate on the various research questions, and finally conclusions can be drawn about the quality of the model predictions. The research questions that have been investigated in this thesis are presented below (see also section 1.3).

- What is the influence of a stress path on the amount of horizontal soil deformation?
- How is creep simulated in the constitutive models of Plaxis?
- Under which circumstances are the empirical and analytical models still useful?
- What is quality of the predictions obtained with the constitutive models in Plaxis?
- Which degree of uncertainty can be expected in the horizontal soil deformation prediction?
- Which soil features could be included to improve the present state of the art models even further?

This chapter concludes with a list of recommendations, these explain what is still missing and what topics need further research. Note that the conclusions and recommendations are presented in such a way that one should be able to read them independently from the rest of the thesis.

5.1. Conclusions

This paragraph elaborates on the various research questions, which have been presented in the summation above. The results can be used to draw conclusions about the constitutive behaviour of soils related to the determination of the horizontal soil deformations.

5.1.1. *What is the influence of a stress path on the amount of horizontal soil deformation?*

The course of a stress path determines the response of a soil to a foundation load. A proper knowledge about the development of a stress path is required to make a justified choice about the strength and stiffness parameters which are used in the constitutive models. The findings indicated that the magnitude of the horizontal deformation was chiefly influenced by the same factors, which are:

- Applied embankment load
- Stress history
- Safety factor of the embankment
- Subsoil type
- Location under the embankment
- Construction rate
- Drainage conditions

The applied embankment load has a large influence on the magnitude of horizontal soil deformation. If the load exceeded the stress history, the deformation rate progressively increases. During the initially overconsolidated state, the effective stress path stays close to the K_0^{NC} line as shown in figure 75 (path A to B). The development of pore pressures is limited during this stage, and consequently a small amount of deformation will develop.

When the preconsolidation pressure is exceeded in the subsoil the effective stress path starts to deviate from the K_0^{NC} line and follows the yield contour towards the Mohr Coulomb failure line (path B to C). In this stage the horizontal deformations are much higher than in the initially overconsolidated state. In addition, the distance between C and F gives an indication about the safety factor of the embankment. If a stress path exceeds point F a local failure will occur, and a new equilibrium will be reached in point F'.
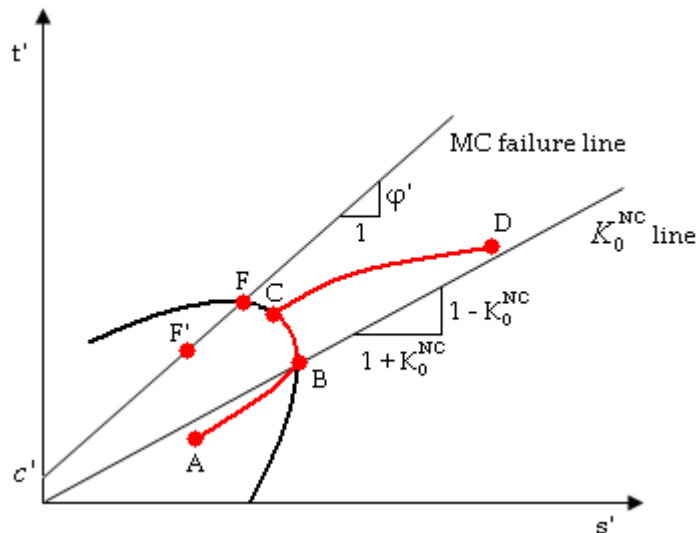
Figure 75 – Indicative effective stress path during the construction of an embankment

Another factor which has a significant influence on the horizontal deformation is the subsoil type. It appears that the development of the horizontal deformations is different for a clayey subsoil than an organic subsoil. This difference is mainly due to the value of K_0^{NC}, which is much higher for clay than for peat. According to Den Haan and Feddema (2009) this difference can be attributed to the fibre structure of peat. This fibre structure restricts the development of horizontal deformations. As a result, the inclination of the K_0^{NC} line is lower for a clayey soil.

For the evaluation of the horizontal deformations, it is also important to consider the effect of the location under the embankment. The first case study has shown that the magnitude and shape of the horizontal deformation profile is entirely different under toe of the embankment than 10.0 m outside the toe of the embankment. This is predominantly the result of the different stress conditions under the embankment. Under the toe the stress condition is about similar to a simple shear test, while the stress condition outside the toe has some similarities with a triaxial extension test.

Finally, the rate of construction and the drainage conditions have a notable influence on the course of the stress path. These factors determine if a soil response is drained, partially drained or undrained. Figure 48 illustrates that a lightly overconsolidated soil behaves much different in a drained triaxial test and in an undrained triaxial test. The stress path and the size of the yield contour are both entirely different. In the undrained case the size of the yield is substantially smaller, and larger horizontal deformations can be expected.

5.1.2. *How is creep simulated in the constitutive models of Plaxis?*

This discussion starts with the question whether creep should be conceived as a constitutive process that occurs after or together with primary consolidation. Ladd *et al.* (1977) defined two extremes, which are also known as hypothesis A and B. In hypothesis A creep occurs after the primary consolidation, while for hypothesis B creep occurs together with primary consolidation. It is important to state that the conclusions drawn about hypotheses A and B are based on findings reported in literature. The validity of these hypothesises are not examined with own in-situ measurements.

Hypothesis A is supported by Mesri and co-workers, they believed that a unique EoP curve could be determined that is independent on the duration of the primary consolidation stage. If such a EoP relation is assumed, it becomes easy to translate a laboratory stress-strain curve to an in-situ stress-strain curve (Mesri and Choi, 1985). The deformation under constant effective stress, which is also known as the secondary compression, is determined from an empirical relation between C_α/C_c.

Hypothesis B considers that creep is inextricably related with the primary consolidation stage. This assumption implies that soils are strain rate dependent during consolidation. The validity of strain rate dependency is graphically illustrated in figure 27. This figure indicates that hypothesis A cannot be true, because the ratio C_α/C_c is not constant value, but a ratio that is dependent on the strain rate. Another critical notion is given by Schiffman *et al.* (1987) and Imai (1989), they showed that the mass balance was also not satisfied in hypothesis A. In spite of the promising results that have been reported by Mesri *et al.* (1997), hypothesis A is from a theoretical point of view fundamentally wrong. It is therefore advised to use strain rate dependent formulations, which are in line with hypothesis B.

The strain rate dependent models are in principle isotache models. In numerical modelling these isotache models are often simulated within an elasto-viscoplastic framework. It important to state that these model formulations are particular cases of the isotache model proposed by Šuklje (1957). For the simulations performed with the FE program Plaxis this discussion is only relevant for the SSC and AC model, because the other models do not consider creep behaviour. In the original model formulation of the SSC model as proposed by Vermeer *et al.* (1998), it becomes clear that this model is line with hypothesis B. The creep behaviour in the SSC model is formulated with principles of Bjerrum (1967), Janbu (1969) and Garlanger (1972); these principles were combined to define an unique relation between the vertical effective stress, strain and stain rate. This also applies for the AC model, because this model is actually an anisotropic extension of the SSC model.

However, one has to be aware that the modelling of the time-dependent behaviour in Plaxis is not fully correct. A limitation is that stress states are not reliable at the dry site of the CSL, because softening behaviour that has to occur at the dry site results in mesh dependency and poor convergence of the equilibrium iterations (Brinkgreve, 1994). Regularization techniques can be applied to prevent mesh dependency, but the accuracy of these techniques is often limited. Notice that the SSC and AC model both use a Mohr Coulomb failure criterion to prevent stress states at the dry side of the CSL, which implies that softening cannot occur anymore. Another limitation is that the pore pressures are not coupled with the stress history

for a soil that is modelled as an undrained material. The simulations in Plaxis indicate that the generated pore pressures are similar before and after the preconsolidation pressure, while the in-situ measurements indicate that a smaller amount of pore pressure is generated in the initially overconsolidated state than during the primary compression. Plaxis ignores this distinction, and predicts therefore to much pore pressures. This overestimation increases for soils which are more overconsolidated. Nevertheless, the soils treated in this research have a small OCR or POP value, which implies that the error remains relatively low.

5.1.3. *Under which circumstances are the empirical and analytical models still useful?*

The empirical and analytical models are often used to obtain a relatively quick estimation of the horizontal soil deformation, especially when the amount of available soil data is limited. However, one has to be aware that the applicability of these models is limited.

The considered empirical model of Bourgens and Mieussens (1979) relates the settlements under the centre of the embankment to the maximum horizontal soil deformation under the toe of the embankment. The horizontal deformation profiles are obtained from normalized curves, which describe a particular distribution with depth (see figure 41). Figure 76 presents the advantages and limitations of this empirical model.

Advantages	*Limitations*
▪ Gives an relatively quick estimation of the horizontal deformations ▪ Predictions with this model are reasonably accurate, mostly slightly conservative	▪ Only valid at the toe of the embankment ▪ It should be used with caution for organic soils ▪ Safety factor of the embankment should be above 1.3 ▪ Horizontal deformations 5 years after construction cannot be predicted ▪ Not possible to analyze the influence of distinctive soil features separately ▪ Not possible to simulate layered soil profiles

Figure 76 – Advantages and limitations of the empirical model Bourgens and Mieussens

The results of the first case study indicate that the horizontal deformations predicted with this model are slightly conservative. Similar findings are reported by Feddema *et al.* (2009) for the embankments at Bricor and the Betuweroute. This overestimation is presumably the result of the empirical relation of Tavenas *et al.* (1979), which is used to determine lateral deformations during consolidation. This relation uses the factor 0.16 to relate the settlements under the centre of the embankment to the lateral deformation at the toe of the embankment. However, the in-situ measurements indicated that this factor varied from 0.03 to 0.32. In addition, Long and O'Riordan (2001) emphasize that the use of this model should limited to embankments that are constructed on a clayey soils, because the relation is not accurate for organic soils. Despite these limitations this empirical model has significant potential.

The considered analytical models are Van IJsseldijk and Loof. The first simulates a uniform soft soil layer that is subjected to an embankment loading, while the latter also simulates a uniform soft soil layer that is subjected to an embankment loading, but in this case it is overlain by stiff rigid top layer. Both analytical models are based on the undrained elastic theory of Jürgenson (1934). The horizontal stress increments and horizontal deformations can be easily predicted from the normalized tables of De Leeuw (1963), which are presented for Van IJsseldijk in Appendix 1 and for Loof in Appendix 2. Figure 77 shows the advantages and limitations of both analytical models.

Advantages	*Limitations*
■ Gives an relatively quick estimation of the horizontal deformations	■ Predictions are inaccurate, the in-situ measurements are largely overestimated ■ Elastic soil response assumption is not valid for clayey and organic soils ■ Time-dependent processes like consolidation and creep are not included ■ Predictions can only be made at the toe and outside the toe of the embankment ■ Not possible to analyze the influence of distinctive soil features separately ■ Not possible to simulate layered soil profiles

Figure 77 – Advantages and limitations of the analytical models Van IJsseldijk and Loof

The results of the first case study have shown that the quality of the model predictions with Van IJsseldijk and Loof is usually poor, especially Van IJsseldijk which hugely overestimates the in-situ horizontal deformations. Furthermore, the shape of the horizontal deformation profiles is only accurate near the toe. If these predictions were used for the determination of the forces and moments in a pile foundation, it would definitely lead to very conservative estimates, and consequently too much reinforcement will be prescribed.

5.1.4. *What is quality of the predictions obtained with the constitutive models in Plaxis?*

The constitutive models that are simulated in the FE program Plaxis are LEPP-MC, MCC, SSC, S-Clay1 and AC. Notice that the last two models are used-defined models, which are not commercially available in Plaxis yet. The simulations performed with these models are validated with the in-situ measurements of two different case studies. The first case study is a road embankment founded on a thick organic layer, while the second case study deals with an embankment that is situated on a layered soil profile of clay and sand layers.

The LEPP-MC model uses Hooke's law and a Mohr Coulomb failure criterion to describe elastic and plastic behaviour respectively. In geotechnical engineering this model is often used as first approximation for the description of in-situ soil behaviour. The simulations for both case studies indicated that the accuracy of the predictions with this model is mainly dependent on the value of stiffness parameter E_{oed}. When E_{oed} is selected at the in-situ stress level the predicted horizontal deformations are much lower than the values measured in the

field. However, a solution to obtain better predictions is reduce the E_{oed} manually by fitting. The advantages and limitations of this constitutive model are presented in figure 78.

Advantages	Limitations
▪ It requires a small amount of input parameters ▪ Predicted horizontal deformation profile is reasonably in line with the in-situ horizontal deformation profile	▪ Predicted horizontal deformations are too low with an oedometer stiffness that corresponds to the in-situ stress level ▪ Yield contour remains static during plastic straining ▪ Creep deformation is not included ▪ Soil behaviour is assumed to be isotropic ▪ Single stiffness parameter is applied for primary loading and reloading

Figure 78 – Advantages and limitations of the numerical model LEPP-MC

The second case study has shown that this model is not suitable to simulate embankments that contain loading and unloading / reloading stages at the same time, because the same stiffness parameter is applied to represent both types of loadings. It is therefore advised to use this model only in a single stage embankment construction with reduced value of E_{oed}.

The MCC is a model that is originally developed by Roscoe *et al.* (1958). This model uses a hardening rule to describe the relation between the increase of the preconsolidation pressure and the development of plastic volumetric strains. The sensitivity analysis performed in this thesis indicated that parameter M has a major influence on the magnitude of the horizontal deformation. This parameter M is friction constant that is solely based on critical state value of the friction angle as shown in formula 64.

$$M = \frac{6\sin \varphi'_{cv}}{3 - \sin \varphi'_{cv}}$$

(64)

The parameter φ'_{cv} should preferably be determined from a CU-triaxial test. The advantages and limitations of this model are presented in figure 79.

Advantages	Limitations
▪ Preconsolidation pressure increases during plastic straining ▪ Different stiffness parameters are used for primary loading and reloading ▪ Predicted horizontal deformation profile is reasonably in line with the in-situ horizontal deformation profile	▪ Predicted horizontal deformations are generally too high ▪ Creep deformation is not included ▪ Soil behaviour is assumed to isotropic ▪ Value of K_0^{NC} is overestimated with the conventional critical state theory

Figure 79 – Advantages and limitations of the numerical model MCC

Both case studies indicate that the predictions made with the MCC model overestimate the in-situ horizontal deformations. This is mainly the result of the associative flow rule, which determines plastic strain components perpendicular to the yield function. This leads to a substantial overestimation of the plastic volumetric strains. Similar findings are reported by Ladd *et al.* (1999) for an embankment on Boston blue clay.

The SSC model is a viscoplastic extension of the MCC model. The additional feature of this model is that strain can develop under constant effective stress. This is in contrast with the elastoplastic models, which only generate strains when the stress state is altered. Note that the critical state parameter M is not based on φ'_{cv} in triaxial compression, but on a relation with parameter K_0^{NC} as shown in formula 2. Brinkgreve (1994) explained that this adaption is necessary, because the conventional equation for M overestimates the value of K_0^{NC}.

$$M = 3 \cdot \sqrt{\frac{\left(1-K_0^{NC}\right)^2}{\left(1+2K_0^{NC}\right)^2} + \frac{\left(1-K_0^{NC}\right) \cdot \left(1-2.\nu_{ur}\right) \cdot \left(\lambda^*/\kappa^* -1\right)}{\left(1+2K_0^{NC}\right) \cdot \left(1-2\nu_{ur}\right) \cdot \left(\lambda^*/\kappa^*\right) - \left(1-K_0^{NC}\right) \cdot \left(1+\nu_{ur}\right)}} \tag{2}$$

However, a Mohr Coulomb failure criterion has to be used to prevent an overestimation of the shear strength, because the slope of the CSL is usually steeper when M is based on K_0^{NC}. The value of K_0^{NC} should preferably be determined with a K_0-CRS oedometer test, because the relation presented in formula 2 is valid for one-dimensional compression at a constant rate of strain in the normally consolidated range. These conditions exactly correspond to the last part of the K_0-CRS oedometer test. In addition, figure 80 presents the advantages and limitations of the SSC model.

Advantages	Limitations
▪ Preconsolidation pressure increases during plastic straining	▪ Predicted horizontal deformations are generally too high
▪ Different stiffness parameters are used for primary loading and reloading	▪ Soil behaviour is assumed to be isotropic
▪ Creep deformation is included	
▪ Alternative formulation of M ensures that a more realistic value of K_0^{NC} is used	
▪ Predicted horizontal deformation profile is reasonably in line with the in-situ horizontal deformation profile	

Figure 80 – Advantages and limitations of the numerical model SSC

The case studies Abcoude and Brass indicate that the SSC and MCC model produces nearly similar results during construction. This is explainable because both models are essentially based on the critical state theory. In the long-term when the subsoil is significant dissipated creep gets more dominant, and the difference between these models becomes clearly visible. Furthermore, the predicted horizontal deformations are larger than the measured horizontal deformations. This is again the results of the associative flow rule in combination with an isotropic yield contour. As a result, it is possible to use this model for the prediction of the

horizontal deformations during and after the construction period. However, one has to be aware that the predicted horizontal deformations are generally too large.

The S-Clay1 model is an anisotropic extension of the traditional MCC model. The extension compromises a hardening rule that accounts for anisotropy during plastic straining. This model requires just two additional parameters (μ and β) in comparison to the MCC model. A limitation of this model is that hardening parameter μ cannot be determined in direct way. This parameter has to be determined from the empirical relation of Zentar *et al.* (2002), which assumes that μ lies between $10/\lambda$ and $15/\lambda$. The hardening rule causes the yield surface to be sheared during plastic straining, which reduces the amount of plastic volumetric strain, and consequently a smaller amount of horizontal deformation. In addition, figure 81 presents the other advantages and limitations of the S-Clay1 model.

Advantages	*Limitations*
▪ Preconsolidation pressure increases during plastic straining ▪ Different stiffness parameters are used for primary loading and reloading ▪ It is possible to simulate anisotropy during plastic straining ▪ Predicted horizontal deformations fit nicely with the in-situ measurements	▪ Empirical relation is required to determine parameter μ ▪ Creep deformation is not included ▪ Value of K_0^{NC} is overestimated with the conventional critical state theory

Figure 81 – Advantages and limitations of the numerical model S-Clay1

Both case studies produce excellent matches with the in-situ measurements, in particular during the construction period of the embankment. This is an indication that anisotropy plays at least an important during the early stage of consolidation. Unfortunately, it was not possible to validate the S-Clay1 model with long-term in-situ measurements, because all inclinometers were removed shortly after construction. It is expected that the predictions with the S-Clay1 model are less good in the long-term, because creep is not included. As a result, this model is this in particular suitable to simulate the horizontal soil deformations during the construction period of an embankment. Nevertheless, this model could also be used after construction, but this is mainly dependent on the rate of dissipation within a soil. If the permeability of the soil is extremely low and no vertical drainage has been installed, it could take several years before a creep model yields better results.

A model that is recently developed is the AC model, this model includes anisotropy as well as creep (Leonie *et al.*, 2008). Such a model is desirable, because there is evidence that creep cannot be disregarded after construction. For example, Neher *et al.* (2001) showed for a test embankment in Skå Edeby that the horizontal deformations are dominated by creep 20 years after construction. The predictions with the MCC model indicate that the horizontal soil deformations are underestimated with approximately 10 cm in a clay layer. Note that higher underestimations are expected for organic soils. Unfortunately, the current predictions with the AC model are not very satisfying, because the in-situ horizontal deformations are largely underestimated. When the available dll (ACM_MC.dll) was analyzed in more detail, it appears that the creep was not correctly implemented. It was not possible to examine the

creep formulation more closely, because the Fortran codes were not available. Nevertheless, besides these problems, a constitutive model that incorporates both anisotropy and creep has a great potential. It is therefore advised to put more effort in the correctness of the constitutive formulation and the stability of the numerical procedures.

5.1.5. *Which degree of uncertainty can be expected in the horizontal deformation prediction?*

The uncertainty in the model predictions is evaluated with an extended version of the simple reliability method proposed by Duncan (2000). This method is based on a first-order Taylor series approach, and gives therefore roughly an idea about the uncertainty margins in the considered models. The extension embraces the spatial variability of soils and the inclusion of the model uncertainty. The incorporation of the spatial variability is absolutely necessary, because the point estimates obtained from the laboratory tests overestimate the variability of the spatial average. Lo and Li (2007) suggested formula 92 to account for the uncertainty in the estimation of the average value and the uncertainty caused by spatial variability.

$$\sigma_{net} = \sqrt{\frac{1}{N} + \Gamma^2} \cdot \sigma_{\text{point}} \tag{92}$$

If more independent sample points are available factor N increases, and consequently the net standard deviation σ_{net} decreases. The variance reduction factor Γ^2 has a value of about 0.1 for a relatively uniform soils and can be 0.5 for highly variable soils.

The model uncertainty is incorporated in a pragmatic way in the determination of coefficient of variation with a factor ε as shown in formula 96. This factor represents the difference between the prediction and the in-situ observation.

$$CV = \frac{\sqrt{\left(\left(\frac{\Delta HD_1}{2}\right)^2 + \left(\frac{\Delta HD_2}{2}\right)^2 + \left(\frac{\Delta HD_n}{2}\right)^2\right)} + |\varepsilon|}{HD_{MLV}} \tag{96}$$

The ΔHD values are obtained from a sensitivity analysis where each parameter has been decreased respectively increased with one standard deviation, while the other parameters remained fixed to their mean value. It is assumed that the parameters are not correlated with each other.

The results of the sensitivity analysis show that the E_{oed} and ν are essential for the prediction of the horizontal soil deformations with the LEPP-MC model. The isotropic critical state models (MCC and SSC) indicate that parameter M and the POP (or OCR) have a large influence on the amount of lateral deformation. This large influence is explainable, because these parameters largely determine the shape of the yield contour. The lateral deformation predictions with S-Clay1 show again that the M and POP (or OCR) are important. Besides these two parameters, the value of hardening parameter β is also crucial in the S-Clay1 model. A higher value of β increases the rotation rate of the yield contour, and consequently a lower amount of horizontal deformation will be expected.

The results of the sensitivity analysis can be used to determine the variation coefficients of the various considered models. This coefficient gives the relation between the total standard deviation and the mean value. Table 23 presents some indicative classification categories for the coefficient of variation. It is important to emphasize that these categories are indicative, and should not be interpreted as precise values.

Table 23 – Indicative classification categories for the coefficient of variation

CV [%]	Classification [-]
0 - 25	Good
25 - 50	Reasonable
50 - 75	Mediocre
> 75	Poor

For the case studies in Abcoude and Brass the coefficients of variation have been determined for the considered models at the toe of the embankment. The results of these analyses have been summarized in table 24.

Table 24 – Calculated coefficients of variation for the considered models

Model	CV [%]	Quality Prediction [-]
Bourgens & Mieussens	50	Reasonable
Van IJsseldijk	85	Poor
Loof	60	Mediocre
LEPP-MC	60	Mediocre
MCC	45	Reasonable
SSC	35	Reasonable
S-Clay1	25	Good

Table 24 shows that the highest variation coefficient is obtained for the analytical model Van IJsseldijk. In this model the total standard deviation is almost equal to the predicted mean value. This high variation coefficient is mainly the results of the model uncertainty, because this model simulates fully undrained behaviour during construction and assumes that the soil behaves in a linear elastic manner. Furthermore, the other analytical model Loof and the LEPP-MC model also have a relatively high coefficient of variation, and the quality of the prediction is therefore classified as mediocre. More acceptable values are obtained for the traditional critical state models. The calculated variation coefficient is approximately 45% for MCC and about 35% for SSC. Nearly similar findings are reported by Mestat (2001), which showed that the uncertainty in the prediction of the horizontal deformations at the toe of an embankment was on average about 50% for the MCC model. The variation coefficient for the empirical model Bourgens and Mieussens is in line with the MCC model. However, it is noted that the magnitude of the variation coefficient for Bourgens and Mieussens is entirely dependent on the characteristics of the subsoil. The use of this model is restricted to cases that match with the empirical data set. The table above indicates that the lowest variation coefficient is obtained for the S-Clay1 model, and the quality of the prediction is classified as good. This sophisticated model has a relatively high parameter uncertainty, because it

requires a larger amount of uncertain input parameters (more ΔHD values in formula 96) in comparison to the LEPP-MC model that only needs a small amount of input parameters (few ΔHD values). However, the effect of the parameter uncertainty seems to be less dominant than the model uncertainty.

As a result, there are several effective measures to reduce the coefficient of variation:

- Use case specific soil investigation data, and minimize the use of the empirical relations for example the ones proposed by Vermeer *et al.* (2009)
- Increase the number of laboratory and field tests to reduce the net standard deviation, especially for the parameters that have a high ΔHD value
- Use higher order model formulations, even if the quality of the soil investigation data is somewhat meagre

Finally, table 24 indicates that the uncertainty margins in the prediction of the horizontal deformations are still quite high compared to the uncertainty margins generally observed for settlement predictions. The use of these models can be problematic in Design & Construct contracts which often specify very strict deformation requirements. For example, it is not uncommon that these contracts specify a maximum horizontal deformation of 1.0 or 2.0 cm on an adjacent structure. Such values are definitely not realistic, because the uncertainty related to the model already exceeds this value. A solution to deal with the uncertainties in a more convenient way is to define horizontal deformation values that corresponds to a particular probability of exceedance. The choice for a particular probability of exceedance should be related to the risk profile of the project. If the consequences of failure are high a lower probability of exceedance should be specified.

5.1.6. *Which soil features could be included to improve the considered models even further?*

For the modelling of normally and lightly overconsolidated soft soils it is not very useful to include features like the small-strain nonlinearity or the anisotropy during elastic straining. Karstunen and Koskinen (2008) indicated that these features are only relevant for highly overconsolidated soils, and not the soils considered in this thesis (OCR<2). However, a feature that could be included is the effect of destructuration. In some stress path controlled triaxial tests, which are performed by Koskinen *et al.* (2002), it appears that the effect of destructuration becomes important when the stress state of a soil gets close to the CSL. In order words, destructuration is only relevant when the safety factor of the embankment is close to unity (FS≈ 1.0).

Krenn *et al.* (2003) showed for an embankment on soft clay that the accurateness of the rotational hardening law as used in the S-Clay1 model is highly dependent on the ratio q/p'. If the ratio is high, which indicates that the soil is close to the CSL, the plastic volumetric strains are significantly underestimated. It is believed that the underestimation of the plastic strains is the result of destructuration. For lower q/p' ratios the plastic volumetric strains are accurately predicted with the S-Clay1 model. This implies that the destructuration effect is most relevant when a soil is close to failure.

An extension of the S-Clay1 model that accounts for the effect of destructuration has already been proposed by Karstunen and Koskinen (2004) under the name S-Clay1S. This effect is expressed with an intrinsic yield contour, which is the theoretical yield contour for the same soil with the same void ratio and fabric but without bonding. The shape and inclination of this intrinsic yield contour are the same as the yield contour of a natural soil. However, the size of the intrinsic yield contour is smaller than the yield contour of a natural soil with bonding. The destructuration is simulated in this model with an additional hardening rule, which is presented in formula 99.

$$\partial x = -a \cdot x_0 \cdot \left(\left| \partial \varepsilon_v^p \right| + b \cdot \left| \partial \varepsilon_q^p \right| \right) \tag{99}$$

The parameters a and b are both destructuration parameters, while parameter x_0 represents the initial amount of bonding. The S-Clay1S model requires thus three additional input parameters, which consequently increases the parameter uncertainty. Especially, x_0 is a quite uncertain parameter, because a portion of the bonding is always lost during sampling and testing.

5.2. Recommendations

This research about the modelling of horizontal soil deformations closes with a list of recommendations. Most of these recommendations directly follow from the conclusions and require only a little further explanation.

- Testing in general has to be recognized as an important, if not the most important part of a geotechnical analysis. For example, the parameter φ'_{cv} should be estimated from a CU-triaxial test to give an indication of the residual value of the effective strength. Another essential parameter is the K_0^{NC}, which is preferably determined from K_0-CRS oedometer tests. If possible, try to avoid Jaky's rule of thumb, especially in the case of organic soils. Jaky's rule tends to underestimate the value of M. The cause of the underestimation lies predominantly in the determination of the friction angle. In the Dutch geotechnical practice is customary to cut the friction angles off at strain values 2% or 5% strain. This approach is quite conservative for organic soils.
- It is recommended to use linear strain parameters in combination with a small strain analysis in Plaxis. An updated mesh analysis is numerically more complex, and needs considerably more calculation time. It is important to state that the input parameters of a linear and a natural strain formulation are not the same (see subsection 3.3.3). Simulations have been performed with both strain formulations, and resulted only in marginal differences.
- It is advised to extend the monitoring period of the inclinometers after the end of construction. If these data becomes available, it becomes possible to validate the considered models in the long-term.
- It is desirable to apply more advanced reliability methods than the first-order Taylor series approximation. For example, Bayesian methods or Kalman filters can be used to improve the reliability of the horizontal deformation prediction even further.

- It is desirable investigate the effect of the flexural rigidity of an inclinometer rod on the development of the horizontal soil deformations. For example, it is interesting to know if there a difference between a steel inclinometer and a synthetic inclinometer.

- Use the horizontal deformation measurements also as an indicator of the safety factor during the construction of an embankment. A progressive increase of the horizontal movement in time indicates that the soil is close to failure (FS≈ 1.0).

- It is recommended to extend the applicability of the empirical model of Bourgens and Mieussens (1979) to organic soils, and to improve the accuracy of the factor 0.16 that is used to determine the horizontal consolidation deformations for clayey soils. The construction of a new database to develop comparable relations is highly desirable.

- Effort should be put in the development of numerical models that use a coupled pore pressure formulation. These models should be able to predict the pore pressures more accurately. A limitation of Plaxis is that excess pore pressures are not coupled with the stress history. This assumption results in an overestimation of the excess pore pressure during the initially overconsolidated state of a soil.

- When accurate predictions of the horizontal deformation are required, it is advised to use the S-Clay1 model that accounts for anisotropy during plastic straining. This model is in particular suitable to determine the horizontal deformations during the construction period.

- Additional research should concentrate on the development of a robust anisotropic creep model, which is suitable to simulate the horizontal deformations during and after the construction of an embankment. More robust means in this case that more effort should be put in the correctness of the constitutive formulation and the stability of the numerical procedures.

In spite of the significant number of recommendations, it is believed that the results in this thesis have improved the insights into the constitutive behaviour of soft soils. This is needed to increase the predictability of the horizontal soil deformations. Hopefully, this thesis has reduced the gap a bit that is often observed between theoretical soil mechanics and the engineering practice.

References

Atkinson, J.H. *et al.* (1990). Effect of recent stress history on the stiffness of overconsolidated soil. Géotechnique, Vol. 40, pp. 531-540.

Baecher, G.B. and Christian, J.T. (2003). Reliability and statistics in geotechnical engineering. Wiley, New Jersey.

Ballard, T.A. (2006). Brass LNG project – LNG tank settlement study and preliminary seismic analysis. SC-Solutions, Sunnyvale.

Banerjee, P.K. and Yousif, N.B. (1986). A plasticity model for the mechanical behaviour anisotropically consolidated clay. International Journal for Numerical and Analytical Methods in Geomechanics, Vol. 10, pp. 521-541.

Beckwith, C.W. *et al.* (2003). Anisotropy and depth-related heterogeneity of hydraulic conductivity in a bog peat – I: laboratory measurements. Journal of Hydrological Processes, Vol. 17, pp. 89-101.

Berengo, V. *et al.* (2008). Numerical modelling of the time-dependent behaviour of Venice lagoon silts. 12th International Conference of IACMAC, Goa.

Berry, P.L. and Poskitt, T.J. (1972). The consolidation of peat. Géotechnique, Vol. 22, pp. 27-52.

Biot, M.A. (1941). General theory of three-dimensional consolidation. Journal of Applied Physics, Vol. 12, pp. 155-164.

Bishop, A.W. (1966). The strength of soils as engineering materials. Géotechnique, Vol. 18, pp. 91-130.

Bjerrum, L. (1967). Engineering geology of Norwegian normally-consolidated marine clays as related to settlements of buildings. Géotechnique, Vol.17, pp. 81-118.

Bjerrum, L. (1973). Problems of soil mechanics and construction on soft clays and structurally unstable soils (collapsible, expansive and other): state of the art report. Proceedings of the 8th ICSMFE, Moscow.

Boekhorst, C.W.J. te and Nguyen, B.L. (2007). Memo – beïnvloeding verkeersportalen. Combinatie A2HoMa, Breukelen.

Borja, R.I. et al. (1990). Double yield surface model – part II: implementation and verification. Journal of Geotechnical Engineering, ASCE, Vol. 116, pp. 1402-1421.

Boudali, M. (1995). Comportement tridimensionnel et visqueux des argyles naturelles. PhD thesis, Université Laval, Québec.

Bourges, F. and Mieussens, C. (1979). Déplacement latéraux à proximité des remblais sur sols compressibles. Bulletin des Laboratoires des Ponts et Chaussées, No. 101, pp. 73-100.

Boussinesq, J. (1885). Application des potentiels a l'etude de le l'equilibre et du mouvement des solides elastiques. Gauthier-Villars, Paris.

Brinkgreve, R.B.J. (1994). Geomaterial models and numerical analysis of softening. PhD thesis, Delft University of Technology, Delft.

Brinkgreve, R.B.J. (2004). Time-dependent behaviour of soft soils during embankment construction – a numerical study. Proceedings of the 9th NUMOG, Ottawa.

Brinkgreve, R.B.J. and Broere, W. (2008). Plaxis 2D manual version 9. Plaxis Company, Delft.

Brisbois, J.J. (1999). Performance of Route 106 interchange embankments in Sackville, New Brunswick Canada. MSc Thesis, University of New Brunswick, Fredericton.

Budhu, M. (2007). Soil mechanics and foundations. John Wiley & Sons, New Jersey.

Buisman, K.A.S. (1940). Grondmechanica (*heruitgave 1996*). Balkema, Rotterdam.

Christie, I.F. (1964). A re-appraisal of Merchant's contribution to the theory of consolidation. Géotechnique, Vol. 14, pp. 309-320.

Duncan, J.M. (2000). Factor of safety and reliability in geotechnical engineering. Journal of Geotechnical and Geoenvironmental Engineering, Vol. 126, pp. 307-316.

Dykstra, C.J. (2008). Brass LNG project – preload settlement design. Royal Boskalis Westminster, Papendrecht.

Dykstra, C.J. *et al.* (2009). Settlement predictions of embankments on organic soils in engineering practice. Geotechnics of Soft Soils, London.

Feddema, A. *et al.* (2009). Ontwerpmethode door grond horizontaal belaste palen (*concept version*). CUR Report H408, Gouda.

Fellenius, B.H. and Johansson, B. (1972). Buckling of piles due to lateral soil movements. Proceedings of the 5th European Conference on Soil Mechanics and Foundation Engineering, Vol. 2, pp. 282-284.

Floquet, F. (2006). Modelling creep of soft Finnish clay. MSc thesis, Helsinki University of Technology, Helsinki.

Folayan, J.I. *et al.* (1970). Decision theory applied to settlement predictions. Journal of Soil Mechanics and Foundation Engineering, ASCE, Vol. 96, pp. 1127-1141.

Folkes, D.J. and Crooks, J.H.A. (1985). Effective stress path and yielding in soft clays below embankments. Canadian Geotechnical Journal, Vol. 22. pp. 357-374.

Gaberc, A. (1999). Some experience in the construction of embankments on soft soils. Geotechnical Engineering for Transport Infrastructure, Balkema, Rotterdam.

Garlanger, J.E. (1972). The consolidation of soils exhibiting creep under constant effective stress. Géotechnique, Vol. 22, pp. 71-78.

Gibson, R.E. *et al.* (1967). The theory of one-dimensional consolidation of saturated clays. Géotechnique, Vol. 17, pp. 261-273.

Graham, J. and Houlsby, G.T. (1983). Elastic anisotropy of a natural clay. Géotechnique, Vol. 33, pp. 165-180.

Haan, E.J. den (1994). Vertical compression of soils. PhD thesis, TU Delft, Delft.

Haan, E.J. den (1996). A compression model for non-brittle soft clays and peat. Géotechnique, Vol. 46, pp. 1-16.

Haan, E.J. den and Sellmeijer, J.B. (2000). Calculation of soft ground settlement with Isotache model. Proceedings of Soft Ground Technology Conference, ASCE, Noordwijkerhout.

Haan, E.J. den (2001). Evaluation of creep models for soft soils. Delft Cluster, Delft.

Haan, E.J. den and Feddema, A. (2009). Deformatie en sterkte van ophogingen en dijken op slappe Nederlandse grond. Geotechniek, Vol. 13, pp. 52-55.

Havinga, H.R. (1995). Berekening landhoofdconstructie Betuweroute (*rapport CO360760/39*). Grondmechanica Delft, Delft.

Heeres, O.M. (2008). Lecture numerical modelling of geotechnical problems – discretisation errors. TU Delft, Delft.

Hight, D.W. *et al.* (1997). Wave velocity and stiffness measurements of the Crag and Lower Londen Tertiaries at Sizewell. Géotechnique, Vol. 47, pp. 451-474.

Hill, R. (1950). The mathematical theory of plasticity. Oxford University Press, London.

Hoefsloot, F.J.M. (2008). Door grond horizontal belaste palen – bestaande ontwerpmodellen. Fugro Ingenieursburo, Leidschendam.

Hvorslev, M.J. (1937). Physical properties of remoulded cohesive soils (*English translation*). U.S. Waterways Experimental Station, Vicksburg.

Hughes, T.J.R. (2000). The finite element method – linear static and dynamic finite element analysis. Dover, New York.

Imai, G. (1989). A unified theory of one-dimensional consolidation with creep. Proceedings of the 12th ICSMFE, Rio de Janeiro.

Jamiolkowski, M. *et al.* (1985). New developments in field and laboratory testing of soils. Proceedings of the 11th ICSMFE, San Francisco.

Janbu, N. (1969). The resistance concept applied to deformations of soils. Proceedings of 7th ICSMFE, Mexico.

Jeong, S. *et al.* (2004). Time-dependent behaviour of pile groups by staged construction of an adjacent embankment on soft clay. Canadian Geotechnical Journal, Vol. 41, pp. 644-656.

Jürgenson, L. (1934). The application of theories of elasticity and plasticity to foundation problems. Contributions to Soil Mechanics 1925-1940, Boston Society of Civil Engineers, Boston.

Kabbaj, M. *et al.* (1986). Consolidation of natural clays and laboratory testing. Proceedings of Consolidation of Soils: Testing and Evaluation, ASTM, pp. 378-404.

Kabbaj, M. *et al.* (1988). In situ and laboratory stress-strain relationships. Géotechnique, Vol. 38, pp. 83-100.

Kamien, D. (1995). Introduction to probability and reliability methods for use in geotechnical engineering. U.S. Army Corps of Engineers, Technical Letter no. 1110-2-547, Washington DC.

Karstunen, M. and Koskinen M. (2004). Anisotropy and destructuration of Murro clay. In Advances on Geotechnical Engineering: The Skempton Memorial Conference, London.

Karstunen, M. (2005). Modeling anisotropy and destructuration. Amgiss Workshop, Glasgow.

Karstunen, M. *et al.* (2006). Modelling the behaviour of an embankment on soft clay with different constitutive models. International Journal for Numerical and Analytical Methods in Geomechanics, Vol. 30, pp. 953-982.

Karstunen, M. (2008). Plastic anisotropy of soft reconstituted clays. Canadian Geotechnical Journal, Vol. 45, pp. 314-328.

Karstunen, M. (2010). Guest lecture – Modelling time-dependent behaviour of natural clays. TU Delft, Delft.

Kim, Y.H. and Leroueil, S. (2001). Modeling the viscoplastic behaviour of clays during consolidation: application to Berthierville clay in both laboratory and field conditions. Canadian Geotechnical Journal, Vol. 38, pp. 484-497.

Koskinen, M. *et al.* (2002). Modelling anisotropic behaviour of clays. Finnish Road Administration, Report No. 16, Helsinki.

Krenn, H. *et al.* (2003). Influence of anisotropy and destructuration on an embankment on soft clay. Proceedings of the International Workshop on Geotechnics of Soft Soils – Theory and Practice, Noordwijkerhout.

Kulhawy, F.H. (1992). On the evaluation of soil properties. Geotechnical Special Publication No. 31, ASCE, pp. 95-115.

Lacasse, S. and Nadim, F. (1997). Uncertainties in characterizing soil properties. Publication No. 201, NGI, pp. 49-75.

Ladd, C.C. *et al.* (1977). Stress-deformation and strength characteristics. Proceedings of the 9th ICSMFE, Tokyo, pp. 421-494.

Ladd, C.C. (1991). Stability evaluation during staged construction. Journal of Geotechnical Engineering, ASCE, Vol. 117, pp. 540-615.

Ladd, C.C. *et al.* (1994). Stress-deformation behaviour of an embankment on Boston Blue Clay. Vertical and horizontal deformations of foundations and embankments. Geotechnical Special Publication No. 40, ASCE, pp. 1730-1759.

Lambe, T.W. (1967). Stress path method. Journal of Soil Mechanics and Foundation Engineering, ASCE, Vol. 93, pp. 309-331.

Landva, A.O. and La Rochelle, P. (1982). Compressibility and shear characteristics of Radforth peats. Testing of Peats and Organic Soils, ASTM, pp. 157-191.

Larsson, R. *et al.* (1997). Prediction of settlements of embankments on soft, fine grained soils. Swedish Geotechnical Institute, Information No. 13E, Linköping.

Larsson, R. and Mattsson H. (2003). Settlement and shear strength increase below embankments. Swedish Geotechnical Institute, Report No. 63, Linköping.

Leeuw, E.H. de (1963). Horizontale spanningen en verplaatsingen in een homogene elastische laag van eindige dikte. Laboratorium voor Grondmechanica, Delft.

Leonie, M. *et al.* (2008). Anisotropic creep model for soft soils. Géotechnique, Vol. 15, pp. 215-226.

Leonie *et al.*, M. (2009). Validation of anisotropic creep model for soft soils. Geotechnics of Soft Soils, London.

Leroueil, S. *et al.* (1979). Behaviour of destructed natural clays. Journal of Geotechnical Engineering, Vol. 105, pp. 759-778.

Leroueil, S. *et al.* (1985). Stress-strain-strain rate relation for the compressibility of sensitive natural clays. Géotechnique, Vol. 35, pp. 159-180.

Leroueil, S. *et al.* (1990). Embankments on soft clays (*English translation*). Ellis Horwood, London.

Leroueil, S. (2006). The isotache approach. Where are we 50 years after its development by Professor Šuklje? Proceedings of the 13th Danube European Conference on Geotechnical Engineering, Ljubljana.

Li, K.S.V. (1989). Discussion: In situ and laboratory stress-strain relationships. Géotechnique, Vol. 39, pp. 553-560.

Lings, M.L. *et al.* (2000). Anisotropic stiffness parameters and their measurement in a stiff natural clay. Géotechnique, Vol. 50, pp. 109-125.

Long, M.M. and O'Riordan, N.J. (2001). Field behaviour of very soft clays at the Athlone embankments. Géotechnique, Vol. 51, pp. 293-309.

Lo, S.R. and Li, K.S.V. (2007). Characteristic and design soil parameters: use of statistics. Journal of Geotechnical Engineering, Vol. 160, pp. 141-146.

Lumb, P. and Wong, C.Y. (1971). Influence of anisotropy and dilatancy on pore-water pressure dissipation. University of Hong Kong, Hong Kong.

Maas, M. and Wuite, M. (2006). Vertraging HSL door schuivende ondergrond. Cobouw, Den Haag .

MacFarlane, I.C. (1969). Muskeg engineering handbook. University of Toronto Press, Toronto.

Marche, R. and Chapuis, R. (1974). Contrôle de la stabilité des remblais par la mesure des déplacements horizontaux. Canadian Geotechnical Journal, Vol. 11, pp. 182-201.

Matsou, M. and Kawamura, K. (1977). Diagram for construction control of embankment on soft ground. Soils and Foundations, Vol. 17, pp. 37-52.

McGinty, K. *et al.* (2009). Modelling destructuration and anisotropy of Bothkennar clay. Geotechnics of Soft Soils, London.

Mesri, G. and Godlewski, P.M. (1977). Time and stress compressibility interrelationship. Journal of Geotechnical Engineering Division, ASCE, Vol. 103, pp. 417-430.

Mesri, G. and Choi, Y.K. (1985). The uniqueness of end of primary (EOP) void ratio-effective stress relationship. Proceedings of the 11th ICSMFE, San Francisco.

Mesri, G. *et al.* (1997). Secondary compression of peat with or without surcharging. Journal of Geotechnical and Geoenvironmental Engineering, ASCE, Vol. 123, pp. 411-422.

Mesri, G. and Vardhanabhuti, B. (2005). Secondary compression. Journal of Geotechnical and Geoenvironmental Engineering, ASCE, Vol. 131, pp. 398-401.

Mestat, P.H. (2001). Momis: a database for the numerical modelling of embankments on soft soils and the comparison between computational results and in situ measurements. Bulletin des Laboratoires des Ponts et Chaussées, Ref. 4376, pp. 45-59.

Molenkamp, F. and Heshmati, A.A.R. (1998). Axial shear testing for measuring anisotropy of fibrous peat. Problematic Soils, Balkema, Rotterdam.

Muir Wood, D. (1990). Soil behaviour and critical state soil mechanics. Cambridge University, Cambridge.

Muir Wood, D. (2004). Geotechnical modelling. Spon Press, Oxfordshire.

Näätänen, A. and Lojander, M. (2000). Modelling of anisotropy of Finnish clays. In Proceedings of the 7th Finnish Symposium on Mechanics, Tampere University of Technology, Tampere.

Nash, D.F.T. *et al.* (1992). Initial investigation of the soft clay test bed site at Bothkennar. Géotechnique, Vol. 42, pp. 163-181.

Neher, H.P. *et al.* (2001). An evaluation of soft soil models based on trial embankments. University of Stuttgart, Stuttgart.

Nishimura, S. (2005). Laboratory study on anisotropy of natural London clay. PhD thesis, Imperial College London, London.

Pande, G.N. and Sharma, K.G. (1983). Multi-laminate model of clays – a numerical evaluation of the influence of rotation of principal stress axes. International Journal for Numerical and Analytical Methods in Geomechanics, Vol. 7, pp. 397-418.

Peters, M.G.J.M. and Steenbrink, R. (2008). Berekening van door grond zijdelings belaste palen, conservatief of niet? Geotechniek, April, pp. 30-37.

Perzyna, P. (1963). The constitutive equations for rate sensitive plastic materials. Quarterly of Applied Mechanics, Vol. 20, pp. 321-332.

Pestana , J.M. and Whittle, A.J. (1999). Formulation of a unified constitutive model for clays and sands. International Journal for Numerical and Analytical Methods in Geomechanics, Vol. 23, pp. 1215-1243.

Peuchen, L.J. (2006). Geotechnical Report: Onshore investigation data LNG/CDS Tanks, LNG Downstream Project, Brass Nigeria, Report no. N4525/024. Fugro, Leidschendam.

Poulos, H.G. (1972). Difficulties in prediction of horizontal deformations of foundations. ASCE Journal of the Soil Mechanics and Foundation Division, Vol. 98, pp. 843-848.

Raymond, G.P. (1972). Prediction of undrained deformations and pore pressures in weak clay under two embankments. Géotechnique, Vol. 22, pp. 381-401.

Roscoe, K.H. *et al.* (1958). On the yielding of soils. Géotechnique, Vol. 8, pp. 22-53.

Roscoe, K.H. and Burland, J.B. (1968). On the generalized stress-strain behaviour of wet clay. Cambridge University Press, Cambridge.

Rowe, R.K. *et al.* (2001). Performance of a test embankment constructed on an organic clayey silt deposit. Canadian Geotechnical Journal, Vol. 38, pp. 1283-1296.

Russell, D. (1992). Finite element analysis of soil containing vertical drains. Journal of Ground Engineering, August, pp. 20-24.

Sánchez-Alciturri, J.M. *et al.* (1999). Field performance of staged construction of an embankment. Geotechnical Engineering for Transportation Infrastructure, Balkema, Rotterdam.

Schiffman, R.L. *et al.* (1987). Discussion of "settlement analysis of embankments on soft clays" by G. Mesri and Y.K. Choi. Journal of Geotechnical and Geoenvironmental Engineering, Vol. 113, pp. 1070-1073.

Schofield, A. and Wroth P. (1968). Critical state soil mechanics. Cambridge University Press, Cambridge.

Servais, R. (2006). Plaxis soft soil creep: de toepassing van een isotroop kruipmodel op de anisotrope ondergrond. MSc thesis, TU Delft, Delft.

Skempton, A.W. (1954). The pore water coefficients A and B. Gèotechnique, Vol. 4, pp. 143-147.

Skempton, A.W. (1984). Effective stress in soils, concrete and rocks. Selected Papers on Soil Mechanics, Thomas Telford, London.

Smith, I.M. and Griffiths, D.V. (1982). Programming the finite element method – 2th Edition. John Wiley & Sons, New Jersey.

Spencer, E. (1967). A method of analysis of the stability of embankments assuming parallel inter-slice forces. Géotechnique, Vol. 17, pp. 11-26.

Stermac, A.G. *et al.* (1968). Unusual movements of abutments supported on end bearing piles. Canadian Geotechnical Journal, Vol. 5, pp. 69-79.

Stewart, D.P. *et al.* (1996). Design of bridge abutments on soft clay for loading from lateral soil movements. Géotechnique, Vol. 46, pp. 165-173.

Šuklje L. (1957). The analysis of the consolidation process by the isotaches method. Proceedings of 4th ICSMFE, London.

Šuklje, L. and Majes, B. (1989). Consolidation and creep of soils in plane-strain conditions. Géotechnique, Vol. 39, pp. 231-250.

Symes *et al.* (1988). Drained principle stress rotation in saturated sand. Géotechnique, Vol. 38, pp. 58-81.

Tavenas, F. *et al.* (1978). Creep behaviour of an undisturbed lightly overconsolidated clay. Canadian Geotechnical Journal, Vol. 15, pp. 402-423.

Tavenas, F. *et al.* (1979). Lateral displacements in clay foundations under embankments. Canadian Geotechnical Journal, Vol. 16, pp. 532-550.

Tavenas, F. and Leroueil, S. (1980). The behaviour of embankments on clay foundations. Canadian Geotechnical Journal, Vol. 17, pp. 236-260.

Termaten, H.W. *et al.* (1992). Construeren met grond. CUR Report 162, Gouda.

Terzaghi, K. (1923). Die berechnung der durchlassigkeitziffer des tones aus dem verlauf der hydronamischen spannungserscheinungen. Akademie der Wissenschaften, Wien.

Terzaghi, K. *et al.* (1996). Soil mechanics in engineering practice – 3rd edition. John Wiley & Sons, New York.

Turnhout, P.J. *et al.* (2006). Ontwerpnota Onderbouw A2 Holendrecht – Maarssen. Combinatie A2HoMa, Breukelen.

Valliappan, S. (1981). Continuum mechanics fundamentals. Balkema, Rotterdam.

Vanmarcke, E.H. (1977). Probabilistic modelling of soil properties. Journal of the Geotechnical Engineering Division, Vol. 103, pp. 1227-1246.

Vermeer, P.A. (1978). A double hardening model for sand. Géotechnique, Vol. 28, pp. 413-433.

Vermeer, P.A. *et al.* (1998). From the classical theory of secondary compression to modern creep analysis. Proceedings Computer Methods and Advances in Geomechanics, Wuhan.

Vermeer, P.A. and Neher, H. (1999). A soft soil model that accounts for creep. 10 years of Plaxis International, Balkema, Rotterdam.

Vermeer, P.A. *et al.* (2009). Computational geotechnics. Stichting PostAcedemisch Onderwijs, Delft.

Wheeler, S.J. *et al.* (2003). An anisotropic elasto-plastic model for soft clays. Canadian Geotechnical Journal, Vol. 40, pp. 403-418.

Whittle, A.J. (1993). Evaluation of a constitutive model for overconsolidated clays. Géotechnique, Vol. 43, pp. 289-313.

Wiltafsky, C. (2003). S-Clay1S – user-defined soil model for Plaxis. University of Glasgow, Glasgow.

Yimsiri, S. (2001). Pre-failure deformation characteristics of soils: anisotropy and soil fabric. PhD thesis, University of Cambridge, Cambridge.

Yin, J.H. and Graham, J. (1989). Viscous-elastic-plastic modelling of one-dimensional time-dependent behaviour of clays. Canadian Geotechnical Journal, Vol. 26, pp. 199-209.

Yin, J.H. and Graham, J. (1994). Equivalent times and one-dimensional viscoplastic modelling of time-dependent stress-strain behaviour of clays. Canadian Geotechnical Journal, Vol. 31, pp. 42-52.

Yin, J.H. *et al.* (2002). A new elastic viscoplastic model for time-dependent behaviour of normally and overconsolidated clays: theory and verification. Canadian Geotechnical Journal, Vol. 39, pp. 157-173.

Yin, Z.Y. and Karstunen, M. (2008). Influence of anisotropy, destructuration and viscosity on the behaviour of an embankment on soft clay. The 12th International Conference of IACMAG, Goa.

Zdravković, L. *et al.* (2001). A parametric study of the pull-out capacity of bucket foundations in soft clay. Géotechnique, Vol. 51, pp. 55-67.

Zdravković, L. and Jardine, R.J. (2001). The effect of rotating the principal stress axes during consolidation. Géotechnique, Vol. 51, pp. 69-83.

Zdravković, L. *et al.* (2002). The effect of strength anisotropy on the behaviour of embankments on soft ground. Géotechnique, Vol. 52, pp. 447-457.

Zentar, R. *et al.* (2002). Comparison of two approaches for modelling anisotropy of soft clays. Proceedings of the 8th NUMOG, Rome.

Zhang, L.M. and Ng, A.M.Y. (2005). Probabilistic limiting displacements for serviceability limit state design of foundations. Géotechnique, Vol. 55, pp. 151-161.

Zwanenburg, C. and F.B.J. Barends (2005). Unravelling the anisotropy of peat. Proceedings of the 16th ICSMGE, Osaka.

Appendixes

Appendix 1 – Tables of Van IJsseldijk model

Appendix 1 shows a table for the determination of the horizontal soil deformation and another table for the determination of the increase in horizontal soil stress (Hoefsloot, 2008). These tables are valid for terrace loading without rigid top layer.

$\dfrac{E}{h \cdot q} \cdot u$	y = z/h					
	0.00	0.20	0.40	0.60	0.80	1.00
-8.00	-0.001	-0.001	-0.001	-0.001	-0.001	0.000
-6.00	-0.007	-0.006	-0.005	-0.004	-0.002	0.000
-5.00	-0.015	-0.014	-0.011	-0.008	-0.004	0.000
-4.50	-0.022	-0.020	-0.016	-0.012	-0.006	0.000
-4.00	-0.032	-0.028	-0.024	-0.017	-0.009	0.000
-3.50	-0.046	-0.041	-0.034	-0.025	-0.013	0.000
-3.00	-0.066	-0.060	-0.049	-0.035	-0.019	0.000
-2.50	-0.096	-0.086	-0.071	-0.051	-0.027	0.000
-2.00	-0.140	-0.125	-0.103	-0.074	-0.039	0.000
-1.50	-0.203	-0.181	-0.150	-0.109	-0.058	0.000
-1.00	-0.284	-0.259	-0.224	-0.170	-0.095	0.000
-0.75	-0.327	-0.307	-0.275	-0.216	-0.124	0.000
-0.50	-0.364	-0.361	-0.336	-0.270	-0.159	0.000
-0.25	-0.390	-0.425	-0.400	-0.321	-0.191	0.000
0.00	-0.400	-0.475	-0.434	-0.344	-0.205	0.000
0.25	-0.390	-0.425	-0.400	-0.321	-0.191	0.000
0.50	-0.364	-0.361	-0.336	-0.270	-0.159	0.000
0.75	-0.327	-0.307	-0.275	-0.216	-0.124	0.000
1.00	-0.284	-0.259	-0.224	-0.170	-0.095	0.000
1.50	-0.203	-0.181	-0.150	-0.109	-0.058	0.000
2.00	-0.140	-0.125	-0.103	-0.074	-0.039	0.000
2.50	-0.096	-0.086	-0.071	-0.051	-0.027	0.000
3.00	-0.066	-0.060	-0.049	-0.035	-0.019	0.000
3.50	-0.046	-0.041	-0.034	-0.025	-0.013	0.000
4.00	-0.032	-0.028	-0.024	-0.017	-0.009	0.000
4.50	-0.022	-0.020	-0.016	-0.012	-0.006	0.000
5.00	-0.015	-0.014	-0.011	-0.008	-0.004	0.000
6.00	-0.007	-0.006	-0.005	-0.004	-0.002	0.000
8.00	-0.001	-0.001	-0.001	-0.001	-0.001	0.000

x = t/h

$\frac{1}{q} \cdot \sigma_{xx}$	y = z/h					
	0.00	0.20	0.40	0.60	0.80	1.00
-8.00	0.002	0.002	0.001	0.001	0.001	0.000
-6.00	0.007	0.007	0.006	0.004	0.003	0.001
-5.00	0.015	0.014	0.012	0.009	0.007	0.004
-4.50	0.022	0.020	0.017	0.013	0.009	0.004
-4.00	0.031	0.028	0.024	0.019	0.013	0.006
-3.50	0.045	0.041	0.035	0.028	0.020	0.011
-3.00	0.065	0.060	0.051	0.041	0.028	0.015
-2.50	0.096	0.087	0.074	0.058	0.040	0.020
-2.00	0.141	0.125	0.106	0.083	0.056	0.027
-1.50	0.196	0.176	0.155	0.126	0.085	0.034
-1.00	0.231	0.234	0.235	0.212	0.152	0.050
-0.75	0.219	0.266	0.297	0.283	0.216	0.084
-0.50	0.175	0.314	0.380	0.371	0.304	0.162
-0.25	0.098	0.417	0.472	0.454	0.404	0.304
-0.01	0.004	0.502	0.500	0.499	0.496	0.492
0.00		0.500	0.500	0.500	0.500	0.500
0.01	0.996	0.498	0.500	0.501	0.504	0.508
0.25	0.902	0.583	0.528	0.546	0.596	0.696
0.50	0.825	0.686	0.620	0.629	0.696	0.838
0.75	0.781	0.734	0.703	0.717	0.784	0.916
1.00	0.769	0.766	0.765	0.788	0.848	0.950
1.50	0.804	0.824	0.845	0.874	0.915	0.966
2.00	0.859	0.875	0.894	0.917	0.944	0.973
2.50	0.904	0.913	0.926	0.942	0.960	0.980
3.00	0.935	0.940	0.949	0.959	0.972	0.985
3.50	0.955	0.959	0.965	0.972	0.980	0.989
4.00	0.969	0.972	0.976	0.981	0.987	0.994
4.50	0.978	0.980	0.983	0.987	0.991	0.996
5.00	0.985	0.986	0.988	0.991	0.993	0.996
6.00	0.933	0.993	0.994	0.996	0.997	0.999
8.00	0.998	0.998	0.999	0.999	0.999	1.000

x = t/h

Appendix 2 – Tables of Loof model

Appendix 2 shows a table for the determination of the horizontal soil deformation and another table for the determination of the increase in horizontal soil stress (Hoefsloot, 2008). These tables are valid for terrace loading with rigid top layer. Notice that the x coordinate for this model extends till +/- 4 instead of +/- 8. This emphasises the large influence of a rigid top layer on the overall result.

$\frac{E}{h \cdot q} \cdot u$		y = z/h					
		0.00	0.20	0.40	0.60	0.80	1.00
x = t/h	-4.00	0.000	0.000	0.000	0.000	0.000	0.000
	-3.00	0.000	0.000	0.001	0.001	0.000	0.000
	-2.00	0.000	-0.002	-0.004	-0.003	-0.002	0.000
	-1.50	0.000	-0.012	-0.019	-0.019	-0.012	0.000
	-1.25	0.000	-0.022	-0.036	-0.037	-0.024	0.000
	-1.00	0.000	-0.038	-0.063	-0.066	-0.044	0.000
	-0.75	0.000	-0.062	-0.101	-0.106	-0.072	0.000
	-0.50	0.000	-0.096	-0.154	-0.158	-0.107	0.000
	-0.25	0.000	-0.147	-0.213	-0.208	-0.140	0.000
	0.00	0.000	-0.192	-0.245	-0.230	-0.153	0.000
	0.25	0.000	-0.147	-0.213	-0.208	-0.140	0.000
	0.50	0.000	-0.096	-0.154	-0.158	-0.107	0.000
	0.75	0.000	-0.062	-0.101	-0.106	-0.072	0.000
	1.00	0.000	-0.038	-0.063	-0.066	-0.044	0.000
	1.25	0.000	-0.022	-0.036	-0.037	-0.024	0.000
	1.50	0.000	-0.012	-0.019	-0.019	-0.012	0.000
	2.00	0.000	-0.002	-0.004	-0.003	-0.002	0.000
	3.00	0.000	0.000	0.001	0.001	0.000	0.000
	4.00	0.000	0.000	0.000	0.000	0.000	0.000

$\dfrac{1}{q} \cdot \sigma_{xx}$		$y = z/h$					
		0.00	0.20	0.40	0.60	0.80	1.00
x = t/h	-4.00	0.000	0.000	0.000	0.000	0.000	0.000
	-3.00	0.000	0.000	-0.001	-0.001	-0.001	-0.001
	-2.00	0.000	-0.005	0.007	0.005	-0.002	-0.012
	-1.50	0.000	-0.023	0.037	0.035	0.015	-0.022
	-1.25	0.000	-0.042	0.069	0.070	0.039	-0.023
	-1.00	0.000	-0.072	0.120	0.127	0.085	-0.011
	-0.75	0.000	-0.121	0.198	0.212	0.159	0.029
	-0.50	0.000	-0.203	0.307	0.320	0.262	0.120
	-0.25	0.000	-0.356	0.433	0.426	0.382	0.281
	-0.01	0.000	0.499	0.499	0.498	0.495	0.491
	0.00		0.500	0.500	0.500	0.500	0.500
	0.01	1.000	0.501	0.501	0.502	0.505	0.509
	0.25	1.000	0.644	0.567	0.574	0.618	0.719
	0.50	1.000	0.797	0.693	0.680	0.738	0.880
	0.75	1.000	0.879	0.802	0.788	0.841	0.971
	1.00	1.000	0.928	0.880	0.873	0.915	1.011
	1.25	1.000	0.958	0.931	0.930	0.961	1.023
	1.50	1.000	0.977	0.963	0.965	0.985	1.022
	2.00	1.000	0.995	0.993	0.995	1.002	1.012
	3.00	1.000	1.000	1.001	1.001	1.001	1.001
	4.00	1.000	1.000	1.000	1.000	1.000	1.000

Appendix 3 – Inclinometers installed in the A2 reconstruction project

Appendix 3 shows a Google Earth plot of the installed inclinometers in the neighbourhood of Abcoude.
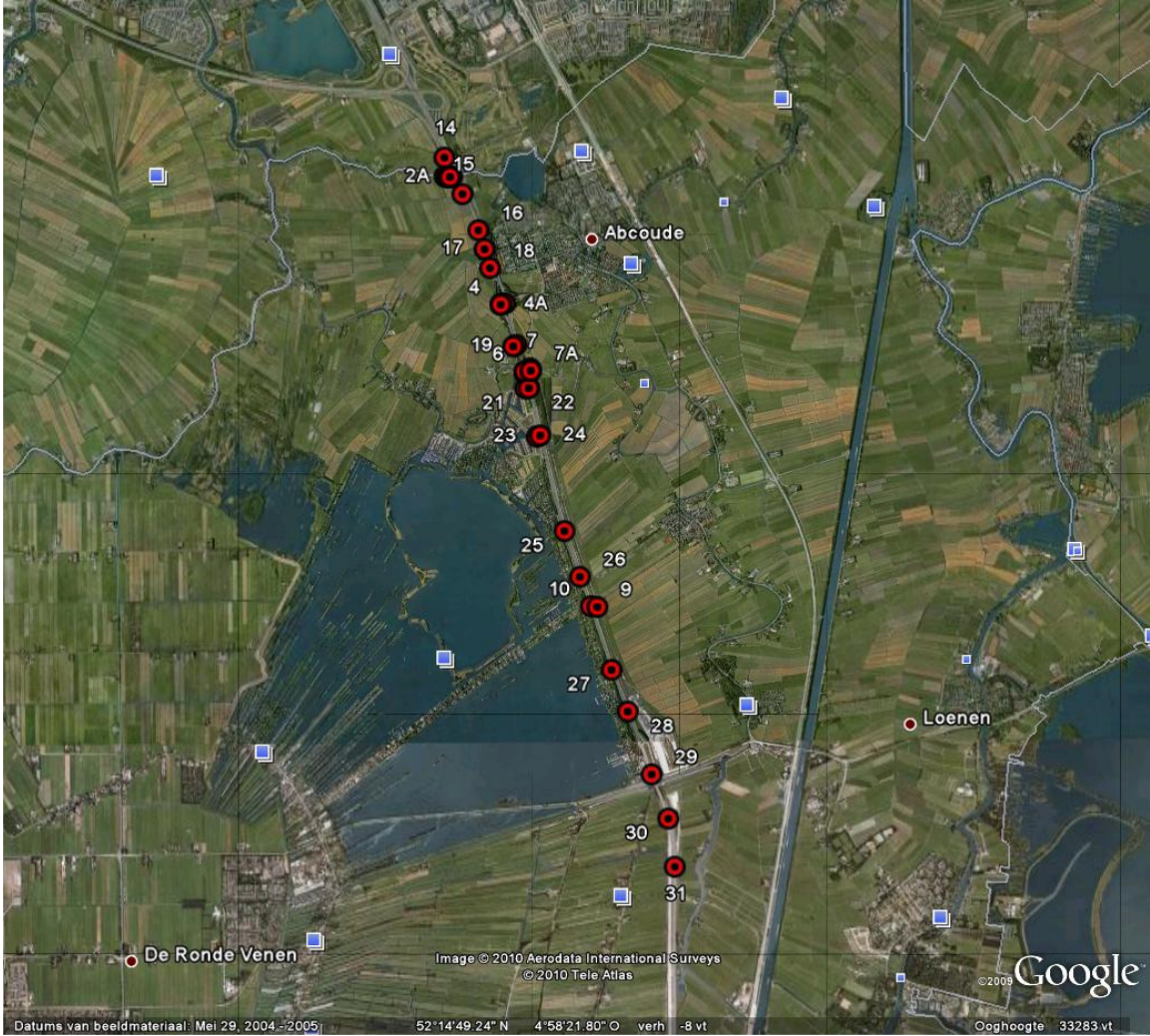
Appendix 4 – Graphical Plaxis output for the Abcoude case study

Appendix 4 presents the graphical output of the horizontal deformations 10.000 days after construction for all considered models in Plaxis.
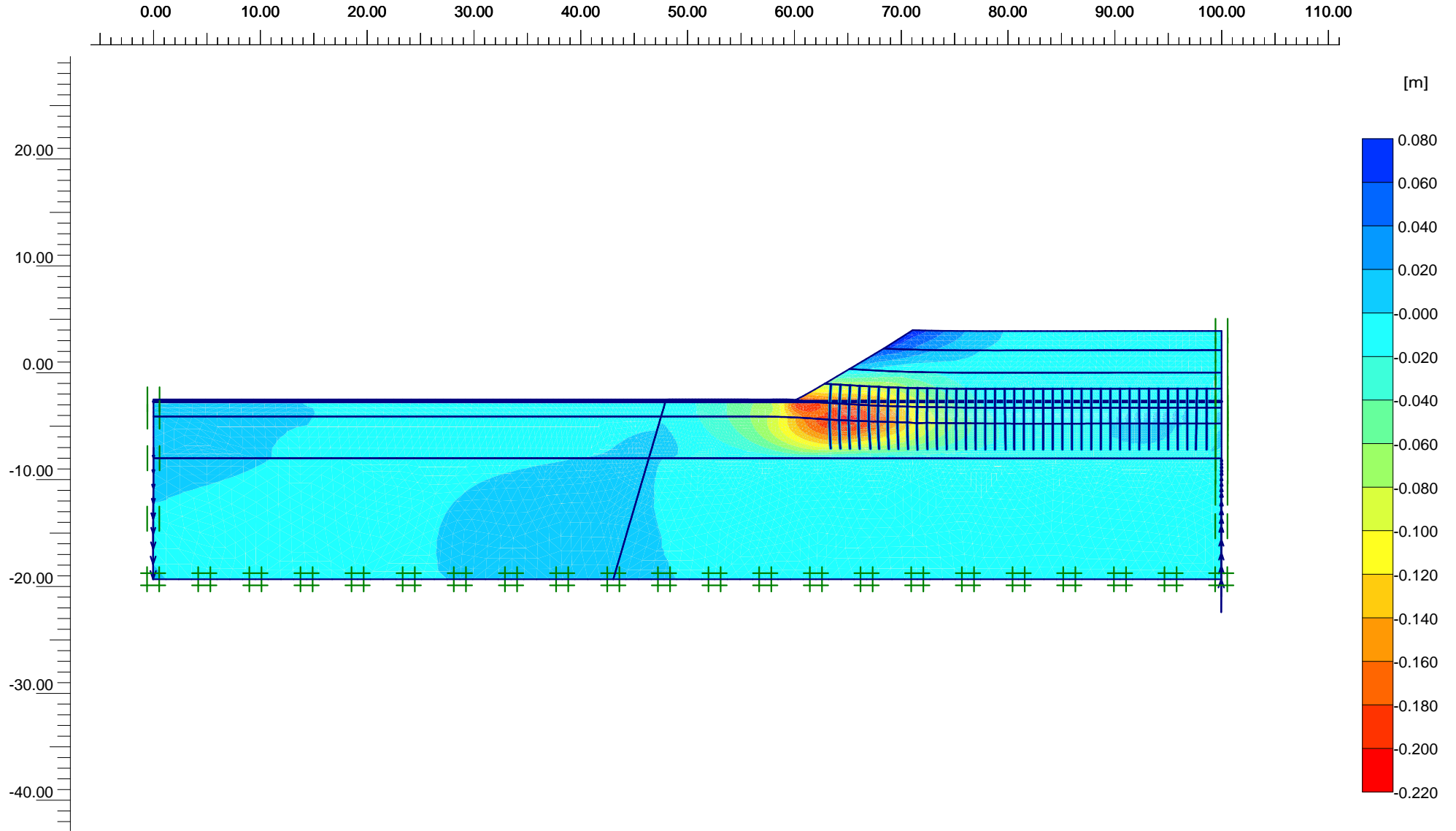
Horizontal displacements (Ux)

Extreme Ux -207,78*10^{-3} m

[m]

0.080
0.060
0.040
0.020
-0.000
-0.020
-0.040
-0.060
-0.080
-0.100
-0.120
-0.140
-0.160
-0.180
-0.200
-0.220

PLAXIS	Project description	Horizontal deformations after 10.000 days (LEPP-MC)		
Finite Element Code for Soil and Rock Analyses	Project name	Step	Date	User name
	Case Study Abco...	27	19-03-10	Hydronamic bv

Version 9.0.2.1182
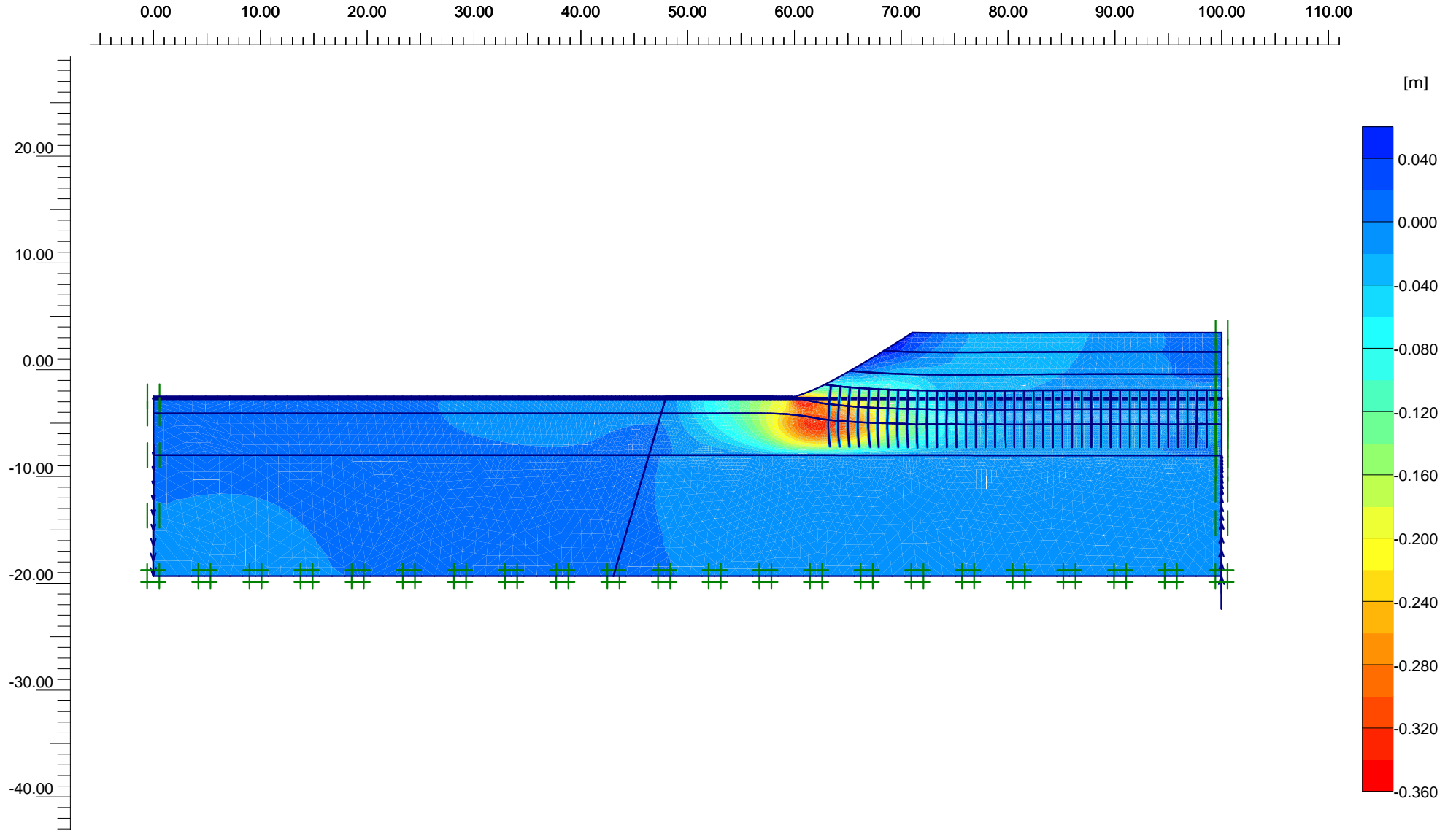
Horizontal displacements (Ux)

Extreme Ux -341,19*10^{-3} m

Project description				
Horizontal deformations after 10.000 days (MCC)				
Project name		Step	Date	User name
Case Study Abco...		45	19-03-10	Hydronamic bv
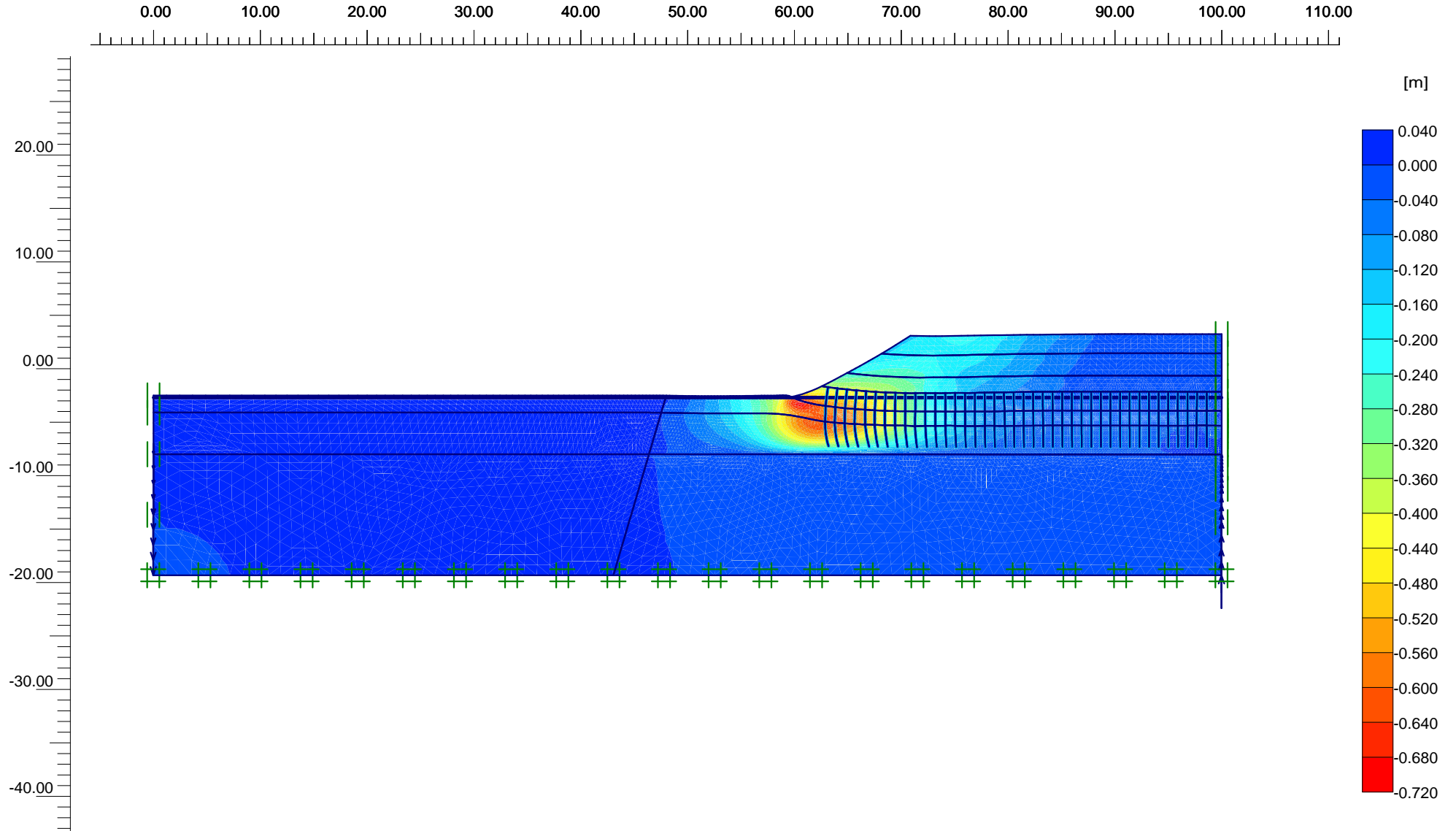
Horizontal displacements (Ux)

Extreme Ux -695,59*10^{-3} m

Project description				
Horizontal deformations after 10.000 days (SSC)				
Project name	Step	Date	User name	
Case Study Abco...	120	19-03-10	Hydronamic bv	

Plaxis 2D
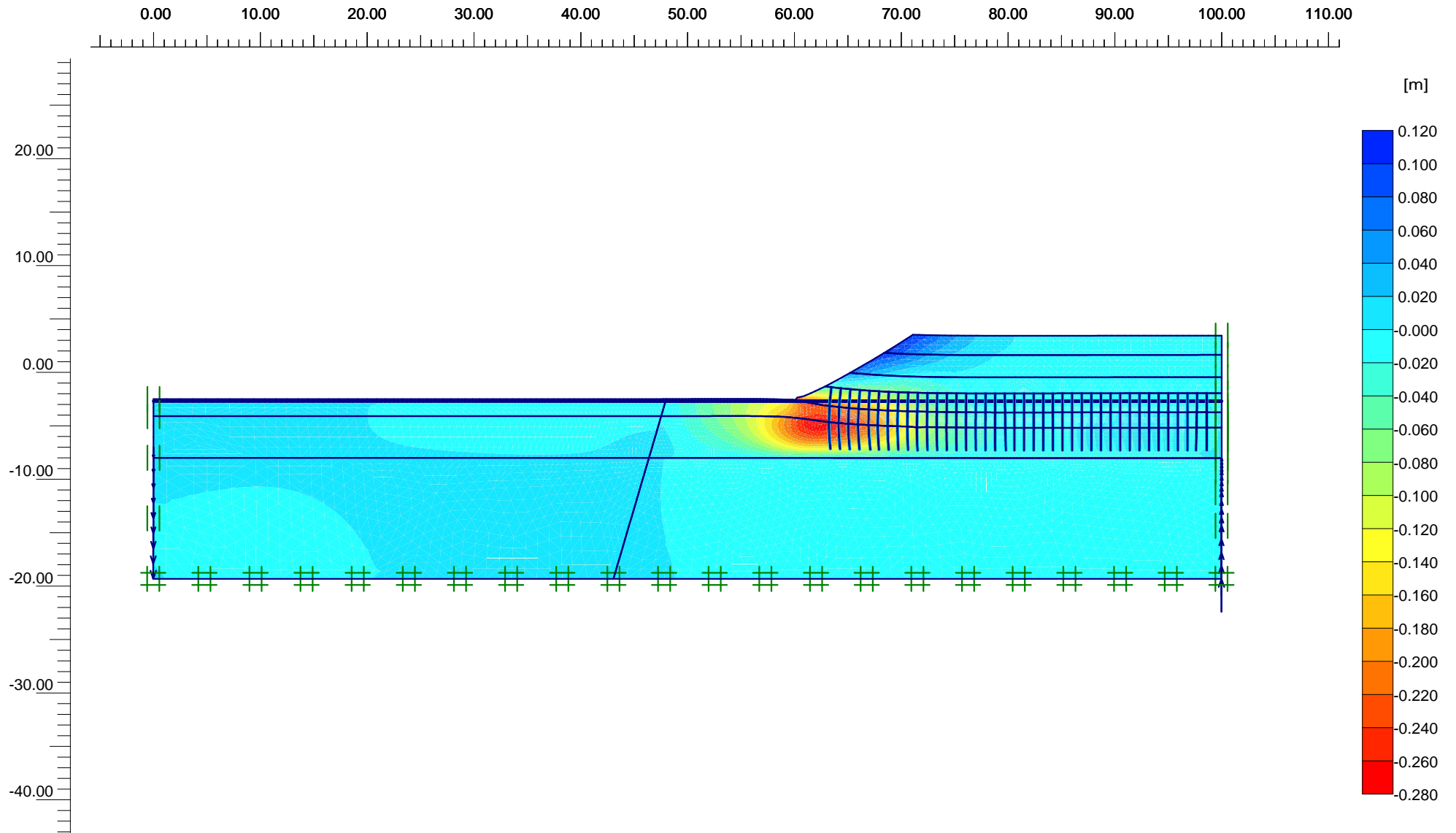
Horizontal displacements (Ux)

Extreme Ux -277,84*10^{-3} m

	[m]
	0.120
	0.100
	0.080
	0.060
	0.040
	0.020
	-0.000
	-0.020
	-0.040
	-0.060
	-0.080
	-0.100
	-0.120
	-0.140
	-0.160
	-0.180
	-0.200
	-0.220
	-0.240
	-0.260
	-0.280

Project description			
Horizontal deformations after 10.000 days (S-Clay1)			
Project name	Step	Date	User name
Case Study Abco...	55	19-03-10	Hydronamic bv

Appendix 5 – Sensitivity analysis for the Abcoude case study

Appendix 5 presents the results of the sensitivity analysis for the considered empirical, analytical and numerical models in this thesis. Before a proper sensitivity analysis can be performed, the standard deviations of the model parameters have to be converted from point values to net values. Notice that such a conversion is only required for the parameters which are determined in the laboratory. It is not useful to apply this correction for parameters that are based on empirical rules or experience. For these parameters the point value is equal to the net value, which is actually a conservative estimate of the standard deviation.

The magnitude of the spatial variability parameters N and Γ^2 are determined from the geotechnical database. In which N and Γ^2 represent the number of independent sample points and the variance reduction factor for spatial averaging over the thickness of the soft soil layer. A precise determination of Γ^2 is usually not possible, because the complete picture of the soil property with depth is mostly not known. Li (1989) showed that the value of Γ^2 values usually varied between 0.1 and 0.5. For example, the friction angle of a 1.5 m thick clay layer is obtained from a triaxial test sample of approximately 0.15 m. A reasonable value of Γ^2 would be 0.1, which is the ratio between the real thickness and the laboratory thickness.

The sensitivity analysis is performed after the 2nd and 4th construction stage at the toe of the embankment. In this analysis each geotechnical parameter is increased respectively decreased with one net standard deviation. The difference gives an indication of the sensitivity of the parameter.

<u>Determination of the net standard deviations:</u>

Table A5.1 – Standard deviations for the Bourgens and Mieussens model

Soil	Parameter	Unit	Point value	Spatial Variability	Net Value
Peat	c_u	kPa	$\sigma_{point} = 5.3$	N = 177 $\Gamma^2 = 0{,}2$	$\sigma_{net} = 2.4$
Sand Fill	γ_{dry}	m/s	$\sigma_{point} = 0.5$	N = - [1] $\Gamma^2 = -$	$\sigma_{net} = 0.5$
Sand Fill	H	m	$\sigma_{point} = 0.2$	N = - $\Gamma^2 = -$	$\sigma_{net} = 0.2$
Sand Fill	L	m	$\sigma_{point} = 1.0$	N = - $\Gamma^2 = -$	$\sigma_{net} = 1.0$
Clay / Peat	S_t	m	$\sigma_{point} = 0.1$	N = - $\Gamma^2 = -$	$\sigma_{net} = 0.1$

[1] A correction for spatial variability is not required for model parameters or parameters that are based on empirical rules

Table A5.2 – Standard deviations for the Van IJsseldijk and Loof model

Soil	Parameter	Unit	Point value	Spatial Variability	Net Value
Sand Fill	B	m	$\sigma_{point} = 1.0$	N = - [1] $\Gamma^2 = -$	$\sigma_{net} = 1.0$
Sand Fill	t	m	$\sigma_{point} = 1.0$	N = - $\Gamma^2 = -$	$\sigma_{net} = 1.0$
Sand Fill	h	m	$\sigma_{point} = 0.5$	N = - $\Gamma^2 = -$	$\sigma_{net} = 0.5$
Sand Fill	q	kPa	$\sigma_{point} = 2.0$	N = - $\Gamma^2 = -$	$\sigma_{net} = 2.0$
Peat	S_t	m	$\sigma_{point} = 0.1$	N = - $\Gamma^2 = -$	$\sigma_{net} = 0.1$

[1] A correction for spatial variability is not required for model parameters or parameters that are based on empirical rules

Table A5.3 – Standard deviations for the general Plaxis parameters

Soil	Parameter	Unit	Point value	Spatial Variability	Net Value
Clay	γ_{sat}	kN/m³	$\sigma_{point} = 0.5$	N = 71 $\Gamma^2 = 0.1$	$\sigma_{net} = 0.2$
	k_x	m/day	$\sigma_{point} = 8.0 \cdot 10^{-5}$	N = 42 $\Gamma^2 = 0.2$	$\sigma_{net} = 3.8 \cdot 10^{-5}$
	k_y	m/day	$\sigma_{point} = 5.4 \cdot 10^{-5}$	N = 42 $\Gamma^2 = 0.2$	$\sigma_{net} = 2.5 \cdot 10^{-5}$
Peat	γ_{sat}	kN/m³	$\sigma_{point} = 0.9$	N = 255 $\Gamma^2 = 0.1$	$\sigma_{net} = 0.3$
	k_x	m/day	$\sigma_{point} = 4.7 \cdot 10^{-3}$	N = 66 $\Gamma^2 = 0.2$	$\sigma_{net} = 2.2 \cdot 10^{-3}$
	k_y	m/day	$\sigma_{point} = 4.7 \cdot 10^{-4}$	N = 66 $\Gamma^2 = 0.2$	$\sigma_{net} = 2.2 \cdot 10^{-4}$

Table A5.4 – Standard deviations for the LEPP-MC model

Soil	Parameter	Unit	Point value	Spatial Variability	Net Value
Clay	E_{oed}	kPa	$\sigma_{point} = 159$	N = 11 $\Gamma^2 = 0.1$	$\sigma_{net} = 69.5$
	ν	-	$\sigma_{point} = 5.0 \cdot 10^{-2}$	N = - [1] $\Gamma^2 = -$	$\sigma_{net} = 5.0 \cdot 10^{-2}$
	c	kPa	$\sigma_{point} = 2.0$	N = 4 $\Gamma^2 = 0.1$	$\sigma_{net} = 1.2$
	φ'_{cv}	°	$\sigma_{point} = 4.0$	N = 4 $\Gamma^2 = 0.1$	$\sigma_{net} = 2.4$
Peat	E_{oed}	kPa	$\sigma_{point} = 156$	N = 65 $\Gamma^2 = 0.1$	$\sigma_{net} = 53.0$
	ν	-	$\sigma_{point} = 5.0 \cdot 10^{-2}$	N = - $\Gamma^2 = -$	$\sigma_{net} = 5.0 \cdot 10^{-2}$
	c	kPa	$\sigma_{point} = 4.3$	N = 14 $\Gamma^2 = 0.1$	$\sigma_{net} = 1.8$
	φ'_{cv}	°	$\sigma_{point} = 5.0$	N = 13 $\Gamma^2 = 0.1$	$\sigma_{net} = 2.1$

[1] A correction for spatial variability is not required for model parameters or parameters that are based on empirical rules

Table A5.5 – Standard deviations for the MCC model

Soil	Parameter	Unit	Point value	Spatial Variability	Net Value
Clay	M	-	$\sigma_{point} = 0.1$	N = - [1] $\Gamma^2 = -$	$\sigma_{net} = 0.1$
	POP	kPa	$\sigma_{point} = 8.5$	N = 21 $\Gamma^2 = 0.2$	$\sigma_{net} = 4.2$
	ν_{ur}	-	$\sigma_{point} = 5.0 \cdot 10^{-2}$	N = - $\Gamma^2 = -$	$\sigma_{net} = 5.0 \cdot 10^{-2}$
	φ'_{cv}	°	$\sigma_{point} = 4.0$	N = 4 $\Gamma^2 = 0.1$	$\sigma_{net} = 2.4$
	c	kPa	$\sigma_{point} = 2.0$	N = 4 $\Gamma^2 = 0.1$	$\sigma_{net} = 1.2$
	e_0	-	$\sigma_{point} = 0.8$	N = 21 $\Gamma^2 = 0.2$	$\sigma_{net} = 0.4$
	λ	-	$\sigma_{point} = 5.0 \cdot 10^{-3}$	N = 11 $\Gamma^2 = 0.1$	$\sigma_{net} = 2.0 \cdot 10^{-3}$
	κ	-	$\sigma_{point} = 2.0 \cdot 10^{-3}$	N = 11 $\Gamma^2 = 0.1$	$\sigma_{net} = 1.0 \cdot 10^{-3}$
Peat	M	-	$\sigma_{point} = 0.1$	N = - $\Gamma^2 = -$	$\sigma_{net} = 0.1$
	POP	kPa	$\sigma_{point} = 5.1$	N = 50 $\Gamma^2 = 0.2$	$\sigma_{net} = 2.4$
	ν_{ur}	-	$\sigma_{point} = 5.0 \cdot 10^{-2}$	N = - $\Gamma^2 = -$	$\sigma_{net} = 5.0 \cdot 10^{-2}$
	φ'_{cv}	°	$\sigma_{point} = 5.0$	N = 13 $\Gamma^2 = 0.1$	$\sigma_{net} = 2.1$
	c	kPa	$\sigma_{point} = 4.3$	N = 14 $\Gamma^2 = 0.1$	$\sigma_{net} = 1.8$
	e_0	-	$\sigma_{point} = 2.6$	N = 83 $\Gamma^2 = 0.2$	$\sigma_{net} = 0.9$
	λ	-	$\sigma_{point} = 8.5 \cdot 10^{-2}$	N = 65 $\Gamma^2 = 0.1$	$\sigma_{net} = 2.9 \cdot 10^{-2}$
	κ	-	$\sigma_{point} = 2.4 \cdot 10^{-2}$	N = 65 $\Gamma^2 = 0.1$	$\sigma_{net} = 8.0 \cdot 10^{-3}$

[1] A correction for spatial variability is not required for model parameters or parameters that are based on empirical rules

Table A5.6 – Standard deviations for the SSC model

Soil	Parameter	Unit	Point value	Spatial Variability	Net Value
Clay	K_0^{NC}	-	$\sigma_{point} = 9.0 \cdot 10^{-2}$	$N = 4$ $\Gamma^2 = 0.2$	$\sigma_{net} = 6.0 \cdot 10^{-2}$
	POP	kPa	$\sigma_{point} = 8.5$	$N = 21$ $\Gamma^2 = 0.2$	$\sigma_{net} = 4.2$
	ν_{ur}	-	$\sigma_{point} = 5.0 \cdot 10^{-2}$	$N = -$ [1] $\Gamma^2 = -$	$\sigma_{net} = 5.0 \cdot 10^{-2}$
	φ'_{cv}	°	$\sigma_{point} = 4.0$	$N = 4$ $\Gamma^2 = 0.1$	$\sigma_{net} = 2.4$
	c	kPa	$\sigma_{point} = 2.0$	$N = 4$ $\Gamma^2 = 0.1$	$\sigma_{net} = 1.2$
	λ^*	-	$\sigma_{point} = 2.0 \cdot 10^{-3}$	$N = 11$ $\Gamma^2 = 0.1$	$\sigma_{net} = 8.7 \cdot 10^{-4}$
	κ^*	-	$\sigma_{point} = 1.0 \cdot 10^{-3}$	$N = 11$ $\Gamma^2 = 0.1$	$\sigma_{net} = 4.4 \cdot 10^{-4}$
	μ^*	-	$\sigma_{point} = 3.0 \cdot 10^{-4}$	$N = 11$ $\Gamma^2 = 0.1$	$\sigma_{net} = 1.3 . \cdot 10^{-4}$
Peat	K_0^{NC}	-	$\sigma_{point} = 6.0 \cdot 10^{-2}$	$N = 22$ $\Gamma^2 = 0.2$	$\sigma_{net} = 3.0 \cdot 10^{-2}$
	POP	kPa	$\sigma_{point} = 5.1$	$N = 50$ $\Gamma^2 = 0.2$	$\sigma_{net} = 2.4$
	ν_{ur}	-	$\sigma_{point} = 5.0 \cdot 10^{-2}$	$N = -$ $\Gamma^2 = -$	$\sigma_{net} = 5.0 \cdot 10^{-2}$
	φ'_{cv}	°	$\sigma_{point} = 5.0$	$N = 13$ $\Gamma^2 = 0.1$	$\sigma_{net} = 2.1$
	c	kPa	$\sigma_{point} = 4.3$	$N = 14$ $\Gamma^2 = 0.1$	$\sigma_{net} = 1.8$
	λ^*	-	$\sigma_{point} = 1.3 \cdot 10^{-2}$	$N = 65$ $\Gamma^2 = 0.1$	$\sigma_{net} = 4.4 \cdot 10^{-3}$
	κ^*	-	$\sigma_{point} = 4.0 \cdot 10^{-3}$	$N = 65$ $\Gamma^2 = 0.1$	$\sigma_{net} = 1.4 \cdot 10^{-3}$
	μ^*	-	$\sigma_{point} = 1.0 \cdot 10^{-3}$	$N = 65$ $\Gamma^2 = 0.1$	$\sigma_{net} = 3.4 \cdot 10^{-4}$

[1] A correction for spatial variability is not required for model parameters or parameters that are based on empirical rules

Table A5.7 – Standard deviations for the S-Clay1 model

Soil	Parameter	Unit	Point value	Spatial Variability	Net Value
Clay	M	-	$\sigma_{point} = 0.1$	N = - Γ^2 = -	$\sigma_{net} = 0.1$
	POP	kPa	$\sigma_{point} = 8.5$	N = 21 $\Gamma^2 = 0.2$	$\sigma_{net} = 4.2$
	ν_{ur}	-	$\sigma_{point} = 5.0 \cdot 10^{-2}$	N = - Γ^2 = -	$\sigma_{net} = 5.0 \cdot 10^{-2}$
	φ'_{cv}	°	$\sigma_{point} = 4.0$	N = 4 $\Gamma^2 = 0.1$	$\sigma_{net} = 2.4$
	c	kPa	$\sigma_{point} = 2.0$	N = 4 $\Gamma^2 = 0.1$	$\sigma_{net} = 1.2$
	e_0	-	$\sigma_{point} = 0.8$	N = 21 $\Gamma^2 = 0.2$	$\sigma_{net} = 0.4$
	λ	-	$\sigma_{point} = 5.0 \cdot 10^{-3}$	N = 11 $\Gamma^2 = 0.1$	$\sigma_{net} = 2.0 \cdot 10^{-3}$
	κ	-	$\sigma_{point} = 2.0 \cdot 10^{-3}$	N = 11 $\Gamma^2 = 0.1$	$\sigma_{net} = 1.0 \cdot 10^{-3}$
	μ	-	$\sigma_{point} = 4.8$	N = - Γ^2 = -	$\sigma_{net} = 4.8$
	β	-	$\sigma_{point} = 0.1$	N = - Γ^2 = -	$\sigma_{net} = 0.1$
Peat	M	-	$\sigma_{point} = 0.1$	N = - Γ^2 = -	$\sigma_{net} = 0.1$
	POP	kPa	$\sigma_{point} = 5.1$	N = 50 $\Gamma^2 = 0.2$	$\sigma_{net} = 2.4$
	ν_{ur}	-	$\sigma_{point} = 5.0 \cdot 10^{-2}$	N = - Γ^2 = -	$\sigma_{net} = 5.0 \cdot 10^{-2}$
	φ'_{cv}	°	$\sigma_{point} = 5.0$	N = 13 $\Gamma^2 = 0.1$	$\sigma_{net} = 2.1$
	c	kPa	$\sigma_{point} = 4.3$	N = 14 $\Gamma^2 = 0.1$	$\sigma_{net} = 1.8$
	e_0	-	$\sigma_{point} = 2.6$	N = 83 $\Gamma^2 = 0.2$	$\sigma_{net} = 0.9$
	λ	-	$\sigma_{point} = 8.5 \cdot 10^{-2}$	N = 65 $\Gamma^2 = 0.1$	$\sigma_{net} = 2.9 \cdot 10^{-2}$
	κ	-	$\sigma_{point} = 2.4 \cdot 10^{-2}$	N = 65 $\Gamma^2 = 0.1$	$\sigma_{net} = 8.0 \cdot 10^{-3}$
	μ	-	$\sigma_{point} = 0.7$	N = - Γ^2 = -	$\sigma_{net} = 0.7$
	β	-	$\sigma_{point} = 0.1$	N = - Γ^2 = -	$\sigma_{net} = 0.1$

<u>Results of the sensitivity analysis:</u>

Table A5.8 –Sensitivity of the parameters of the Bourgens and Mieussens model

Soil	Parameter	2nd stage [cm]	2nd stage [cm]	4th stage [cm]	4th stage [cm]
Peat	c_u	HD$^+$ = 25.7 [1] HD$^-$ = 28.2 [2]	ΔHD = 2.5 [3]	HD$^+$ = 41.0 HD$^-$ = 41.4	ΔHD = 0.4
Sand Fill	γ_{dry}	HD$^+$ = 27.8 HD$^-$ =27.3	ΔHD = 0.5	HD$^+$ = 41.1 HD$^-$ = 41.3	ΔHD = 0.2
Sand Fill	H	HD$^+$ = 28.0 HD$^-$ = 26.5	ΔHD = 1.5	HD$^+$ = 39.9 HD$^-$ = 41.5	ΔHD = 0.6
Sand Fill	L	HD$^+$ = 25.5 HD$^-$ = 28.2	ΔHD = 2.7	HD$^+$ = 38.4 HD$^-$ = 42.1	ΔHD = 3.3
Clay / Peat	S_t	HD$^+$ = 28.9 HD$^-$ = 25.7	ΔHD = 3.2	HD$^+$ = 42.7 HD$^-$ = 39.6	ΔHD = 3.1

[1] HD$^+$ represents the horizontal deformation plus one standard deviation

[2] HD$^-$ represents the horizontal deformation minus one standard deviation

[3] ΔHD represents the difference in horizontal deformation

Table A5.9 –Sensitivity of the parameters of the Van IJsseldijk model

Soil	Parameter	2nd stage [cm]	2nd stage [cm]	4th stage [cm]	4th stage [cm]
Sand Fill	B	HD$^+$ = 51.1 HD$^-$ = 50.9	ΔHD = 0.2	HD$^+$ = 82.0 HD$^-$ = 81.9	ΔHD = 0.1
Sand Fill	t	HD$^+$ = 42.5 HD$^-$ = 47.7	ΔHD = 5.2	HD$^+$ = 68.2 HD$^-$ = 76.6	ΔHD = 8.4
Sand Fill	h	HD$^+$ = 55.4 HD$^-$ = 46.6	ΔHD = 8.8	HD$^+$ = 89.2 HD$^-$ = 74.7	ΔHD = 14.5
Sand Fill	q	HD$^+$ = 52.9 HD$^-$ = 49.2	ΔHD = 3.7	HD$^+$ = 83.3 HD$^-$ = 80.7	ΔHD = 2.6
Peat	S_t	HD$^+$ = 54.8 HD$^-$ = 47.3	ΔHD = 7.5	HD$^+$ = 85.8 HD$^-$ = 78.2	ΔHD = 7.6

Table A5.10 –Sensitivity of the parameters of the Loof model

Soil	Parameter	2nd stage [cm]	2nd stage [cm]	4th stage [cm]	4th stage [cm]
Sand Fill	B	HD$^+$ = 26.7 HD$^-$ = 26.7	ΔHD = 0.0	HD$^+$ = 42.6 HD$^-$ = 42.5	ΔHD = 0.1
Sand Fill	t	HD$^+$ = 20.3 HD$^-$ = 24.7	ΔHD = 4.4	HD$^+$ = 32.4 HD$^-$ = 39.3	ΔHD = 6.9
Sand Fill	h	HD$^+$ = 29.1 HD$^-$ = 24.2	ΔHD = 4.9	HD$^+$ =46.3 HD$^-$ =38.6	ΔHD = 7.7
Sand Fill	q	HD$^+$ = 27.6 HD$^-$ =25.7	ΔHD = 1.9	HD$^+$ = 43.2 HD$^-$ = 41.8	ΔHD = 1.4
Peat	S_t	HD$^+$ = 27.6 HD$^-$ =23.8	ΔHD = 3.8	HD$^+$ = 44.4 HD$^-$ = 40.5	ΔHD = 3.9

Table A5.11 –Sensitivity of the parameters of the LEPP-MC model

Soil	Parameter	2nd stage [cm]	2nd stage [cm]	4th stage [cm]	4th stage [cm]
Clay	γ_{sat}	HD$^+$ = 5.9 HD$^-$ = 6.0	ΔHD = 0.1	HD$^+$ = 16.9 HD$^-$ = 17.2	ΔHD = 0.3
	k_x	HD$^+$ = 6.2 HD$^-$ = 5.8	ΔHD = 0.4	HD$^+$ = 17.3 HD$^-$ = 16.8	ΔHD = 0.5
	k_y	HD$^+$ = 5.8 HD$^-$ = 6.0	ΔHD = 0.2	HD$^+$ =16.7 HD$^-$ = 17.6	ΔHD = 0.9
	E_{oed}	HD$^+$ = 5.8 HD$^-$ = 6.1	ΔHD = 0.3	HD$^+$ = 15.7 HD$^-$ = 17.7	ΔHD = 2.0
	ν	HD$^+$ = 6.4 HD$^-$ = 5.9	ΔHD = 0.5	HD$^+$ = 20.2 HD$^-$ = 14.9	ΔHD = 5.3
	c	HD$^+$ = 5.7 HD$^-$ = 5.9	ΔHD = 0.2	HD$^+$ = 17.3 HD$^-$ = 17.5	ΔHD = 0.2
	φ'_{cv}	HD$^+$ = 5.8 HD$^-$ = 5.9	ΔHD = 0.1	HD$^+$ = 16.1 HD$^-$ = 20.2	ΔHD = 2.9
Peat	γ_{sat}	HD$^+$ = 5.7 HD$^-$ = 6.0	ΔHD = 0.3	HD$^+$ = 16.8 HD$^-$ = 17.3	ΔHD = 0.5
	k_x	HD$^+$ = 6.0 HD$^-$ = 5.8	ΔHD = 0.2	HD$^+$ =17.6 HD$^-$ = 16.5	ΔHD = 1.1
	k_y	HD$^+$ = 6.0 HD$^-$ = 5.8	ΔHD = 0.2	HD$^+$ =17.4 HD$^-$ = 16.6	ΔHD = 0.8
	E_{oed}	HD$^+$ = 5.4 HD$^-$ = 6.3	ΔHD = 0.9	HD$^+$ = 16.4 HD$^-$ = 18.5	ΔHD = 2.1
	ν	HD$^+$ = 7.1 HD$^-$ = 5.3	ΔHD = 1.8	HD$^+$ = 19.2 HD$^-$ = 17.0	ΔHD = 2.2
	c	HD$^+$ = 5.8 HD$^-$ = 6.1	ΔHD = 0.3	HD$^+$ = 16.7 HD$^-$ = 18.4	ΔHD = 1.7
	φ'_{cv}	HD$^+$ = 5.8 HD$^-$ = 5.9	ΔHD = 0.1	HD$^+$ = 16.5 HD$^-$ = 18.2	ΔHD = 1.7

Table A5.12 –Sensitivity of the parameters of the MCC model

Soil	Parameter	2nd stage [cm]	2nd stage [cm]	4th stage [cm]	4th stage [cm]
Clay	γ_{sat}	HD+ =15.2 HD- = 16.0	ΔHD = 0.8	HD+ = 27.5 HD- = 28.9	ΔHD = 1.5
	k_x	HD+ = 16.4 HD- = 15.4	ΔHD = 1.0	HD+ = 28.4 HD- = 26.3	ΔHD = 2.1
	k_y	HD+ =15.9 HD- = 15.3	ΔHD = 0.6	HD+ = 27.9 HD- = 26.3	ΔHD = 1.6
	M	HD+ = 14.9 HD- = 17.3	ΔHD = 2.4	HD+ = 24.7 HD- = 30.1	ΔHD = 5.4
	POP	HD+ = 14.7 HD- = 16.8	ΔHD = 2.1	HD+ = 26.0 HD- = 28.6	ΔHD = 2.6
	ν_{ur}	HD+ =15.7 HD- = 15.5	ΔHD = 0.2	HD+ = 27.5 HD- = 27.2	ΔHD = 0.3
	φ'_{cv}	HD+ = 15.6 HD- = 15.7	ΔHD = 0.1	HD+ = 27.3 HD- = 27.4	ΔHD = 0.1
	c	HD+ = 15.6 HD- = 15.6	ΔHD = 0.0	HD+ = 27.4 HD- =27.5	ΔHD = 0.1
	e_0	HD+ = 14.5 HD- = 16.9	ΔHD = 2.4	HD+ = 25.1 HD- = 29.5	ΔHD = 4.4
	λ	HD+ = 15.8 HD- = 15.3	ΔHD = 0.5	HD+ = 27.7 HD- = 27.0	ΔHD = 0.7
	κ	HD+ = 15.5 HD- = 15.7	ΔHD = 0.2	HD+ = 27.4 HD- = 27.5	ΔHD = 0.1
Peat	γ_{sat}	HD+ = 15.0 HD- = 16.5	ΔHD = 1.5	HD+ = 26.9 HD- = 28.4	ΔHD = 1.5
	k_x	HD+ = 16.4 HD- = 15.3	ΔHD = 1.1	HD+ = 27.9 HD- = 26.8	ΔHD = 1.1
	k_y	HD+ = 15.9 HD- = 15.5	ΔHD = 0.4	HD+ = 27.9 HD- = 27.1	ΔHD = 0.8
	M	HD+ = 14.4 HD- = 17.6	ΔHD = 3.2	HD+ = 24.1 HD- = 29.9	ΔHD = 5.8
	POP	HD+ = 15.1 HD- = 16.3	ΔHD = 1.2	HD+ = 26.3 HD- = 28.5	ΔHD = 2.2
	ν_{ur}	HD+ = 15.8 HD- = 15.5	ΔHD = 0.3	HD+ = 27.5 HD- = 27.1	ΔHD = 0.4
	φ'_{cv}	HD+ = 15.4 HD- = 15.6	ΔHD = 0.2	HD+ = 27.4 HD- =27.5	ΔHD = 0.1
	c	HD+ = 15.5 HD- = 15.6	ΔHD = 0.1	HD+ = 27.4 HD- = 27.5	ΔHD = 0.1
	e_0	HD+ =14.7 HD- = 17.1	ΔHD = 2.4	HD+ =24.7 HD- = 29.9	ΔHD = 5.2
	λ	HD+ = 15.7 HD- = 15.4	ΔHD = 0.3	HD+ = 27.5 HD- = 27.2	ΔHD = 0.3
	κ	HD+ = 15.4 HD- = 15.8	ΔHD = 0.4	HD+ = 27.2 HD- = 27.4	ΔHD = 0.2

Table A5.13 –Sensitivity of the parameters of the SSC model

Soil	Parameter	2nd stage [cm]	2nd stage [cm]	4th stage [cm]	4th stage [cm]
Clay	γ_{sat}	HD+ = 15.3 HD- = 15.8	ΔHD = 0.5	HD+ =25.8 HD- = 26.7	ΔHD = 0.9
	k_x	HD+ = 16.2 HD- = 15.3	ΔHD = 0.9	HD+ = 27.0 HD- = 25.5	ΔHD = 1.5
	k_y	HD+ = 16.0 HD- = 15.5	ΔHD = 0.5	HD+ = 26.6 HD- = 25.6	ΔHD = 1.0
	K_0^{NC}	HD+ = 16.1 HD- = 15.5	ΔHD = 0.6	HD+ = 26.9 HD- = 25.6	ΔHD = 1.3
	POP	HD+ =14.5 HD- = 17.4	ΔHD = 2.9	HD+ = 25.0 HD- = 27.8	ΔHD = 2.8
	ν_{ur}	HD+ =15.7 HD- = 15.6	ΔHD = 0.1	HD+ = 26.2 HD- = 26.1	ΔHD = 0.1
	φ'_{cv}	HD+ = 14.3 HD- = 17.0	ΔHD = 2.7	HD+ = 24.0 HD- = 28.9	ΔHD = 4.9
	c	HD+ = 14.0 HD- = 17.6	ΔHD = 3.6	HD+ = 24.8 HD- = 27.9	ΔHD = 3.1
	λ^*	HD+ =15.8 HD- = 15.6	ΔHD = 0.2	HD+ = 26.2 HD- = 25.9	ΔHD = 0.3
	κ^*	HD+ = 15.5 HD- = 16.1	ΔHD = 0.6	HD+ = 26.0 HD- = 26.4	ΔHD = 0.4
	μ^*	HD+ = 17.3 HD- = 15.1	ΔHD = 2.1	HD+ = 27.9 HD- = 25.3	ΔHD = 2.6
Peat	γ_{sat}	HD+ = 15.3 HD- = 15.9	ΔHD = 0.6	HD+ = 26.2 HD- = 26.9	ΔHD = 0.7
	k_x	HD+ = 16.7 HD- = 15.3	ΔHD = 1.5	HD+ = 27.1 HD- = 25.5	ΔHD = 1.6
	k_y	HD+ = 16.0 HD- = 15.5	ΔHD = 0.5	HD+ = 25.5 HD- = 26.3	ΔHD = 0.8
	K_0^{NC}	HD+ = 17.0 HD- = 14.4	ΔHD = 2.6	HD+ = 29,8 HD- = 24.1	ΔHD = 5.7
	POP	HD+ = 15.5 HD- =15.8	ΔHD = 0.3	HD+ = 25.8 HD- = 26.3	ΔHD = 0.5
	ν_{ur}	HD+ =15.8 HD- = 15.7	ΔHD = 0.1	HD+ = 26.2 HD- = 26.1	ΔHD = 0.1
	φ'_{cv}	HD+ = 15.0 HD- = 17.7	ΔHD = 2.7	HD+ = 23.8 HD- = 28.3	ΔHD = 4.5
	c	HD+ = 14.9 HD- = 16.5	ΔHD = 1.6	HD+ =25.3 HD- = 27.3	ΔHD = 2.0
	λ^*	HD+ = 15.9 HD- = 15.5	ΔHD = 0.4	HD+ = 26.2 HD- = 25.8	ΔHD = 0.4
	κ^*	HD+ = 15.7 HD- = 15.9	ΔHD = 0.2	HD+ = 26.0 HD- = 26.1	ΔHD = 0.1
	μ^*	HD+ = 16.3 HD- = 15.2	ΔHD = 1.1	HD+ = 27.4 HD- = 25.1	ΔHD = 2.3

Table A5.14 –Sensitivity of the parameters of the S-Clay1 model

Soil	Parameter	2nd stage [cm]	2nd stage [cm]	4th stage [cm]	4th stage [cm]
Clay	γ_{sat}	HD+ = 12.8 HD- = 13.3	ΔHD = 0.5	HD+ = 23.1 HD- = 24.3	ΔHD = 1.2
	k_x	HD+ = 13.4 HD- = 13.0	ΔHD = 0.4	HD+ = 23.5 HD- = 22.9	ΔHD = 0.6
	k_y	HD+ = 13.3 HD- = 13.0	ΔHD = 0.3	HD+ = 23.9 HD- = 23.3	ΔHD = 0.6
	M	HD+ = 11.0 HD- = 14.5	ΔHD = 3.5	HD+ = 21.9 HD- = 26.7	ΔHD = 4.8
	POP	HD+ = 12.3 HD- = 13.5	ΔHD = 1.2	HD+ = 22.9 HD- = 25.2	ΔHD = 2.3
	ν_{ur}	HD+ = 13.2 HD- = 13.1	ΔHD = 0.1	HD+ = 23.7 HD- = 23.6	ΔHD = 0.1
	φ'_{cv}	HD+ = 12.7 HD- = 14.1	ΔHD = 1.4	HD+ = 22.9 HD- = 24.7	ΔHD = 1.8
	c	HD+ = 12.6 HD- = 13.5	ΔHD = 0.9	HD+ = 23.0 HD- = 24.4	ΔHD = 1.4
	e_0	HD+ = 12.5 HD- = 14.9	ΔHD = 2.4	HD+ = 21.9 HD- = 25.1	ΔHD = 3.2
	λ	HD+ = 13.4 HD- = 12.9	ΔHD = 0.5	HD+ = 24.0 HD- = 23.3	ΔHD = 0.7
	κ	HD+ = 13.0 HD- = 13.3	ΔHD = 0.3	HD+ = 23.6 HD- = 23.9	ΔHD = 0.3
	μ	HD+ = 12.9 HD- = 13.2	ΔHD = 0.3	HD+ = 23.5 HD- = 23.9	ΔHD = 0.4
	β	HD+ = 12.1 HD- = 14.3	ΔHD = 2.2	HD+ = 22.7 HD- = 24.0	ΔHD = 1.3
Peat	γ_{sat}	HD+ = 12.7 HD- = 13.8	ΔHD = 1.1	HD+ = 23.1 HD- = 24.8	ΔHD = 1.7
	k_x	HD+ = 13.5 HD- = 12.4	ΔHD = 1.1	HD+ = 24.5 HD- = 22.9	ΔHD = 1.6
	k_y	HD+ = 13.5 HD- = 12.9	ΔHD = 0.6	HD+ = 24.4 HD- = 23.1	ΔHD = 1.3
	M	HD+ = 11.9 HD- = 14.5	ΔHD = 2.6	HD+ = 21.8 HD- = 26.0	ΔHD = 5.2
	POP	HD+ = 12.3 HD- = 13.9	ΔHD = 1.6	HD+ = 22.9 HD- = 24.8	ΔHD = 2.1
	ν_{ur}	HD+ = 13.4 HD- = 12.7	ΔHD = 0.6	HD+ = 24.0 HD- = 23.1	ΔHD = 0.9
	φ'_{cv}	HD+ = 12.3 HD- = 13.6	ΔHD = 1.3	HD+ = 23.1 HD- = 24.6	ΔHD = 1.5
	c	HD+ = 12.8 HD- = 13.7	ΔHD = 0.9	HD+ =23.5 HD- = 24.2	ΔHD = 0.7
	e_0	HD+ = 11.5 HD- = 14.9	ΔHD = 3.4	HD+ = 22.0 HD- = 27.4	ΔHD = 5.4
	λ	HD+ = 13.5 HD- = 12.6	ΔHD = 0.9	HD+ = 24.2 HD- = 23.1	ΔHD = 1.1
	κ	HD+ = 12.8 HD- = 13.5	ΔHD = 0.7	HD+ = 23.3 HD- = 24.2	ΔHD = 0.9
	μ	HD+ = 12.9 HD- = 13.4	ΔHD = 0.5	HD+ = 23.6 HD- = 24.1	ΔHD = 0.5
	β	HD+ = 12.2 HD- = 14.5	ΔHD = 2.3	HD+ = 22.1 HD- = 25.5	ΔHD = 3.4

Appendix 6 – Graphical Plaxis output for the Brass case study

Appendix 6 presents the graphical output of the horizontal deformations at the end of the operational lifetime. Notice that the end of the operational lifetime is planned 20 years after the end of construction.
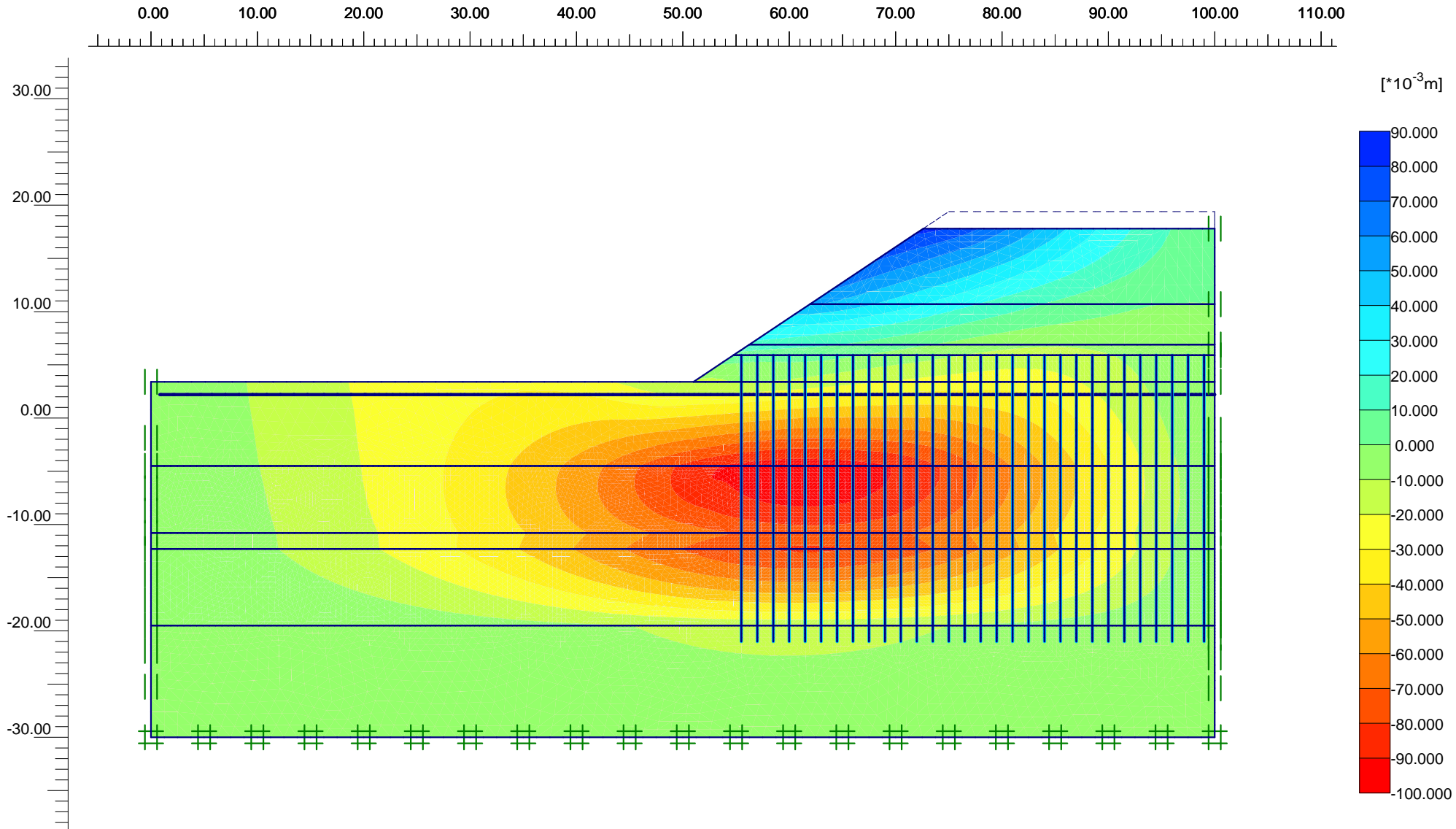
Horizontal displacements (Ux)

Extreme Ux -97,24*10^{-3} m

PLAXIS

Finite Element Code for Soil and Rock Analyses

Project description				
Horizontal deformations at the end of design life (LEPP-MC)				
Project name	Step	Date	User name	
Case Study Bras...	52	07-06-10	Hydronamic bv	

Version 9.0.2.1182

Horizontal displacements (Ux)

Extreme Ux -201,31*10^{-3} m

PLAXIS	Project description			
	Horizontal deformations at the end of design life (MCC)			
Finite Element Code for Soil and Rock Analyses	Project name	Step	Date	User name
	Case Study Bras...	29	07-06-10	Hydronamic bv

Version 9.0.2.1182
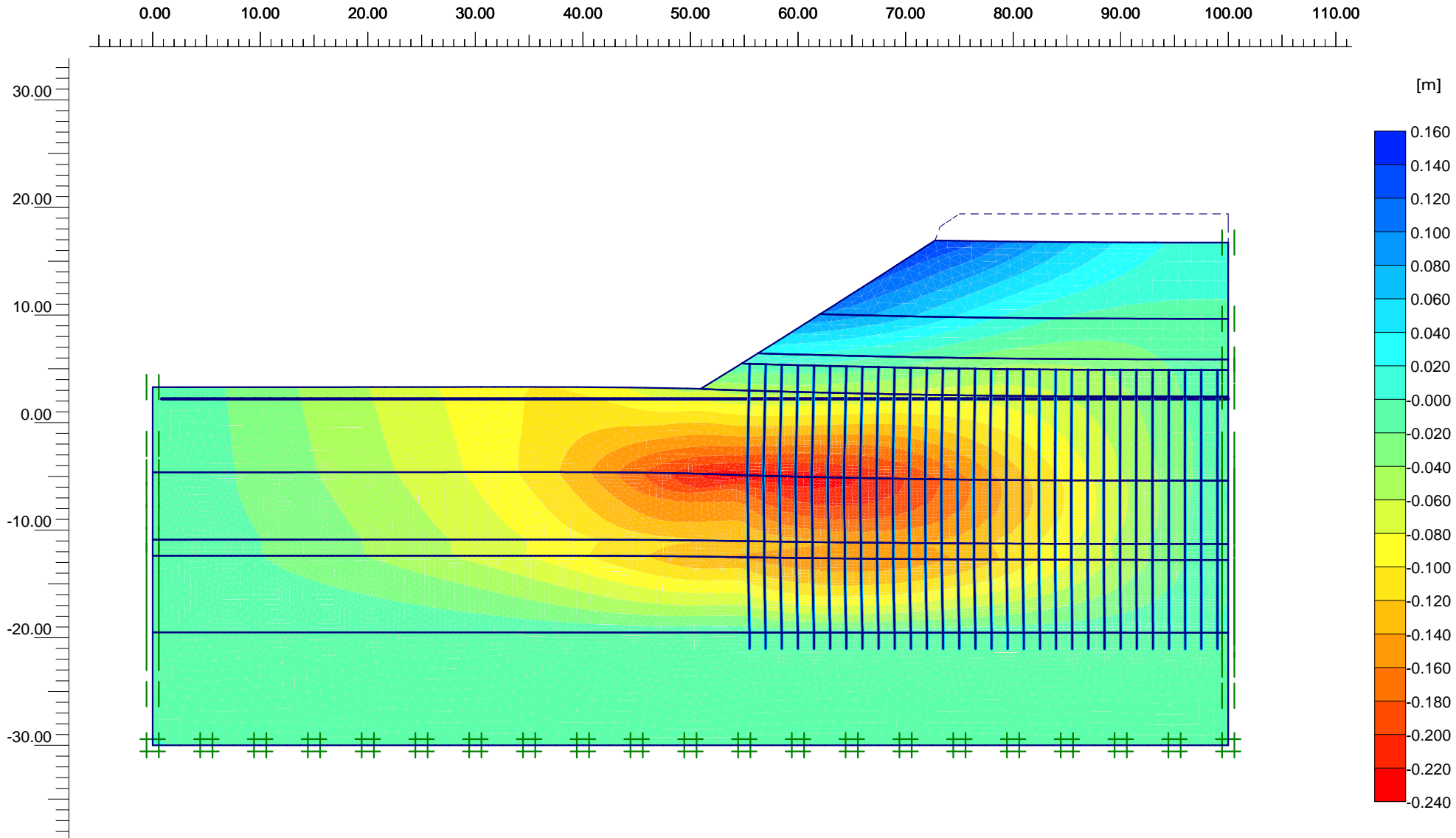
Horizontal displacements (Ux)

Extreme Ux -233,17*10^{-3} m

Project description				
Horizontal deformations at the end of design life (SSC)				
Project name	Step	Date	User name	
Case Study Bras...	49	07-06-10	Hydronamic bv	
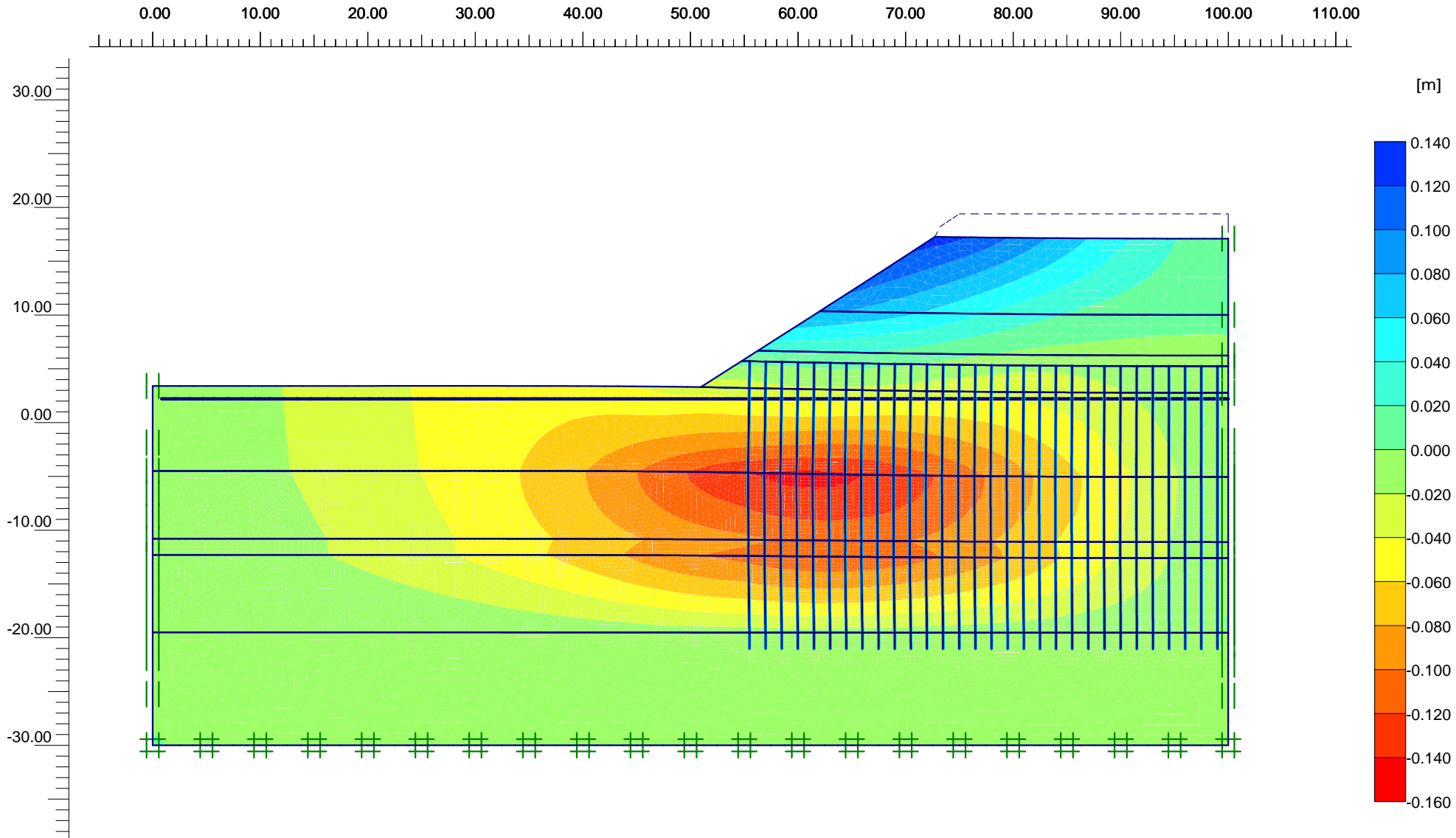
Horizontal displacements (Ux)

Extreme Ux -144,77*10^{-3} m

Project description				
Horizontal deformations at the end of design life (S-Clay1)				
Project name	Step	Date	User name	
Case Study Bras...	23	07-06-10	Hydronamic bv	

Appendix 7 – Sensitivity analysis for the Brass case study

Appendix 7 presents the results of the sensitivity analysis for the considered constitutive models in Plaxis. In contrast to Appendix 5 the net standard deviations are already reported in tables 19 and 20 of the main text.

The sensitivity analysis is performed for the last construction stage where sand thickness is increased from 3.5 m till 16.0 m. In this analysis each geotechnical parameter is increased respectively decreased with one net standard deviation. The difference gives an indication of the sensitivity of the parameter.

Table A7.1 –Sensitivity of the parameters of the LEPP-MC model

Soil	Parameter	Last stage [cm]	Last stage [cm]
Sandy Clay	γ_{sat}	$HD^+ = 9.1$ $HD^- = 9.2$	$\Delta HD = 0.1$
	k_x	$HD^+ = 9.6$ $HD^- = 8.9$	$\Delta HD = 0.7$
	k_y	$HD^+ = 9.3$ $HD^- = 9.0$	$\Delta HD = 0.3$
	E_{oed}	$HD^+ = 7.5$ $HD^- = 10.9$	$\Delta HD = 3.4$
	ν	$HD^+ = 9.6$ $HD^- = 8.4$	$\Delta HD = 1.2$
	c	$HD^+ = 9.1$ $HD^- = 9.3$	$\Delta HD = 0.2$
	φ'_{cv}	$HD^+ = 9.1$ $HD^- = 9.4$	$\Delta HD = 0.3$
Soft Clay I	γ_{sat}	$HD^+ = 9.1$ $HD^- = 9.2$	$\Delta HD = 0.1$
	k_x	$HD^+ = 9.3$ $HD^- = 9.1$	$\Delta HD = 0.2$
	k_y	$HD^+ = 9.4$ $HD^- = 9.2$	$\Delta HD = 0.2$
	E_{oed}	$HD^+ = 8.8$ $HD^- = 9.6$	$\Delta HD = 0.8$
	ν	$HD^+ = 9.7$ $HD^- = 8.9$	$\Delta HD = 0.8$
	c	$HD^+ = 9.1$ $HD^- = 9.2$	$\Delta HD = 0.1$
	φ'_{cv}	$HD^+ = 9.0$ $HD^- = 9.4$	$\Delta HD = 0.4$

Table A7.2 –Sensitivity of the parameters of the MCC model

Soil	Parameter	Last stage [cm]	Last stage [cm]
Sandy Clay	γ_{sat}	HD$^+$ = 17.3 HD$^-$ = 17.6	ΔHD = 0.3
	k_x	HD$^+$ = 17.8 HD$^-$ = 17.0	ΔHD = 0.8
	k_y	HD$^+$ = 17.7 HD$^-$ = 17.3	ΔHD = 0.4
	M	HD$^+$ =15.2 HD$^-$ = 18.7	ΔHD = 3.5
	OCR	HD$^+$ = 15.8 HD$^-$ = 19.0	ΔHD = 3.2
	ν_{ur}	HD$^+$ = 17.8 HD$^-$ = 17.1	ΔHD = 0.7
	φ'_{cv}	HD$^+$ = 17.3 HD$^-$ = 17.5	ΔHD = 0.2
	c	HD$^+$ = 17.3 HD$^-$ = 17.4	ΔHD = 0.1
	e_0	HD$^+$ =16.0 HD$^-$ = 19.4	ΔHD = 4.4
	λ	HD$^+$ = 18.4 HD$^-$ = 16.8	ΔHD = 1.6
	κ	HD$^+$ = 17.3 HD$^-$ = 17.5	ΔHD = 0.2
Soft Clay I	γ_{sat}	HD$^+$ = 17.4 HD$^-$ = 17.5	ΔHD = 0.1
	k_x	HD$^+$ = 17.7 HD$^-$ = 17.2	ΔHD = 0.5
	k_y	HD$^+$ = 17.6 HD$^-$ = 17.3	ΔHD = 0.3
	M	HD$^+$ = 16.1 HD$^-$ = 18.0	ΔHD = 1.9
	OCR	HD$^+$ = 15.9 HD$^-$ = 18.3	ΔHD = 2.4
	ν_{ur}	HD$^+$ = 17.7 HD$^-$ = 16.9	ΔHD = 0.8
	φ'_{cv}	HD$^+$ = 17.4 HD$^-$ = 17.5	ΔHD = 0.1
	c	HD$^+$ = 17.4 HD$^-$ = 17.4	ΔHD = 0.0
	e_0	HD$^+$ = 16.8 HD$^-$ = 18.5	ΔHD = 1.7
	λ	HD$^+$ =17.6 HD$^-$ = 17.3	ΔHD = 0.3
	κ	HD$^+$ = 17.4 HD$^-$ = 17.6	ΔHD = 0.2

Table A7.3 –Sensitivity of the parameters of the SSC model

Soil	Parameter	Last stage [cm]	Last stage [cm]
Sandy Clay	γ_{sat}	$HD^+ = 14.6$ $HD^- = 15.0$	$\Delta HD = 0.4$
	k_x	$HD^+ = 15.2$ $HD^- = 14.0$	$\Delta HD = 1.2$
	k_y	$HD^+ = 14.9$ $HD^- = 14.3$	$\Delta HD = 0.6$
	K_0^{NC}	$HD^+ = 16.3$ $HD^- = 14.1$	$\Delta HD = 2.1$
	OCR	$HD^+ = 13.3$ $HD^- = 16.4$	$\Delta HD = 3.1$
	ν_{ur}	$HD^+ = 15.0$ $HD^- = 14.5$	$\Delta HD = 0.5$
	φ'_{cv}	$HD^+ = 14.2$ $HD^- = 14.8$	$\Delta HD = 0.6$
	c	$HD^+ = 14.3$ $HD^- = 14.9$	$\Delta HD = 0.6$
	λ^*	$HD^+ = 15.9$ $HD^- = 13.9$	$\Delta HD = 2.0$
	κ^*	$HD^+ = 14.3$ $HD^- = 15.1$	$\Delta HD = 0.8$
	μ^*	$HD^+ = 15.5$ $HD^- = 14.1$	$\Delta HD = 1.4$
Soft Clay I	γ_{sat}	$HD^+ = 14.6$ $HD^- = 14.9$	$\Delta HD = 0.3$
	k_x	$HD^+ = 15.6$ $HD^- = 14.1$	$\Delta HD = 1.5$
	k_y	$HD^+ = 15.2$ $HD^- = 14.3$	$\Delta HD = 0.9$
	K_0^{NC}	$HD^+ = 15.8$ $HD^- = 13.7$	$\Delta HD = 2.1$
	OCR	$HD^+ = 13.2$ $HD^- = 16.0$	$\Delta HD = 2.8$
	ν_{ur}	$HD^+ = 14.9$ $HD^- = 14.7$	$\Delta HD = 0.2$
	φ'_{cv}	$HD^+ = 14.2$ $HD^- = 15.6$	$\Delta HD = 1.4$
	c	$HD^+ = 14.0$ $HD^- = 15.2$	$\Delta HD = 1.2$
	λ^*	$HD^+ = 15.5$ $HD^- = 13.9$	$\Delta HD = 1.6$
	κ^*	$HD^+ = 14.5$ $HD^- = 15.0$	$\Delta HD = 0.5$
	μ^*	$HD^+ = 15.3$ $HD^- = 14.3$	$\Delta HD = 1.0$

Table A7.4 –Sensitivity of the parameters of the S–Clay1 model

Soil	Parameter	Last stage [cm]	Last stage [cm]
Sandy Clay	γ_{sat}	HD$^+$ = 12.6 HD$^-$ = 12.8	ΔHD = 0.2
	k_x	HD$^+$ = 13.3 HD$^-$ = 12.5	ΔHD = 0.8
	k_y	HD$^+$ = 13.0 HD$^-$ = 12.5	ΔHD = 0.5
	M	HD$^+$ = 11.1 HD$^-$ = 14.5	ΔHD = 3.4
	OCR	HD$^+$ = 11.6 HD$^-$ = 14.6	ΔHD = 3.0
	ν_{ur}	HD$^+$ = 13.2 HD$^-$ = 12.5	ΔHD = 0.7
	φ'_{cv}	HD$^+$ = 12.4 HD$^-$ = 12.8	ΔHD = 0.4
	c	HD$^+$ = 12.5 HD$^-$ = 12.9	ΔHD = 0.4
	e_0	HD$^+$ = 11.6 HD$^-$ = 13.5	ΔHD = 1.9
	λ	HD$^+$ = 13.5 HD$^-$ = 12.3	ΔHD = 1.2
	κ	HD$^+$ = 12.3 HD$^-$ = 13.0	ΔHD = 0.7
	μ	HD$^+$ = 12.5 HD$^-$ = 13.0	ΔHD = 0.5
	β	HD$^+$ = 11.7 HD$^-$ = 13.7	ΔHD = 2.0
Soft Clay I	γ_{sat}	HD$^+$ = 12.6 HD$^-$ = 13.0	ΔHD = 0.4
	k_x	HD$^+$ = 12.1 HD$^-$ = 13.0	ΔHD = 0.9
	k_y	HD$^+$ = 12.9 HD$^-$ = 12.5	ΔHD = 0.4
	M	HD$^+$ = 11.7 HD$^-$ = 13.8	ΔHD = 2.1
	OCR	HD$^+$ = 11.9 HD$^-$ = 13.6	ΔHD = 1.7
	ν_{ur}	HD$^+$ = 12.9 HD$^-$ = 12.6	ΔHD = 0.3
	φ'_{cv}	HD$^+$ = 12.6 HD$^-$ = 12.8	ΔHD = 0.2
	c	HD$^+$ = 12.7 HD$^-$ = 12.8	ΔHD = 0.1
	e_0	HD$^+$ = 12.3 HD$^-$ = 13.3	ΔHD = 1.0
	λ	HD$^+$ = 13.0 HD$^-$ = 12.4	ΔHD = 0.6
	κ	HD$^+$ = 12.6 HD$^-$ = 13.0	ΔHD = 0.4
	μ	HD$^+$ = 12.6 HD$^-$ = 12.9	ΔHD = 0.3
	β	HD$^+$ = 12.1 HD$^-$ = 13.6	ΔHD = 1.5